Institut für Biologie und Biochemie

Arbeitsgruppe Molekulare Enzymologie

Role of the tRNA thiouridine modification protein (TUM1) as a sulfurtransferase in humans

Dissertation

zur Erlangung des akademischen Grades
“doctor rerum naturalium”
(Dr. rer. nat.)
in der Wissenschaftsdisziplin “Biochemie”

eingereicht an der
Mathematisch-Naturwissenschaftlichen Fakultät
an der Universität Potsdam

von

Moses Ogunkola

Potsdam, 2023.

Published online on the
Publication Server of the University of Potsdam:
https://doi.org/10.25932/publishup-61135
https://nbn-resolving.org/urn:nbn:de:kobv:517-opus4-611357

Abstract

Sulfur is essential for the functionality of some important biomolecules in humans. Biomolecules like the Iron-sulfur clusters, tRNAs, Molybdenum cofactor, and some vitamins. The trafficking of sulfur involves proteins collectively called sulfurtransferase. Among these are TUM1, MOCS3, and NFS1.

This research investigated the role of TUM1 for molybdenum cofactor biosynthesis and cytosolic tRNA thiolation in humans. The rhodanese-like protein MOCS3 and the L-cysteine desulfurase (NFS1) have been previously demonstrated to interact with TUM1. These interactions suggested a dual function of TUM1 in sulfur transfer for Moco biosynthesis and cytosolic tRNA thiolation. TUM1 deficiency has been implicated to be responsible for a rare inheritable disorder known as mercaptolactate cysteine disulfiduria (MCDU), which is associated with a mental disorder. This mental disorder is similar to the symptoms of sulfite oxidase deficiency which is characterised by neurological disorders. Therefore, the role of TUM1 as a sulfurtransferase in humans was investigated, in CRISPR/Cas9 generated *TUM1* knockout HEK 293T cell lines.

For the first time, TUM1 was implicated in Moco biosynthesis in humans by quantifying the intermediate product cPMP and Moco using HPLC. Comparing the *TUM1* knockout cell lines to the wild-type, accumulation and reduction of cPMP and Moco were observed respectively. The effect of *TUM1* knockout on the activity of a Moco-dependent enzyme, Sulfite oxidase, was also investigated. Sulfite oxidase is essential for the detoxification of sulfite to sulfate. Sulfite oxidase activity and protein abundance were reduced due to less availability of Moco. This shows that TUM1 is essential for efficient sulfur transfer for Moco biosynthesis. Reduction in cystathionin γ-lyase in *TUM1* knockout cells was quantified, a possible coping mechanism of the cell against sulfite production through cysteine catabolism.

Secondly, the involvement of TUM1 in tRNA thio-modification at the wobble Uridine-34 was reported by quantifying the amount of mcm^5s^2U and mcm^5U via HPLC. The reduction and accumulation of mcm^5s^2U and mcm^5U in *TUM1* knockout cells were observed in the nucleoside analysis. Herein, exogenous treatment with NaHS, a hydrogen sulfide donor, rescued the Moco biosynthesis, cytosolic tRNA thiolation, and cell proliferation deficits in *TUM1* knockout cells.

Further, TUM1 was shown to impact mitochondria bioenergetics through the measurement of the oxygen consumption rate and extracellular acidification rate (ECAR) via the seahorse cell

Mito stress analyzer. Reduction in total ATP production was also measured. This reveals how important TUM1 is for H_2S biosynthesis in the mitochondria of HEK 293T.

Finally, the inhibition of NFS1 in HEK 293T and purified NFS1 protein by 2-methylene 3-quinuclidinone was demonstrated via spectrophotometric and radioactivity quantification. Inhibition of NFS1 by MQ further affected the iron-sulfur cluster-dependent enzyme aconitase activity.

Zusammenfassung

Schwefel ist für die Funktionalität einiger wichtiger Biomoleküle beim Menschen wie die Eisen-Schwefel-Cluster, tRNA, Molybdän-Cofaktoren und einige Vitamine unerlässlich. Am Schwefelverkehr ist eine weit verbreitete Gruppe von Proteinen beteiligt, die als Rhodanese (Sulfurtransferase) bezeichnet wird. Zu dieser Klasse von Enzymen gehören die humanen (Proteine) TUM1, MOCS3 und NFS1.

Es hat sich gezeigt, dass TUM1 mit der L-Cystein-Desulfurase (NFS1) und dem rhodaneseähnlichen Protein MOCS3 interagiert. Diese Wechselwirkungen deuten auf eine Doppelfunktion von TUM1 beim Schwefeltransfer für die Moco-Biosynthese und die zytosolische tRNA-Thiolierung hin. Ein TUM1-Mangel wird für eine seltene vererbbare Störung verantwortlich gemacht, die als Mercaptolactat-Cystein-Disulfidurie (MCDU) bekannt ist und mit geistigen Störungen einhergeht. Diese psychische Störung könnte auf die Symptome des Sulfit-Oxidase-Mangels zurückzuführen sein, der auch durch neurologische Störungen gekennzeichnet ist. In dieser Studie wurde zum ersten Mal die Rolle von TUM1 bei der Biosynthese von Molybdän-Cofaktoren und der zytosolischen tRNA-Thiolierung beim Menschen untersucht. Dies wurde durch die Verwendung von einer zuvor generierten TUM1-Deletion in HEK 293T-Zelllinien unter Verwendung von CRISPR/Cas9 erreicht.

Hier wurde zum ersten Mal die Funktion von TUM1 in der Moco-Biosynthese im Menschen untersucht, wobei das Zwischenprodukt cPMP und Moco mittels HPLC quantifiziert wurde. Beim Vergleich der TUM1-deletierten-Zelllinien mit dem Wildtyp wurde eine Akkumulation bzw. Reduktion von cPMP und Moco beobachtet. Die Auswirkungen der TUM1-Deletion auf die Aktivität eines Moco-abhängigen Enzyms, der Sulfit-Oxidase, wurden ebenfalls untersucht. Sulfit ist wichtig für die Entgiftung von Sulfit zu Sulfat. Die Aktivität der Sulfit-Oxidase und die Proteinquantität waren aufgrund der geringeren Verfügbarkeit von Moco reduziert. Dies zeigt, dass TUM1 für einen effizienten Schwefeltransfer für die Moco-Biosynthese wichtig ist. Wir berichteten auch über die Verringerung der Cystathionin -Lyase in TUM1-deletierten-Zellen, ein möglicher Bewältigungsmechanismus der Zelle gegen die Sulfitproduktion.

Zweitens wurde die Beteiligung von TUM1 an der tRNA-ThioModifikation am Wobble Uridin-34 durch Quantifizierung der Menge an mcm^5s^2U und mcm^5U mittels HPLC untersucht. Es wurde eine Reduktion bzw. Akkumulation von mcm^5s^2U und mcm^5U in TUM1-Knockout-Zellen beobachtet. Die exogene Behandlung mit NaHS, einem Schwefelwasserstoff-

Donor, rettete die Moco-Biosynthese, die zytosolische tRNA-Thiolation und das Defizit der Zellproliferation in TUM1-deletion-Zellen.

Darüber hinaus wurde gezeigt, dass TUM1 die Bioenergetik der Mitochondrien beeinflusst, indem die Sauerstoffverbrauchsrate und die extrazelluläre Versauerungsrate (ECAR) über den Seahorse XF Analyzer gemessen wurden. Eine Verringerung der gesamten ATP-Produktion war ebenfalls erkennbar. Dies zeigt, wie wichtig TUM1 für die H_2S-Biosynthese in den Mitochondrien von HEK 293T ist.

Schließlich wurde die Hemmung von NFS1 in HEK 293T und gereinigtem NFS1-Protein durch 2-Methylen-3-chinuclidinon mittels spektrophotometrischer und radioaktiver Quantifizierung nachgewiesen. Die Hemmung von NFS1 durch 2-Methylen-3-chinuclidinon verringerte die Aktivität des von Eisen-Schwefel-Clustern abhängigen Enzyms Aconitase in HEK 293T.

Table of Contents

List of Figures

List of abbreviations

ABA	Abscisic acid
Aco	Aconitase
AHCY	Adenosylhomocysteinase
AMP	Adenine monophosphate
AO	Aldehyde oxidase
ATP	Adenosine triphosphate
BHMT	Betaine-homocysteine S-methyltransferase
BSA	Bovine serum albumin
CBS	Cystathionine β-synthase
CDO	Cysteine dioxygenase
CIA	Cytosolic iron-sulfur-protein assembly
cPMP	Cyclic pyranopterin monophosphate
CRISPR	Clustered regularly interspaced short palindromic repeats
CSA	Cysteine sulfinic acid
CSAD	Cysteine sulfinic acid decarboxylase
CTH	Cystathionine-γ-lyase
CTU	Cytoplasmic tRNA 2-thiolation protein
DAO	D-amino acid oxidase.
DHLA	Dihydrolipoic acid
ELP	Elongator protein
ETC	Electron transport chain
FBS	Fetal bovine serum
FDX	Ferredoxin
Fe-S	Iron-sulfur
FRET	Förster resonance energy transfer
FXN	Frataxin
GLRX5	Glutaredoxin 5
GOT	glutamate oxaloacetate transaminase
GS	Glutathione synthetase
GTP	Guanosine triphosphate
GTPBP3	GTP binding protein 3

H_2S	Hydrogen sulfide
HPLC	High-pressure liquid chromatography
IMS	Intermembrane space
ISD11	Iron-sulfur biogenesis desulfurase interacting protein
LYRM	Lysine, tyrosine arginine motif
MAPK	Mitogen-activated protein kinases
mARC	Mitochondrial amidoxime reductase component
MAT	Methionine-adenosyltransferase
MCDU	Mercaptolactate- cysteine disulfuiduria
mcm^5s^2U34	5-Methoxycarbonylmethyl-2-thiouridine
mcm^5U	5-methoxycarbonylmethyl uridine
MERRF	Myoclonic epilepsy with ragged red fibres
mnm^5s^2U34	5-methylaminomethyl-2-thiouridine
Mo	Molybdenum
Moco	Molybdenum cofactor
MOCOS	Molybdenum cofactor sulfurase
MOCS	Molybdenum cofactor synthesis
MPST	3-mercaptopyruvate sulfurtransferases
MPT	Molybdopterin
MQ	2-methylene 3-quinuclidinone
ms^2i^6A37	2-methylthio-N6-isopentenyladenosine,
MTO1	Mitochondrial tRNA translation optimisation 1
MTR	Methionine synthase
MTS	Mitochondria targeting sequence
MTU1	Mitochondrial tRNA-specific 2-thiouridylase 1
PLP	Pyridoxal-5'-phosphate
RHD	Rhodanese homology domain
RLD	Rhodanese-like domain
s^2C32	2-thiocytidine
s^4U8	4 thiouridine
SAH	S-adenosylhomocysteine
SAM	S-adenosylmethionine
SDO	Sulfur dioxygenase
SO	Sulfite oxidase

SQR	Sulfide:quinone oxidoreductase
ST	Sulfur transferase
TST	Thiosulfate sulfurtransferase
TUM1	tRNA thiouridine modification protein
Ub	Ubiquitin
Uba4	Ubiquitin-like protein activator 4
URM1	Ubiquitin-related modifier 1
WT	Wild type
XOR	Xanthine oxidoreductase
τm^5U	5-taurinomethyl uridine
τm^5s^2U	5-taurinomethyl-2-thiouridine

1 Introduction

1.1 Sulfur in human biomolecules

Sulfur is an element that is essential for life. It is unique in its chemical diversity, primarily due to the easy cleavage of its chemical bonds. Sulfur can serve as a nucleophile or an electrophile, enhancing the functionality of various biomolecules (Beinert, 2000). Sulfur is present in essential amino acids (cysteine and methionine) (Brosnan *et al.*, 2006), which can be used for the synthesis of other crucial molecules like hydrogen sulfide (H_2S) (Kabil *et al.*, 2014). Sulfur is present in vitamins such as biotin and thiamine. Sulfur is also present in essential cofactors such as the iron-sulfur clusters (Fe-S) and the Molybdenum cofactor (Moco) (Leimkühler, 2017). The sulfuration of tRNAs also plays a critical role in ensuring the stabilisation of tRNA during translation (Liu *et al.*, 2016).

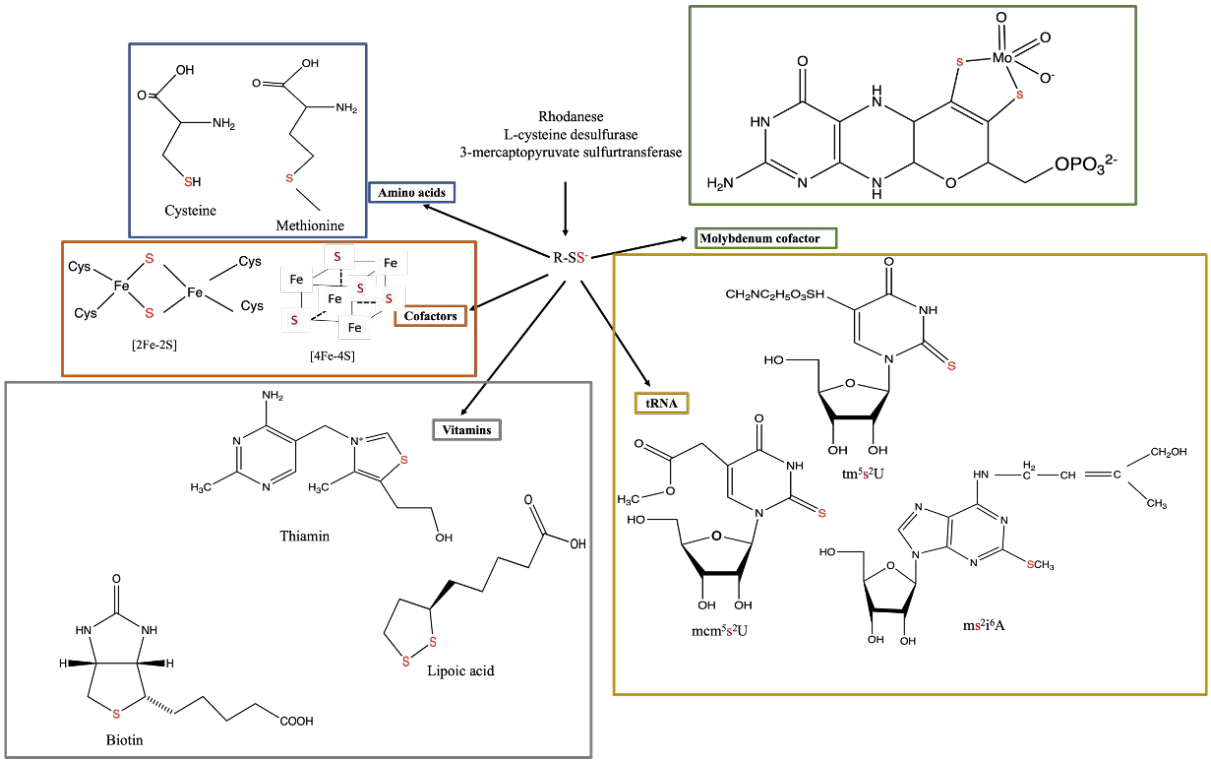

Figure 1: Sulfur-dependent biomolecules relying on persulfide transfer from sulfurtransferases. Both L-cysteine desulfurases and rhodanese can bind sulfur as protein-persulfide (R-S-SH). L-cysteine desulfurases mobilised sulfur is transferred to sulfur transferases such as rhodanese or directly into biomolecules such as amino acids like cysteine and methionine, cofactors like iron-sulfur clusters, Molybdenum cofactor. This sulfur can also be incorporated into vitamins like biotin, thiamine and lipoic acid and tRNAs.

1.1.1 Sulfur metabolism in eukaryotes

Sulfur is present in methionine and cysteine. Methionine is an essential amino acid that cannot be synthesised by the body (Townsend *et al.*, 2004). Cysteine can be synthesised through the transsulfuration pathway of methionine. In the first step of the transsulfuration pathway, S-adenosylmethionine (SAM) is synthesised from methionine in an ATP-dependent manner by methionine S-adenosyltransferase (MAT) (Stipanuk, 2020). The majority of the SAM synthesised goes through transmethylation reactions leading to the transfer of its methyl group to other small molecules, DNA, and RNA with S-adenosylhomocysteine (SAH) as a by-product (Mudd *et al.*, 1975; Jeltsch *et al.*, 2018; Du *et al.*, 2015; Roundtree *et al.*, 2017). SAH is further hydrolysed to form homocysteine and adenosine through the enzymatic reaction of adenosylhomocysteinase (AHCY) (Stipanuk, 2020). This step is essential for removing SAH, an inhibitor of methyltransferases that competes with SAM. However, the accumulation of homocysteine leads to the production of SAH due to the reversibility of the step (Grubbs *et al.*, 2010; Buist *et al.*, 2006; Strauss *et al.*, 2015; Barić *et al.*, 2005; Stender *et al.*, 2015). Homocysteine produced undergoes either transsulfuration or remethylation. The transsulfuration pathway is responsible for cysteine's catabolism, while homocysteine's remethylation synthesises methionine (Stipanuk, 2020). The remethylation reaction is catalysed by either methionine synthase (MTR) or betaine-homocysteine S-methyltransferase (BHMT), using methyl donated from folate coenzyme or betaine respectively (Stipanuk, 2004)(Figure 2). In the transsulfuration pathway, Cystathionine ß synthase (CBS) catalyses the formation of cystathionine from homocysteine and serine. Cystathionine γ lyase (CTH) cleaves cystathionine to form cysteine and α ketobutyrate (Figure 2). CBS and CTH are pyridoxal-5`-phosphate (PLP) enzymes, making the transsulfuration pathway vitamin B6 dependent (Stipanuk, 2020).

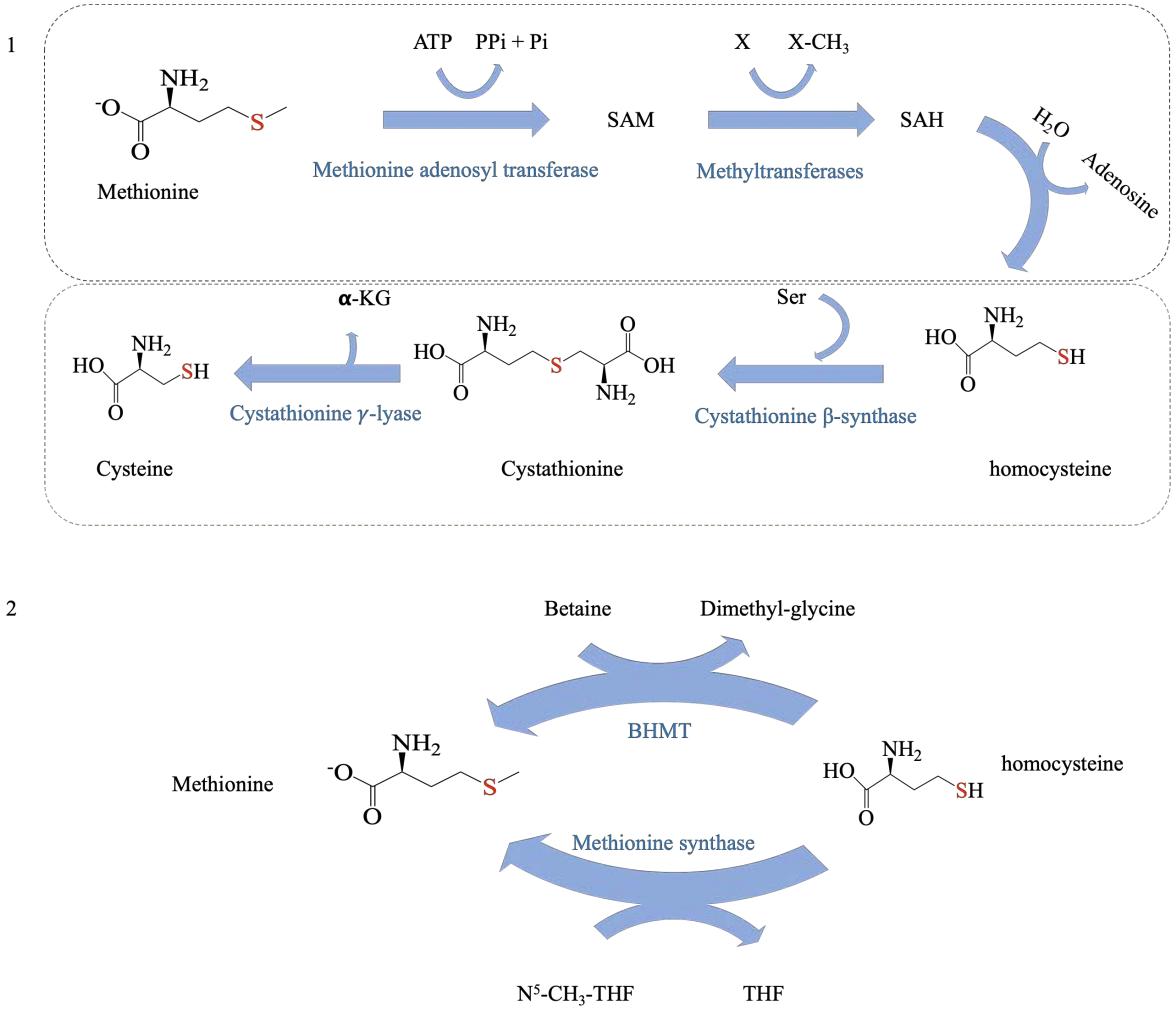

Figure 2: Biosynthesis of cysteine from the transmethylation and transsulfuration pathway. Homocysteine derived from the catalytic activity of methionine adenosyl transferase (MAT) and S-adenosylhomocysteine hydrolase (SAH) (Transmethylation blue dots) condenses with serine to form cystathionine in a reaction catalysed by cystathionine ß synthase (CBS). Cystathionine is finally converted to L-cysteine by cystathionine γ lyase (Transsulfuration yellow dot). (2) Remethylation of homocysteine to methionine by the catalytic action of betaine-homocysteine S-methyltransferase (BHMT) or methionine synthase (Stipanuk, 2020).

In the presence of a high concentration of sulfur-containing amino acids, the oxidative pathway is the main pathway for cysteine degradation. The process is catalysed by cysteine dioxygenase (CDO1) to produce cysteine sulfinic acid (CSA). CSA is either metabolised to form 3-sufinylpyruvate or hypotaurine. For the formation of hypotaurine, cysteine sulfinic acid decarboxylase (CSAD) decarboxylates CSA. Hypotaurine undergoes further oxidation to taurine (Stipanuk, 2020). Pyruvate is produced through transamination of CSA with α-ketoglutarate in a reaction catalysed by glutamate oxaloacetate (GOT) to produce 3-

sufinylpyruvate, which decomposes to pyruvate and sulfite. Sulfite is further detoxified to sulfate by sulfite oxidase (SO).

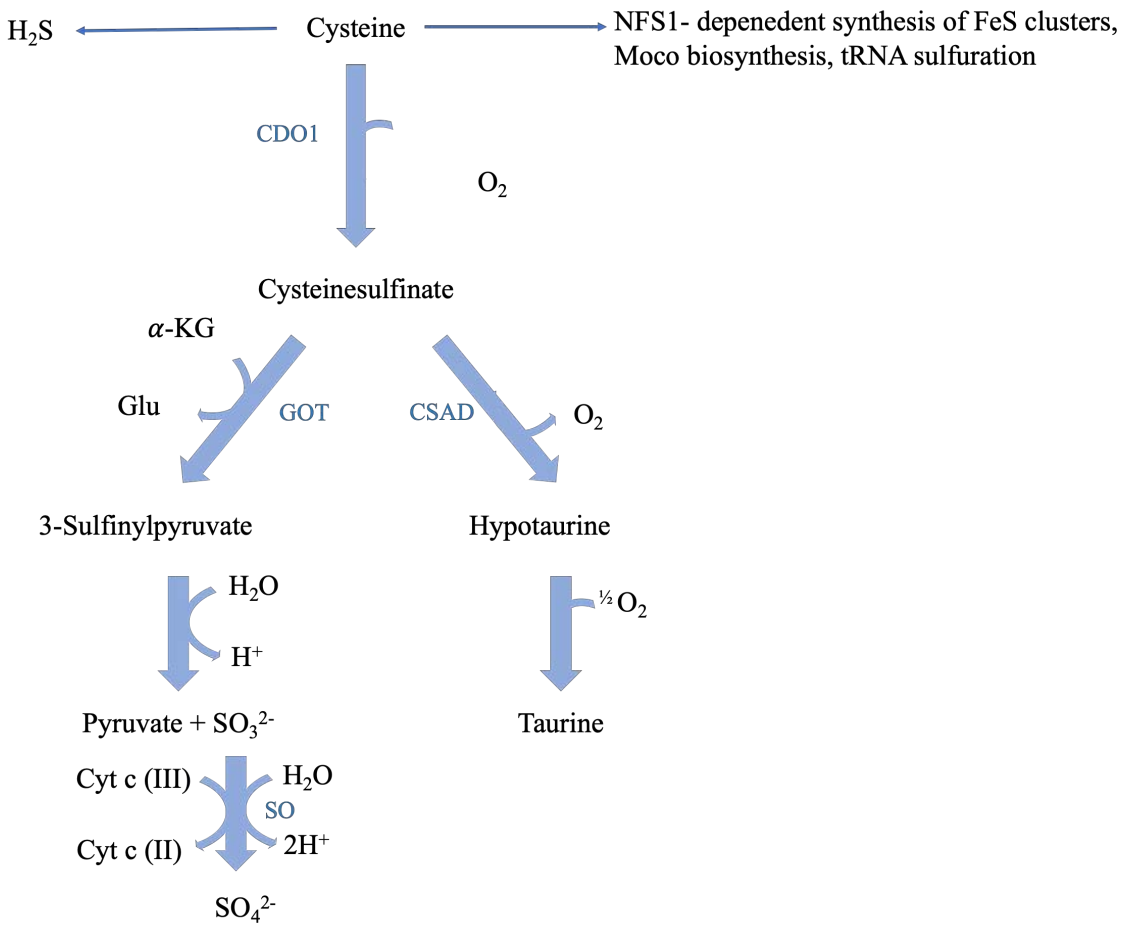

Figure 3: Metabolism of cysteine by CDO. Oxidation of cysteine by CDO produces cysteine sulfinate, which is either decarboxylated to form taurine as an end-product or transamination by glutamate oxaloacetate transaminase to form pyruvate and sulfate. L-cysteine desulfurase uses cysteine as a substrate to provide sulfur for biomolecules like Fe-S clusters, Moco biosynthesis and tRNA sulfuration.

The cysteine produced from the transsulfuration pathway can be further utilised to form persulfides, which are additionally incorporated into biomolecules for their functionality. A particular class of enzymes called the Rhodaneses (sulfurtransferases) catalyses this process of persulfide formation and transfer.

1.1.2 Rhodanese-like proteins

Rhodaneses were discovered first in the mitochondria of bovine (Bos taurus) as a thiosulfate sulfurtransferase (TST)(Westley *et al.*, 1983). Characterisation studies showed that they contain an inactive N-terminal domain and an active C-terminal domain. The C-terminal has a

conserved six-amino acid active site loop unique for all rhodanese-like proteins. They can be classified into four categories based on the number and type of rhodanese-like domains they possess. The first group comprises a single domain consisting an active or an inactive rhodanese-like domains. An example of this group with a functional part is the *E.coli* GlpE with only one rhodanese domain which is enough for the formation of thiocyanate in the presence of cyanide (Ray *et al.*, 2000). The eukaryotic MAPK-phosphatases and ubiquitin hydrolases are examples of inactive single rhodanese domains which have their active cysteine missing (Fauman *et al.*, 1998; Hofmann *et al.*, 1998). The second group of rhodanese-like proteins comprises the tandem-domain proteins with one catalytic active and one inactive rhodanese-like domain. This double domain includes TST (Thiosulfate sulfurtransferase) and the 3-mercaptopyruvate sulfurtransferase (MPST). MPST and TST subfamily are similar structurally and functionally, but on the other hand, MPST uses a specific substrate 3-mercaptopyruvate (3-MP) (Nagahara *et al.*, 1995). The amino acid sequence in the active site of both enzymes differs CRXGX[R/T] for TSTs and CG[S/T]GVT for MPST, respectively (Spallarossa *et al.*, 2001).

A

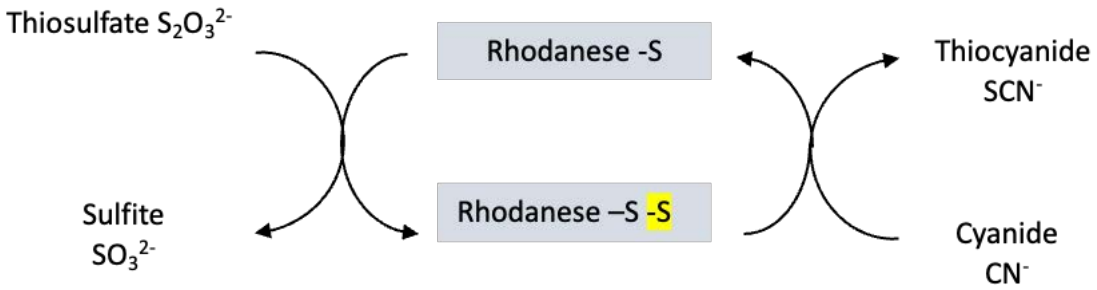

B

TST:	CRXGX(T/R)	MPST:	CG(S/T)GV(T/S)
EcYnjE	CGTGWR	EcSsea	CGSGVT
AvRhdA	CQTHHR	hTUM1	CGSGVT
hTST	CRKGVT	ScTum1	CGTGVS
DmMOCS3-RLD	CRRGND	LmajMST	CGSGVT
hMOCS3-RLD	CKLGND	BtMPST	CGSGVT

Figure 4: Schematic representation of the sulfur transfer catalysed by rhodanese and motive of the catalytic loop of TSTs and MSTs. (A) schematic representation of the catalytic reaction of rhodanese. In the first step, sulfane sulfur is transferred from thiosulfate to the thiol group at the active cysteine residue of the catalytic loop, generating a persulfide and subsequently followed by the transfer of the persulfide sulfur to cyanide, leading to the

formation of a less toxic thiocyanate (B) Amino acid sequence motif of the catalytic centre of TSTs (EcYnjE from *E. coli*, AvRhdA from *Acetobacter vinelandii*, hTST from *H.sapiens*, DmMOCS3-RLD from *Drosophilia melanogaster*, hMOCS3-RLD from *H. sapiens*) and MSTs (EcSseA from *E. coli*, hTUM1 from *H. sapiens*, ScTum1 from *S. cerevisiae*, LmajMST *from Leichmania major*, BtMPST from Bos taurus). X represents any alternative amino acid separated by a slash, and the catalytic cysteines are described in yellow. (Bordo *et al.*, 2002)

The third group of rhodanese-like proteins consists of a catalytic rhodanese-like domain and another domain with another known function. Examples of multi-domain proteins are MOCS3, Thil- and ThiF/MoeB-related proteins (Matthies *et al.*, 2004; Palenchar *et al.*, 2000). The fourth group of rhodanese-like proteins comprises the elongated active site loop proteins. These proteins are only present in eukaryotes and can recognise phosphate as a substrate. An example of this group of rhodanese is the Cdc25A phosphatase which has an active–site loop that is a long stretch of the rhodanese active-site loop (Bordo *et al.*, 2002; Hofmann *et al.*, 1998).

1.1.3 The L-cysteine desulfurase NFS1

L-cysteine desulfurase catalyses the formation of L-alanine and protein-bound persulfide from the breakdown of the L-cysteine protein-bound PLP (Zheng *et al.*, 1994). L-cysteine is bound to the PLP cofactor by forming a Schiff base (Kessler, 2006). In the process that leads to the formation of this persulfide, the PLP cofactor of the L-cysteine desulfurase binds the α-amino group of the substrate L-cysteine to form an external aldimine, which is subsequently converted to a Ketimine intermediate. The hydrolysis of the Ketimine intermediate leads to the formation of L-alanine and the release of the PLP cofactor. A catalytic cycle is established following the nucleophilic attack on the persulfide sulfur atom through the cysteine residue (Zheng *et al.*, 1994).

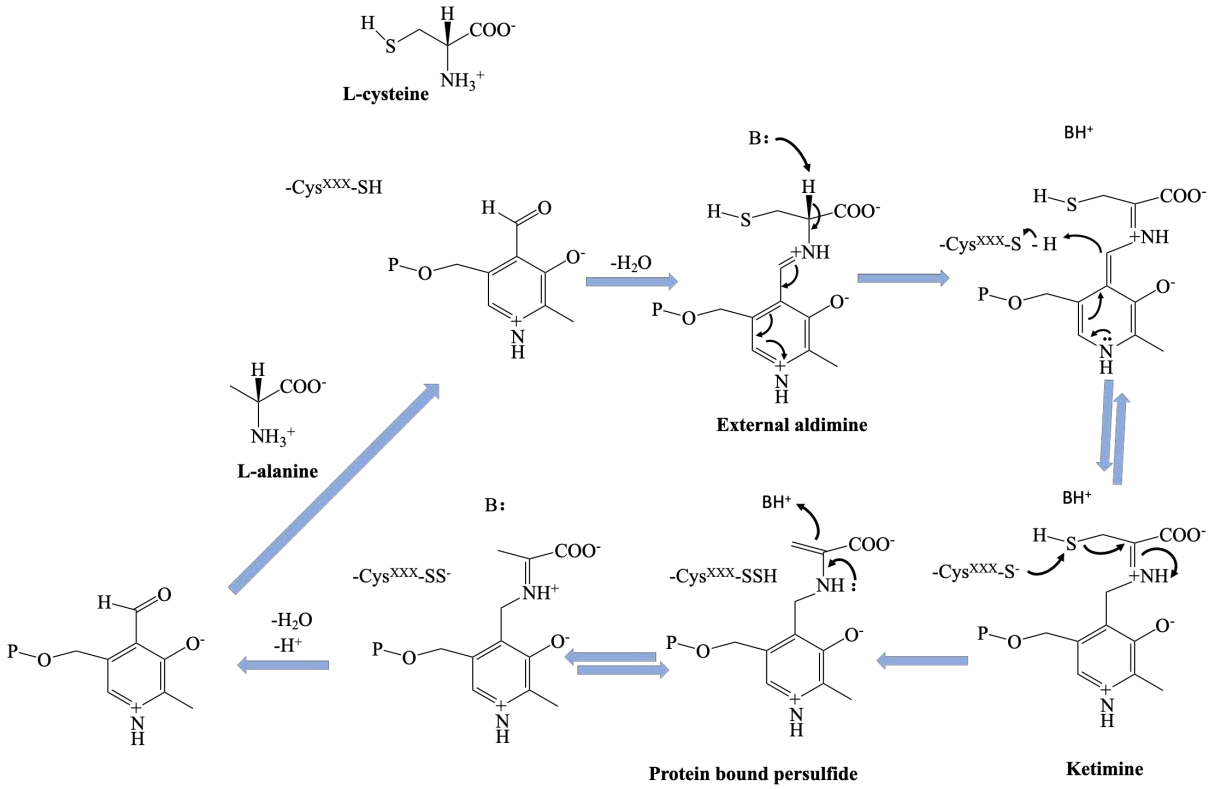

Figure 5: Mechanism of persulfide formation from L-cysteine by catalytic reaction of L-cysteine desulfurase. The α-amino group of L-cysteine attaches to PLP and creates an exterior aldimine. The nucleophilic attack from the L-cysteine sulfur to the active-site cysteine residue of the L-cysteine desulfurase causes cleavage of the C-S bond of the L-cysteine bound PLP (-CysXXX-S-), leading to the formation of an enzyme-bound persulfide (-CysXXX-SS-) and alanine enamine bound to PLP. Alanine is subsequently released to bind to another L-cysteine molecule.

The persulfide is utilised in a wide range of sulfur-dependent pathways like Fe-S clusters biosynthesis, Moco biosynthesis, cytosolic and mitochondrial tRNA thiolation (Hidese *et al.*, 2011; Noma *et al.*, 2009; Lill *et al.*, 2008; Leimkühler, 2017). In humans, two proteins have been identified to possess the L-cysteine desulfurase activity, namely the NFS1 and molybdenum cofactor sulfurase (MOCOS). MOCOS contain an N-terminal L-cysteine desulfurase domain for the sulfuration of Moco, which is essential for the two sulfurated Moco-containing enzyme aldehyde oxidase and xanthine oxidoreductase (Ichida *et al.*, 2001; Bittner *et al.*, 2001; Amrani *et al.*, 2000). The L-cysteine desulfurase NFS1 in humans is majorly located in the mitochondria compartment. However, a small amount is also present in the cytosol and nucleus and has also been reported recently to be at the centrosome (Land *et al.*, 1998; Nakai *et al.*, 1998; Neukranz *et al.*, 2019). The difference between the mitochondria-localized NFS1 and the cytosolic localised NFS1 is the mitochondria targeting sequence (MTS), which is absent in the cytosolic NFS1 (Tong *et al.*, 2006; Land *et al.*, 1998). The

primary role of NFS1 in humans is the donation of sulfur for the Fe-S cluster assembly from the L-cysteine (Zheng *et al.*, 1994).

1.1.4 Fe-S biosynthesis and pathophysiological relevance

Iron–sulfur clusters are present in all forms of life, serving as a cofactor in numerous enzymes involved in important metabolic pathways in prokaryotes and eukaryotes (Fontecave, 2006). These proteins are involved in diverse functions ranging but not limited to electron transfer, respiration, photosynthesis, metabolism of nitrogen, sulfur, carbon, and hydrogen, biosynthesis of antibiotics, gene regulation, protein translation replication, DNA repair, protection from oxidising agents, and neurotransmission (Lill, 2006; Beinert *et al.*, 1997; Fuss *et al.*, 2015; Wiedemann *et al.*, 2006; Mettert *et al.*, 2015; Roche *et al.*, 2013). More than 200 identified Fe-S cluster proteins exist in humans (Shi *et al.*, 2021). The biosynthesis of Fe-S is governed by the Fe-S assembly machinery (ISC) and divided into two steps. Firstly, the cluster is formed on the scaffold, followed by the incorporation of the Fe-S cluster into the apo Fe-S cluster containing protein with the help of chaperones. For denovo synthesis of the Fe-S cluster, the scaffold protein ISCU forms a quaternary complex with NFS1.ISD11.FDX. For direct transfer of sulfur ISD11 which belongs to the LYRM (Lysine, tyrosine arginine motif) family, stabilises NFS1 to form the active L-cysteine desulfurase complex (Adam *et al.*, 2006; Wiedemann *et al.*, 2006). The electrons necessary for converting sulfur to sulfide are provided by ferredoxin 2 (Lange *et al.*, 2000; Shi *et al.*, 2012; Mühlenhoff *et al.*, 2003). Following the formation of the [2Fe-2S] cluster on ISCU, it must be transported to the respective apoproteins. However, little is known about the proteins necessary for the transport of Fe-S. Recently, a co-chaperone HSC20 mainly localised in the mitochondria was implicated as a chaperone for delivering Fe-S to apoproteins based on evidence from bacteria and yeast (Uhrigshardt *et al.*, 2010; Vickery *et al.*, 2007; Craig *et al.*, 2002). A dimerised Glutaredoxin 5 (GLRX5) transports and recognises target proteins by connecting them to the [2Fe-2S] cluster. In *S. cerevisiae*, a binding site of the Grx5 homologue of human GLRX5 on the Ssq1 homologue of human HSP70 was found near Isu1, the human homologue of ISCU. This allows for the quick transfer of [2Fe-2S] clusters to GLRX5.

Mutations in the gene of Fe-S cluster biosynthesis proteins have been linked to several diseases, such as Friedreich's ataxia (Frataxin), Sideroblastic anaemia (GLRX5), Myopathy (ISCU), X-linked sideroblastic Anaemia (ABCB7) (Campuzano *et al.*, 1996; Camaschella *et al.*, 2007; Mochel *et al.*, 2008; Olsson *et al.*, 2008; Bergmann *et al.*, 2010). NFS1 provides sulfur for the

ISC, which is responsible for Fe-S cluster biogenesis (Stehling *et al.*, 2014; Netz *et al.*, 2014). Due to the vital functions of Fe-S clusters, Researchers have recently focused on developing drugs that affect the biogenesis of Fe-S clusters through the inhibition of NFS1 (Fujihara *et al.*, 2022). The level of oxygen has been shown to affect the activity of oxygen-consuming enzymes (Alvarez *et al.*, 2017). Recently Alvarez, Sviderskiy and colleagues discovered through RNAi-based loss of function screens that NFS1 is required in the lungs at 21 % oxygen (Alvarez *et al.*, 2017). Due to the oxygen sensitivity of essential cofactors like Fe-S clusters (Imlay, 2006), tumours in oxygen-perfused environments require the high activity of NFS1 to meet up with Fe-S cluster biogenesis (Alvarez *et al.*, 2017). Research has shown that NFS1 inhibition does not affect the growth of tumours in a low-oxygen environment but suppresses tumour growth in the Lungs (Alvarez *et al.*, 2017). Eprenetapopt, a prodrug with active compound 2-methylene 3-quinuclidinone (MQ), was recently shown to limit NFS1 activity (Fujihara *et al.*, 2022). MQ is a Michael acceptor that binds to thiols like GSH and cysteine (Lambert *et al.*, 2009). The mode of action of Eprenetapopt has been previously linked to the reactivation of mutant p53 in tumour cells. p53 is a transcription factor activated in the stress response (Lane, 2004; Vousden *et al.*, 2002). p53 induces cell cycle arrest, senescence, cell death and apoptosis (Mijit *et al.*, 2020). Cancer cells are known to express mutation in p53 in other to invade the cell death (Hollstein *et al.*, 1991; Olivier *et al.*, 2002). p53 contains ten cysteine residues in its DNA binding core domain which are essential for its activation (Méplan *et al.*, 2000). MQ was shown to bind Cys122 and Cys277 (Wassman *et al.*, 2013; Zhang *et al.*, 2018). However, the exact mechanism of the reactivation of the mutated p53 is not well understood. Kenji and colleagues have shown the upregulation of Ferredoxin (FDX1) through the proteomics database. It was hypothesised to be caused by the binding of MQ to free cysteine, thereby limiting the NFS1 activity (Fujihara *et al.*, 2022). MQ was shown to inhibit the activity of NFS1 in millimolar concentration and the activity of aconitase, an iron-sulfur cluster-dependent enzyme (Fujihara *et al.*, 2022; Tong *et al.*, 2006). Cancer requires a high iron level to survive (Guo *et al.*, 2021). Studies have shown that NFS1 and ISC stability regulates cellular sensitivity to the ferroptosis (Alvarez *et al.*, 2017; Du *et al.*, 2020). The loss of iron-sulfur cluster biosynthesis increases the intracellular iron load, thereby promoting cell death by ferroptosis (Terzi *et al.*, 2021).

1.1.5 The molybdenum cofactor biosynthesis protein MOCS3

MOCS3 is an important sulfurtransferase for Molybdenum cofactor biosynthesis and thiolation modification of mcm^5s^2U at the wobble uridine 34 of Lys, Gln, Glu (Chowdhury *et al.*, 2012; Schmitz *et al.*, 2008a). MOCS3 consists of two domains, an N-terminal domain with a conserved cysteine at position 239 which is vital for its adenylyltransferase role (Chowdhury *et al.*, 2012; Matthies *et al.*, 2004). The C-terminus of MOCS3 sheltering the rhodanese-like domain contains a highly conserved cysteine residue at position 412 which is indispensable for the sulfur transfer (Matthies *et al.*, 2004).

A

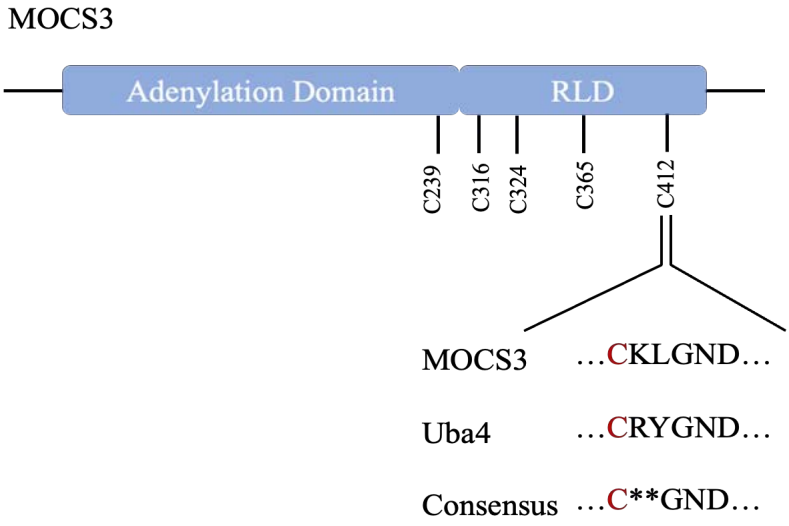

B

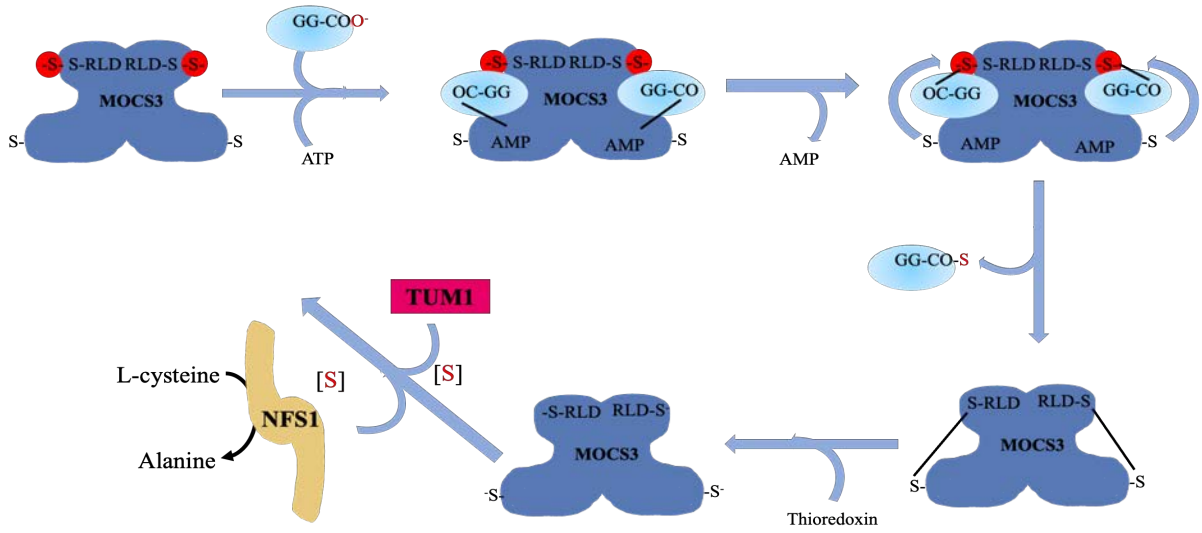

Figure 6: The sulfur transfer mechanism of MOCS3 and its catalytic centre. (A) Depiction of the adenylation and rhodanese-like domains of the MOCS3 protein. The MOCS3 active site loop, which has six amino acids, is typical of rhodanese-like proteins, containing highly conserved cysteine at position 412. (B) MOCS3 adenylates MOCS2A and URM1. The acyl-disulfide link between the two proteins and MOCS3 is broken due to a nucleophilic attack on the persulfide group on C412 of MOCS3 and a subsequent attack on C239 of MOCS3. As a result, a disulfide bond is created between C239 and C412. tRNA thiolation and Moco biosynthesis receive the sulfur from the thiocarboxylated MOCS2A and URM1, respectively (Chowdhury et al., 2012). A thioredoxin mechanism in MOCS3 reduces the disulfide bond between the two cysteines, and either directly or indirectly, a new persulfide can be transmitted from NFS1 to MOCS3 (Fräsdorf et al., 2014; Marelja et al., 2008).

This catalytic cysteine is highly homologous to the active-site loop of the TST (Chowdhury *et al.*, 2012; Matthies *et al.*, 2004). MOCS3 activates its protein interaction partners URM1 and MOCS2A by adenylating their C terminus. Due to the nucleophilic attack on the Cys412 of MOCS3, an acyl-disulfide bond is formed between MOCS3 and URM1/MOCS2A. The bond formed is cleaved by another nucleophilic attack by the Cys239 of MOCS3, leading to the formation of a thiocarboxylate group on URM1/MOCS2A. This results in the formation of a new disulfide bond between Cys239 and Cys412. To further accept sulfur from NFS1 or TUM1, the disulfide bond is reduced by a thioredoxin system (Marelja *et al.*, 2008; Marelja *et al.*, 2013; Krepinsky *et al.*, 2007). Recently, the human TUM1 was reported to interact with NFS1 and MOCS3, suggesting a role in tRNA thiolation and Molybdenum cofactor (Moco) biosynthesis (Fräsdorf *et al.*, 2014). Moco biosynthesis and tRNA thiolation are suggested to share the same sulfur delivery pathway composed of NFS1, TUM1 and MOCS3 (Fräsdorf *et al.*, 2014).

1.1.6 The human Mercaptopyruvate sulfurtransferase TUM1

Human TUM1, also designated as 3-mercaptopyruvate sulfur transferase (MPST), has been suggested to be involved in many physiological processes in the cell. TUM1 catalyses the transfer of sulfur from 3- mercaptopyruvate to other protein acceptors (Huang *et al.*, 2016). The human TUM1 has two isoforms, TUM1 Iso1, which localises solely in the cytosol and TUM1 Iso2, which localises both in the mitochondria and cytosol (Fräsdorf *et al.*, 2014). It belongs to a protein superfamily of enzymes that contains the RLD (rhodanese-like domain) (Bordo *et al.*, 2002). Representatives of this enzyme family are made up of one to four RLDs, with the catalytically active site loop typically only present in the C-terminal domain. The N-terminal part plays a regulatory role and participates in signalling pathways (Bordo *et al.*,

2002). Several domains of other enzyme families, like adenylation domains, RNA-binding motifs, phosphatase families, and ubiquitinating enzymes, have been discovered to be connected with catalytically active or inactive single RLDs (Keyse *et al.*, 1993; Bordo *et al.*, 2002). In the interaction of the catalytic active site loop with pyruvate, the two conserved arginine residues R188 and R197 orientate the substrate by forming a hydrogen bond with the carboxylate in Arg188 and Arg197 and the carbonyl group of 3- mercaptopyruvate (3-MP). The former is essential for desulfuration and persulfidation, while the latter is less critical for the MPST activity (Lec *et al.*, 2018; Mikami *et al.*, 2011; Kimura *et al.*, 2015; Kimura *et al.*, 2017; Nagahara *et al.*, 1996). Ser250 and Thr253 orchestrate the substrate binding by forming a water-mediated link with the 3-MP carboxylate.

A

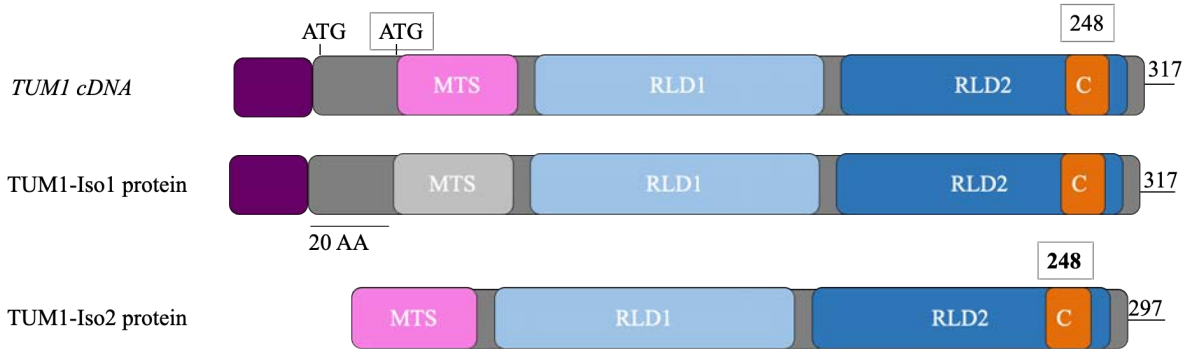

ATG: start codon, MTS: mitochondrial targeting sequence,
RLD: rhodanese like domain, C: active side cysteine residue,
AA: amino acids

B

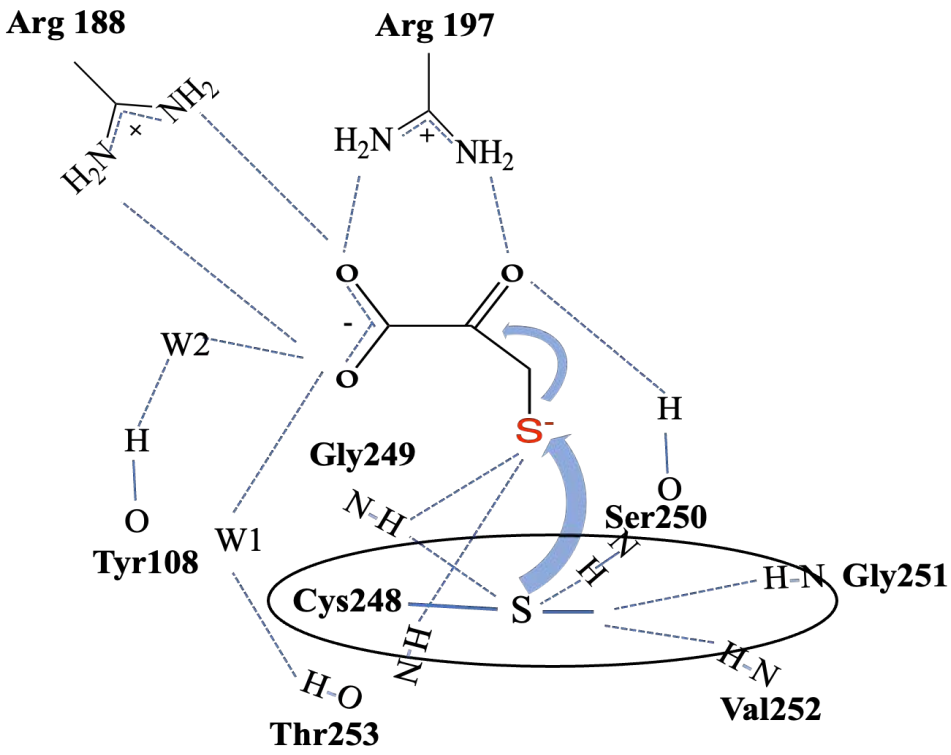

Figure 7: Schematic representation of the rhodanese domains of TUM1. (A) Upper displaying the 20 amino acids capping the mitochondria targeting sequence (TUM1-Iso1) Below: (TUM-Iso2). ATG: start codon, MTS: mitochondrial targeting sequence, RLD: rhodanese-like domain, C: active site cysteine residue, AA: amino acid. (B) hydrogen bonding network based on the crystal structure of human MPST showing the active site Cys248 and pyruvate in the active site pocket (PDB ID: 4jgt) Adapted from (Pedre *et al.*, 2021)

TUM1 catalyses the desulfuration of 3-MP, generating an enzyme-bound persulfide TUM1(-S-S-) and pyruvate (Pedre *et al.*, 2021). Pyruvate is liberated from the active site allowing the acceptor protein to bind to the active site. Further, TUM1 bound persulfide of the active site loop undergoes nucleophilic attack by the acceptor protein on the outermost sulfur atom. The electrophilicity of the innermost sulfur atom is strengthened, protecting it from the nucleophilic attack (Huang *et al.*, 2016). The outermost sulfur atom is then transferred to the acceptor protein leading to the regeneration of the active site thiol (Figure 8).

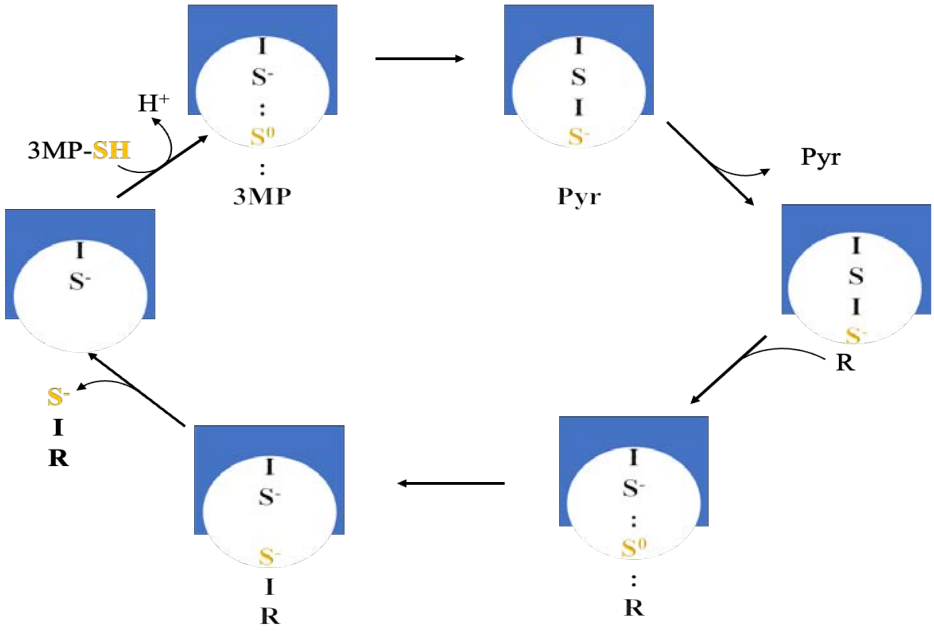

Figure 8: Persulfide transfer to the recipient by TUM1 and its regeneration cycle. MPST orchestrate the transfer of the outermost sulfur atom to the recipient protein. After the binding of 3MP to the active site, it is desulfurized to form an active site cysteine and pyruvate. Pyruvate is subsequently removed from the active site allowing the binding of an acceptor protein. The persulfide recipient protein is then released from the active site (Pedre *et al.*, 2021).

The physiological substrate of MPST is the 3-mercaptopyruvate for persulfide formation. 3-MP can be generated in the cytosol, mitochondria and peroxisome. The formation of 3-MP in the cytosol and mitochondria is through the transamination of L-cysteine by the cytosolic glutamate oxaloacetate transaminase (GOT1) and mitochondria GOT2. 3-MP can also be synthesized in the peroxisome by the oxidative deamination of D-cysteine by D-amino acid oxidase (DAO) (Figure 9).

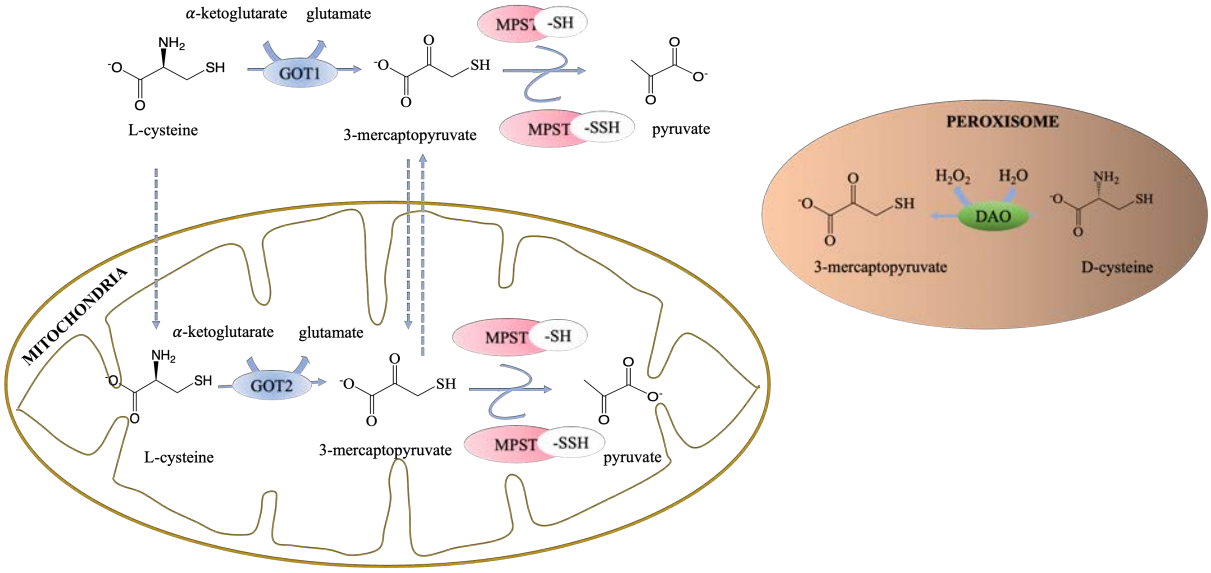

Figure 9: Compartmentalization of 3-MP production. In the cytosol, 3-MP is formed by the transamination of L-cysteine by the enzymatic action of glutamate oxaloacetate transaminase 1 (GOT1). Similarly, in the mitochondria, 3-MP is created by the transamination of L-cysteine by glutamate-oxaloacetate transaminase 2. Additionally, 3-MP can be synthesised in the peroxisomes from the oxidative deamination of D-cysteine by D-amino acid oxidase.

Generally, TUM1 transfers its outermost sulfur to L-Cysteine, glutathione (GSH), MOCS3 and cyanide. The sulfur transfer to L-Cys and GSH generates persulfides like L-CysSSH and GSSH, respectively. Persulfidated MOCS3 transfers its sulfur to the C-terminal of URM or MOCS2A, forming a thiocarboxylate at their C-terminal. TUM1 can also produce H_2S and a disulfide in a process being facilitated by dihydrolipoic acid (DHLA) or thioredoxin (Yadav *et al.*, 2013)(Mikami *et al.*, 2011) (Figure 10).

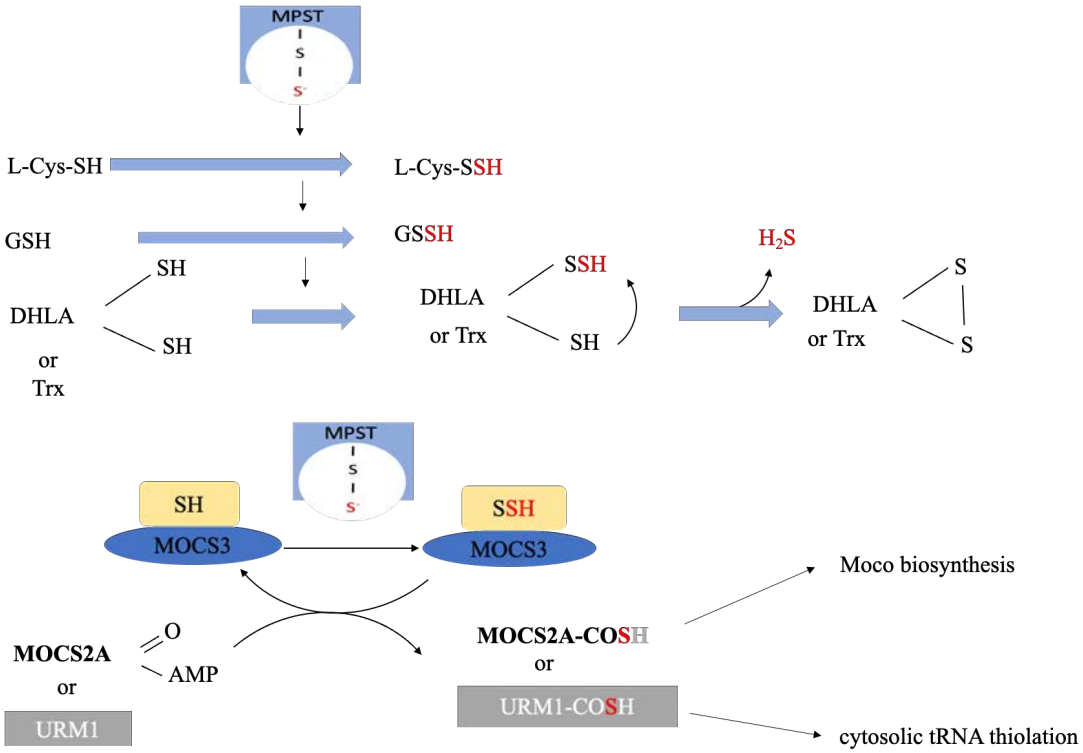

Figure 10: Sulfur transfer from MPST to thiol molecules and proteins. MPST transfers protein to thiol-containing molecules like L-cysteine, glutathione and dihydrolipoic acid (DHLA). Thiol-containing protein MOCS3 transfers its sulfur to URM1 or MOCS2A from a thiocaboxylate (COSH) which are essential for cytosolic tRNA thiolation and Moco biosynthesis in human. Additionally, thioredoxin and DHLA produce H_2S by the rapid attack of the persulfide bond by nearby thiol.

1.1.7 Interaction partners of TUM1

TUM1 has two distinct isoforms which have different localisation. TUM1-Iso1 localises solely in the cytosol, while TUM1-Iso2 localises in the cytosol and mitochondria. The difference in their sequence is the 20 amino acids capping the mitochondria targeting sequence in TUM1-Iso1. Interaction studies have shown that TUM1 interacts with NFS1, MOCS3, and MTU1 (Fräsdorf *et al.*, 2014). However, the interaction partners of the two isoforms were different. In the cytosol, the TUM1-Iso1 interacted with NFS1 and MOCS3, while the TUM1 Iso2 interacted with only MOCS3, not NFS1(Fräsdorf *et al.*, 2014). In the mitochondria, TUM1 Iso2 interacted with NFS1 and MTU1. NFS1 and MOCS3 share a dual role in the sulfur transfer for the cytosolic tRNA thiolation and Moco biosynthesis (Leimkühler *et al.*, 2017). This interaction implicates TUM1 in the sulfur transfer for these critical pathways in humans. The interaction of TUM1 Iso2 with NFS1 and MTU1 also suggests a role as sulfurtransferase for taurine modification in the mitochondria.

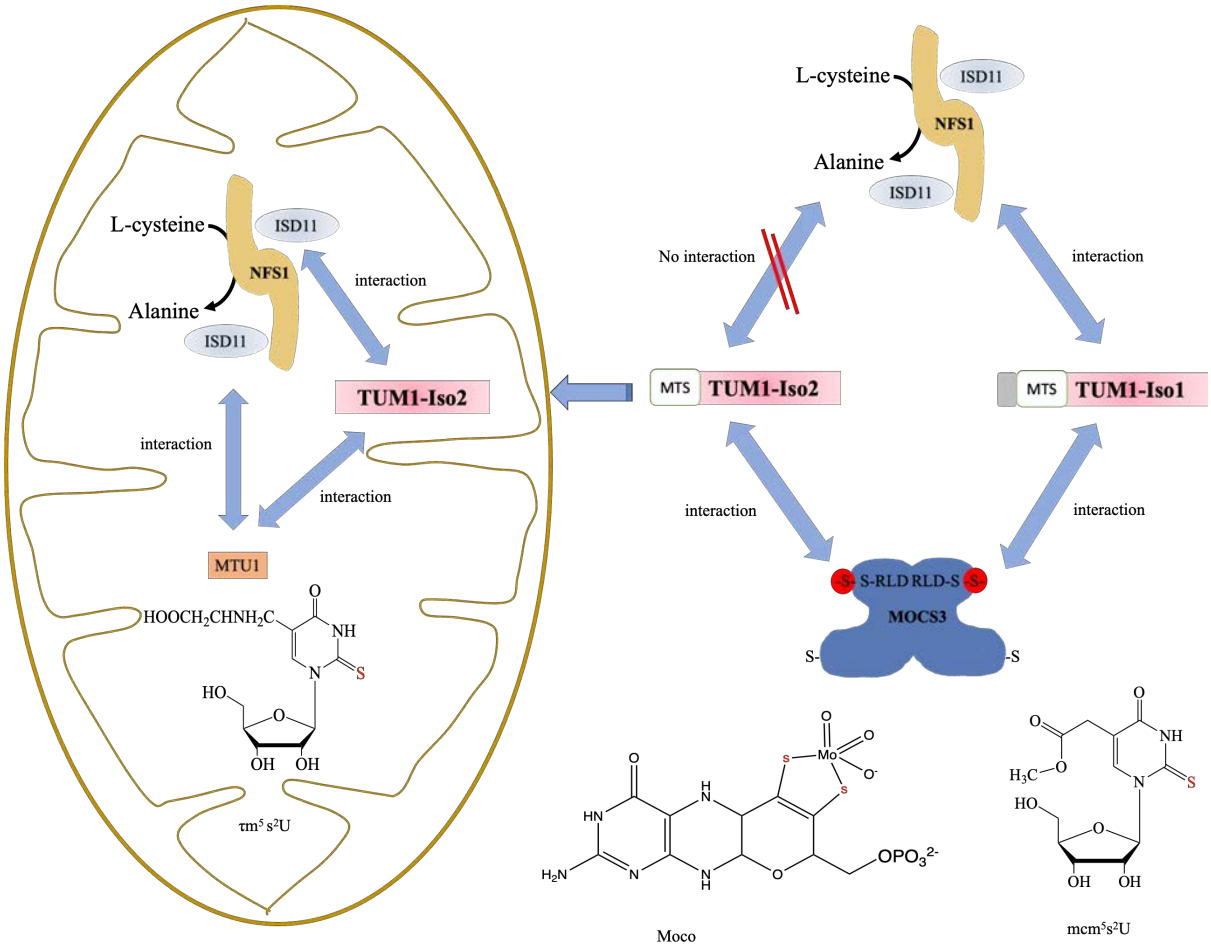

Figure 11: Interaction partners of TUM1 isoforms. TUM1 has two isoforms: TUM1 Iso1 localising in the cytosol, interacting with NFS1 and MOCS3. TUM1 Iso2 localizes both in the cytosol and mitochondria. It interacts with NFS1 and MTU1 in the mitochondria, both only with MOCS3 in the cytosol.

1.1.8 The physiological relevance of TUM1

Human TUM1 is mainly expressed in the kidney, liver, heart and neurological cells (Taniguchi et al., 1974). Tissue-specific changes in MPST expression correlate with ageing and the development of metabolic disease. Recently, high expression of MPST has been reported in cancer tissues due to its H_2S biosynthesis capability and subsequent influence on the cellular bioenergetics (Bronowicka-Adamska *et al.*, 2017; Ramasamy *et al.*, 2006; Zuhra *et al.*, 2019). Deletion and overexpression experiments suggested that MPST contributes to oxidative stress resistance, mitochondrial respiratory function and the regulation of fatty acid metabolism. Patients have been reported to accumulate 3-Mercaptolactate (3ML) in the urine. 3-mercaptopyruvate is converted to 3-ML due to the deficiency of TUM1, which converts the former to pyruvate (Crawhall *et al.*, 1968)(Hannestad *et al.*, 1981). Patients with

Mercaptolactate- cysteine disulfiduria (MCDU) have been shown to have mental retardation, while in some cases, mental retardation was not recorded. It has since been classified as a hereditary abnormality due to the detection of a high level of MCDU in the urine and deficiency in TUM1 in father and daughter (Niederwieser *et al.*, 1973)(Akahoshi *et al.*, 2017). While patients with TUM1 mutations display Mercaptolactate-cysteine disulfiduria (MCDU), an autosomal recessive disorder with elevated mercaptolactate urine levels (Hannestad *et al.*, 1981). MPST knockout mice showed increased anxiety-like behaviour. In addition, an investigation of MPST knockout mouse brains revealed a lack of cysteine-SSH and GSSH production with 50% decreased levels of total persulfate species (Kimura *et al.*, 2012).

1.2 Sulfur transfer for tRNA modifications in eukaryotes

Across the kingdom of life, accurate and efficient gene translation into proteins is vital. tRNA molecules function as translation machinery and the transport of amino acids to the ribosomes. This ensures the translation of the genetic information of mRNA into amino acids that form a protein (Hoagland *et al.*, 1958). Protein synthesis takes place both in the cytoplasm and mitochondria. In the cytoplasm, proteins are synthesized from cytosolic tRNA molecules encoded by different tRNA genes (Chan *et al.*, 2016). Protein synthesis is essential in the mitochondria for the oxidative phosphorylation complex proteins transcribed from about 22 tRNAs (Chujo *et al.*, 2021). For proper functionality of tRNA molecules, they require cleavage and chemical modifications (Shigi, 2021). These modifications on tRNAs are essential for appropriate codon recognition and stability regulation (Shigi, 2014). The wobble uridine at position 34 (U_{34}) is shared across living organisms. In eukaryotes, sulfur modifications at different positions around their anticodons are essential for an accurate codon recognition (Yokoyama *et al.*, 1985). Generally, uridines are flexible and weakly bind with nucleosides in close proximity (Schaffrath *et al.*, 2017). This is due to the relative flexibility of the C2'-endoform adopted by the 5'modification (xm5) (Sierzputowska-Gracz *et al.*, 1987; Agris *et al.*, 1992). The thio-modification of tRNA favours the C3'-endoform, which is more rigid than the C2'-endoform (Figure 12). The C3'-endoform is hydrophobic, restricted and well-suited for anticodon base piling, stabilising the anticodon stem loop (ASL) for interaction with A in the codon (Sierzputowska-Gracz *et al.*, 1987; Agris *et al.*, 1992). s^2U modification makes the ASL structure rigid, while the xm^5 modifications relax the conformation for interacting with G-ending codons. The N6-threonylcarbamoyladenosine (t^6A37) coordinates with U34

modification to position the ASL for proper binding to the mRNA codons (Schaffrath *et al.*, 2017).

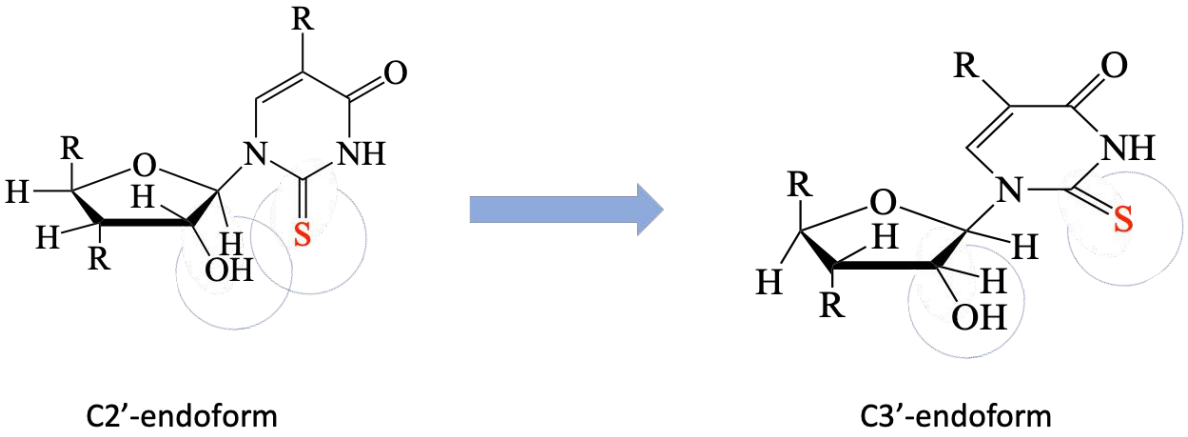

Figure 12: Thiomodification-dependent ribose conformational change. The combined effect of the 2-thiocarbonyl group and the 5-substituent, there is a conformational change from the less stable C2'-endo to the more stable C3'- endo form of the ribose ring. The mcm^{5}U, however, favours the C2'-endo. (Yokoyama *et al.*, 1985)

There are different types of sulfur modifications across the kingdom of life. For example, the sulfur modification of tRNA at the wobble Uridine-34 (34) of lysine, glutamine or glutamic acid is specifically reported to enhance codon and anticodon pairing and prevent frameshifting during the translation process (El Yacoubi *et al.*, 2012)(Umeda *et al.*, 2005). The s^{2}U modification is present in a wide range of organisms, from eukaryotes and bacteria. Most of the knowledge of the biosynthesis pathway of s^{2}U is from *S.cerevisiae* and *E.coli* (Zheng *et al.*, 2021). In *E.coli*, there are four different forms of tRNA thiolation: 4-thiouridine at position 8 (s^{4}U8), 2-thiocytidine at position 32 (s^{2}C32), 5-methylaminomethyl-2-thiouridine at position 34 (mnm^{5}s^{2}U34) and 2-methylthio-N6-Isopentyladenosine at position 37 (Shigi, 2014). In human, there are two important sulfur modifications; the 5methoxycarbonylmethyl-2-thiouridine (mcm^{5}s^{2}U34) in the cytosol and 5-taurinomethyl-2-thiouridine (τm^{5}s^{2}U34) in the mitochondria.

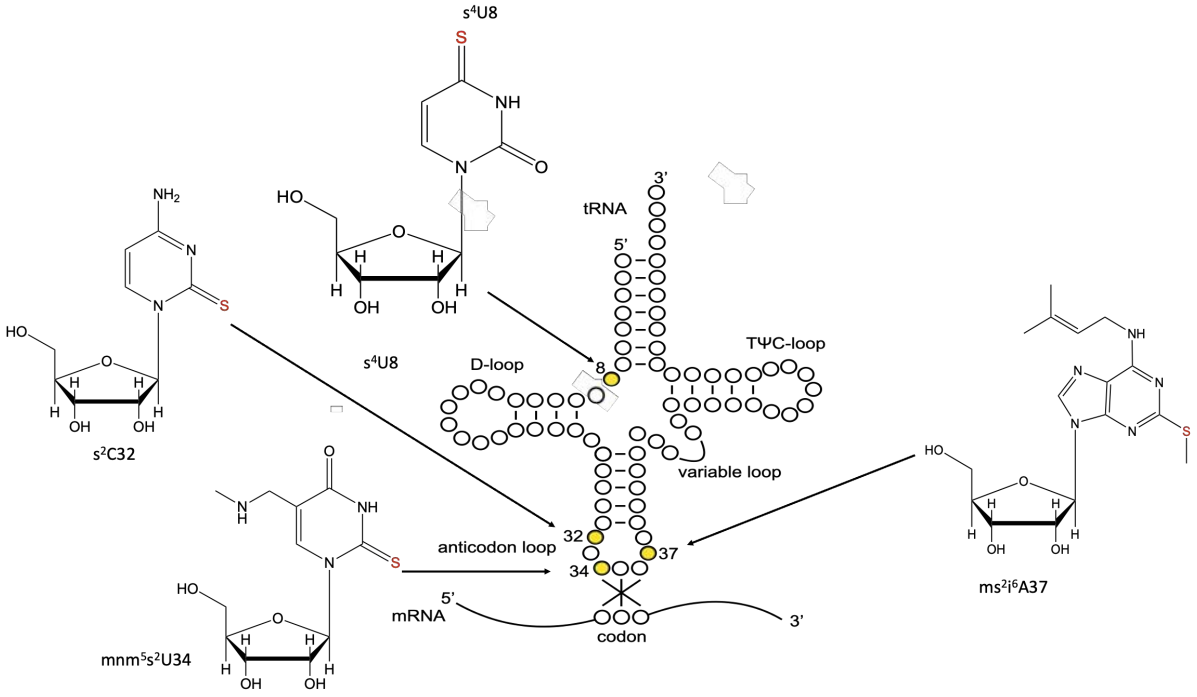

Figure 13: Structure and distribution of the different thio-nucleosides in eukaryotes. (A) E.coli: 4-thiouridine at position 8 (s^4U8), 2-thiocytidine at position 32 (s^2C32), 2-thiouridine at position 34 (mnm^5s^2U34), and 2-methylthio-N6-isopentenyladenosine at position 37 (ms^2i^6A37).

The modification at the wobble uridine requires two independent pathways—the URM1-dependent pathway to form the thiouridine. The second is the elongator complex-dependent pathway for synthesizing the xm^5U34 side chain (Schaffrath *et al.*, 2017). The insertion of sulfur into tRNA consists of highly conserved proteins. In humans, the proteins NFS1,MOCS2, TUM1, URM1, CTU1 and CTU2 are involved. The cytosolic tRNA in yeast is facilitated by Nfs1p, Tum1p, Urm1p, Ncs2p and Ncs6p.

1.2.1 URM1-dependent thiouridine formation in eukaryotes

The Ubiquitin-like protein (Ubl) URM1 serves as a protein modifier in a process called urmylation and as a sulfur transfer mediator (Nakai *et al.*, 2008). In humans, the N-terminus containing the E1 domain is activated by MOCS3. Its C-terminal contains a rhodanese homology domain (RHD) (Bordo *et al.*, 2002)(Hofmann *et al.*, 1998). The initial sulfur relay for URM1 originates from NFS1 using L-cysteine as a substrate. The sulfur is incorporated for 2-thiolation formation by interacting with the two CTU proteins in an ATP-dependent manner (Dewez *et al.*, 2008; Philipp *et al.*, 2014; Liu *et al.*, 2016)

1.2.2 Thiouridine modification in yeast

S. cerevisiae Tump1 and the human TUM1 have the same conserved catalytic loop and about 40 % amino acid sequence similarity. In *S.cerevisiae*, Tum1 is involved in the transfer of sulfur between Nfs1p and Uba4p homologues of human NFS1 and MOCS3 (Huang *et al.*, 2008)(Noma *et al.*, 2009). It has been shown that Tum1p is involved in efficient cytosolic tRNA thiolation in yeast (Noma *et al.*, 2009). For the mcm^5s^2U34 formation in *S. cerevisiae*, the Nfs1p catalyses the sulfur transfer to Tum1p and subsequently to the rhodanese domain on Uba4p (Noma *et al.*, 2009). As previously elucidated, rhodanese functions as a sulfur carrier and subsequent catalysis of transfer to acceptor protein. In the case of *S. cerevisiae*, the acceptor protein is the ubiquitin-related modifier (Urm1p) (Zheng *et al.*, 2021). Firstly, Urm1p is activated to an acyl adenylate intermediate (-COAMP) and subsequently thiocarboxylated by Uba4p at the C-terminal. Thiocarboxylated Urm1 interacts with Ncs2p and Ncs6p complex; this complex prepares the tRNA for final sulfur transfer from Urm1p to the tRNALys, tRNAGln, tRNAGlu.

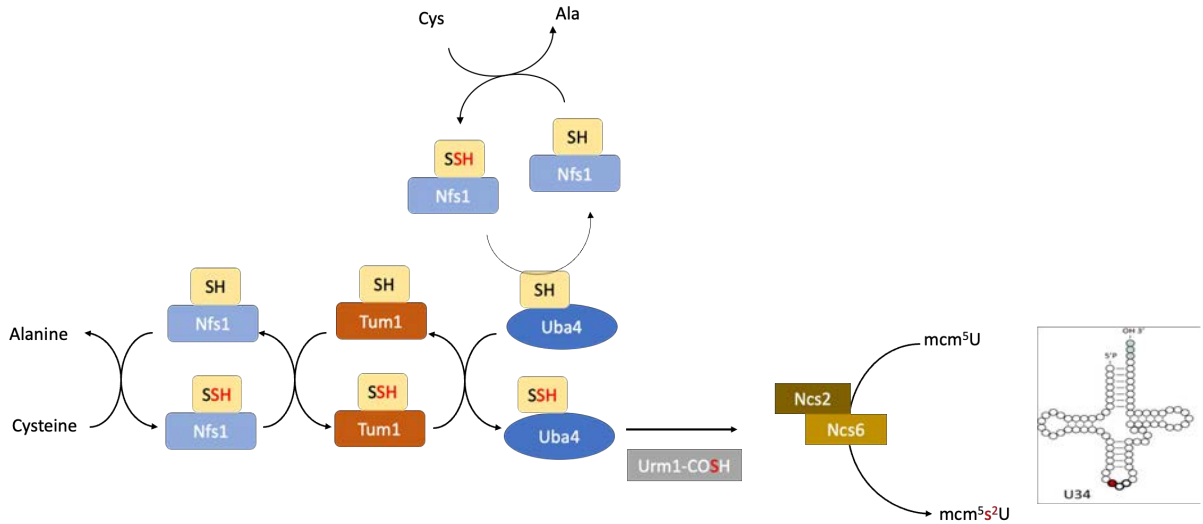

Figure 14: s^2U biosynthesis in *S.cerevisiae*. L-cysteine provides sulfur for Nfs1p, which is transferred to Tum1p (indirect) or Uba4p (direct and less efficient). Tum1p then transfers the sulfur to Uba4p, after which the persulfide is transferred to the C-terminal of Urm1p, forming a thiocarboxylate group. Ncs2p and Ncs6p catalyse the formation of s^2U in which the thiocarboxylate group of Urm1p serves as a substrate.

1.2.3 Thiouridine modification in human

Cytosolic tRNA thiolation

In human cytosol, the tRNA wobble bases for Glu, Gln and Lys are sulfurated to 5-methoxycarbonylmethyl-2-thiouridine (mcm^5s^2U34). The proteins responsible for sulfur modification of tRNA in the cytosol were reported to be NFS1, TUM1, MOCS3, URM1, CTU1 and CTU2 (Nakai *et al.*, 2007)(Schmitz *et al.*, 2008)(Leidel, Patrick G. A. Pedrioli, *et al.*, 2009)(Noma *et al.*, 2009)(Chowdhury *et al.*, 2012). The formation of the mcm^5s^2U modification in cytosol involves the biosynthesis of the side chain 5-methoxycarbonylmethyl-group by the elongator protein complex (ELP) and subsequent sulfur insertion (Leimkühler, 2017). In this pathway, the sulfur from NFS1 is efficiently transferred to MOCS3 in the presence of TUM1 (Fräsdorf *et al.*, 2014). MOCS3-bound persulfide is transferred to URM1, forming a thiocrboxylate group at the C-terminal glycine (Schmitz *et al.*, 2008). The sulfur C-terminus of URM1 is first adenylated, followed by the formation of the thiocarboxylate group. After that, URM1 interacts with the CTUCTU2 complex facilitating the final incorporation of sulfur into the U 34 in Lys, Gln and Glu tRNA after an adenylation step (Figure 15). For the biosynthesis of the mcm5-group, which is essential for an efficient translation (Johansson *et al.*, 2008), the ELP complex is required. The ELP complex comprises two copies of ELP1-ELP6 (Krogan *et al.*, 2001; Sebastiaan Winkler *et al.*, 2001; Dauden *et al.*, 2017). The ELP1-ELP3 forms a symmetrical homodimer complex and binds the heterotetrameric ring of ELP4-ELP6 (Glatt *et al.*, 2012; Lin *et al.*, 2012; Dauden *et al.*, 2017; Setiaputra *et al.*, 2017). All the units of the complex are essential for the biosynthesis of the mcm^5U-group, with ELP3 serving as the catalytic subunit (Butler *et al.*, 1994; Yajima *et al.*, 1997; Frohloff *et al.*, 2001; Huang *et al.*, 2005; Esberg *et al.*, 2006) (Figure 15).

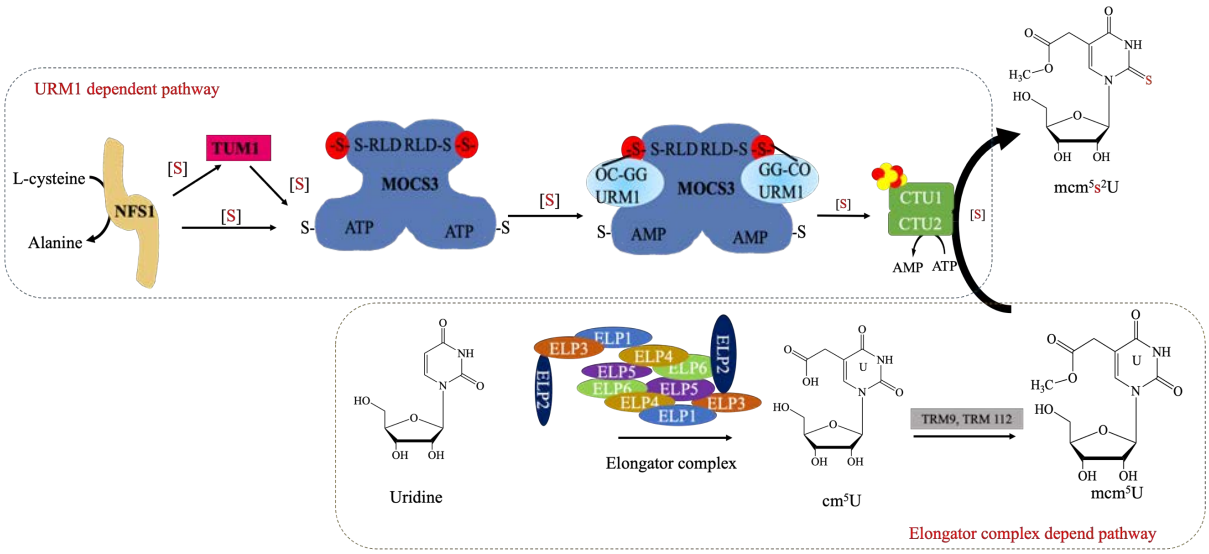

Figure 15: Biosynthesis of mcm^{5}s^{2}U in human cytosol. For the s^{2}U formation, the NFS1 mobilises sulfur from L-cysteine in the form of persulfide and is transferred to TUM1 (indirect) or the RLD of MOCS3 (direct and less efficient). URM1 is activated and forms an acyl-adenylated intermediate, followed by the transfer of persulfide sulfur from MOCS3, and thiocarboxylated URM1 is formed with the release of AMP. The sulfur of the URM1-COSH group is then moved to position 34 with the help of CTU1 and CTU2, consuming ATP of the tRNAs Lys, Glu and Gln (blue dots). The cm^{5}U is formed by the elongator complex, after which methyltransferase Trm9 and Trm 112 transfer the methyl group to form mcm^{5}U(yellow dots). The pathway for the formation of s^{2}U and mcm^{5}U occurs independently.

For the final sulfur insertion into the tRNA, CTU1 and CTU2 are involved. However, the mechanism of insertion still needs to be better understood in humans. CTU1 has three cysteine residues at positions 130, 133 and 222. This cysteine residue harbours the 3Fe-4S cluster (Liu *et al.*, 2016), which is implicated in the final sulfur transfer incorporation with the thiocarboxylate group formed by the ubiquitin-related modifier (URM1). Similar to the Thermus thermophilus TtuA, it is proposed that the Fe-S clusters on CTU1 binds the C-terminal of URM1 and subsequently adenylated. After that, it liberates the sulfur from URM1 via nucleophilic attack with a hydroxide ion with the charge donated by the Lys137 on the side chain. In the final step, the adenylated group of the tRNA is attacked and substituted by the sulfide bound to the Fe site leading to the release of the adenyl group and the incorporation of sulfur into the tRNA (Figure 16).

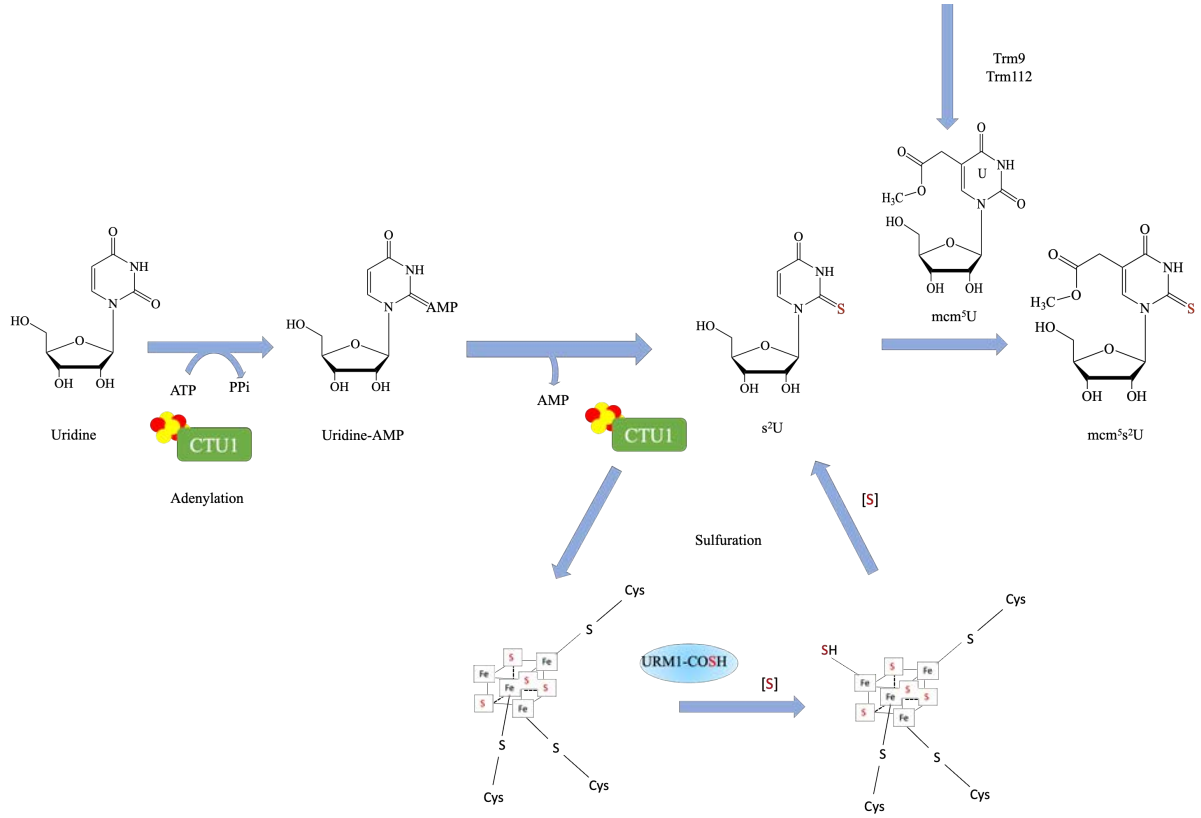

Figure 16: Proposed mechanism of sulfur transfer to tRNA from cytoplasmic tRNA 2-thiolation protein 1. CTU1 uses a Fe-S cluster to grasp the C-terminal of URM1, after adenylation the sulfur is released from URM1 through a nucleophilic attack with a hydroxide ion while making use of a charge on the side chain at Lys137. The unique Fe site-bound sulfide targets the adenylated tRNA and replaces the adenyl group.

Mitochondria tRNA thiolation

In humans, the mitochondrial tRNA-specific 2-thiouridylase 1 (MTU1) is involved in the thio-modification of 5-taurinomethyluridine (τm^5U) to 5-taurinomethyl-2-thiouridine (τm^5s^2U) of tRNAs of Gln, Glu and Lys. This is essential for the recognition of codons and accurate translation. The NFS1 is believed to transfer sulfur to the MTU1 for sulfur modification. However, interaction studies have recently shown an interaction between mitochondria-localized TUM-Iso2 and MTU1. This suggests a possible sulfur transfer from NFS1 to TUM1 Iso2 and MTU1. The mechanism of sulfur transfer from MTU1 to the tRNA, which leads to the formation of τm^5s^2U, is not well understood yet in humans. However, the L-cysteine desulfurase is believed to be the initial sulfur donor for the formation of τm^5s^2U. For the insertion of the taurine side group, the proteins mitochondrial tRNA translation optimisation 1 (MTO1) and the GTP binding protein 3 (GTPBP3) are involved (Umeda *et al.*, 2005). The proteins responsible for the formation of the taurine group are yet unknown (Fräsdorf *et al.*, 2014; Suzuki, 2005). MTU1 is homologous to the MnmA protein in *E.coli* (Shigi, 2014).

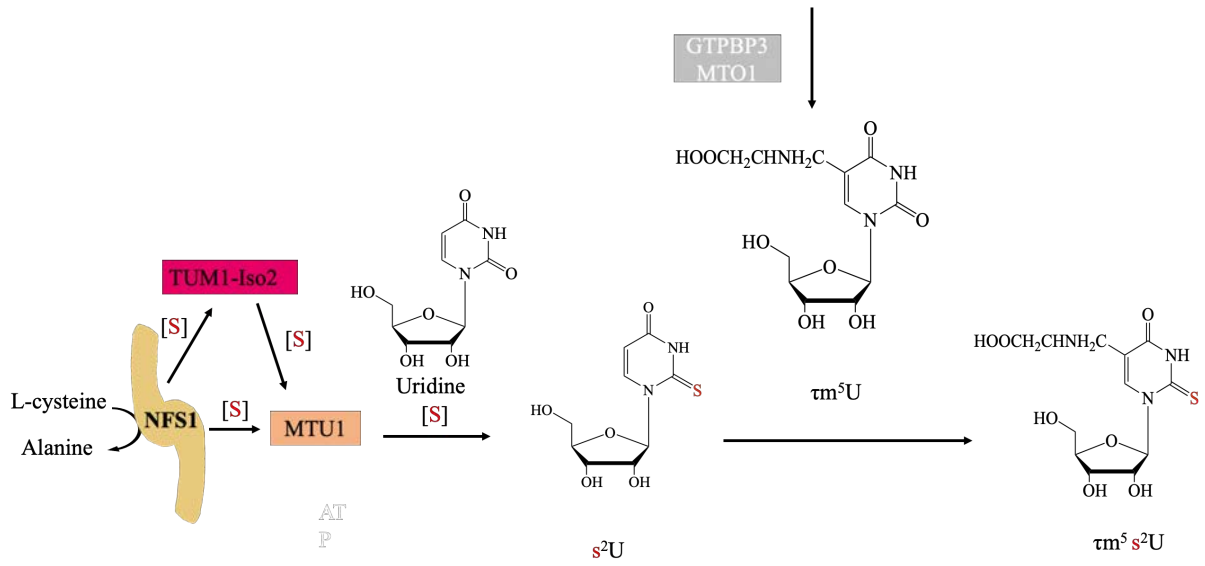

Figure 17: Proposed biosynthesis of τm^{5}s^{2}U in human mitochondria. For the formation of the s^{2}U, the sulfur is mobilised from L-cysteine by NFS1 and then transferred to TUM1-Iso2 (indirectly) or MTU1 (directly). The taurine side chain τm^{5}U, is synthesized by GTPBP3 and MTO1

The *E.coli* MnmA contains catalytic residues such as aspartic acid (Asp) 99, cysteine (Cys) 102, and Cys199. This differs from the conserved residue from other bacteria by replacing the aspartic acid with a cysteine residue. For the final transfer of sulfur to the tRNA in *E.coli*, MnmA binds to tRNA, thereby inducing a conformational change. This conformational change leads to the binding of the anticodon loop of the tRNA deeply in the MnmA active site. Different tRNAs are distinguished due to the Van der Waals interactions and hydrogen bond between the Uridine 34 and 35 with the catalytic centre of MnmA. The conserved PP-loop motif participates in the rotation of the carbon-2 in the Uridine 34, exposing it to the persulfurated Cysteine-199 of MnmA. A covalent bond is formed between MnmA and tRNA by a nucleophilic attack of persulfide sulfur on the carbon-2 U34. This is followed by another nucleophilic attack by the cysteine 102, leading to the liberation of AMP and the thiolated tRNA. MnmA is regenerated by the breakage of the disulfide bridge between cysteine 102 and 199, leading to reduction.

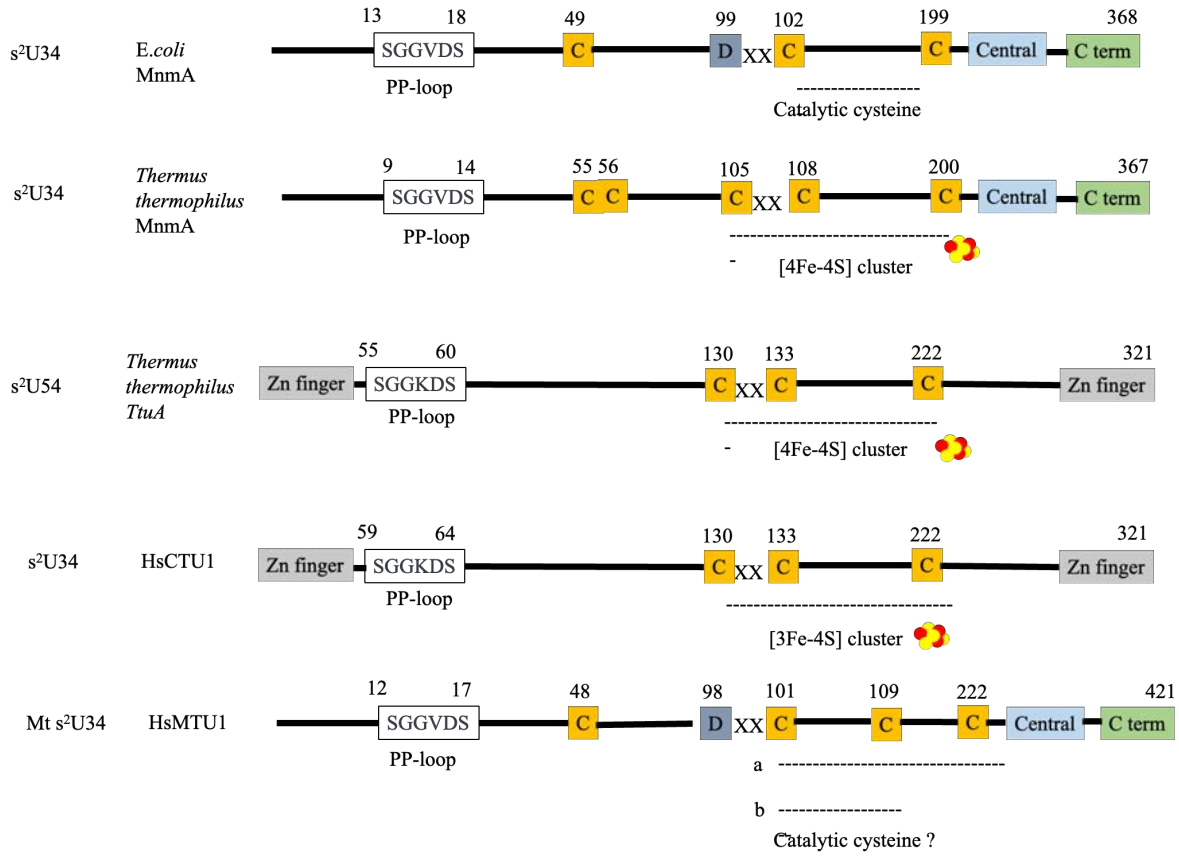

Figure 18: Schematic representation of catalytic motifs of eukaryotic thiouridylases. The amino acid sequence motif of the catalytic centre and PP-loop of *E.coli* MnmA (tRNA specific 2-thiouridylase), Thermus thermophilus MnmA, Thermus thermophilus TtuA (tRNA-5-methyluridine (54) 2-sulfurtransferase), Homo sapiens CTU1 (cytoplasmic tRNA 2-thiolation protein 1) and Homo sapiens MTU1 (mitochondrial tRNA- specific 2-thiouridylase 1) modification X represents any or alternative amino acid.

1.2.4 The physiological relevance of tRNA modifications

Over 150 types of RNA modifications are present in all kingdoms of life which about 80 % were found to be tRNA (Boccaletto *et al.*, 2022). These chemical modifications may range from methylation, sulfuration, hydroxylation and acetylation, amongst others (Suzuki, 2021). Hypo-modified tRNAs are eliminated in the process of tRNA maturation and are degraded by endonucleases through rapid tRNA decay (RTD) (Copela *et al.*, 2008; Dewe *et al.*, 2012; Alexandrov *et al.*, 2006; Kadaba *et al.*, 2004). Deficiency in taurine in animals has been reported to cause developmental defects, central retinal degradation, hepatitis lipidosis and dilated cardiomyopathy (Suzuki, 2021). These symptoms resemble human mitochondrial encephalomyopathies (Schaffer *et al.*, 2013). In the mitochondria, mutants lacking the τm^5s^2U were unable to optimally decode the AAA or AAG codons causing perturbation of

mitochondrial translation and respiration. Mutation in the MTU1 gene has been linked to the cause of infantile liver failure (Zeharia *et al.*, 2009). Myoclonic epilepsy with ragged red fibres (MERRF) like disorder has also been associated with a mutation in 8344A>G of mitochondrial $tRNA^{Lys}$ gene (Goto *et al.*, 1990). Hypertrophic cardiomyopathy and lactic acidosis were observed in humans with mutations in the MTO1 gene, catalyses the formation of τthe m^5U modification (Baruffini *et al.*, 2013; Ghezzi *et al.*, 2012). However, in mouse embryos, knockout of Mto1 caused death at the early stage of development. This demonstrates the essentiality of MTO in animal development. The abnormal splicing of ELP1 protein which is essential for mcm^5U34 formation is a cause of familial dysautonomia. In the cells of patients with familial dysautonomia, the levels of mcm^5U were observed to be reduced. A knockout of Elp1 in mice was similarly lethal owing to the perturbation of cardiovascular development and function (Chen *et al.*, 2009). Mutation of ELP2 and ELP3 causes intellectual disability and amyotrophic lateral sclerosis, respectively (Cohen *et al.*, 2015; Simpson *et al.*, 2009). The mutation of CTU2, which is essential for the formation of the URM1-dependent thiouridine formation, is also associated with intellectual disability (Shaheen *et al.*, 2016). Higher expression of ELP1 corresponding to a higher level of mcm^5s^2U modification was observed in drug-resistant melanomas. This upregulation was associated with promoting tumour growth due to the efficient translation of mRNA. Asides from tRNA thiolation, the TUM1 is linked to Moco biosynthesis in humans based on the interaction studies shown in previous studies (Fräsdorf *et al.*, 2014). It is widely essential for the functionality of many enzymes across the kingdom of life.

1.3 Sulfur transfer for Moco biosynthesis in humans

1.3.1 Moco biosynthesis in humans

The biosynthesis of Moco is highly conserved, comprising four significant steps that are enzymatically catalysed (Leimkühler, 2017). The proteins involved in Moco biosynthesis are named the MOCS (molybdenum cofactor biosynthesis). The first step of the Moco biosynthesis occurs in the mitochondria starting from the conversion of Guanosine 5'-triphosphate (GTP) to cyclic pyranopterin monophosphate (cPMP) by MOCS1A and MOCS1B (Leimkühler, 2017). MOCS1A is a radical S-adenosyl methionine (SAM) enzyme containing two [4Fe-4S] clusters which act as the catalytic subunit of the complex while MOCS1B regulates it's function (Hänzelmann *et al.*, 2002). An intermediate substrate for MOCS1B 3', 8-cyclo-7,8-dihydro-GTP (3',8-cH_2GTP) is formed by MOCS1A leading to the formation of cPMP (Hover *et al.*,

2015). In the second step occurring in the cytosol, the intermediate product cPMP is exported from the mitochondria. The transport mechanism in humans is yet unknown; however, in plants, the inner mitochondrial membrane transporter 3 Atm3 is implicated in this transport process (Teschner *et al.*, 2012). Subsequently, after the export two sulfur atoms are inserted into cPMP, leading to molybdopterin (MPT) formation. The reaction leading to the formation of MPT is catalysed by MOCS2A and MOCS2B complex forming a hetero-tetrameric structure known as MPT synthase. The reaction leading to the formation of MPT is catalysed by MOCS2A and MOCS2B complex comprising a hetero-tetrameric structure known as MPT synthase. This complex consists of two smaller subunits, MOC2A carrying the sulfur in the form of thio-carboxylate which is subsequently transferred to cPMP, and two larger subunits of MOCS2B mediating the oligomerisation (Gutzke *et al.*, 2001)(Matthies *et al.*, 2004). The thiocaboxylate is formed on MOCS2A by MOCS3, the sulfur atoms originate from the L-cysteine desulfurase before being relayed directly to MOCS3 or, more efficiently through TUM1 before subsequent transfer to MOCS3 (Figure 19).

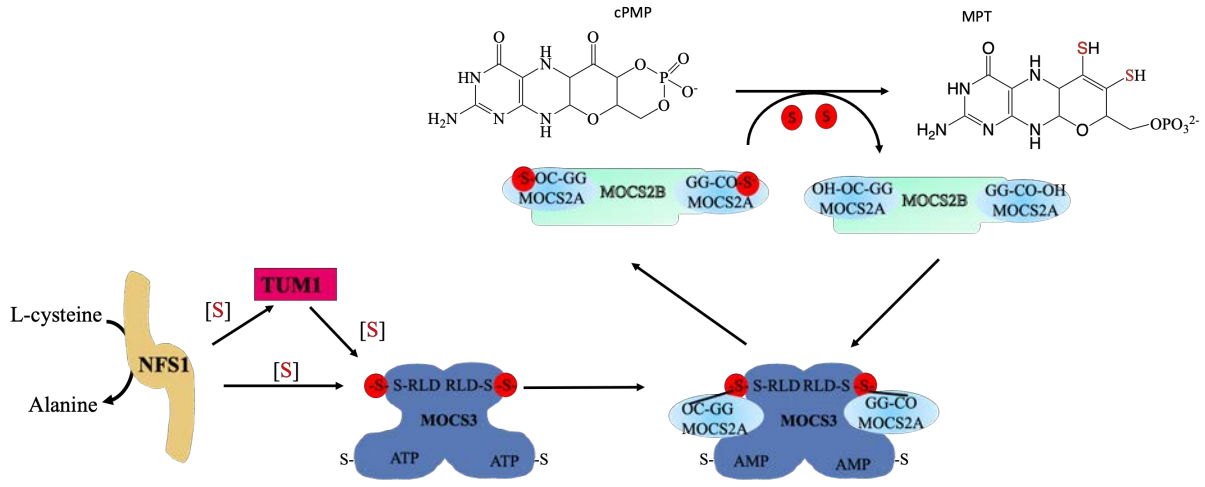

Figure 19: Sulfuration of cPMP for the formation of Molybdopterin ring. In the second phase of Moco biosynthesis, two sulfur atoms are incorporated into cPMP to form MPT. L-cysteine desulfurase serves as the sulfur donor for this sulfur transfer relay. The sulfur is transferred efficiently in the presence of TUM1 to MOCS3 in the cytosol. MOCS3 delivers the sulfur to MOCS2A, where a thio-carboxylate group is formed, activating MOCS2A through adenylation. A complex formed by MOCS2A and MOCS2B incorporated the sulfur into cPMP.

The penultimate and the last steps of Moco biosynthesis involve the insertion of molybdate by gephyrin. Gephyrin contains an N-terminal G-domain and a C-terminal E-domain. These

domains catalyses different reactions in the final step of the Moco biosynthesis (Schwarz *et al.*, 2006). First, in an ATP and Mg2+-dependent reaction, the G-domain attaches to MPT generating an MPT-AMP complex—the MPT-AMP complex is transferred to the E domain. Here, the complex is hydrolysed, and the AMP is detached following the insertion of Mo. This leads to the formation of di-oxo Moco, which is readily inserted into SO and mARC. However, Moco sulfurase (MOCOS) requires further sulfuration step for XOR and AO. (Amrani *et al.*, 2000)(Bittner *et al.*, 2001)

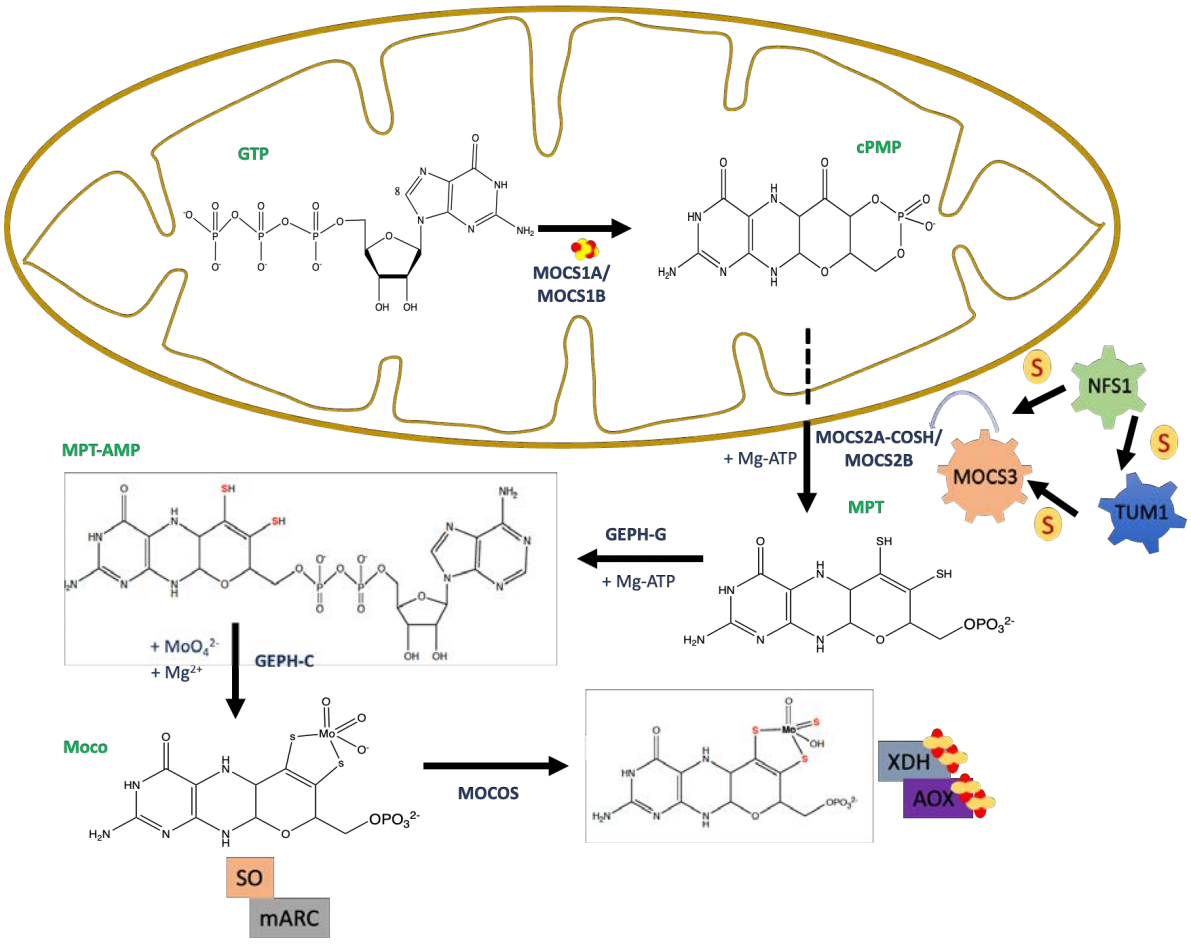

Figure 20: Biosynthetic pathway of the Moco in humans. In the first step, 5'GTP is converted to cPMP by the MOCS1 proteins. This is followed by the export of cPMP into the cytosol. cPMP is converted to MPT by the incorporation of 2 sulfur atoms. The sulfur is provided by the L-cysteine desulfurase NFS1 and transferred onto TUM1 (indirect) or the rhodanese-like domain of MOCS3 (direct and less efficient). After that, the sulfur is further transferred to MOCS2A, which forms a complex with MOCS2B enabling the incorporation. Finally, Gephyrin converts MPT to the Moco by the insertion of molybdate. The Moco is then incorporated into sulfite oxidase and mARC or further sulfuration by Moco sulfurase for xanthine dehydrogenase and aldehyde oxidase.

1.3.2 Molybdoenzymes in humans

Molybdoenzymes are enzyme classes that have molybdenum coordinated at their active site. They are several molybdoenzymes in prokaryotes and eukaryotes. There are three classes of molybdoenzmes; sulfite oxidase (SO), Xanthine oxidase (XO) and the dimethyl sulfoxide (DMSO) reductase family. The two classes present in humans are the SO and XO families. In humans, there are four different types of molybdoenzymes; sulfite oxidase (SO), mitochondria amidoxime compound 1 & 2 (mARC), aldehyde oxidase (AO) and xanthine oxidoreductase.
SO is the most essential and abundant molybdoenzyme in humans (Zhang *et al.*, 2008). SO catalyses the detoxification of sulfite to sulfate in humans (Johnson-Winters *et al.*, 2010). SO harbours its Moco with a conserved cysteine in the main domain. SO also contains a non-covalently bound cytochrome b5-type heme on its N-terminal domain (Mayr *et al.*, 2021). Sulfite oxidation occurs in the intermembrane space (IMS) of the mitochondria with the reduction of the physiological electron acceptor cytochrome c. SO is highly expressed in the liver, the leading site for methionine and cysteine catabolism. However, it is described in the kidney, heart and to some lower extent in the brain. Common expression protects the brain from sulfite toxification (Moriwaki *et al.*, 1997). SO is localised in the IMS as a soluble enzyme (Ito, 1971); it is synthesised in the cytosol and imported into the mitochondria. However, in the absence of Moco, which is required to induce mitochondria trapping and retention, SO is localised in the cytosol (Klein *et al.*, 2012). The second mitochondria localised Molybdoenzyme mARC is involved in reducing and activating N-hydroxylation of pro-drugs. mARC1 and mARC2 were recently identified as having sequence similarities to the MOCS1 and MOCS2 genes, respectively (Gruenewald *et al.*, 2008).

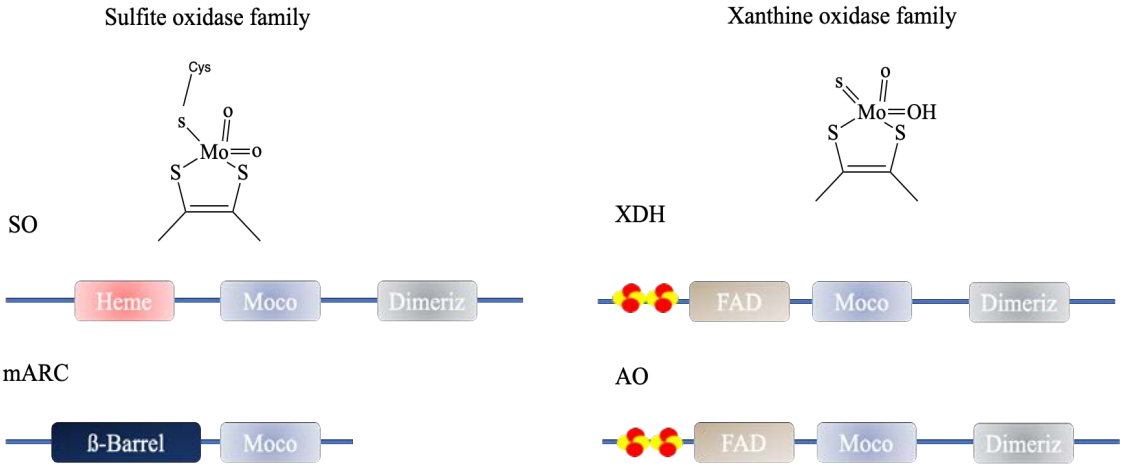

Figure 21: Classification of Molybdoenzymes in humans. The molybdenum centre of the sulfite oxidase family is bound to two oxide ligands and cysteine ligands. Sulfite oxidase and mARC are members of this class of molybdoenzyme. mARC contains only Moco as a cofactor

in contrast to sulfite oxidase, having heme as an additional cofactor. The XO and AO enzymes make up the Xanthine oxidase family. They require a second sulfuration process, resulting in the attachment of a third terminal sulfur ligand to the molybdenum centre. They also have 2 [2Fe-2S] and FAD as additional cofactors.

In humans, there are two cytosolic localised molybdoenzymes: AO and XO. Both enzymes are structurally and functionally similar. They anchor Moco at their C-terminal domains, which orchestrates their homodimerisation (Garattini *et al.*, 2003). In contrast to SO and mARC, AO and XO contains a third terminal sulfide group instead of the protein-derived cysteine. The sulfur atom is attached to Moco by the Moco sulfurase (MOCOS) (Hille *et al.*, 2011). There is biochemical evidence of the human Moco sulfurase, although the loss of MOCOS resulted in Xanthinuria type II (Ichida *et al.*, 2001). However, most evidence is from the plant homologue ABA3. Invitro experiment using ABA3 reported sulfur transfer to Aldehyde oxidase (Schwarz, 2005). The N-terminus of ABA3 is similar to the L-cysteine desulfurases in bacteria. ABA3 desulfurates L-cysteine in a PLP-dependent manner and is subsequently transferred to the molybdenum centre. The C-terminal domain of ABA3 facilitates binding AO or XO to the trans-sulfurase domain of ABA3.

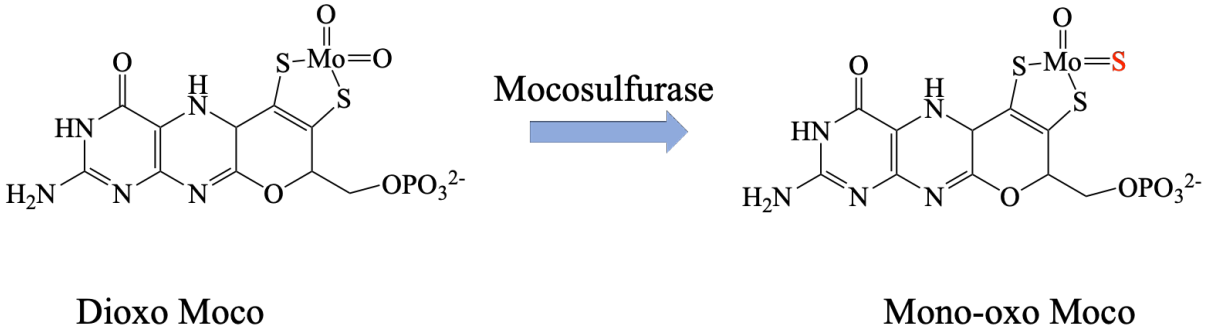

Figure 22: Sulfuration of Moco by Moco sulfurase. A sulfur atom replaces the oxygen atom being facilitated by Moco sulfurase. Moco sulfurase contains an L-cysteine desulfurase domain for the mobilisation of the sulfur atom incorporated into the dioxo Moco.

AO and XO contain [2Fe-2S] clusters in their N-terminal and a central FAD domain. AO catalyses a wide range of substrates, majorly the oxidation of aldehydes and, in part, hydroxylation of some heterocycles. XO can be found in two forms, xanthine oxidase (XO) and xanthine dehydrogenase. Xanthine dehydrogenase uses NAD+ as the primary electron acceptor, while Xanthine oxidase utilises O_2 (Ichida et al., 2012) both enzymes can catalyse

the conversion of xanthine to uric acid (Hille et al., 2011). XO catalyses the oxidation of hypoxanthine to xanthine and the transformation of xanthine to uric acid

1.3.3 Pathophysiological relevance of molybdoenzymes

Molybdoenzymes without their cofactor are inactive, disrupting their known function. Perturbation in the pathway that leads to Moco biosynthesis causes diseases termed molybdenum cofactor deficiency (MOCD) (Johnson *et al.*, 1980). Moco deficiency can be grouped into three types: A, B and C. Type A, B and C are caused by mutations in MOCS1, MOCS2/MOCS3 and gephyrin, respectively (Reiss *et al.*, 2011). The most common of the three types is type A. Treatment therapy for patients with MOCS1 mutation is available with the injection of cPMP, the first intermediate product of the Moco biosynthesis pathway (Veldman *et al.*, 2010). Deficiency in Moco enzymes has been linked to a wide range of disorders. They are usually marked by neurodegenerative diseases like mental retardation, microcephaly, dislocated ocular lenses, seizures and dysmorphic features (Tan *et al.*, 2005). Patients with this deficiency usually have early infancy mortality. Most symptoms are linked to SO disorders (Tan *et al.*, 2005), arising from sulfite accumulation in the liver, which eventually spreads to the brain. However, the mechanism by which the toxic level of sulfite causes neurological disorders is not well-understood. Sulfite is a potent nucleophile capable of disintegrating disulfide bonds and disrupting protein structures (Zhang *et al.*, 2004). The deficiency of uric acid usually clarifies Moco deficiency and SO deficiency since XOR leads to the accumulation of hypoxanthine and Xanthine. Sulfite also inhibits glutamate dehydrogenase leading to glutamate accumulation. Glutamate accumulation in the brain causes energy deficit and subsequently generates brain lesions (Zhang *et al.*, 2004).

Accumulation of sulfite also leads to the generation of a structural analogue of glutamate s-sulfocysteine, which is detrimental to the neuron (Olney *et al.*, 1975). Recently, the effect of Moco deficiency was alleviated by the suppression of CTH and CDO in *C.elegans* (Warnhoff *et al.*, 2019a). CTH catalyses cysteine formation from cystathionine and the forward production of hydrogen sulfide (Chiku *et al.*, 2009)(Figure 2). Increased production in H_2S could also add up to the sulfite pool in the cell. In close cooperation with SQR, a persulfidated sulfite is formed from the oxidation of H_2S, which is later converted to sulfite by thiosulfate sulfurtransferase (TST)/rhodanese (Paul *et al.*, 2021) (Figure 23 & 26).

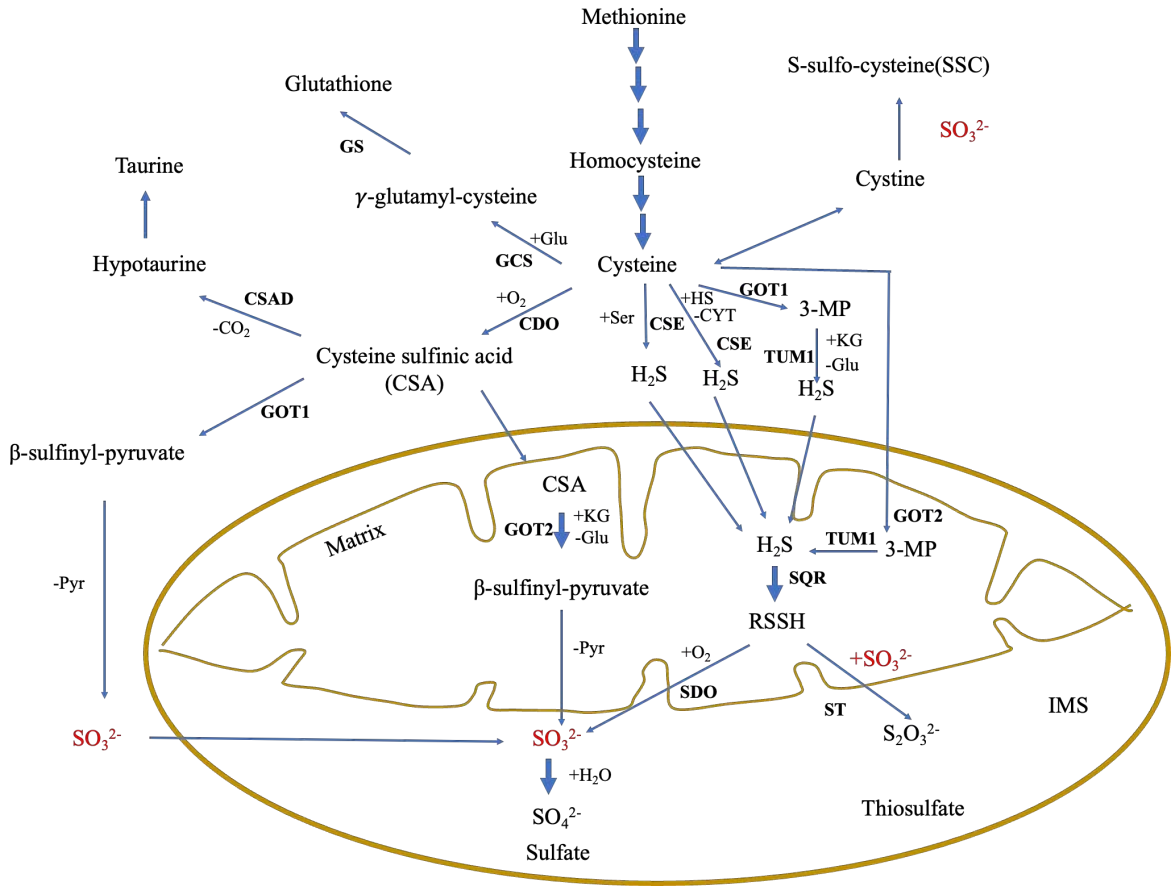

Figure 23: Interconnection between cysteine catabolism and sulfite production. Cysteine is derived from the transmethylation and transsulfuration pathway with methionine as substrate. Oxidative catabolism of cysteine produces taurine and sulfate as end-product. H_2S is the intermediate product of the non-oxidative path. H_2S is subsequently converted into sulfite and thiosulfate. The intermediate product of both pathways, sulfite, is converted to the non-toxic sulfate by sulfite oxidase in the IMS.

CSE, cystathionine γ-lyase; CBS, cystathionine β-synthase; CDO, cysteine dioxygenase; CSAD, cysteine sulfinate decarboxylase; GOT, glutamate oxaloacetate transaminase; SO, sulfite oxidase; MPST, 3-mercaptopyruvate sulfurtransferase; SQR, quinone oxidoreductase; SDO, sulfur dioxygenase; ST, sulfur transferase. GS, Glutathione synthetase. Adapted from (Kohl *et al.*, 2018) and Gunter schwarz metabolism revision

TUM1 is the main H_2S biosynthesis enzyme in the mitochondria. TUM1 can also produce H_2S and a disulfide in a process facilitated by dihydrolipoic acid (DHLA) or thioredoxin (Yadav *et al.*, 2013; Mikami *et al.*, 2011)

1.4 H_2S biosynthesis in humans

Hydrogen sulfide (H_2S), nitric oxide and carbon monoxide are the three crucial gasotransmitters recognised in humans (Kolluru *et al.*, 2017). Gasotransmitters are a subclass

of neurotransmitters which controls numerous cellular functions in an organism. Over the year, attention has been given to research on these three small molecules due to their up-downregulation in pathophysiological conditions (Fukuto *et al.*, 2012). H_2S can be toxic at high concentrations by inhibiting enzymes like cytochrome oxidase, carbonic anhydrase, and Na+/K+ ATPase. (Nicholson *et al.*, 1998; Reiffenstein *et al.*, 1992). H_2S has been implicated in pathophysiological and physiological in various organs (Abe *et al.*, 1996a; Geng *et al.*, 2004; Trédan *et al.*, 2007; Fu *et al.*, 2008; Wallace *et al.*, 2015; Distrutti *et al.*, 2006). The two enzymes CTH and CBS, which are essential in the transsulfuration pathway production of cysteine, can also catalyse the production of H_2S from the product cysteine. TUM1, in like manner, produces H_2S with the additional step of converting cysteine to 3-mercaptopyruvate in combination with Glutamate oxaloacetate transaminase 1 and 2 in the cytosol and mitochondria, respectively. However, under hypoxia, CBS and CTH translocate to the mitochondria when TUM1 is suppressed by the oxidative stress (Tay *et al.*, 2010). CBS is localized in the cytosol and widely expressed in different tissues (Enokido *et al.*, 2005). CBS is a pyridoxal phosphate-dependent (PLP) enzyme which contains a heme domain essential for interaction with the oxidative environment, thereby inducing an increased PLP reactivity. CBS produces H_2S from L-cysteine β-the replacement and the production of serine. In L-homocysteine presence, H_2S production increases by folds compared to L-cysteine alone (Singh *et al.*, 2009). CBS is the main H_2S enzyme in the central nervous system. It is expressed in the kidney, liver, uterus and other organs (Patel *et al.*, 2009). CTH utilises L-cysteine and L-homocysteine as substrates to produce hydrogen sulfide, pyruvate and ammonia through α-and β elimination (Chiku *et al.*, 2009).

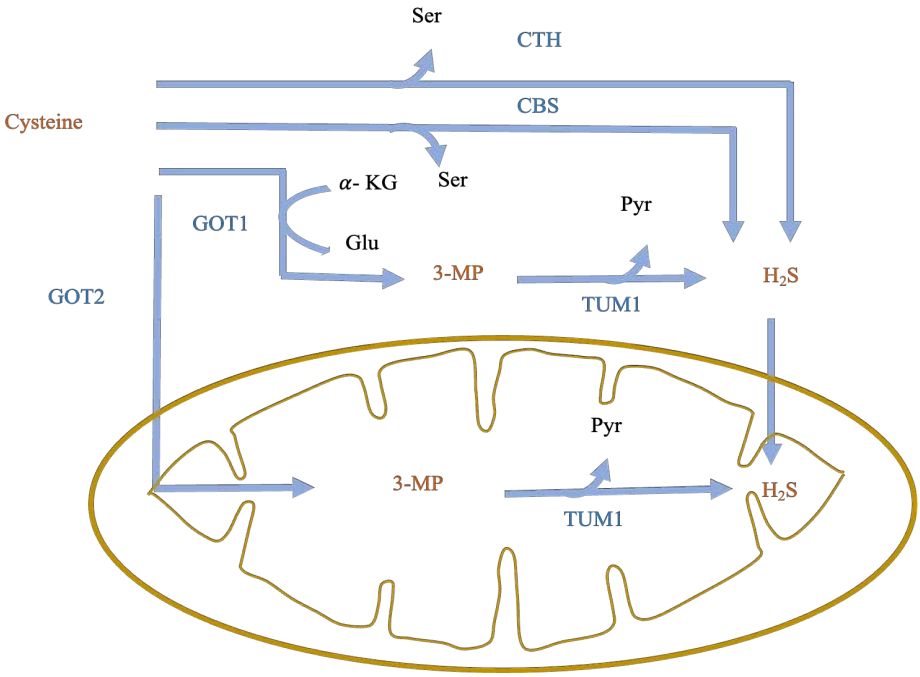

Figure 24: Biosynthetic pathway of hydrogen sulfide in humans. CSE and CBS utilise cysteine derived from the transsulfuration pathway to produce H_2S (Figure 2). TUM1 requires an additional step involving forming 3-MP by glutamate oxaloacetate transaminase (GOT) before the final release of H_2S, which can occur both in the cytosol and mitochondria.

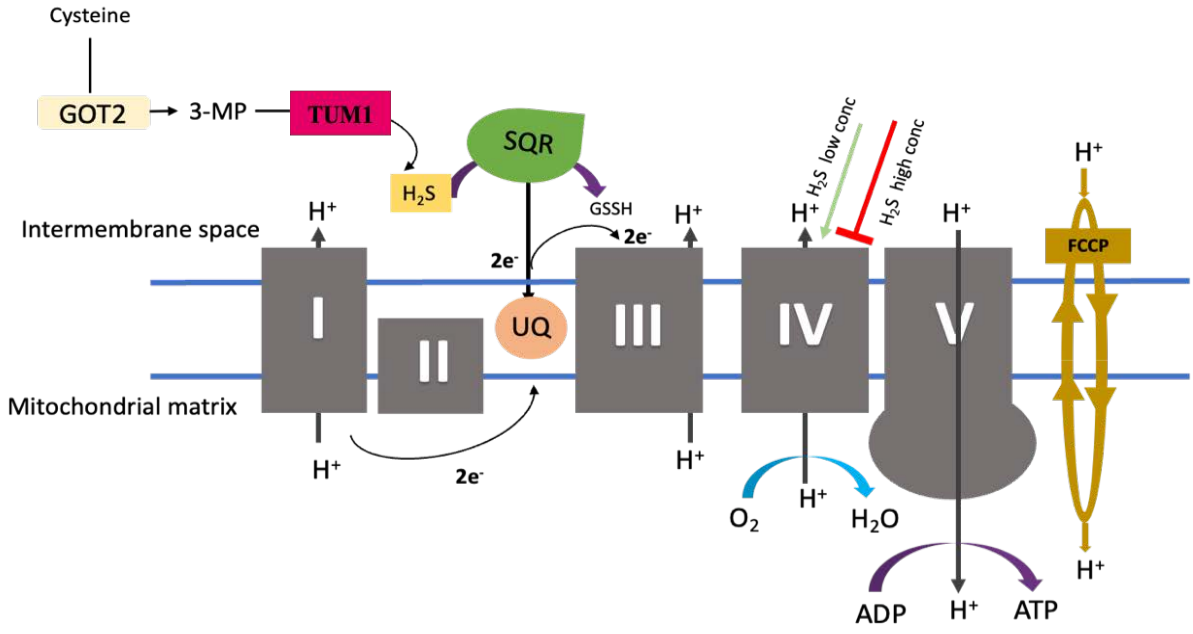

Figure 25: Stimulation of mitochondria bioenergetics by hydrogen sulfide. The ETC is made up of five complexes. Complexes I and II donate an electron to Coenzyme Q via the oxidation of NADH and succinate, respectively. These electrons are relayed to Complex III and subsequently to complex IV. The electron is finally transferred to oxygen; oxygen is

reduced to water, pumping electrons across the membrane. The force is utilised by the complex V to catalyse the formation of ATP from ADP.

H_2S produced in the vicinity of the mitochondria, usually by TUM1, stimulates the ETC by donating electrons to Coenzyme Q. The electron produced contributes to the electron transport chain's electron pump and promotes the mitochondria ATP generation Field (Szabo et al., 2014). The oxidation of H_2S facilitates this by Sulfide quinone oxidoreductase (SQR) Field (Abou-Hamdan et al., 2015). SQR oxidises two H_2S molecules, forming two disulfides and two electrons (Szabo et al., 2014).

1.4.1 H_2S metabolism in mitochondria

H_2S can also be oxidised to thiosulfate in the mitochondria through the enzyme sulfide quinone oxidoreductase (SQR). In this reaction, the persulfide is either on GSH or sulfite. However, studies have shown that sulfite is the more favoured substrate as the persulfide acceptor than GSH (Libiad *et al.*, 2014). The persulfidated glutathione formed is converted to thiosulfate by sulfur dioxygenase (SDO). Further, the persulfidated sulfite is converted to sulfite by rhodanese enzyme and, in the final step, to its non-toxic form, sulfate by sulfite oxidase in the intermembrane space of the mitochondria.

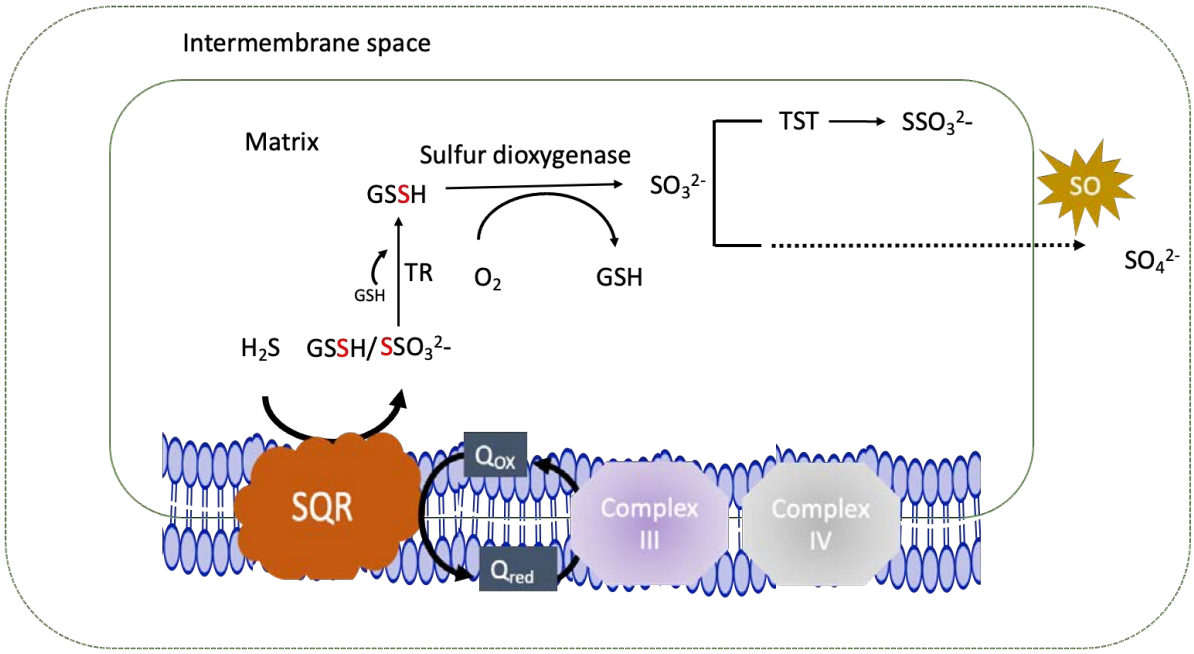

Figure 26: Oxidation of H_2S by sulfide quinone oxidoreductase in the mitochondria. SQR oxidises H_2S to GSSH and SSO_3^{2-} using GSH and sulfite as acceptors. SSO_3^{2-} is further

converted to GSSH by thiosulfate reductase. GSSH is converted to SO_3^{2-} by sulfur dioxygenase, which is finally converted to thiosulfate and sulfate by TST and SO, respectively.

1.5 Aims of this work

This research aimed to investigate the influence of TUM1 on the sulfur transfer for Moco biosynthesis, cytosolic tRNA and mitochondria bioenergetics in human embryonic kidney cells. The interaction of TUM1 with NFS1 and MOCS3 was previously confirmed (Fräsdorf *et al.*, 2014). In view of this, the following questions were addressed

I. Does *TUM1* deletion influence Moco biosynthesis?

The main goal is to investigate the level of Moco biosynthesis in *TUM1* knockout cells compared to the wild type. To achieve this, the level of Moco and accumulation of cPMP in the cells were quantified. Further, it was interesting to determine the activity and abundance of a vital molybdoenzyme.

II. Is cytosolic tRNA thiolation impaired in TUM1 absence?

It is of interest to know if the deletion of *TUM*1 affects the sulfur transfer for the cytosolic tRNA thiolation. The proposed reduction of mcm^5s^2U and accumulation of mcm^5U modifications were investigated to achieve this.

III. Is TUM1 an important H_2S enzyme in kidney cells, and does it link to the disruption of mitochondria bioenergetics?

The goal was to investigate the effect of TUM1 on the general H_2S metabolism and whether this affects mitochondria bioenergetics in human embryonic kidney cells.

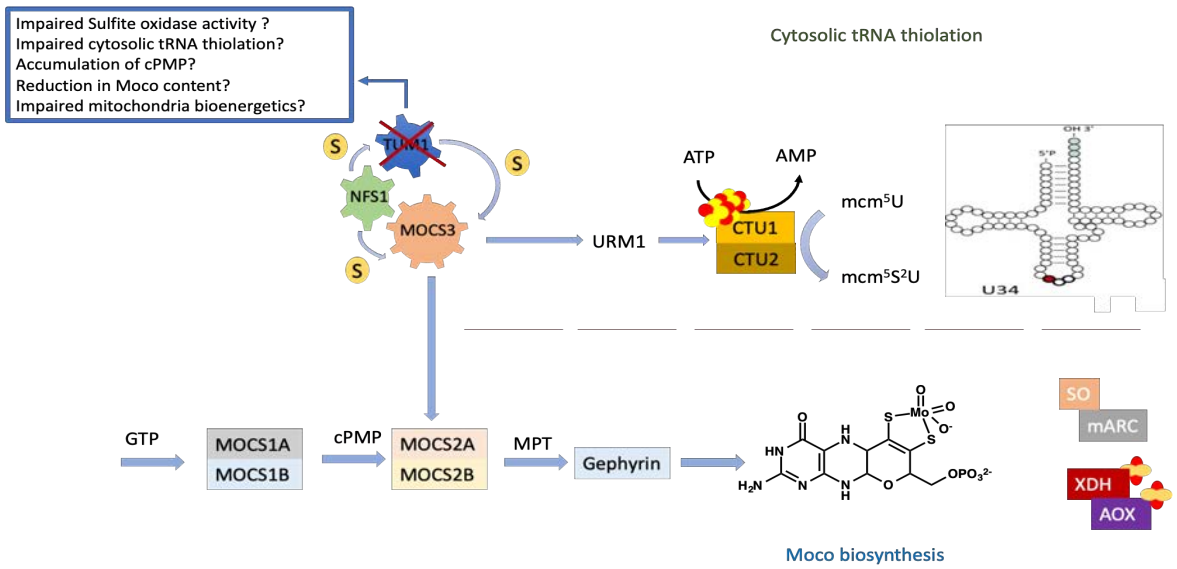

Figure 27: Overview of the research. Deletion of TUM1 in human embryonic kidney cells via CRISPR/Cas9. Investigation of the effect on Moco biosynthesis quantifying the cPMP and Moco content. Analysis of possible decrement in thiolation of tRNA. Further, the impact on H_2S biosynthesis linking to lower bioenergetics.

2 Overview of manuscripts

2.1 Overview manuscript I

The Human Mercaptopyruvate Sulfurtransferase TUM1 Is Involved in Moco Biosynthesis, Cytosolic tRNA Thiolation and Cellular Bioenergetics in Human Embryonic Kidney Cells.

Moses Olalekan Ogunkola [1],Gaelle Guiraudie-Capraz [2], and Francois Feron [2] Silke Leimkühler[1,*]

Biomolecules 2023, 13(1), 144; https://doi.org/10.3390/biom13010144

The first part of this thesis focused on the role of TUM1, a sulfurtransferase in humans, on tRNA thiolation, Moco biosynthesis and H_2S metabolism. TUM1 has previously been shown to interact with NFS1 and MOCS3 proteins involved in sulfur transfer for two pathways; the cytosolic tRNA thiolation and Moco biosynthesis (Fräsdorf *et al.*, 2014). Data from *S.cerevisiae* have already shown that Tum1p, the yeast homologue for TUM1, is involved in efficient sulfur transfer for cytosolic tRNA thiolation in yeast (Noma *et al.*, 2009a). However, the proteins necessary for Moco biosynthesis are absent in yeast. Therefore, the role of the human TUM1 on cytosolic tRNA thiolation was investigated.

On the other hand, the involvement of TUM1 on sulfur transfer for Moco biosynthesis was also investigated due to the prior interaction studies.

Further, its role in maintaining mitochondrial bioenergetics was investigated due to the capability of producing H_2S. H_2S serves as an electron donor for the mitochondrial respiratory chain via sulfide quinone oxidoreductase, stimulating the ETC at low concentrations. To address these questions, previously generated Human Embryonic kidney *TUM1* KO cells using CRISPR/Cas9 were investigated.

Research questions

Is TUM1 involved in the sulfur transfer cascade for cytosolic tRNA thiolation?

Is TUM1 involved in sulfur transfer for the Moco biosynthesis?

Does exogenous NaHS treatment complement the effect of TUM1's deletion on the pathways mentioned above?

Does TUM1 deficiency affect mitochondria bioenergetics?

2.2 Overview of manuscript II

Sulfur transferases in the pathways of molybdenum cofactor biosynthesis and tRNA thiolation in humans

Silke Leimkühler* and Moses Olalekan Ogunkola.

The second part is an overall review of the Sulfurtransferases in the pathways of molybdenum cofactor biosynthesis and tRNA thiolation in humans. This review discusses the sulfurtrasferases involved in cytosolic tRNA thiolation in humans. The role of the proteins NFS1, MOCS3, TUM1, URM1 CTU1 and MTU1 in sulfur transfer for the tRNA thiolation in the cytosol and mitochondria are presented. Further, the role and mechanism of sulfur transfer for Moco biosynthesis in humans are summarized.

2.3 Overview of manuscript III

Eprenetapopt triggers ferroptosis, inhibits NFS1 cysteine desulfurase and synergises with serine and glycine dietary restriction.

Kenji M. Fujihara, Bonnie Z. Zhang, Thomas D. Jackson, Moses O. Ogunkola, Brunda Nijagal, Julia V. Milne David A. Sallman, Ching-Seng Ang, Iva Nikolic, and Nicholas J. Clemons

Science advances 2022, 8 (37), DOI: 10.1126/sci-adv.abm9427

In the third aspect of the thesis, a collaborative work to investigate the effect of Eprenetapopt, an anticancer agent with active compound 2-methylene 3-quinuclidinone (MQ), on the activity of the sulfurtransferase in human L-cysteine desulfurase (NFS1) was done. NFS1 is the sulfur donor for ISC biogenesis, and MQ is known to bind to thiols like free cysteine, which is hypothesized to inhibit the activity of NFS1 Field (Fujihara et al., 2022). Prior proteomics data have shown that (Ferrodoxin) FDX1, which is essential for ISC biogenesis, was up-regulated (Fujihara et al., 2022).

Research questions (Contribution to the article)

Does MQ affect cell proliferation in human embryonic kidney cells?

Does MQ affect NFS1 activity?

Which type of inhibition does MQ pose?

Is persulfide formation on L-cysteine desulfurase affected?

Is the Fe-S cluster-dependent enzyme affected?

2.4 Contribution to the publications

My contributions to the accomplishment of the manuscripts discussed in this thesis are listed below in Table.

	Manuscript I	Manuscript II	Manuscript III
Conceptualization and experimentation	XX	N/A	X
investigation	XX	N/A	X
writing—original draft	XX	X	-
writing—review and editing	XX	X	X
software	XX	X	X

N/A – Not applicable

XX- Full contribution

X- Partial contribution

3 Discussion

Sulfur improves the efficiency of biomolecules in living organisms (Kessler, 2006). Numerous human macromolecules, including the Fe-S cluster, lipoic acid, biotin, Moco, and tRNA, have been found to include sulfur (Leimkühler *et al.*, 2017). In humans, several proteins are required for the trafficking of sulfur before final insertion into biomolecules. For sulfur to be integrated into biomolecules, it must first undergo reduction or activation (Kessler, 2006). L-cysteine is typically used as a key building component for adding sulfur to a variety of biomolecules (Hidese *et al.*, 2011). Sulfur carrier proteins provide sulfur from L-cysteine as a persulfide (Black *et al.*, 2015). The thiocarboxylate group is an alternative method of transferring sulfur (Hochstrasser, 2000). Ubiquitin-like proteins produce thiocarboxylate sulfur, which is transferred by thioester intermediates to sulfur acceptor proteins or the final biomolecule (Hochstrasser, 2000; Leidel, Patrick G. A. Pedrioli, *et al.*, 2009). L-cysteine desulfurases mobilises sulfur predominantly from L-cysteine and generates a protein-bound persulfide that can be transferred to acceptor proteins (Black *et al.*, 2015; Cupp-Vickery *et al.*, 2003; Zheng *et al.*, 1993). They use L-cysteine as a substrate and create a persulfide on a conserved cysteine residue that can be transported to acceptor proteins through transpersulfidation. Molybdenum cofactor biosynthesis, the formation of s^2U-modified nucleosides in tRNAs, and the synthesis of thiamine all occur through pathways that combine both the transpersulfidation of sulfur mobilised by L-cysteine desulfurases and the thiocarboxylate formation by ubiquitin-like proteins with thioester intermediates (Leimkühler *et al.*, 2017). Additionally, the sulfur can be transferred to rhodanese-like proteins in the form of an enzyme-bound persulfide. The transfer of sulfane sulfur from a donor molecule to a thiophilic acceptor is catalysed by sulfurtransferases (Bordo *et al.*, 2002). In-vitro, rhodaneses (thiosulfate: cyanide sulfur transferases) can convert thiosulfate to cyanide (Bordo *et al.*, 2002). Similar reactions are catalysed by 3-mercaptopyruvate: cyanide sulfur transferases (MSTs, EC 2.8.1.2), which use 3-mercaptopyruvate as the sulfur donor (Kessler, 2006; Pedre *et al.*, 2021). Thiocarboxylation of sulfur carrier proteins can be the last step in the sulfur transfer to the thio-containing cofactors (Pedre *et al.*, 2021). Interaction studies have shown previously that TUM1 interacts with the sulfurtransferases NFS1 and MOCS3 (Fräsdorf *et al.*, 2014). This interaction suggests a sulfur relay between the three sulfurtransferases.

3.1 TUM1 is required for efficient cytosolic thiolation in HEK293T

Here, the effect of *TUM1* knockout on the 5-methoxycarbonylmethyl-2-thiouridine (mcm^5s^2U) modification was investigated. Thio-modification on tRNA at wobble U34 of lysine (UUU), glutamine(UUG), and glutamate (UUC) is essential for efficient translation, proper codon-anticodon pairing, and prevention of frameshifting (El Yacoubi *et al.*, 2012; Suzuki, 2005). Impairment of cytosolic tRNA thiolation in yeast was reported to cause hypersensitivity to higher temperatures and oxidative stress (Goehring *et al.*, 2003; Laxman *et al.*, 2013; Leidel, Patrick G.A. Pedrioli, *et al.*, 2009). For tRNA modification in eukaryotes, proteins which are highly conserved are involved (Suzuki, 2005). NFS1, TUM1, MOCS3, URM1, CTU1, and CTU2 are involved in cytosolic thiouridine modification in humans. TUM1 was not implicated in cytosolic tRNA thiolation until genetic investigations in *S. cerevisiae* (Noma *et al.*, 2009). The genetic investigation reported Nfs1p, Uba4p, Tum1p, Urm1, Ncs2, and Ncs6 in 2 thiouridine formation in *S.cerevisiae* (Noma *et al.*, 2009). Tum1p has about 60 % amino acid similarity with the human TUM1 protein (Fräsdorf *et al.*, 2014). Interaction studies have shown that TUM1 interacts with NFS1 and MOCS3 in the cytosol (Fräsdorf *et al.*, 2014). This implicates TUM1 in sulfur transfer for cytosolic tRNA thiolation (Fräsdorf *et al.*, 2014). As determined by FRET and split eGFP experiments, NFS1 was proposed as the sulfur donor for this thio-modification since it could interact with MOCS3 in the cytosol (Marelja *et al.*, 2008). Prior research has shown that the yeast homologue of MOCS3 (Uba4) and MOCS3 itself, together with URM1 and the yeast homologue of CTU1 (Ncs6), are both capable of forming 2-thiouridine in an in vitro system using isolated lysine tRNAs (Chowdhury *et al.*, 2012; Noma *et al.*, 2009). Recent studies demonstrated the interaction of TUM1 with NFS1 and MOCS3 (Fräsdorf *et al.*, 2014). NFS1 is known to use L-cysteine as a substrate to produce protein-bound persulfide and alanine (Zheng *et al.*, 1994). The sulfur originating from NFS1 is directly incorporated into biomolecules like Fe-S (Nakai *et al.*, 2007), or transferred to other sulfurtransferases like TUM1 and MOCS3 before the final insertion of the sulfur into biomolecules like tRNA and Moco. In humans, MOCS3 is known to be involved in sulfur transfer for cytosolic tRNA thiolation (Neukranz *et al.*, 2019). In *MOCS3* deletion, mcm^5s^2U modification was undetectable, implying an abolishment of the s^2U formation at position 34 of tRNA Glu, Gln, and Lys (Neukranz *et al.*, 2019). Here, *TUM1* knockout cells exhibited decreased mcm^5s^2U thio-modification using HPLC analysis of nucleosides. In the wild-type cells, sulfur transfers from NFS1 to MOCS3 efficiently and further to URM1 to form mcm^5s^2U. In the absence of TUM1, there was no optimum transfer of sulfur from NFS1 to MOCS3 for

the thio-modification on tRNA hence the reduction in the level of mcm^{5}s^{2}U. In *S.cerevisiae*, a similar effect was reported in Tum1p deletion strains (Noma *et al.*, 2009). It was postulated from the results that Tum1p presence makes the sulfur transfer more efficient compared to a direct transfer from Nfs1p to Uba4p (Noma *et al.*, 2009). The report from the Tum1p is in line with the findings of this work. Further, invitro L-cysteine desulfurase activity has shown that four folds of TUM1 and MOCS3 doubled the sulfur release by NFS1 (Fräsdorf *et al.*, 2014). Bringing all these findings together, it can be suggested that TUM1 is involved for optimum sulfur transfer for cytosolic tRNA thiolation in humans.

TUM1 KO -/-

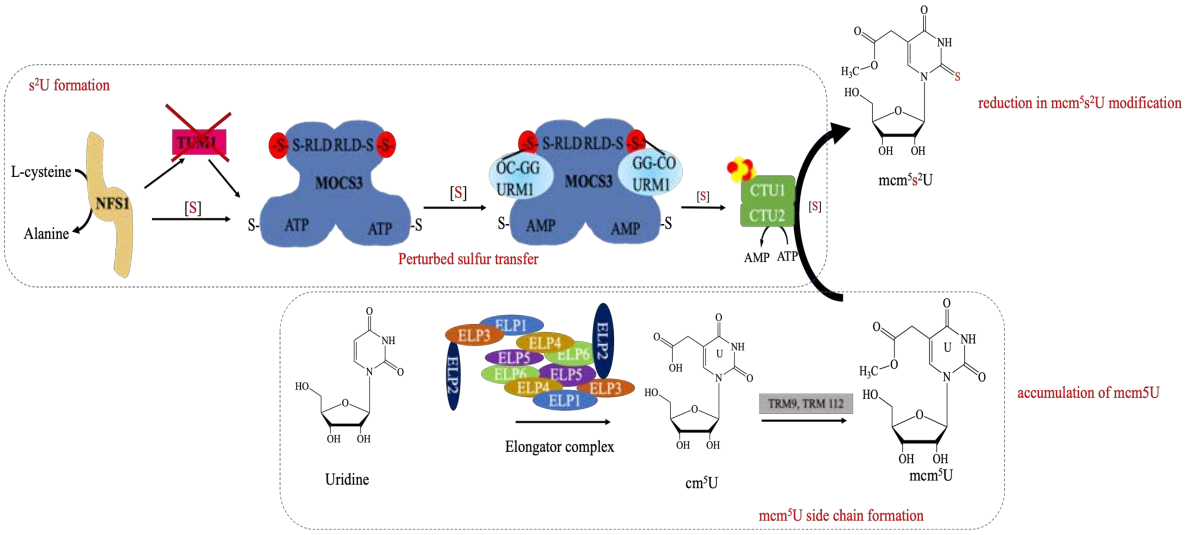

WT

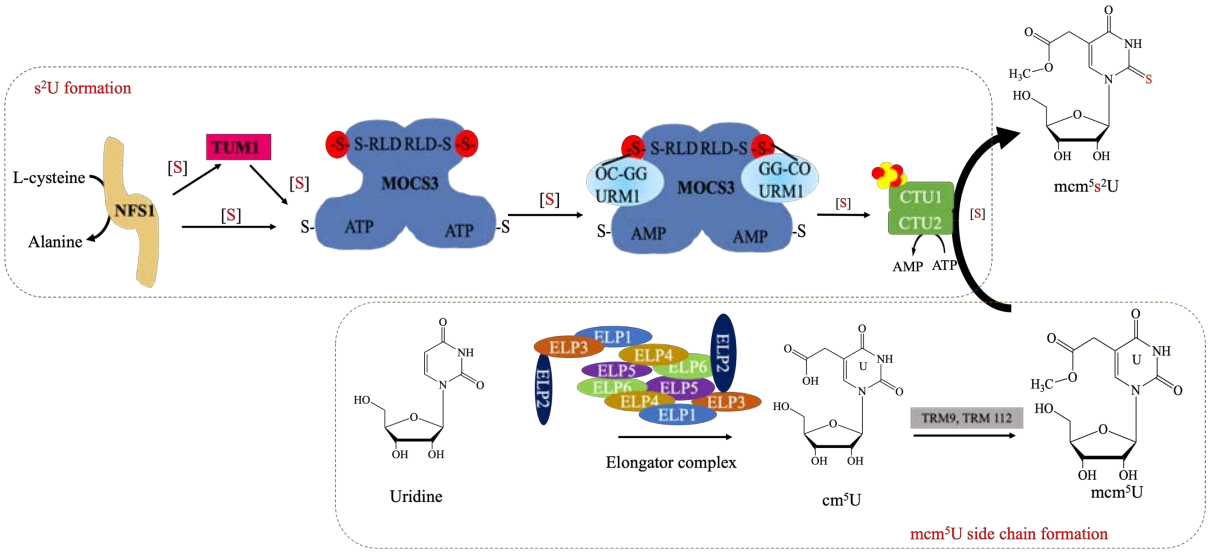

Figure 28: TUM1 is involved in efficient sulfur transfer for mcm^{5}s^{2}U thio-modification in the cytosol. In the *TUM1* knockout, L-cysteine desulfurase NFS1 distributes sulfur directly to the MOCS3 protein. However, there is perturbed persulfide transfer due to the absence of

TUM1. The persulfide is then transferred to URM1 by MOCS3, which activates URM1 through adenylation. After obtaining the sulfur, the CTU1/CTU2 incorporates it into the 2-thiouridine modification of the tRNA anticodon. The inefficient persulfide transfer reduces mcm^5s^2U and an accumulation of mcm^5U in *TUM1* knockout cells.

The elongator complex is the leading player in forming the mcm^5 side chain at the U34 (Schaffrath *et al.*, 2017). Additionally, the tRNA methyltransferase 9 and 112 are also crucial for the formation of the mcm^5U (Schaffrath *et al.*, 2017). Most studies that investigated the thio-modification levels using chemical stress did not separate the involvement of the s^2 and mcm^5 formation (Chan *et al.*, 2010; Chan *et al.*, 2015; Chan *et al.*, 2012).

The formation of the s^2U and xm5 in *E.coli* were found to be independent of each other. The formation of the mnm^5s^2U modification in E.*coli* is divided into two steps. The first is the formation of the s^2U by MnmA (Kambampati *et al.*, 2003; Ikeuchi *et al.*, 2006) in an ATP-dependent manner and the modification at the C5 which is formed by the MnmG, MnmE and MnmC (Armengod *et al.*, 2012; Moukadiri *et al.*, 2014). Previous research has reported mcm^5U modification accumulation in *MOCS3* knockout cells lacking the mcm^5s^2U modification (Neukranz *et al.*, 2019). Herein, *TUM1* knockout cells exhibited accumulation of mcm^5U. However, it was undetectable in the wild-type cells. This suggests that the majority of the mcm^5U synthesized were incorporated into s^2U for the formation of mcm^5s^2U, making the mcm^5U undetectable in the wild type. However, attempts to quantify the s^2U proves difficult as most of the s^2U were already incorporated for the formation of mcm^5s^2U. However, further analysis on the deletion of the elongator factors or the methyltransferase Trm9 and 112, which are responsible for the formation of the mcm^5U, would shed more light. In the *S.cerevisiae* Elp3 mutant, the s^2U modification was present, while the mcm^5U modification was undetectable (Huang *et al.*, 2005). These findings further buttress the hypothesis on the involvement of TUM1 in the s^2U formation in humans due to the accumulation of the mcm^5U.

3.2 TUM1 is involved in sulfur transfer for Moco biosynthesis.

TUM1 knockout cells were analysed to investigate the influence on Moco biosynthesis. The sulfur relay for forming the dithiolene group of Moco, the NFS1, MOCS3, and MOCS2A are previously believed to be involved. However, interaction studies by Fräsdorf and colleagues implicated the TUM1 protein in the sulfur relay due to its interaction with NFS1 and MOCS3 (Fräsdorf *et al.*, 2014). An invitro MPT production assay using purified proteins has shown that the interaction of NFS1 with either TUM1 Iso1 or Iso 2 increased the amount of MPT formed

compared to NFS1 alone (Fräsdorf *et al.*, 2014). Previously, cPMP accumulation and unquantifiable MPT were reported in *MOCS3* knockout (Neukranz *et al.*, 2019). Also, in-vitro studies demonstrated the alteration of the C-terminus of MOCS2A; the sulfur acceptor from MOCS3 affected the MPT production (Chowdhury *et al.*, 2012; Schmitz *et al.*, 2008b). cPMP is the first intermediate product of Moco biosynthesis. The formation of cPMP in the mitochondria involves the rearrangement of GTP by the catalytic activity of MOCS1A and MOCS2A (Schwarz, 2016). Subsequently, two sulfur atoms are inserted into cPMP, forming molybdopterin (MPT) (Leimkühler *et al.*, 2017). Using HPLC, the fluorescent derivatives of cPMP and MPT were quantified to analyse the effect of *TUM1* knockout on Moco biosynthesis for the first time. As expected, there was a reduction in MPT production in the absence of TUM1. Accumulation of cPMP was also observed, holding to the impairment in the MPT formation. These results confirm the involvement of TUM1 in sulfur transfer for the formation of Moco in humans. Past studies in the lab have reported that the absence of MOCS3 resulted in the accumulation of cPMP and the total abolishment of the MPT production (Neukranz *et al.*, 2019). Mutation in the gene that leads to Moco biosynthesis (MoCD) has been characterised by the loss of all molybdoenzymes. Patients have symptoms like mental retardation, epileptic seizures, brain atrophy, and dislocated ocular lenses (Schwarz 2016). Moco deficiency in most patients has been described by MOCS1, MOCS2 or GEPH (Reiss *et al.*, 2011)

Moco is an essential cofactor in humans' four known molybdoenzymes: sulfite oxidase, mitochondrial amidoxime reducing compounds 1&2, Aldehyde oxidase, and Xanthine oxidoreductase. Recently, the deletion of the *MOCS3* gene was reported to affect the activity of sulfite oxidase (Neukranz *et al.*, 2019), a molybdoenzyme responsible for detoxifying sulfite to its non-toxic metabolite sulfate (Cohen *et al.*, 1971). Accumulated sulfite can spread through the plasma membrane to other body parts. This results in reduced disulfide bridges vital for protein folding, stability and activity (Schwarz, 2016). Isolated SO deficiency caused by the mutations in *SUOX* gene displayed symptoms of MOCD. This indicates that sulfite oxidase is the most important out of the four molybdoenzyme in humans (Schwarz, 2016). It has been previously reported that sulfite accumulation increased reactive oxygen species in Neuro-2a, PC12, HepG2, and human fetal liver (Zhang *et al.*, 2004). Zhang and colleagues also reported that sulfite inhibits glutamate dehydrogenase. In this work, TUM1 deletion exhibited a reduction in sulfite oxidase activity with a concomitant increase in ROS level and a decrease in glutamate dehydrogenase.

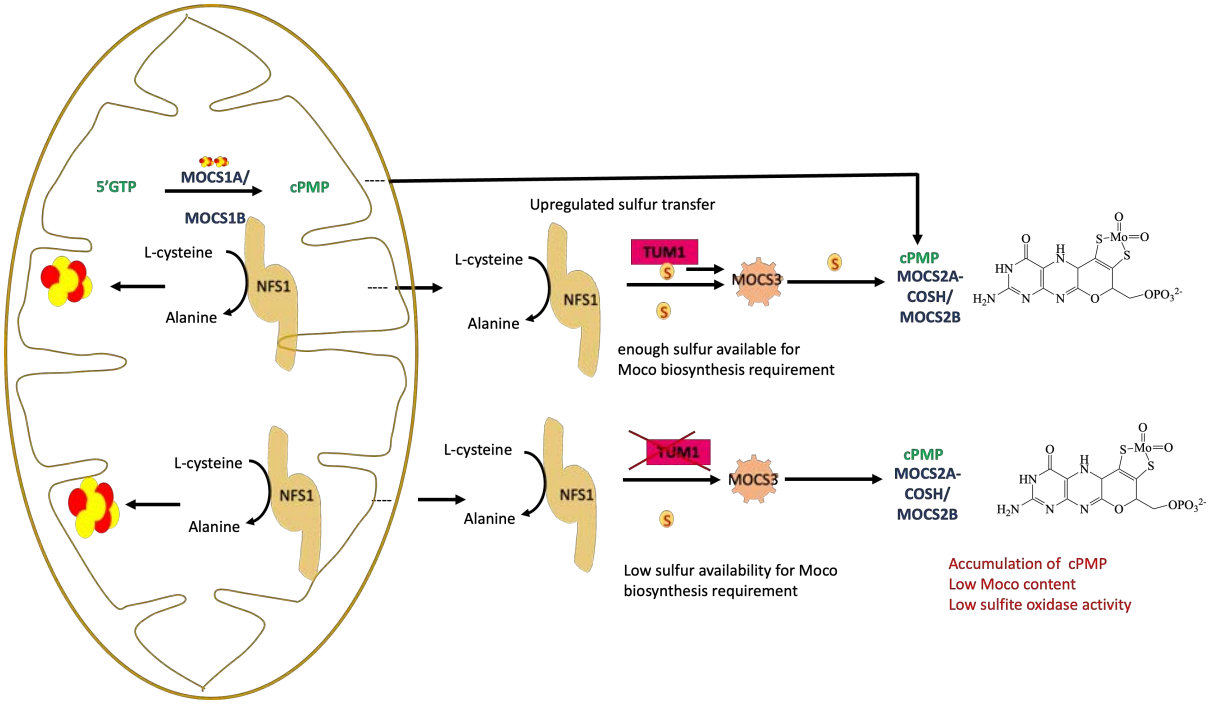

Figure 29: TUM1 is involved in sulfur transfer for Moco biosynthesis. In the wild type, the L-cysteine desulfurase NFS1 and TUM1 provide the sulfur to MOCS3. MOCS3 activates the thiocarboxylated MOCS2A and subsequently forms a complex with MOCS2B leading to the formation of MPT, and eventually, Moco can be produced. Moco is then integrated into the molybdoenzymes. sulfite oxidases, XDH, AOX, and mARC. In *TUM1* knockout cells, the sulfur availability is reduced. The sulfur acquired by MOCS2A from MOCS3 is limited. As a result, cPMP builds up, and a limited amount of MPT is formed. This influences the activity of molybdoenzymes due to the limited amount of Moco formed.

Sulfite oxidase requires Moco and heme cofactors for homodimerisation for an active form (Kisker et al., 1997; Klein et al., 2012). Further, it has been previously reported that sulfite oxidase is found in the cytosol rather than the inner mitochondrial space in the absence of Moco. SO requires not only its N-terminal targeting signal but also Moco integration for the translocation and retention in the inner mitochondria membrane (Klein et al., 2012). Klein and colleagues also reported that Moco is the rate-limiting step for the maturation of SO (Klein *et al.*, 2012). In this research, the reduction in the abundance of sulfite oxidase protein in the *TUM1* knockout cells was reported, suggesting apo-SO degradation. This is concomitant with the decrease in MPT production. Here, it is proposed that in the absence of TUM1, there is a reduction in the transfer of persulfide to MOCS3. The amount of persulfidated MOCS3 is reduced, limiting the sulfuration of cPMP for MPT formation. This results in a limited amount of Moco available for incorporation into SO.

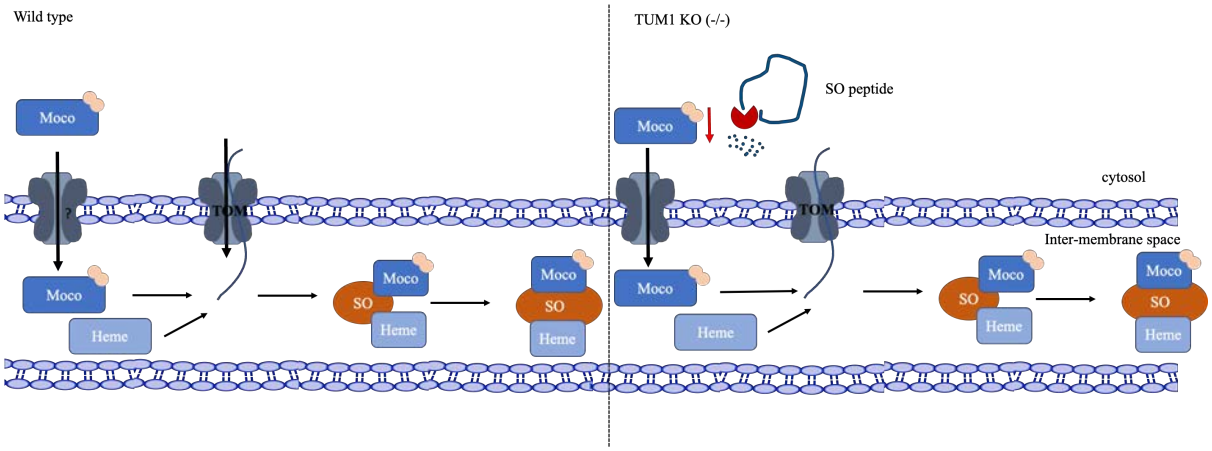

Figure 30: The absence of TUM1 leads to partial degradation of Sulfite oxidase. The mechanism of transport of Moco into the inter-membrane space is still yet unknown. Sulfite oxidase is transported to the IMS through the TOM system. The incorporation of Moco makes the heme binding site accessible, resulting in SO folding and its dimerization. In TUM1 knockout cells, there is a reduction in Moco, leading to reduced binding of Moco to SO and partial degradation of sulfite oxidase. (Adapted from Klein et al., 2012)

3.3 Exogenous sulfur donor affected cytosolic tRNA thiolation and Moco biosynthesis.

NaHS could serve as direct sulfur donor through NaHS dissociation in neutral solution (H_2S, HS-, S2), leading to pool of sulfide and polysulfides (Greiner *et al.*, 2013). In addition, investigation of *MPST* knockout mouse brains revealed lack of cysteine-SSH and GSSH production with 50% decrease in the levels of total persulfated species (Kimura *et al.*, 2017). H_2S has been reported to produce cysteine persulfides and polysulfides in SH-SY5Y cells (Koike *et al.*, 2017). MPST has produced similar persulfides like cysteine persulfide (CysSSH) and GSH persulfide (GSSH). Studies in yeast have linked tRNA sulfur modification to nutrient availability. The mcm^5s^2U was shown to utilise metabolites derived from sulfur metabolism which is important during cell growth (Laxman *et al.*, 2013). Yeast grown without free amino acid had less mcm^5s^2U modification compared to when supplemented with cysteine and methionine. Cysteine and methionine can be interconverted (Figure 2). Laxman and colleagues also reported a low level of cysteine and methionine abundance. In humans, Cysteine can be metabolised to hydrogen sulfide by TUM1, CBS and CSE. Dissociation of H_2S can produce sulfide. Cysteine is the substrate for NFS1 to form persulfide. This persulfide is further transferred to TUM1, MOCS3, URM1, and CTU1 before final insertion into tRNA. An increase in mcm^5s^2U was observed after HPLC analysis of nucleosides in NaHS-treated cells, including the *TUM1* knockout cells. However, NaHS treatment did not affect *MOCS3*

knockout, indicating the importance of MOCS3 in the sulfur transfer for tRNA thio-modification. The reduction of mcm^{5}s^{2}U in *TUM1* deletion could be linked to the stimulation of NFS1 activity for increased persulfide production. Therefore, the sulfide availability through NaHS increased the pool of sulfide, increasing mcm^{5}s^{2}U formation. Consequently, the effect of *TUM1* knockout on cytosolic tRNA thiolation can be ascribed to the sulfur availability.

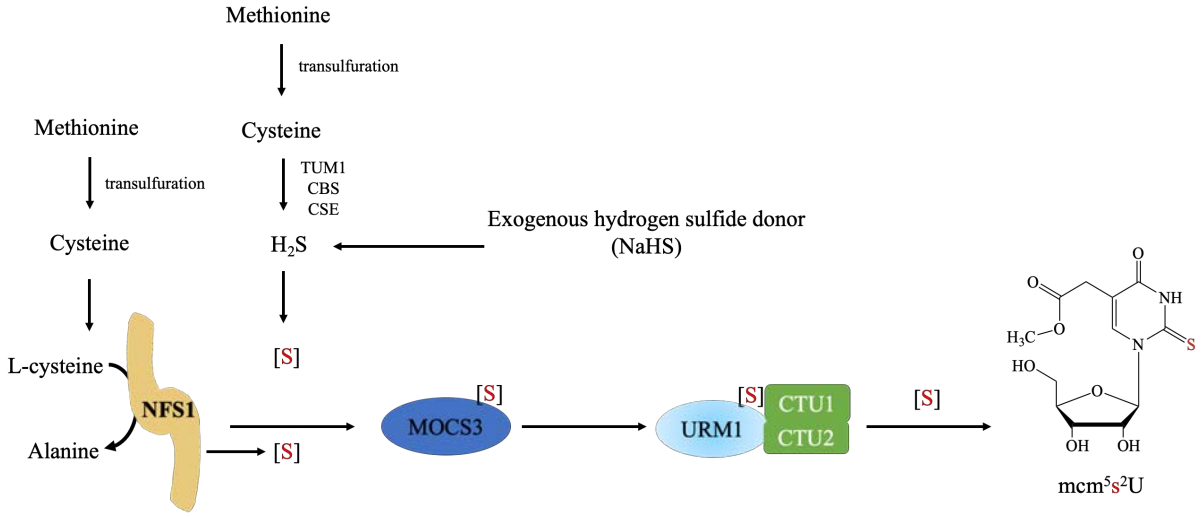

Figure 31: Sulfur availability affects thio-modification. The availability of sulfur-containing amino acids methionine and cysteine increases thio-modification. Cysteine is a substrate for L-cysteine desulfurase for persulfide formation, which MOCS3 utilises, URM1 and CTU1 for the thiolation of tRNA at wobble Uridine position 34. In the alternative, cysteine can be replaced by exogenous supplementation with H_2S donor NaHS Cysteine can be oxidised to H_2S, which can dissociate to form sulfide, MOCS3, URM1 and CTU1 for mcm5s2U modification, can use.

H_2S has been mentioned to act via the *S*-sulfhydration of target proteins. Transfer of sulfur is essential for the formation of Moco in humans. NFS1 facilitates the donation of the initial sulfur for this process. The sulfur is further transferred to MOCS3 and MOC2A before the final incorporation to form MPT. For the availability of sulfur, TUM1 has been reported to increase the sulfide pool by upregulating the activity of NFS1 in the presence of MOCS3 in an invitro experiment (Fräsdorf *et al.*, 2014). Here, *MOCS3* knockout cells were not affected by NaHS treatment due to their importance in further sulfur transfer to MOCS2A. However, SO activity increased in *TUM1* knockout cells. The sulfur generated from the dissociation of NaHS is suggested to increase the persulfide pool for further incorporation into MOCS3, which is subsequently transferred to MOCS2A for the sulfuration of cPMP to MPT. Invitro MPT production assay has shown that sulfide can serve as a direct sulfur donor instead of NFS1 (Fräsdorf *et al.*, 2014). It is impossible to disprove a direct transfer of sulfur within a cell.

However, sulfur requires reduction to sulfide before incorporation into biomolecules like Moco and tRNAs. The activated sulfur can also be utilised to form sulfane sulfur, which is incorporated into the biomolecules (Kessler, 2006). Further, the activated sulfur can be used for the biosynthesis of cysteine, which NFS1 uses to form persulfide. Therefore, the hypothesis of direct sulphur transfer can be annulled (Kessler, 2006)

3.4 Moco deficiency affects the H_2S biosynthesis enzyme.

In humans, H_2S biosynthesis emerges from the desulfhydration of cysteine by CBS, CTH and TUM1 (Chiku *et al.*, 2009). However, TUM1 requires an intermediate step of conversion of cysteine to 3-mercaptopyruvate by GOT. Cysteine is usually synthesised from the transmethylation and transsulfuration of methionine (Stipanuk, 2020). CTH can produce L-cysteine from cystathionine through α, and γ elimination. Also, H_2S can be biosynthesised from L-cysteine through α, and β elimination by CTH (Chiku *et al.*, 2009). H_2S has been reported to be toxic at high concentrations therefore the need for its regulation (Nicholson *et al.*, 1998; Reiffenstein *et al.*, 1992). One of the end products of H_2S catabolism is sulfite. Through the sulfide oxidizing unit, the oxidation of H_2S in the mitochondria produces sulfite (Paul *et al.*, 2021) (Figure 26). H_2S is oxidized by SQR to GSSH, this is further oxidized by sulfur dioxygenase to sulfite (Paul *et al.*, 2021). SO further catalyses the metabolic detoxification of sulfite to inorganic sulfate within the intermembrane space of the mitochondria (Cohen *et al.*, 1971). Sulfite toxicity has been proposed to arise from the conversion of excess sulfite to sulfite radicals in the absence and presence of oxidative stress due to deficiency in SO (Velayutham *et al.*, 2016). In rat hepatocytes, sulfite resulted in the formation of ROS and lipid peroxidation (Niknahad *et al.*, 2008). Niknahad and colleagues reported that sulfite depleted GSSH and GSH. Sulfite can react with disulphide bonds to produce thiols and S-sulfonate compounds, which has been reported in rat's small intestine (Robinson *et al.*, 1964). Marshall and colleagues have previously reported GSH depletion enhanced sulfite-linked neurotoxicity (Marshall *et al.*, 1999). In this research, increased ROS was observed on *TUM1* deletion. Moco is essential for the activity of SO and its incorporation is essential for the maturation of SO (Klein *et al.*, 2012). *MOCS3* deletion resulted in Moco deficit, which makes SO inactive. (Neukranz *et al.*, 2019). However, only a mild impairment of sulfite oxidase was observed in *TUM1* deletion. Since there is an impairment in SO in *TUM1* deletion, there is a possibility that the cells tend to regulate cysteine production by CTH suppression, reducing the level of H_2S in the cell. In HEK293T *TUM1* knockout cells, CTH protein level was reduced. It was previously reported

in *C.elegans* (Warnhoff *et al.*, 2019) that the suppression of CTH and CDO attenuated the effect of Moco deficiency (Warnhoff *et al.*, 2019). The reduction in CTH was an adaptive mechanism by the cell to suppress the effect of Moco deficiency. *TUM1* deletion in mice was previously reported to cause a reduction in the expression of CTH (Trautwein *et al.*, 2021). However, the effect of CDO was not investigated in this present research. CDO is responsible for the oxidative pathway of cysteine catabolism with sulfite as one of its end-products (Paul *et al.*, 2021). It has been previously reported in CDO -/- mice that the capability of the mouse to produce H_2S exceeds that of detoxification of sulfite to sulfate (Roman *et al.*, 2013). An increased level of H_2S followed this due to the predominance of the non-oxidative pathway of the cysteine catabolism (Roman *et al.*, 2013).

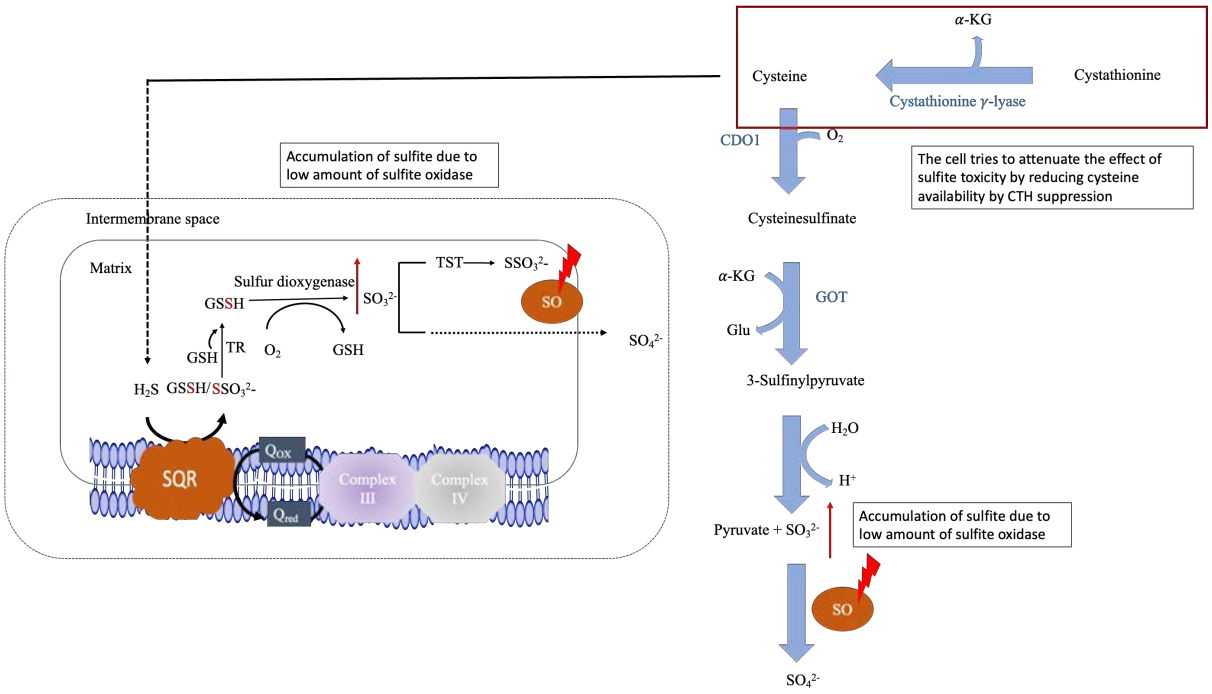

Figure 32: Moco deficiency is attenuated by limiting cysteine availability. The oxidation pathway of cysteine through cysteine dioxygenase leads to the formation of sulfite and pyruvate. However, due to the low availability of SO in *TUM1* knockout cells, there is sulfite accumulation. Likewise, hydrogen sulfide formed through cysteine by CBS and CSE is oxidised in the mitochondria by SQR to persulfide and donates electrons into the ETC. The end product of this pathway is sulfite which is later converted to sulfate in the intermembrane space.

3.5 TUM1 impacts H_2S biosynthesis and links to mitochondria bioenergetics disruption.

H_2S is a gasotransmitter implicated in numerous functions in humans (Módis *et al.*, 2013). H_2S can be produced by three enzymes CBS, CTH and TUM1 (Paul *et al.*, 2021). The three enzymes

are expressed in the kidney. TUM1 produces H_2S and a disulfide in a process facilitated by dihydrolipoic acid (DHLA) or thioredoxin (Yadav *et al.*, 2013; Mikami *et al.*, 2011). Enzymatically, TUM1 can produce H_2S from L-cysteine and α-ketoglutarate after conversion to 3-MP by glutamate oxaloacetate transaminase (GOT) (Shibuya *et al.*, 2009; Taniguchi *et al.*, 1974). H_2S can also be produced through a non-enzymatic pathway through glucose, glutathione, elemental sulfur and polysulfides (Kolluru *et al.*, 2013). The biological importance of H_2S is constantly increasing (Kolluru *et al.*, 2013). Hydrogen sulfide has been implicated in physiological roles like anti-inflammation, oxidative stress, neuromodulation and others (Yonezawa *et al.*, 2007; Zanardo *et al.*, 2006; Laggner *et al.*, 2007; Abe *et al.*, 1996b). TUM1 can produce H_2S both in the cytosol and mitochondria. TUM1 have two isoforms TUM1-Iso1 and TUM1 Iso2. TUM1 Iso2 is localised in both cytosol and mitochondria, while the TUM1 Iso1 only localizes in the cytosol (Fräsdorf *et al.*, 2014). Deletion of TUM1 in various systems exhibited decreased, increased or unchanged H_2S levels (Peleli *et al.*, 2020; Li *et al.*, 2018; Li *et al.*, 2019). In HEK 293T cells, a reduction in H_2S level was observed on the deletion of *TUM1*. H_2S level was significantly decreased using cysteine as substrate respectively. Using cysteine as substrate only reduced the H_2S production since CBS and CTH can also biosynthesise H_2S in the cytosol. However, there was no H_2S production using the physiological substrate of TUM1 3-mercaptopyruvate.

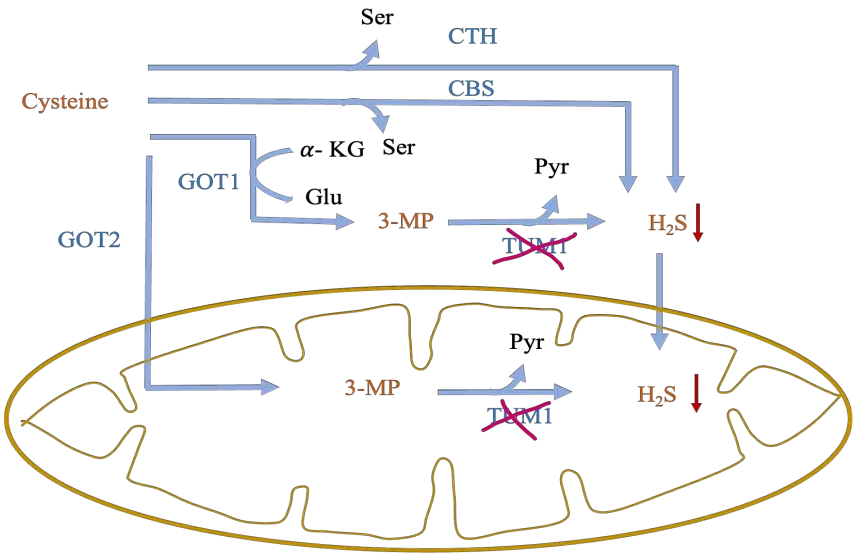

Figure 33: TUM1 attenuates H_2S biosynthesis in HEK 293T cells. Cysteine derived from the transsulfuration pathway (Figure 2) is utilised by CSE, CBS and TUM1 to produce H_2S in the cytosol. Deletion of *TUM1* in the cytosol reduces H_2S biosynthesis. TUM1 requires an additional step involving forming 3-MP by Glutamate oxaloacetate transaminase (GOT). Using the 3-MP H2S biosynthesis is abolished in the absence of TUM1.

3.6 TUM1 affects mitochondria bioenergetics.

It has been reported that the silencing of 3-MST in liver cell cultures led to reduced bioenergetics and concomitant stimulation by 3-MP, at low concentrations (Módis *et al.*, 2013)**.** H_2S biosynthesis in the mitochondria has been implicated in the stimulation of the mitochondria bioenergetics (Szabo *et al.*, 2014) through the sulfite oxidizing unit (SOU). The SOU consists of SQR, which oxidizes two H_2S molecules leading to the formation of two disulfides on SQR and two electrons (Szabo *et al.*, 2014). The electron produced contributes to the electron transport chain's electron pump and promotes the mitochondria ATP generation (Szabo *et al.*, 2014). A higher concentration of H_2S has been reported to inhibit Complex IV, thereby inhibiting potential mitochondrial (Szabo *et al.*, 2014)**.** However, in ΔMST mouse models, the activity of the complex IV was found to be similar to the wild-type (Trautwein *et al.*, 2021). 3-MST suppression in the endothelial cell has been reported to affect the mitochondrial ATP production (Abdollahi Govar *et al.*, 2020). Herein, a lower oxygen consumption rate (OCR) in the *TUM1* knockout cells was observed, indicating deficit in mitochondria bioenergetics. The decrease in OCR corresponds to a decrement in the total ATP production in *TUM1* knockout cells.

Further, an increment in the extracellular acidification rate (ECAR) was observed, suggesting a shift to glycolytic ATP production by the *TUM1* knockout cells. H_2S can be produced from glucose through the glycolytic pathway. Glucose can interact with methionine, homocysteine or cysteine to form gaseous sulfur compounds like hydrogen sulfide (Kolluru *et al.*, 2013). Past experiments have shown that the silencing of 3-mercaptopyruvate sulfurtransferase (3-MST) in liver cell cultures exhibited reduced bioenergetics with a corresponding stimulation of 3-MP (Módis *et al.*, 2013). H_2S produced by CTH and CBS can also diffuse into the mitochondria; therefore, their compensatory effects cannot be annulled (Murphy *et al.*, 2019). Different outcomes on cellular bioenergetics have been reported of CTH deletion in various tissues. In smooth muscle cells, CTH deletion exhibited no effect on the mitochondria bioenergetics but was promoted in blood cells (Fu *et al.*, 2012; Módis *et al.*, 2019). High proton leak was also characteristic of *TUM1* deletion, this can be attributed to the damage of the mitochondria membrane through sulfite. Previous experiments have demonstrated sulfite-dependent damage to the mitochondria with a corresponding decrease in the ATP production (Mellis *et al.*, 2020). To further buttress the sulfite-linked damage, the non-mitochondria oxygen consumption was observed to be increased in the *TUM1* knockout cells. Non-mitochondria oxygen consumption

is influenced by ROS and various oxidative stress conditions (Herst *et al.*, 2004). These findings demonstrates the importance of TUM1 in maintaining the optimum mitochondria bioenergetics by providing electrons into the ETC through the H_2S.

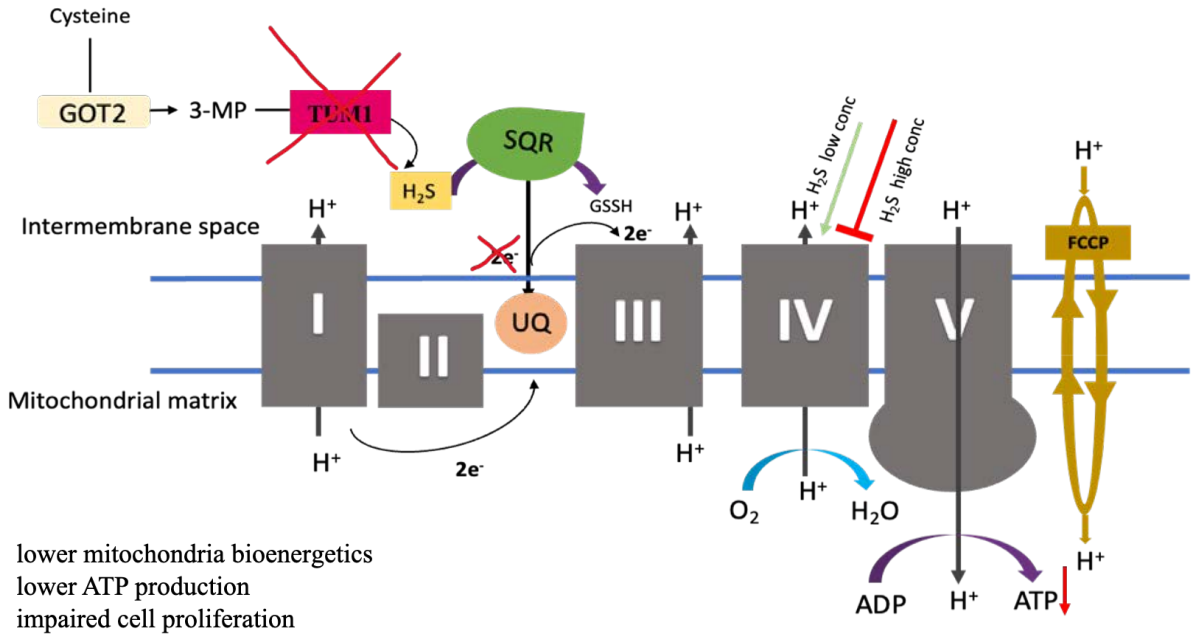

Figure 34: TUM1 absence affects mitochondria bioenergetics. TUM1 is the main H_2S biosynthesis enzyme in the mitochondria. H_2S produced from TUM1 is oxidised by SQR, thereby producing electrons which enter the ETC and stimulate the production of ATP. Without TUM1, ATP production is reduced due to impaired H_2S biosynthesis, leading to decreased growth.

3.7 Absence of TUM1 affected cell proliferation

Cell cycle progression is controlled and regulated by numerous checkpoints (Mandal *et al.*, 2005). Cell division is an energy-intensive process, and inhibition of the cell cycle by an ATP-dependent checkpoint is critical (Mandal *et al.*, 2005). Cellular proliferation and the concomitant DNA replication and translational processes represent significant energetic commitments. This presumably require an increase in energy supply to meet this great ATP-dependent synthetic demand. Therefore insufficient ATP can cause a pause in the cell cycle progression (Johnson *et al.*, 1999). Cell cycle progression is regulated by mitochondrial energetics in Jurkat cells. It was reported that Jurkat cells with ΔΨmL (with low mitochondria potential) fraction were almost exclusively in the G1 phase. The cells obtained from the ΔΨmH (with high mitochondria potential) fraction were in all cell cycle stages, indicating cell cycle arrest in Jurkat cells with low mitochondria potential (Schieke *et al.*, 2008). This work reported reduced ATP and mitochondrial bioenergetic in *TUM1* knockout cells. Following the low ATP

in Jurkat cells cycle arrest was reported. In this thesis, the rate of cell proliferation in *TUM1* knockout cells was significantly reduced. Further, the TCA cycle is essential for the production of energy in the form of ATP for maintaining high energy-demanding physiological functions like cell growth (Martínez-Reyes *et al.*, 2016). Recently, it has been reported that the suppression of TCA cycle enzymes using genetic silencing siRNA showed that aconitase 2 affected the growth of CHO cells (Dhami *et al.*, 2018). The other TCA cycle enzymes did not significantly affect the CHO cells' growth rate and viability. A cytosolic and mitochondrial aconitase reduction was observed in *TUM1* knockout cells.

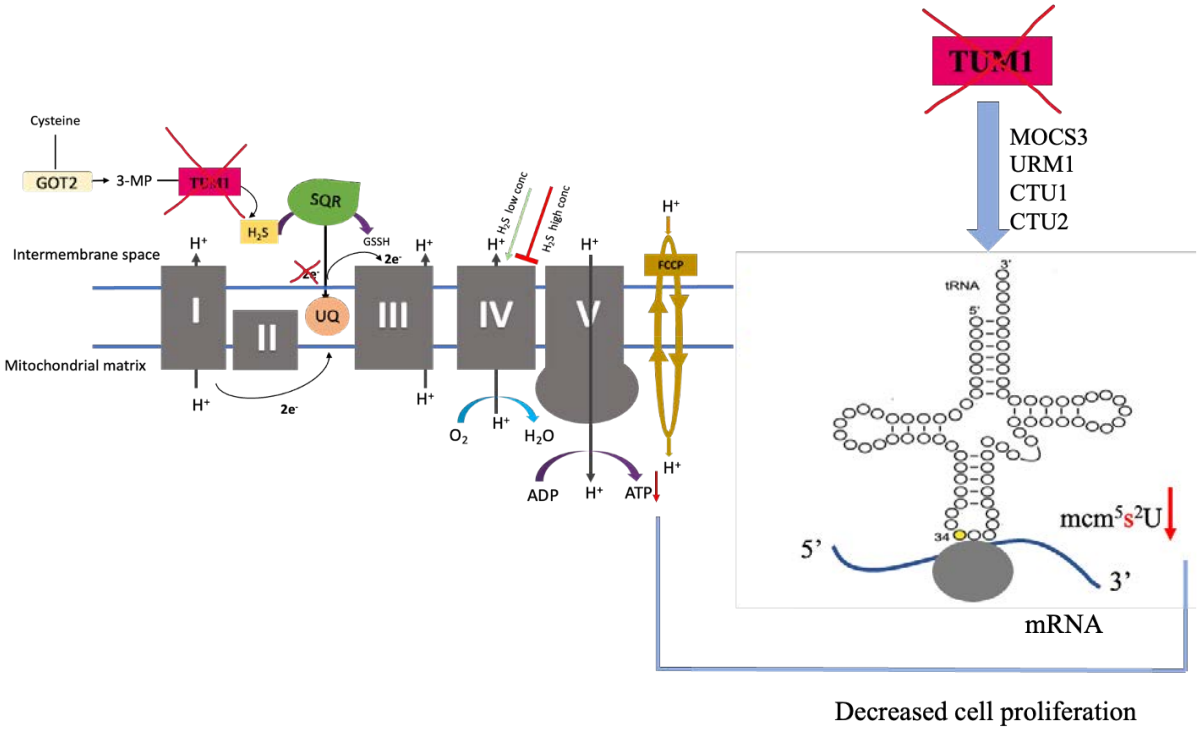

Figure 35: TUM1 affects cell proliferation in HEK 293T cells. TUM1 serves as the central mitochondrial H_2S biosynthesis. Oxidation of H_2S by SQR donates electrons into the ETC, thereby increasing the electron pump. This subsequently increases ATP production in the mitochondria. Also, TUM1 deletion decreases thio-modification, affecting the translation rate, thereby affecting cell proliferation.

The stimulation of mitochondrial bioenergetics has been linked to H_2S production (Szabo *et al.*, 2014). The oxidation of H_2S in the mitochondria by SQR produces two electrons that flow into the ETC and increase ATP production (Figure 25) (Szabo *et al.*, 2014). In this thesis, *TUM1* knockout cells were reported to have perturbed H_2S production. Xie and colleagues have shown previously that NaHS complementation increased cell proliferation in keratinocytes exogenous (Xie *et al.*, 2016). A similar outcome was observed in *TUM1* knockout cells with exogenous NaHS rescuing the growth rate.

Further, the availability of sulfur-containing amino acids in yeast was linked to growth deficiency due to impairment in the tRNA thio-modification (Laxman *et al.*, 2013). We also reported impairment in the tRNA thio-modification in *TUM1* knockout cells. NaHS is an exogenous hydrogen sulfide donor dissociating to sulfide, increasing thio-modification and cell proliferation in *TUM1* knockout cells. Bringing all these together, the effect of *TUM1* knockout on cell proliferation can be linked to its hydrogen sulfide production capability and involvement in thio-modification

3.8 The L-cysteine desulfurase NFS1 activity is inhibited by 2-methylene 3-quinuclidinone (MQ)

2-methylene 3-quinuclidinone (MQ) is an active compound in eprenetapopt. Eprenetapopt is an anticancer drug with yet unknown mode of action (Fujihara *et al.*, 2022). Cancer cells are characterised by a rapid growth rate (Feitelson *et al.*, 2015). Proteomics studies have reported an upregulation of ferredoxin-2 (mitochondrial) in eprenetopopt-treated cells (Fujihara *et al.*, 2022). Ferredoxin 2 provides the electrons necessary for converting sulfur to sulfide (Lange *et al.*, 2000; Shi *et al.*, 2012; Sheftel *et al.*, n.d.; Mühlenhoff *et al.*, 2003) for the formation of iron-sulfur clusters. Iron-sulfur clusters are essential cofactors for several cellular processes (Zhang *et al.*, 2022). NFS1 provides sulfur for ISC biogenesis in humans. A recent study demonstrated that suppression of NFS1 causes iron deprivation followed by iron influx to cells leading to ferroptosis (Alvarez *et al.*, 2017; Alvarez *et al.*, 2018). A high load of iron produces reactive hydroxyl radicals from H_2O_2 (Wardman *et al.*, 1996). Ferroptosis has been characterised by inhibiting Glutamate/cystine antiporter, which depletes the intracellular cysteine (Yang *et al.*, 2014). However, inhibition of GSH did not induce ferroptosis (Yang *et al.*, 2014). This suggests the importance of blocking cysteine availability in ferroptosis induction. In this research, enzyme inhibition assay revealed that MQ inhibits purified NFS1 protein in a non-competitive manner. As a Michael acceptor, MQ can bind to thiols like GSH and cysteine (Lambert *et al.*, 2009). Using human embryonic kidney cells, NFS1 activity was demonstrated to reduce with increasing concentrations of MQ. Using radiolabelled cysteine (35-S) as substrate, the inhibition rate of persulfide formation on NFS1 was affected by MQ treatment. This indicates reduced availability of sulfur for biogenesis of iron-sulfur cluster.
Reduced aconitase activity was also observed with increasing concentrations of MQ. Aconitase is an iron-sulfur cluster containing enzymes and functions under iron starvation as an iron regulatory protein (IRP) (Casey et al., 1988). Aconitase 2 was recently found to impact CHO

cells' growth when TCA cycle enzymes were silenced Field (Dhami et al., 2018). Similarly, the iron-responsive promoted in cancer cells was activated in NFS1 suppression (Alvarez et al., 2018). A decrement in proliferation rate in MQ-treated HEK293T cells was observed in this work. Since evasive growth is characteristic of cancer cells, then this effect of MQ will be beneficial to control the cancer cell growth (Feitelson *et al.*, 2015).

NFS1 uses cysteine to provide sulfur for cytosolic tRNA thiolation and Moco biosynthesis. Reduced thio-modification and Moco deficiency have been shown to cause growth retardation in yeast and *C.elegans,* respectively (Laxman *et al.*, 2013; Warnhoff *et al.*, 2019). However, this was not investigated in this research. The mode of action can then be ascribed to the binding of MQ to cysteine, thereby inhibiting the rate of persulfide formation on NFS1. This indicates that MQ inhibits NFS1 activity by binding to cysteine leading to perturbation of ISC biogenesis and reducing cell proliferation. This therapeutic approach will be helpful in cancer biology due to the energy demand of cancer cells. NFS1 is an essential cofactor for vital proteins as NFS1 is found to be upregulated in some cancer cells. High expression of NFS1 has been reported to be critical for lung tumour growth (Alvarez *et al.*, 2017).

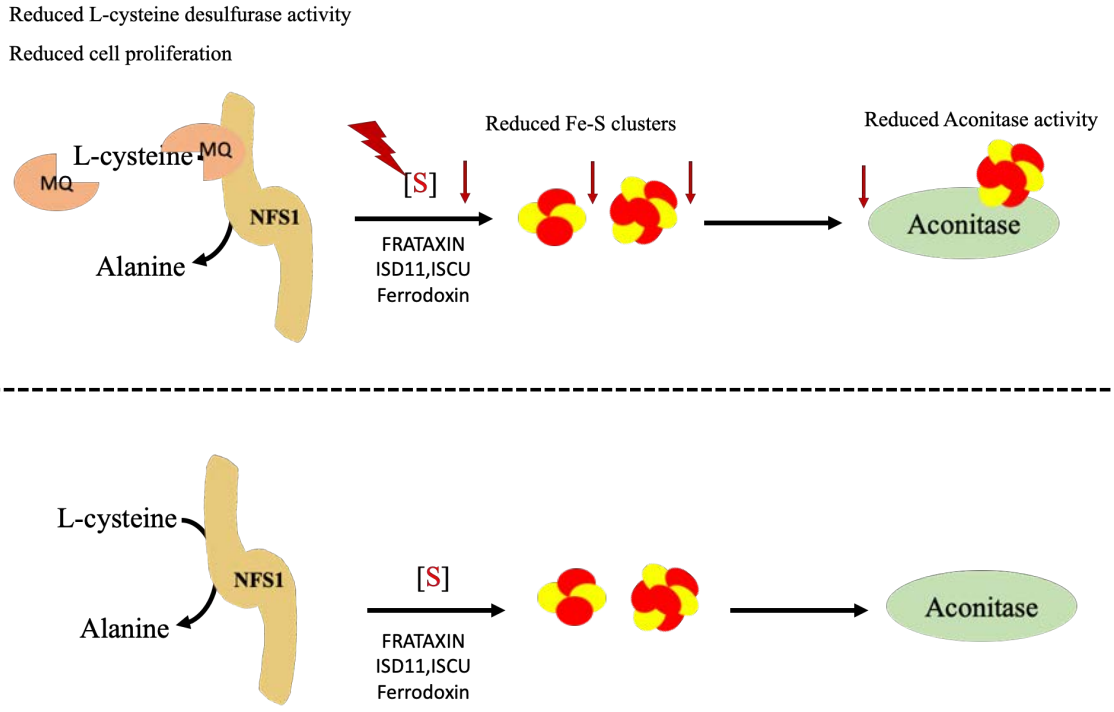

Figure 36: Inhibition of NFS1 activity by MQ. Cysteine serves as a substrate of NFS1 for ISC biogenesis and other biomolecules. MQ binds cysteine, reducing the intracellular cysteine available. This reduces the Fe-S clusters open, causing a reduction in aconitase activity and cell proliferation.

4 Conclusion

In this study, we were able to show for the first time using CRISPR/Cas9 *TUM1* HEK 293T knockout cells the effects of TUM1 on Moco biosynthesis, cytosolic tRNA thiolation and cellular bioenergetics based on previous interaction studies.

Using HPLC quantification of the fluorescent derivative of cPMP and MPT, TUM1 was shown to be involved in the efficient sulfur transfer for the second step of Moco biosynthesis. Further, sulfite oxidase activity and protein levels were reduced in *TUM1* knockout cells, resulting from the degradation of SO due to reduced Moco content in the cell. We also demonstrated the accumulation of cPMP, the first product of Moco biosynthesis. TUM1 is involved in sulfur transfer for Moco biosynthesis in humans based on the above evidence.

The deletion of *TUM1* resulted in the reduction of thio-modification (mcm^5s^2U) in the cell. This caused an accumulation of mcm^5U in the cells due to low sulfur being incorporated for mcm^5s^2U formation. TUM1 can therefore be suggested to be a part player in the sulfur transfer for cytosolic tRNA thiolation in humans. The deficit in Moco biosynthesis, cytosolic tRNA thiolation and cell proliferation is suggested to be caused by sulfur availability as treatment with NaHS rescued the deficits.

TUM1 is an essential enzyme for H_2S biosynthesis in HEK 293T. In the absence of TUM1 in the cells, H_2S biosynthesis was affected, affecting ATP production and mitochondria bioenergetics.

Further, MQ inhibits the activity of L-cysteine desulfurase in HEK293T by limiting substrate availability. This leads to the reduction of the activity of an iron-sulfur cluster-dependent enzyme aconitase indicating impairment in Fe-S cluster biogenesis. However, this still needs to be intensively investigated. Conclusively, TUM1 is an important sulfurtransferase for efficient sulfur transfer for cytosolic tRNA thiolation and Moco biosynthesis. TUM1 is also crucial for maintaining the optimal level of H_2S biosynthesis in kidney cells.

5 Future perspectives

This present research investigated the combined effect of both TUM1 isoforms. In the future, the role of the individual isoforms on cytosolic tRNA thiolation, Moco, and H_2S biosynthesis should be investigated. This is important due to the different localisation of the two isoforms and various interaction partners. The effect of TUM1 on other Moco-dependent enzymes like xanthine oxidase and aldehyde oxidase would also be of interest. Moreover, the low expression of these enzymes in human embryonic kidney cells is a constraint. However, other conventional methods that could detect low levels of products could be employed. Also, the effect of NaHS on the Moco and cPMP levels should be investigated. This might give more insights into the increase in sulfite oxidase activity.

Further, the activity of NFS1 should be analysed in the *TUM1* KO cells. Since the methylene blue assay measures the overall sulfide produced, it is difficult to separate other sulfide-producing enzymes. Using radioactivity for the analysis would have more prospects into measuring NFS1's activity. This might give further knowledge on the sulfur transfer mechanism for Moco biosynthesis and cytosolic tRNA thiolation. It would also be of interest to know the levels of cysteine and glutathione in *TUM1* deletion. A metabolomics analysis would be important to observe the affected metabolisms in the *TUM1* KO. This is important due to the numerous effects already observed in this research. Finally, the impact of TUM1 on the mitochondria tRNA thiolation should be investigated since there is already interaction evidence between MTU1 and TUM1 in the mitochondria.

6 References

Abdollahi Govar A, Törő G, Szaniszlo P, Pavlidou A, Bibli SI, Thanki K, et al. 3-Mercaptopyruvate sulfurtransferase supports endothelial cell angiogenesis and bioenergetics—British Journal of Pharmacology 2020;177(4):866.

Abe K, Kimura H. The possible role of hydrogen sulfide as an endogenous neuromodulator. Journal of neuroscience 1996a;16(3):1066-71.

Abou-Hamdan A, Guedouari-Bounihi H, Lenoir V, Andriamihaja M, Blachier F, Bouillaud F. Oxidation of H_2S in Mammalian Cells and Mitochondria. Methods in Enzymology 2015;554:201-28.

Adam AC, Bornhövd C, Prokisch H, Neupert W, Hell K. The Nfs1 interacting protein Isd11 has an essential role in Fe/S cluster biogenesis in mitochondria. Embo Journal 2006;25(1):174.

Agris PF, Sierzputowska-Gracz H, Smith W, Malkiewicz A, Sochacka E, Nawrot B. Thiolation of Uridine Carbon-2 Restricts the Motional Dynamics of The Transfer RNA Wobble Position Nucleoside. Journal of American Chemical Society 1992;114(7):2652-6.

Ahmad M, Wolberg A, Kahwaji CI. Biochemistry, Electron Transport Chain. StatPearls Publishing; 2022 Jan.

Akahoshi N, Minakawa T, Miyashita M, Sugiyama U, Saito C, Takemoto R, et al. Increased Urinary 3-Mercaptolactate Excretion and Enhanced Passive Systemic Anaphylaxis in Mice Lacking Mercaptopyruvate Sulfurtransferase, a Model of Mercaptolactate-Cysteine Disulfiduria. International journal of molecular sciences,2020 21(3), 818.

Alexandrov A, Chernyakov I, Gu W, Hiley SL, Hughes TR, Grayhack EJ, et al. Rapid tRNA Decay Can Result from Lack of Nonessential Modifications. Molecular Cell 2006;21(1):87-96.

Alvarez SW, Possemato R. Leveraging the iron-starvation response to promote ferroptosis. Oncotarget 2018;9(13):10830.

Alvarez SW, Sviderskiy VO, Terzi EM, Papagiannakopoulos T, Moreira AL, Adams S, et al. NFS1 undergoes positive selection in lung tumours and protects cells from ferroptosis. Nature 2017 5517682 2017;551(7682):639-43.

Amrani L, Primus J, Glatigny A, Arcangeli L, Scazzocchio C, Finnerty V. Comparison of the sequences of the Aspergillus nidulans hxB and Drosophila melanogaster ma-l genes with nifS from Azotobacter vinelandii suggests a mechanism for the insertion of the terminal sulphur atom in the molybdopterin cofactor. Molecular Microbiology 2000;38(1):114-25.

Armengod ME, Moukadiri I, Prado S, Ruiz-Partida R, Benítez-Páez A, Villarroya M, et al. Enzymology of tRNA modification in the bacterial MnmEG pathway. Biochimie 2012;94(7):1510-20.

Barić I, Ćuk M, Fumić K, Vugrek O, Allen RH, Glenn B, et al. S-Adenosylhomocysteine hydrolase deficiency: a second patient, the younger brother of the index patient, and outcomes during therapy. Journal of Inherited Metabolic Disease 2005;28(6):885-902.

Baruffini E, Dallabona C, Invernizzi F, Yarham JW, Melchionda L, Blakely EL, et al. MTO1 Mutations are Associated with Hypertrophic Cardiomyopathy and Lactic Acidosis and Cause Respiratory Chain Deficiency in Humans and Yeast. Human Mutation 2013;34(11):1501.

Beinert H, Holm RH, Münck E. Iron-Sulfur Clusters: Nature's Modular, Multipurpose Structures. Science (80-) 1997;277(5326):653-9.

Beinert H. A tribute to sulfur. European Journal of Biochemistry 2000;267(18):5657-64.

Bergmann AK, Campagna DR, McLoughlin EM, Agarwal S, Fleming MD, Bottomley SS, et al. Systematic molecular genetic analysis of congenital sideroblastic anemia: Evidence for genetic heterogeneity and identification of novel mutations. Pediatric Blood & Cancer 2010;54(2):273-8.

Bittner F, Oreb M, Mendel RR. ABA3 Is a Molybdenum Cofactor Sulfurase Required for Activation of Aldehyde Oxidase and Xanthine Dehydrogenase in Arabidopsis thaliana. Journal of Biology and Chemistry 2001;276(44):40381-4.

Black KA, Dos Santos PC. Shared-intermediates in the biosynthesis of thio-cofactors: Mechanism and functions of cysteine desulfurases and sulfur acceptors. Biochimica et Biophysica Acta 2015;1853(6):1470-80.

Boccaletto P, Stefaniak F, Ray A, Cappannini A, Mukherjee S, Purta E, et al. MODOMICS: a database of RNA modification pathways. 2021 update. Nucleic Acids Research 2022;50(D1):D231-5.

Bordo D, Bork P. The rhodanese/Cdc25 phosphatase superfamily: Sequence-structure-function relations. EMBO reports 2002;3(8):741-6.

Borisov VB, Forte E. Impact of Hydrogen Sulfide on Mitochondrial and Bacterial Bioenergetics. International Jornal of Molecular Science 2021, 22(23), 12688.

Bronowicka-Adamska P, Bentke A, Wróbel M. Hydrogen sulfide generation from l-cysteine in the human glioblastoma-astrocytoma U-87 MG and neuroblastoma SHSY5Y cell lines. Acta Biochimica Polonica 2017;64(1):171-6.

Brosnan JT, Brosnan ME. The sulfur-containing amino acids: an overview. Journal of Nutrition 2006;136 (6 Suppl):1636S-1640S

Buist NRM, Glenn B, Vugrek O, Wagner C, Stabler S, Allen RH, et al. S-adenosylhomocysteine hydrolase deficiency in a 26-year-old man. Journal of Inherited Metabolic Disease 2006;29(4):538-45.

Butler AR, White JH, Folawiyo Y, Edlin A, Gardiner D, Stark MJ. Two Saccharomyces cerevisiae genes which control sensitivity to G1 arrest induced by Kluyveromyces lactis toxin. Molecular Cell Biology 1994;14(9):6306.

Camaschella C, Campanella A, De Falco L, Boschetto L, Merlini R, Silvestri L, et al. The human counterpart of zebrafish shiraz shows sideroblastic-like microcytic anemia and iron overload. Blood 2007;110(4):1353-8.

Campuzano V, Montermini L, Moltò MD, Pianese L, Cossée M, Cavalcanti F, et al. Friedreich's Ataxia: Autosomal Recessive Disease Caused by an Intronic GAA Triplet Repeat Expansion. Science (80-) 1996;271(5254):1423-7.

Casey JL, Hentze MW, Koeller DM, Wright Caughman S, Rouault TA, Klausner RD, et al. Iron-Responsive Elements: Regulatory RNA Sequences That Control mRNA Levels and Translation. Science (80-) 1988;240(4854):924-8.

Chan CTY, Deng W, Li F, Demott MS, Babu IR, Begley TJ, et al. Highly PredictiveReprogramming of tRNA ModificationsIs Linked to Selective Expression of Codon-Biased Genes. Chemical Research in Toxicology 2015;28(5):978.

Chan CTY, Dyavaiah M, DeMott MS, Taghizadeh K, Dedon PC, Begley TJ. A Quantitative Systems Approach Reveals Dynamic Control of tRNA Modifications during Cellular Stress. PLoS Genetics 2010;6(12):e1001247.

Chan CTY, Pang YLJ, Deng W, Babu IR, Dyavaiah M, Begley TJ, et al. Reprogramming of tRNA modifications controls the oxidative stress response by codon-biased translation of proteins. Nature Communications 2012;3:937.

Chan PP, Lowe TM. GtRNAdb 2.0: an expanded database of transfer RNA genes identified in complete and draft genomes. Nucleic Acids Research 2016;44(Database issue):D184.

Chen Y-T, Hims MM, Shetty RS, Mull J, Liu L, Leyne M, et al. Loss of Mouse Ikbkap, a Subunit of Elongator, Leads to Transcriptional Deficits and Embryonic Lethality That Can Be Rescued by Human IKBKAP. Molecular Cell Biology 2009;29(3):736.

Chiku T, Padovani D, Zhu W, Singh S, Vitvitsky V, Banerjee R. H2S biogenesis by human cystathionine gamma-lyase leads to the novel sulfur metabolites lanthionine and

homolanthionine and is responsive to the grade of hyperhomocysteinemia. Journal Biological Chemistry 2009;284(17):11601-12.

Chowdhury MM, Dosche C, Löhmannsröben H-G, Leimkühler S. Dual role of the molybdenum cofactor biosynthesis protein MOCS3 in tRNA thiolation and molybdenum cofactor biosynthesis in humans. Journal of Biological Chemistry 2012;287(21):17297-307.

Chujo T, Tomizawa K. Human transfer RNA modopathies: diseases caused by aberrations in transfer RNA modifications. The FEBS Journal 2021;288(24):7096-122.

Cohen HJ, Fridovich I. Hepatic sulfite oxidase. Purification and properties. Journal of Biological Chemistry 1971;246(2):359-66.

Cohen JS, Srivastava S, Farwell KD, Lu HM, Zeng W, Lu H, et al. ELP2 is a novel gene implicated in neurodevelopmental disabilities. American Journal of Medical Genetics Part A 2015;167(6):1391-5.

Copela LA, Fernandez CF, Sherrer RL, Wolin SL. Competition between the Rex1 exonuclease and the La protein affects both Trf4p-mediated RNA quality control and pre-tRNA maturation. RNA 2008;14(6):1214.

Craig EA, Marszalek J. A specialized mitochondrial molecular chaperone system: a role in formation of Fe/S centers. Cellular and Molecular Life Science 2002;59(10):1658-65.

Crawhall JC, Parker R, Sneddon W, Young EP, Ampola MG, Efron ML, et al. Beta Mercaptolactate-Cysteine Disulfide: Analog of Cystine in the Urine of a Mentally Retarded Patient. Science (80-) 1968;160(3826):419-20.

Cupp-Vickery JR, Urbina H, Vickery LE. Crystal structure of IscS, a cysteine desulfurase from Escherichia coli. Journal of Molecular Biology 2003;330(5):1049-59.

Dauden MI, Kosinski J, Kolaj-Robin O, Desfosses A, Ori A, Faux C, et al. Architecture of the yeast Elongator complex. EMBO Reports 2017;18(2):264-79.

Dewe JM, Whipple JM, Chernyakov I, Jaramillo LN, Phizicky EM. The yeast rapid tRNA decay pathway competes with elongation factor 1A for substrate tRNAs and acts on tRNAs lacking one or more of several modifications. RNA 2012;18(10):1886.

Dewez M, Bauer F, Dieu M, Raes M, Vandenhaute J, Hermand D. The conserved Wobble uridine tRNA thiolase Ctu1-Ctu2 is required to maintain genome integrity. Proceedings of the National Academy of Sciences of the United States of America 2008;105(14):5459-64.

Dhami N, Trivedi DK, Goodacre R, Mainwaring D, Humphreys DP. Mitochondrial aconitase is a key regulator of energy production for growth and protein expression in Chinese hamster ovary cells. Metabolomics 2018a;14(10):1-16.

Distrutti E, Sediari L, Mencarelli A, Renga B, Orlandi S, Antonelli E, et al. Evidence that hydrogen sulfide exerts antinociceptive effects in the gastrointestinal tract by activating KATP channels. Journal of pharmacology & experimental therapeutics 2006;316(1):325-35.

Du J, Johnson LM, Jacobsen SE, Patel DJ. DNA methylation pathways and their crosstalk with histone methylation. National Reviews Molecular Cell Biology 2015;16(9):519-32.

Du Y, Bao J, Zhang M ju, Li L lan, Xu XL, Chen H, et al. Targeting ferroptosis contributes to ATPR-induced AML differentiation via ROS-autophagy-lysosomal pathway. Gene 2020;755:144889.

El Yacoubi B, Bailly M, de Crécy-Lagard V. Biosynthesis and Function of Posttranscriptional Modifications of Transfer RNAs. Annual Review of Genetics 2012;46(1):69-95.

Enokido Y, Suzuki E, Iwasawa K, Namekata K, Okazawa H, Kimura H. Cystathionine β-synthase, a key enzyme for homocysteine metabolism, is preferentially expressed in the radial glia/astrocyte lineage of developing mouse CNS. The FASEB Journal 2005;19(13):1854-6.

Esberg A, Huang B, Johansson MJO, Byström AS. Elevated Levels of Two tRNA Species Bypass the Requirement for Elongator Complex in Transcription and Exocytosis. Molecular Cell 2006;24(1):139-48.

Fauman EB, Cogswell JP, Lovejoy B, Rocque WJ, Holmes W, Montana VG, et al. Crystal structure of the catalytic domain of the human cell cycle control phosphatase, Cdc25A. Cell 1998;93(4):617-25.

Feitelson MA, Arzumanyan A, Kulathinal RJ, Blain SW, Holcombe RF, Mahajna J, et al. Sustained proliferation in cancer: Mechanisms and novel therapeutic targets. Semin Cancer Biol 2015;35(Suppl):S25-54.

Fontecave M. Iron-sulfur clusters: ever-expanding roles. Nature Chemical Biology 2006 24 2006;2(4):171-4.

Fräsdorf B, Radon C, Leimkühler S. Characterization and interaction studies of two isoforms of the dual localized 3-mercaptopyruvate sulfurtransferase TUM1 from humans. Journal of Biological Chemistry 2014;289(50):34543-56.

Frohloff F, Fichtner L, Jablonowski D, Breunig KD, Schaffrath R. Saccharomyces cerevisiae Elongator mutations confer resistance to the Kluyveromyces lactis zymocin. EMBO Journal 2001;20(8):1993.

Fu M, Zhang W, Wu L, Yang G, Li H, Wang R. Hydrogen sulfide (H2S) metabolism in mitochondria and its regulatory role in energy production. Proceedings of the National Academy of Sciences of the United States of America 2012;109(8):2943-8.

Fu Z, Liu X, Geng B, Fang L, Tang C. Hydrogen sulfide protects rat lung from ischemia-reperfusion injury. Life Science 2008;82(23-24):1196-202.

Fujihara KM, Zhang BZ, Jackson TD, et al. Eprenetapopt triggers ferroptosis, inhibits NFS1 cysteine desulfurase, and synergizes with serine and glycine dietary restriction. Science Advances. 2022;8(37)

Fukuto JM, Carrington SJ, Tantillo DJ, Harrison JG, Ignarro LJ, Freeman BA, et al. Small Molecule Signaling Agents: The Integrated Chemistry and Biochemistry of Nitrogen Oxides, Oxides of Carbon, Dioxygen, Hydrogen Sulfide, and Their Derived Species. Chemical Research in Toxicology 2012;25(4):769.

Fuss JO, Tsai CL, Ishida JP, Tainer JA. Emerging critical roles of Fe-S clusters in DNA replication and repair. Biochimica et Biophysica Acta 2015;1853(6):1253.

Garattini E, Mendel R, Romão MJ, Wright R, Terao M. Mammalian molybdo-flavoenzymes, an expanding family of proteins: structure, genetics, regulation, function and pathophysiology. Biochemical Journal 2003;372(Pt 1):15-32.

Geng B, Yang J, Qi Y, Zhao J, Pang Y, Du J, et al. H2S generated by heart in rat and its effects on cardiac function. Biochemical and Biophysical Research Communications 2004;313(2):362-8.

Ghezzi D, Baruffini E, Haack TB, Invernizzi F, Melchionda L, Dallabona C, et al. Mutations of the Mitochondrial-tRNA Modifier MTO1 Cause Hypertrophic Cardiomyopathy and Lactic Acidosis. The American Journal for Human Genetics 2012;90(6):1079.

Glatt S, Létoquart J, Faux C, Taylor NMI, Séraphin B, Müller CW. The Elongator subcomplex Elp456 is a hexameric RecA-like ATPase. Nature Structural & Molecular Biology 2012;19(3):314-20.

Goehring AS, Rivers DM, Sprague GF. Urmylation: A Ubiquitin-like Pathway that Functions during Invasive Growth and Budding in Yeast. Molecular Biology of the cell 2003;14(11):4329.

Goto YI, Nonaka I, Horai S. A mutation in the tRNALeu(UUR) gene associated with the MELAS subgroup of mitochondrial encephalomyopathies. Nature 1990 3486302 1990;348(6302):651-3.

Greiner R, Pálinkás Z, Bäsell K, Becher D, Antelmann H, Nagy P, et al. Polysulfides Link H2S to Protein Thiol Oxidation. Antioxidant Redox Signal 2013;19(15):1749.

Grubbs R, Vugrek O, Deisch J, Wagner C, Stabler S, Allen R, et al. S-adenosylhomocysteine hydrolase deficiency: two siblings with fetal hydrops and fatal outcomes. Journal of Inherited Metabolic Disease 2010;33(6):705-13.

Gruenewald S, Wahl B, Bittner F, Hungeling H, Kanzow S, Kotthaus J, et al. The fourth molybdenum containing enzyme mARC: Cloning and involvement in the activation of N-hydroxylated prodrugs. Journal of Medicinal Chemistry 2008;51(24):8173-7.

Guo Q, Li L, Hou S, Yuan Z, Li C, Zhang W, et al. The Role of Iron in Cancer Progression. Frontiers in Oncology 2021;11:4571.

Gutzke G, Fischer B, Mendel RR, Schwarz G. Thiocarboxylation of Molybdopterin Synthase Provides Evidence for the Mechanism of Dithiolene Formation in Metal-binding Pterins. Journal of Biological Chemistry 2001;276(39):36268-74.

Hannestad U, Mårtensson J, Sjödahl R, Sörbo B. 3-mercaptolactate cysteine disulfiduria: biochemical studies on affected and unaffected members of a family. Biochemical Medicine 1981;26(1):106-14.

Hänzelmann P, Schwarz G, Mendel RR. Functionality of alternative splice forms of the first enzymes involved in human molybdenum cofactor biosynthesis. Journal of Biologcal Chemistry 2002;277(21):18303-12.

Herst PM, Tan AS, Scarlett DJG, Berridge M V. Cell surface oxygen consumption by mitochondrial gene knockout cells. Biochimica et Biophysica Acta 2004;1656(2-3):79-87.

Hidese R, Mihara H, Esaki N. Bacterial cysteine desulfurases: versatile key players in biosynthetic pathways of sulfur-containing biofactors. Applied Microbiology and Biotechnology 2011 911 2011;91(1):47-61.

Hille R, Nishino T, Bittner F. Molybdenum enzymes in higher organisms. Coordination Chemistry Review 2011;255(9-10):1179-205.

Hoagland MB, Stephenson ML, Scott JF, Hecht LI, Zamecnik PC. A soluble ribonucleic acid intermediate in protein synthesis. Journal of Biological Chemistry 1958;231(1):241-57.

Hochstrasser M. Evolution and function of ubiquitin-like protein-conjugation systems. Nature Cell Biology 2000, pagesE153–E157

Hofmann K, Bucher P, Kajava A V. A model of Cdc25 phosphatase catalytic domain and Cdk-interaction surface based on the presence of a rhodanese homology domain. Journal of Molecular Biology 1998;282(1):195-208.

Hollstein M, Sidransky D, Vogelstein B, Harris CC. p53 mutations in human cancers. Science 1991;253(5015):49-53.

Hover BM, Yokoyama K. C-terminal glycine-gated radical initiation by GTP 3′,8-cyclase in the molybdenum cofactor biosynthesis. Journal of American Chemical Society 2015;137(9):3352-9.

Huang B, Jian L, Byström AS. A genome-wide screen identifies genes required for formation of the wobble nucleoside 5-methoxycarbonylmethyl-2-thiouridine in Saccharomyces cerevisiae. RNA 2008;14(10):2183-94.

Huang B, Johansson MJO, Byström AS. An early step in wobble uridine tRNA modification requires the Elongator complex. RNA 2005;11(4):424.

Huang GT, Yu JSK. Enzyme Catalysis that Paves the Way for S-Sulfhydration via Sulfur Atom Transfer. Journal of Physical Chemistry B 2016;120(20):4608-15.

Ichida K, Amaya Y, Okamoto K, Nishino T. Mutations Associated with Functional Disorder of Xanthine Oxidoreductase and Hereditary Xanthinuria in Humans. International Journal of Molecular Sciences 2012, Vol 13, Pages 15475-15495 2012;13(11):15475-95.

Ichida K, Matsumura T, Sakuma R, Hosoya T, Nishino T. Mutation of Human Molybdenum Cofactor Sulfurase Gene Is Responsible for Classical Xanthinuria Type II. Biochemical and Biophysical Research Communications 2001;282(5):1194-200.

Ikeuchi Y, Shigi N, Kato JI, Nishimura A, Suzuki T. Mechanistic Insights into Sulfur Relay by Multiple Sulfur Mediators Involved in Thiouridine Biosynthesis at tRNA Wobble Positions. Molecular Cell 2006;21(1):97-108.

Imlay JA. Iron-sulphur clusters and the problem with oxygen. Molecular Microbiology 2006;59(4):1073-82.

Ito A. Hepatic sulfite oxidase identified as cytochrome b5-like pigment extractable from mitochondria by hypotonic treatment. Journal of Biochemistry 1971;70(6):1061-4.

Jeltsch A, Broche J, Bashtrykov P. Molecular Processes Connecting DNA Methylation Patterns with DNA Methyltransferases and Histone Modifications in Mammalian Genomes. Genes (Basel) 2018; Nov 21;9(11):566.

Johansson MJO, Esberg A, Huang B, Björk GR, Byström AS. Eukaryotic Wobble Uridine Modifications Promote a Functionally Redundant Decoding System. Molecular Cell Biology 2008;28(10):3301-12.

Johnson DG, Walker CL. cyclins and cell cycle checkpoints. Annuual Reviews of Pharmacology and Toxicology 1999;39(1):295-312.

Johnson JL, Waud WR, Rajagopalan K V., Duran M, Beemer FA, Wadman SK. Inborn errors of molybdenum metabolism: combined deficiencies of sulfite oxidase and xanthine dehydrogenase in a patient lacking the molybdenum cofactor. Proceedings of the National Academy of Sciences of the United States of America 1980;77(6):3715-9.

Johnson-Winters K, Tollin G, Enemark JH. Elucidating the Catalytic Mechanism of Sulfite Oxidizing Enzymes using Structural, Spectroscopic and Kinetic Analyses. Biochemistry 2010;49(34):7242.

Kabil O, Vitvitsky V, Banerjee R. Sulfur as a signaling nutrient through hydrogen sulfide. Annual Review of Nutrition 2014;34:171-205.

Kadaba S, Krueger A, Trice T, Krecic AM, Hinnebusch AG, Anderson J. Nuclear surveillance and degradation of hypomodified initiator tRNAMet in S. cerevisiae. Genes & Development 2004;18(11):1227.

Kambampati R, Lauhon CT. MnmA and IscS Are Required for in Vitro 2-Thiouridine Biosynthesis in Escherichia coli. 2003;42(4):1109-17.

Kessler D. Enzymatic activation of sulfur for incorporation into biomolecules in prokaryotes. FEMS Microbiology Reviews 2006;30(6):825-40.

Keyse SM, Ginsburg M. Amino acid sequence similarity between CL100, a dual-specificity MAP kinase phosphatase and cdc25. Trends in Biochemical Sciences 1993;18(10):377-8.

Kimura H, Shibuya N, Kimura Y. Hydrogen sulfide is a signaling molecule and a cytoprotectant. Antioxidants & Redox Signaling 2012;17(1):45-57.

Kimura Y, Koike S, Shibuya N, Lefer D, Ogasawara Y, Kimura H. 3-Mercaptopyruvate sulfurtransferase produces potential redox regulators cysteine- and glutathione-persulfide (Cys-SSH and GSSH) together with signaling molecules H_2S_2, H_2S_3 and H_2S. Science Report

Kimura Y, Toyofuku Y, Koike S, Shibuya N, Nagahara N, Lefer D, et al. Identification of H2S3 and H_2S produced by 3-mercaptopyruvate sulfurtransferase in the brain. Science Reports 2015;5(1):1-11.

Kisker C, Schindelin H, Pacheco A, Wehbi WA, Garrett RM, Rajagopalan K V., et al. Molecular basis of sulfite oxidase deficiency from the structure of sulfite oxidase. Cell 1997;91(7):973-83.

Klein JM, Schwarz G. Cofactor-dependent maturation of mammalian sulfite oxidase links two mitochondrial import pathways. Journal of Cell Science 2012;125(20):4876-4855.

Kohl JB, Mellis A-T, Schwarz G. Homeostatic impact of sulfite and hydrogen sulfide on cysteine catabolism. Bristish Journal of pharmacology 201;176(4):554-570.

Koike S, Nishimoto S, Ogasawara Y. Cysteine persulfides and polysulfides produced by exchange reactions with H2S protect SH-SY5Y cells from methylglyoxal-induced toxicity through Nrf2 activation. Redox Biology 2017;12:530.

Kolluru GK, Shen X, Bir SC, Kevil CG. Hydrogen Sulfide Chemical Biology: Pathophysiological roles and detection. Nitric Oxide 2013;35:5.

Kolluru GK, Shen X, Yuan S, Kevil CG. Gasotransmitter Heterocellular Signaling. Antioxid Redox Signal 2017;26(16):936.

Krepinsky K, Leimkühler S. Site-directed mutagenesis of the active site loop of the rhodanese-like domain of the human molybdopterin synthase sulfurase MOCS3. FEBS Journal 2007;274(11):2778-87.

Krogan NJ, Greenblatt JF. Characterization of a Six-Subunit Holo-Elongator Complex Required for the Regulated Expression of a Group of Genes in Saccharomyces cerevisiae. Molecular and Cellular Biology 2001;21(23):8203.

Laggner H, Hermann M, Esterbauer H, Muellner MK, Exner M, Gmeiner BMK, et al. The novel gaseous vasorelaxant hydrogen sulfide inhibits angiotensin-converting enzyme activity of endothelial cells. Journal of Hypertension 2007;25(10):2100-4.

Lambert JMR, Gorzov P, Veprintsev DB, Söderqvist M, Segerbäck D, Bergman J, et al. PRIMA-1 Reactivates Mutant p53 by Covalent Binding to the Core Domain. Cancer Cell 2009;15(5):376-88.

Land T, Rouault TA. Targeting of a Human Iron–Sulfur Cluster Assembly Enzyme, nifs, to Different Subcellular Compartments Is Regulated through Alternative AUG Utilization. Molecular Cell 1998;2(6):807-15.

Lane DP. p53 from pathway to therapy. Carcinogenesis 2004;25(7):1077-81.

Lange H, Kaut A, Kispal G, Lill R. A mitochondrial ferredoxin is essential for biogenesis of cellular iron-sulfur proteins. Proc Natl Acad Sci U S A 2000;97(3):1050-5.

Laxman S, Sutter BM, Wu X, Kumar S, Guo X, Trudgian DC, et al. Sulfur Amino Acids Regulate Translational Capacity and Metabolic Homeostasis through Modulation of tRNA Thiolation. Cell 2013;154(2):416-29.

Lec JC, Boutserin S, Mazon H, Mulliert G, Boschi-Muller S, Talfournier F. Unraveling the Mechanism of Cysteine Persulfide Formation Catalyzed by 3-Mercaptopyruvate Sulfurtransferases. ACS Catalysis 2018;8(3):2049-59.

Leidel S, Pedrioli Patrick G. A., Bucher T, Brost R, Costanzo M, Schmidt A, et al. Ubiquitin-related modifier Urm1 acts as a sulphur carrier in thiolation of eukaryotic transfer RNA. Nature 2009;458(7235):228-32.

Leimkühler S, Bühning M, Beilschmidt L, Leimkühler S, Bühning M, Beilschmidt L. Shared Sulfur Mobilization Routes for tRNA Thiolation and Molybdenum Cofactor Biosynthesis in Prokaryotes and Eukaryotes. Biomolecules 2017;7(4):5.

Leimkühler S. Shared function and moonlighting proteins in molybdenum cofactor biosynthesis. Biological Chemistry 2017;398(9):1009-26.

Li K, Xin Y, Xuan G, Zhao R, Liu H, Xia Y, et al. Escherichia coli Uses Separate Enzymes to Produce H2S and Reactive Sulfane Sulfur From L-cysteine. Frontiers in Microbiology 2019;10.

Li M, Xu C, Shi J, Ding J, Wan X, Chen D, et al. Fatty acids promote fatty liver disease via the dysregulation of 3-mercaptopyruvate sulfurtransferase/hydrogen sulfide pathway. Gut 2018;67(12)

Libiad M, Yadav PK, Vitvitsky V, Martinov M, Banerjee R. Organization of the human mitochondrial hydrogen sulfide oxidation pathway. Journal of Biological Chemistry 2014;289(45):30901-10.

Lill R, Mühlenhoff U. Maturation of iron-sulfur proteins in eukaryotes: Mechanisms, connected processes, and diseases. Annual Reviews of Biochemistry 2008;77:669-700.

Lill R. Iron-Sulfur Protein Biogenesis in Eukaryotes: Components and Mechanisms Iron-sulfur protein biogenesis View project. Annual Review of Cell and Developmental Biology 2006;22:457-86.

Lin Z, Zhao W, Diao W, Xie X, Wang Z, Zhang J, et al. Crystal structure of elongator subcomplex Elp4-6. Journal of Biological Chemistry 2012;287(25):21501-8.

Liu Y, Vinyard DJ, Reesbeck ME, Suzuki T, Manakongtreecheep K, Holland PL, et al. A [3Fe-4S] cluster is required for tRNA thiolation in archaea and eukaryotes. Proceedings of the National Academy of Sciences of the United States of America 2016;113(45):12703-8.

Mandal S, Guptan P, Owusu-Ansah E, Banerjee U. Mitochondrial Regulation of Cell Cycle Progression during Development as Revealed by the tenured Mutation in Drosophila. Dev Cell 2005;9(6):843-54.

Marelja Z, Mullick Chowdhury M, Dosche C, Hille C, Baumann O, Löhmannsröben HG, et al. The L-Cysteine Desulfurase NFS1 Is Localized in the Cytosol where it Provides the Sulfur for Molybdenum Cofactor Biosynthesis in Humans. PLoS One 2013;8(4):e60869.

Marelja Z, Stöcklein W, Nimtz M, Leimkühler S. A novel role for human Nfs1 in the cytoplasm: Nfs1 acts as a sulfur donor for MOCS3, a protein involved in molybdenum cofactor biosynthesis. Journal of Biological Chemistry 2008;283(37):25178-85.

Marshall KA, Reist M, Jenner P, Halliwell B. The neuronal toxicity of sulfite plus peroxynitrite is enhanced by glutathione depletion: implications for Parkinson's disease. Free Radical Biology and Medicine 1999;27(5-6):515-20.

Martínez-Reyes I, Diebold LP, Kong H, Schieber M, Huang H, Hensley CT, et al. TCA Cycle and Mitochondrial Membrane Potential Are Necessary for Diverse Biological Functions. Molecualr Cell 2016;61(2):199-209.

Matthies A, Rajagopalan K V., Mendel RR, Leimkühler S. Evidence for the physiological role of a rhodanese-like protein for the biosynthesis of the molybdenum cofactor in humans. Proceedings of the National Academy of Sciences of the United States of America 2004;101(16):5946.

Mayr SJ, Mendel RR, Schwarz G. Molybdenum cofactor biology, evolution and deficiency. Biochim Biophys Acta - Molecular Cell Research 2021;1868(1):118883.

Mellis AT, Roeper J, Misko AL, Kohl J, Schwarz G. Sulfite Alters the Mitochondrial Network in Molybdenum Cofactor Deficiency. Frontiers in Genetics 2020;11.

Méplan C, Richard MJ, Hainaut P. Metalloregulation of the tumor suppressor protein p53: zinc mediates the renaturation of p53 after exposure to metal chelators in vitro and in intact cells. Oncogene 2000 1946 2000;19(46):5227-36.

Mettert EL, Kiley PJ. Fe-S Proteins that Regulate Gene Expression. Biochimica et Biophysica Acta 2015;1853(6):1284.

Mijit M, Caracciolo V, Melillo A, Amicarelli F, Giordano A. Role of p53 in the Regulation of Cellular Senescence. Biomolecules 2020;10(3).

Mikami Y, Shibuya N, Kimura Y, Nagahara N, Ogasawara Y, Kimura H. Thioredoxin and dihydrolipoic acid are required for 3-mercaptopyruvate sulfurtransferase to produce hydrogen sulfide. Biochemical Journal 2011;439(3):479-85.

Mochel F, Knight MA, Tong WH, Hernandez D, Ayyad K, Taivassalo T, et al. Splice Mutation in the Iron-Sulfur Cluster Scaffold Protein ISCU Causes Myopathy with Exercise Intolerance. American Journal for Human Genetics 2008;82(3):652-60.

Módis K, Asimakopoulou A, Coletta C, Papapetropoulos A, Szabo C. Oxidative stress suppresses the cellular bioenergetic effect of the 3-mercaptopyruvate sulfurtransferase/hydrogen sulfide pathway. Biochemical & Biophysical Research Communication 2013;433(4):401-7.

Módis K, Ramanujam VMS, Govar AA, Lopez E, Anderson KE, Wang R, et al. Cystathionine-γ-lyase (CSE) deficiency increases erythropoiesis and promotes mitochondrial electron transport via the upregulation of coproporphyrinogen III oxidase and consequent stimulation of heme biosynthesis. Biochemical Pharmacology 2019;169:113604.

Moriwaki Y, Yamamoto T, Higashino K. Distribution and pathophysiologic role of molybdenum-containing enzymes. Histology & Histopathology 1997;12(2):513-24.

Moukadiri I, Garzón MJ, Björk GR, Armengod ME. The output of the tRNA modification pathways controlled by the Escherichia coli MnmEG and MnmC enzymes depends on the growth conditions and the tRNA species. Nucleic Acids Research 2014;42(4):2602.

Mudd SH, Poole JR. Labile methyl balances for normal humans on various dietary regimens. Metabolism 1975;24(6):721-35.

Mühlenhoff U, Stadler JA, Richhardt N, Seubert A, Eickhorst T, Schweyen RJ, et al. A Specific Role of the Yeast Mitochondrial Carriers Mrs3/4p in Mitochondrial Iron Acquisition under Iron-limiting Conditions. Journal of Biological Chemistry 2003;278(42):40612-20.

Murphy B, Bhattacharya R, Mukherjee P. Hydrogen sulfide signaling in mitochondria and disease. FASEB Journal 2019;33(12):13098.

Nagahara N, Nishino T. Role of amino acid residues in the active site of rat liver mercaptopyruvate sulfurtransferase. CDNA cloning, overexpression, and site-directed mutagenesis. Journal of Biological Chemistry 1996;271(44):27395-401.

Nagahara N, Okazaki T, Nishino T. Cytosolic mercaptopyruvate sulfurtransferase is evolutionarily related to mitochondrial rhodanese. Striking similarity in active site amino acid sequence and the increase in the mercaptopyruvate sulfurtransferase activity of rhodanese by site-directed mutagenesis. Journal of Biological Chemistry 1995;270(27):16230-5.

Nakai Y, Nakai M, Hayashi H. Thio-modification of yeast cytosolic tRNA requires a ubiquitin-related system that resembles bacterial sulfur transfer systems. Journal of Biological Chemistry 2008;283(41):27469-76.

Nakai Y, Nakai M, Lill R, Suzuki T, Hayashi H. Thio modification of yeast cytosolic tRNA is an iron-sulfur protein-dependent pathway. Molecular Cell Biology 2007;27(8):2841-7.

Nakai Y, Yoshihara Y, Hayashi H, Kagamiyama H. cDNA cloning and characterization of mouse nifS-like protein, m-Nfs1: mitochondrial localization of eukaryotic NifS-like proteins. FEBS Lett 1998;433(1-2):143-8.

Netz DJA, Mascarenhas J, Stehling O, Pierik AJ, Lill R. Maturation of cytosolic and nuclear iron-sulfur proteins. Trends in Cell Biology 2014;24(5):303-12.

Neukranz Y, Kotter A, Beilschmidt L, Marelja Z, Helm M, Gräf R, et al. Analysis of the Cellular Roles of MOCS3 Identifies a MOCS3-Independent Localization of NFS1 at the Tips of the Centrosome. Biochemistry 2019;58(13):1786-98.

Nicholson RA, Roth SH, Zhang A, Zheng J, Brookes J, Skrajny B, et al. Inhibition of respiratory and bioenergetic mechanisms by hydrogen sulfide in mammalian brain. Journal of Toxicology and Environmental Health 1998;54(6):491-507.

Niederwieser A, Giliberti P, Baerlocher K. β-mercaptolactate cysteine disulfiduria in two normal sisters. Isolation and characterization of β-mercaptolactate cysteine disulfide. Clinica Chimica Acta 1973;43(3):405-16.

Niknahad H, O'Brien PJ. Mechanism of sulfite cytotoxicity in isolated rat hepatocytes. Chemico-Biological Interactions 2008;174(3):147-54.

Noma A, Sakaguchi Y, Suzuki T. Mechanistic characterization of the sulfur-relay system for eukaryotic 2-thiouridine biogenesis at tRNA wobble positions. Nucleic Acids Research 2009;37(4):1335-52.

Olivier M, Eeles R, Hollstein M, Khan MA, Harris CC, Hainaut P. The IARC TP53 database: New online mutation analysis and recommendations to users. Human Mutations 2002;19(6):607-14.

Olney JW, Misra CH, Gubareff T De. Cysteine-S-Sulfate: Brain Damaging Metabolite in Sulfite Oxidase Deficiency. Journal of Neuropathology & Experimental Neurology 1975;34(2):167-77.

Olsson A, Lind L, Thornell LE, Holmberg M. Myopathy with lactic acidosis is linked to chromosome 12q23.3–24.11 and caused by an intron mutation in the ISCU gene resulting in a splicing defect. Human Molecular Genetics 2008;17(11):1666-72.

Palenchar PM, Buck CJ, Cheng H, Larson TJ, Mueller EG. Evidence that ThiI, an enzyme shared between thiamin and 4-thiouridine biosynthesis, may be a sulfurtransferase that proceeds through a persulfide intermediate. Journal of Biological Chemistry 2000;275(12):8283-6.

Patel P, Vatish M, Heptinstall J, Wang R, Carson RJ. The endogenous production of hydrogen sulphide in intrauterine tissues. Reproductive Biology and Endocrinology 2009;7(1):1-9.

Paul BD, Snyder SH, Kashfi K. Effects of hydrogen sulfide on mitochondrial function and cellular bioenergetics. Redox Biology 2021;38:101772.

Pedre B, Dick TP. 3-Mercaptopyruvate sulfurtransferase: An enzyme at the crossroads of sulfane sulfur trafficking. Biological Chemistry 2021;402(3):223-37.

Peleli M, Bibli SI, Li Z, Chatzianastasiou A, Varela A, Katsouda A, et al. Cardiovascular phenotype of mice lacking 3-mercaptopyruvate sulfurtransferase. Biochemical Pharmacology 2020;176.

Philipp M, John F, Ringli C. The cytosolic thiouridylase CTU2 of Arabidopsis thaliana is essential for posttranscriptional thiolation of tRNAs and influences root development. BMC Plant Biology 2014;14(1):1-8.

Ramasamy S, Singh S, Taniere P, Langman MJS, Eggo MC. Sulfide-detoxifying enzymes in the human colon are decreased in cancer and upregulated in differentiation. American Journal of Physiology-Gastrointestinal and Liver 2006;291(2).

Ray WK, Zeng G, Potters MB, Mansuri AM, Larson TJ. Characterization of a 12-kilodalton rhodanese encoded by glpE of Escherichia coli and its interaction with thioredoxin. Journal of Bacteriology 2000;182(8):2277-84.

Reiffenstein RJ, Hulbert WC, Roth SH. Toxicology of hydrogen sulfide [En ligne]. Annual Review of Pharmacology and Toxicology. 1992. p 109-34.

Reiss J, Hahnewald R. Molybdenum cofactor deficiency: Mutations in GPHN, MOCS1, and MOCS2. Human Mutations 2011;32(1):10-8.

Robinson HC, Pasternak CA. The isolation of S-sulphoglutathione from the small intestine of the rat. Biochemical Journal 1964;93(3):487-92.

Roche B, Aussel L, Ezraty B, Mandin P, Py B, Barras F. Iron/sulfur proteins biogenesis in prokaryotes: Formation, regulation and diversity. Biochimica et Biophysica Acta 2013;1827(3):455-69.

Roman HB, Hirschberger LL, Krijt J, Valli A, Kožich V, Stipanuk MH. The cysteine dioxgenase knockout mouse: altered cysteine metabolism in nonhepatic tissues leads to excess H2S/HS(-) production and evidence of pancreatic and lung toxicity. Antioxidant Redox Signal. 2013;19(12):1321-1336.

Roundtree IA, Evans ME, Pan T, He C. Dynamic RNA Modifications in Gene Expression Regulation. Cell 2017;169(7):1187-200.

Schaffer SW, Jong CJ, Warner D, Ito T, Azuma J. Taurine deficiency and MELAS are closely related syndromes. Advances in Experimental Medicine and Biology 2013;776:153-65.

Schaffrath R, Leidel SA. Wobble uridine modifications–a reason to live, a reason to die?! RNA Biology 2017;14(9):1209.

Schieke SM, McCoy JP, Finkel T, Finkel T. Coordination of mitochondrial bioenergetics with G1 phase cell cycle progression. Cell Cycle 2008;7(12):1782-7.

Schmitz J, Chowdhury MM, Hänzelmann P, Nimtz M, Lee EY, Schindelin H, et al. The sulfurtransferase activity of Uba4 presents a link between ubiquitin-like protein conjugation and activation of sulfur carrier proteins. Biochemistry 2008;47(24):6479-89.

Schwarz G, Mendel RR. molybdenum cofactor biosynthesis and molybdenum enzymes. Annual Review of Plant Biology 2006;57(1):623-47.

Schwarz G. Molybdenum cofactor and human disease. Current Opinion in Chemical Biology 2016;31:179-87.

Schwarz G. Molybdenum cofactor biosynthesis and deficiency. Cell Mol Life Sci 2005;62(23):2792-810.

Sebastiaan Winkler G, Petrakis TG, Ethelberg S, Tokunaga M, Erdjument-Bromage H, Tempst P, et al. RNA Polymerase II Elongator Holoenzyme Is Composed of Two Discrete Subcomplexes. Journal of Biological Chemistry 2001;276(35):32743-9.

Setiaputra DT, Cheng DT, Lu S, Hansen JM, Dalwadi U, Lam CH, et al. Molecular architecture of the yeast Elongator complex reveals an unexpected asymmetric subunit arrangement. EMBO Reports 2017;18(2):280-91.

Shaheen R, Al-Salam Z, El-Hattab AW, Alkuraya FS. The syndrome dysmorphic facies, renal agenesis, ambiguous genitalia, microcephaly, polydactyly and lissencephaly (DREAM-PL): Report of two additional patients. American Journal of Medical Genetics A 2016;170(12):3222-6.

Sheftel, Alex D et al. “Humans possess two mitochondrial ferredoxins, Fdx1 and Fdx2, with distinct roles in steroidogenesis, heme, and Fe/S cluster biosynthesis.” Proceedings of the National Academy of Sciences of the United States of America 2010 107,26: 11775-80.

Shi, Ruifeng et al. “Biogenesis of Iron-Sulfur Clusters and Their Role in DNA Metabolism.” Frontiers in cell and developmental biology 2021; 9 735678.

Shi Y, Ghosh M, Kovtunovych G, Crooks DR, Rouault TA. Both human ferredoxins 1 and 2 and ferredoxin reductase are important for iron-sulfur cluster biogenesis. Biochimica et Biophysica Acta - Mol Cell Res 2012;1823(2):484-92.

Shibuya N, Tanaka M, Yoshida M, Ogasawara Y, Togawa T, Ishii K, et al. 3-Mercaptopyruvate Sulfurtransferase Produces Hydrogen Sulfide and Bound Sulfane Sulfur in the Brain. Antioxidant Redox Signal 2009;11(4):703-14.

Shigi N. Biosynthesis and Degradation of Sulfur Modifications in tRNAs. International Journal of Molecular Science 2021;22(21).

Shigi N. Biosynthesis and functions of sulfur modifications in tRNA. Frontiers in Genetics 2014;5(APR):67.

Sierzputowska-Gracz H, Agris PF, Sochacka E, Malkiewiez A, Kuo K, Gehrke CW. Chemistry and Structure of Modified Uridines in the Anticodon, Wobble Position of Transfer RNA Are Determined by Thiolation. Jouranl of American Chemical Society 1987;109(23):7171-7.

Simpson CL, Lemmens R, Miskiewicz K, Broom WJ, Hansen VK, van Vught PWJ, et al. Variants of the elongator protein 3 (ELP3) gene are associated with motor neuron degeneration. Human Molecular Genetics 2009;18(3):472.

Singh S, Madzelan P, Stasser J, Weeks CL, Becker D, Spiro TG, et al. Modulation of the heme electronic structure and cystathionine beta-synthase activity by second coordination sphere ligands: The role of heme ligand switching in redox regulation. Jounral in Inorganic Biochemistry 2009;103(5):689-97.

Spallarossa A, Donahue JL, Larson TJ, Bolognesi M, Bordo D. Escherichia coli GlpE is a prototype sulfurtransferase for the single-domain rhodanese homology superfamily. Structure 2001;9(11):1117-25.

Stehling O, Wilbrecht C, Lill R. Mitochondrial iron–sulfur protein biogenesis and human disease. Biochimie 2014;100(1):61-77.

Stender S, Chakrabarti RS, Xing C, Gotway G, Cohen JC, Hobbs HH. Adult-onset liver disease and hepatocellular carcinoma in S-adenosylhomocysteine hydrolase deficiency. Molecular Genetics and Metabolism 2015;116(4):269-74.

Stipanuk MH. Metabolism of Sulfur-Containing Amino Acids: How the Body Copes with Excess Methionine, Cysteine, and Sulfide. Journal of Nutrition 2020;150(Suppl 1):2494S-2505S.

Stipanuk MH. Sulfur amino acid metabolism: pathways for production and removal of homocysteine and cysteine. Annual Review of Nutrition 2004;24:539-77.

Strauss KA, Ferreira C, Bottiglieri T, Zhao X, Arning E, Zhang S, et al. Liver transplantation for treatment of severe S-adenosylhomocysteine hydrolase deficiency. Molecular Genetics and Metabolism 2015;116(1-2):44-52.

Suzuki T. Biosynthesis and function of tRNA wobble modifications. 2005:23-69.

Suzuki T. The expanding world of tRNA modifications and their disease relevance. Nature Reviews Molecular Cell Biology 2021 226 2021;22(6):375-92.

Szabo C, Ransy C, Módis K, Andriamihaja M, Murghes B, Coletta C, et al. Regulation of mitochondrial bioenergetic function by hydrogen sulfide. Part I. Biochemical and physiological mechanisms. British Journal of Pharmacology 2014;171(8):2099-122.

Tan WH, Eichler FS, Hoda S, Lee MS, Baris H, Hanley CA, et al. Isolated sulfite oxidase deficiency: a case report with a novel mutation and review of the literature. Pediatrics 2005;116(3):757-66.

Taniguchi T, Kimura T. Role of 3-mercaptopyruvate sulfurtransferase in the formation of the iron-sulfur chromophore of adrenal ferredoxin. Biochimica et Biophysica Acta 1974;364(2):284-95.

Tay AS, Hu LF, Lu M, Wong PTH, Bian JS. Hydrogen sulfide protects neurons against hypoxic injury via stimulation of ATP-sensitive potassium channel/protein kinase C/extracellular signal-regulated kinase/heat shock protein 90 pathway. Neuroscience 2010;167(2):277-86.

Terzi EM, Sviderskiy VO, Alvarez SW, Whiten GC, Possemato R. Iron-sulfur cluster deficiency can be sensed by IRP2 and regulates iron homeostasis and sensitivity to ferroptosis independent of IRP1 and FBXL5. Science Advances 2021;7(22).

Teschner J, Lachmann N, Schulze J, Geisler M, Selbach K, Santamaria-Araujo J, et al. A Novel Role for Arabidopsis Mitochondrial ABC Transporter ATM3 in Molybdenum Cofactor Biosynthesis. Plant Cell 2012;22(2):468-80.

Tong WH, Rouault TA. Functions of mitochondrial ISCU and cytosolic ISCU in mammalian iron-sulfur cluster biogenesis and iron homeostasis. Cell Metabolism 2006;3(3):199-210.

Townsend DM, Tew KD, Tapiero H. Sulfur containing amino acids and human disease. Biomedicine & Pharmacotherapy 2004;58(1):47.

Trautwein B, Merz T, Denoix N, Szabo C, Calzia E, Radermacher P, et al. ΔMST and the Regulation of Cardiac CSE and OTR Expression in Trauma and Hemorrhage. Antioxidants 2021;10(2):1-13.

Trédan O, Galmarini CM, Patel K, Tannock IF. Drug Resistance and the Solid Tumor Microenvironment. Journal of the National Cancer Institute 2007;99(19):1441-54.

Uhrigshardt H, Singh A, Kovtunovych G, Ghosh M, Rouault TA. Characterization of the human HSC20, an unusual DnaJ type III protein, involved in iron-sulfur cluster biogenesis. Human Molecular Genetics 2010;19(19):3816-34.

Umeda N, Suzuki Takeo, Yukawa M, Ohya Y, Shindo H, Watanabe K, et al. Mitochondria-specific RNA-modifying enzymes responsible for the biosynthesis of the wobble base in

mitochondrial tRNAs: Implications for the molecular pathogenesis of human mitochondrial diseases. Journal of Biological Chemistry 2005;280(2):1613-24.

Velayutham, Murugesan et al. “Sulfite Oxidase Activity of Cytochrome c: Role of Hydrogen Peroxide.” Biochemistry and biophysics reports 2016; 96-104.

Veldman A, Santamaria-Araujo JA, Sollazzo S, Pitt J, Gianello R, Yaplito-Lee J, et al. Successful Treatment of Molybdenum Cofactor Deficiency Type A With cPMP. Pediatrics 2010;125(5):e1249-54.

Vickery LE, Cupp-Vickery JR. Molecular chaperones HscA/Ssq1 and HscB/Jac1 and their roles in iron-sulfur protein maturation. Critical Reviews in Biochemistry and Molecular Biology 2007;42(2):95-111.

Vousden KH, Lu X. Live or let die: the cell’s response to p53. Nature Reviews Cancer 2002 28 2002;2(8):594-604.

Wallace JL, Wang R. Hydrogen sulfide-based therapeutics: exploiting a unique but ubiquitous gasotransmitter. Nature Reviews Drug Discovery 2015;14(5):329-45.

Wardman P, Candeias LP. Fenton chemistry: An introduction. Radiation Research 1996;145(5):523-31.

Warnhoff K, Ruvkun G. Molybdenum cofactor transfer from bacteria to nematode mediates sulfite detoxification. Nature Chemical Biology 2019;15(5):480.

Wassman CD, Baronio R, Demir Ö, Wallentine BD, Chen CK, Hall L V., et al. Computational identification of a transiently open L1/S3 pocket for reactivation of mutant p53. Nature Communications 2013 41 2013;4(1):1-9.

Westley J, Adler H, Westley L, Nishida C. The sulfurtransferases. Fundamental and Applied Toxicology 1983;3(5):377-82.

Wiedemann N, Urzica E, Guiard B, Müller H, Lohaus C, Meyer HE, et al. Essential role of Isd11 in mitochondrial iron–sulfur cluster synthesis on Isu scaffold proteins. EMBO Journal 2006;25(1):184.

Xie X, Dai H, Zhuang B, Chai L, Xie Y, Li Y. Exogenous hydrogen sulfide promotes cell proliferation and differentiation by modulating autophagy in human keratinocytes. Biochemical and Biophysical Research Communications 2016;472(3):437-43.

Yadav PK, Yamada K, Chiku T, Koutmos M, Banerjee R. Structure and kinetic analysis of H_2S production by human mercaptopyruvate sulfurtransferase. Journal of Biological Chemistry 2013;288(27):20002-13.

Yajima H, Tokunaga M, Nakayama-Murayama A, Hishinuma F. Characterization of IKI1 and IKI3 Genes Conferring pGKL Killer Sensitivity on Saccharomyces cerevisiae. Bioscience, Biotechnology, and Biochemistry 1997;61(4):704-9.

Yang WS, Sriramaratnam R, Welsch ME, Shimada K, Skouta R, Viswanathan VS, et al. Regulation of ferroptotic cancer cell death by GPX4. Cell 2014;156(1-2):317-31.

Yokoyama S, Watanabe T, Murao K, Ishikura H, Yamaizumi Z, Nishimura S, et al. Molecular mechanism of codon recognition by tRNA species with modified uridine in the first position of the anticodon. Proceedings of the National Academy of Sciences of the United States of America 1985;82(15):4905.

Yonezawa D, Sekiguchi F, Miyamoto M, Taniguchi E, Honjo M, Masuko T, et al. A protective role of hydrogen sulfide against oxidative stress in rat gastric mucosal epithelium. Toxicology 2007;241(1-2):11-8.

Zanardo RCO, Brancaleone V, Distrutti E, Fiorucci S, Cirino G, Wallace JL, et al. Hydrogen sulfide is an endogenous modulator of leukocyte-mediated inflammation. FASEB Journal 2006;20(12):2118-20.

Zeharia A, Shaag A, Pappo O, Mager-Heckel AM, Saada A, Beinat M, et al. Acute Infantile Liver Failure Due to Mutations in the TRMU Gene. American Journal of Human Genetics 2009;85(3):401.

Zhang M, Liu Z, Le Y, Gu Z, Zhao H. Iron-Sulfur Clusters: A Key Factor of Regulated Cell Death in Cancer. Oxidative Medicine and Cellular Longevity 2022;7449941.

Zhang Q, Bykov VJN, Wiman KG, Zawacka-Pankau J. APR-246 reactivates mutant p53 by targeting cysteines 124 and 277. Cell Death Dis 2018 95 2018;9(5):1-12.

Zhang X, Vincent AS, Halliwell B, Wong KP. A Mechanism of Sulfite Neurotoxicity. Journal Biological Chemistry 2004;279(41):43035-45.

Zhang Y, Gladyshev VN. Molybdoproteomes and evolution of molybdenum utilization. Journal of Molecula Biology 2008;379(4):881.

Zheng L, White RH, Cash VL, Dean DR. Mechanism for the desulfurization of L-cysteine catalyzed by the nifS gene product. Biochemistry 1994;33(15):4714-20.

Zheng L, White RH, Cash VL, Jack RF, Dean DR. Cysteine desulfurase activity indicates a role for NIFS in metallocluster biosynthesis. Proceedings of the National Academy of Sciences of the United States of America 1993;90(7):2754-8.

Zheng YY, Wu Y, Begley TJ, Sheng J. Sulfur modification in natural RNA and therapeutic oligonucleotides. RSC Chemical Biology 2021;2(4):990-1003.

Zuhra K, Sousa PMF, Paulini G, Lemos AR, Kalme Z, Bisenieks I, et al. Screening Pyridine Derivatives against Human Hydrogen Sulfide-synthesizing Enzymes by Orthogonal Methods. Science Reports 2019 91 2019;9(1):1-14.

7 Acknowledgements

First and foremost, I would like to thank the Almighty God for giving me the knowledge, understanding and strength to complete this thesis.

I would like to express my profound gratitude to Prof. Dr. Silke Leimkühler for the invaluable guidance, patience, and encouragement. I really appreciate the feedbacks and advice, they were really instrumental for the successful completion of this work.

I extend my sincere appreciation to Prof. Dr. Feron Francois, Dr. Capraz Gaelle and Tai Tien of the AIX Marseille for their support during this thesis. I would like to thank them for providing guidance to the usage of the Seahorse instrument for my measurements.

I am also grateful to past and present lab mates and staff of Molecular enzymology, who have provided me with the necessary resources and support during my thesis. Their unwavering support and feedback have been instrumental in shaping this thesis.

I would like to extend my appreciation to my family and friends especially Ogunkola Matthew Olukunle, Ogunkola Michael Oluwatosin, Adebiyi Oluwatomisin Florence, Orukpabo Tokoni, Oginni Olayinka and Sangodare Francis for their unending support, encouragement, and understanding. Their constant support and encouragement have kept me motivated throughout this process, and I am deeply grateful for their love and kindness.

Finally, I thank my late parents Late Israel Olusoji Ogunkola and Late Clementina Iyabo Ogunkola for providing inspiration and drive to push through. I also thank them for giving me the resources to be educated to this level. I will forever be grateful for their sacrifices throughout their lifetime.

Thank you all for your support and encouragement throughout my thesis journey. I would never take this for granted.

8 Affirmation

Hiermit erkläre ich, Moses Ogunkola, dass ich die vorliegende Dissertation selbstständig und ohne unerlaubte Hilfsmittel angefertigt habe und von mir keine anderen als die angegebenen Quellen und Hilfsmittel verwendet wurden.

I, Moses Ogunkola, affirm that I have undertaken this PhD thesis on my own and only with the given references and devices.

_____	_____
Ort, Datum	Unterschrift

Manuscript I

The Human Mercaptopyruvate Sulfurtransferase TUM1 Is Involved in Moco Biosynthesis, Cytosolic tRNA Thiolation and Cellular Bioenergetics in Human Embryonic Kidney Cells.

biomolecules

MDPI

Article

The Human Mercaptopyruvate Sulfurtransferase TUM1 Is Involved in Moco Biosynthesis, Cytosolic tRNA Thiolation andCellular Bioenergetics in Human Embryonic Kidney Cells

Moses Olalekan Ogunkola [1], Gaelle Guiraudie-Capraz [2], Francois Feron [2] and Silke Leimkühler [1,*]

[1] Department of Molecular Enzymology, Institute of Biochemistry and Biology, University of Potsdam,Karl-Liebknecht Strasse 24–25, 14476 Potsdam-Golm, Germany

[2] Institute of NeuroPhysiopathology (INP), CNRS, Aix Marseille University, UMR 7051, CEDEX 5, 13385 Marseille, France

* Correspondence: sleim@uni-potsdam.de; Tel.: +49-331-977-5603

Abstract: Sulfur is an important element that is incorporated into many biomolecules in humans. The incorporation and transfer of sulfur into biomolecules is, however, facilitated by a series of different sulfurtransferases. Among these sulfurtransferases is the human mercaptopyruvate sulfurtransferase (MPST) also designated as tRNA thiouridine modification protein (TUM1). The role of the human TUM1 protein has been suggested in a wide range of physiological processes in the cell among which are but not limited to involvement in Molybdenum cofactor (Moco) biosynthesis, cytosolic tRNA thiolation and generation of H_2S as signaling molecule both in mitochondria and the cytosol.Previous interaction studies showed that TUM1 interacts with the L-cysteine desulfurase NFS1 andthe Molybdenum cofactor biosynthesis protein 3 (MOCS3). Here, we show the roles of TUM1 in human cells using CRISPR/Cas9 genetically modified Human Embryonic Kidney cells. Here, we show that TUM1 is involved in the sulfur transfer for Molybdenum cofactor synthesis and tRNA thiomodification by spectrophotometric measurement of the activity of sulfite oxidase and liquid chromatography quantification of the level of sulfur-modified tRNA. Further, we show that TUM1 has a role in hydrogen sulfide production and cellular bioenergetics.

Keywords: Moco biosynthesis; sulfite oxidase; cytosolic tRNA thiolation; 5-methoxycarbonylmethyl-2-thiouridine; H_2S biosynthesis; cellular bioenergetics

Citation: Ogunkola, M.O.; Guiraudie-Capraz, G.; Feron, F.; Leimkühler, S. The Human Mercaptopyruvate Sulfurtransferase TUM1 Is Involved in Moco Biosynthesis, Cytosolic tRNA Thiolation and Cellular Bioenergetics in Human Embryonic Kidney Cells. *Biomolecules* **2023**, *13*, 144. https://doi.org/10.3390/biom13010144

Academic Editors: Valérie De Crécy-Lagard and Juan Alfonzo

Received: 28 November 2022
Revised: 25 December 2022
Accepted: 28 December 2022
Published: 10 January 2023

1. Introduction

The human 3-mercaptopyruvate sulfurtransferase (MPST) (EC 2.8.1.2), also designated as TUM1 (tRNA thiouridine modification protein 1), belongs to an enzyme superfamily of proteins that contain a rhodanese-like domain (RLD) [1]. To date, the physiological function of rhodanese-like proteins is not fully understood, but rhodaneses have been linked to a wide variety of biological processes, including the detoxification of cyanide, the homeostasis of cellular sulfur in general, the participation in the degradation of L-cysteine, mitochondrial production of hydrogen sulfide (H_2S) as signaling molecule, in addition to the biosynthesis of enzymatic cofactors, vitamins and sulfur-containing nucleic acids in tRNAs [2–6]. A role of the human TUM1 protein was recently suggested to be involved in the two biosynthetic pathways of tRNA thiolation of cytosolic tRNAs and Moco biosynthesis by interacting with the protein MOCS3 in humans [7]. Initially, an involvement of the yeast TUM1 protein (tRNA thiouridine modification protein) in tRNA thiomodification had been identified before [1,8]. Human TUM1 has been shown to catalyze the desulfuration of 3-mercaptopyruvate to generate an enzyme-bound hydropersulfide [9], which then transfers the persulfide's outer sulfur atom to proteins or small molecule acceptors. MPST activity is also known to be involved in hydrogen sulfide generation, tRNA thiolation, protein urmylation and cyanide detoxification [9]. Tissue-specific changes in human MPST

expression correlate with aging and the development of metabolic disease [9]. Recently, high expression of MPST has been reported in cancer tissues due to its H_2S biosynthesis capability and a subsequent influence on cellular bioenergetics [10–13]. Deletion and overexpression experiments suggested that MPST contributes to oxidative stress resistance, mitochondrial respiratory function and the regulation of fatty acid metabolism [9].

Mammalian TUM1/MPST has been mostly studied for its physiological role in H_2S generation in cellular sulfur metabolism [6,14–16]. Human MPST is mainly expressed in kidney, liver, heart and neurological cells [17]. Patients have been reported to accumulate 3-Mercaptolactate (3 ML) in the urine. 3-mercaptopyruvate is converted to 3-ML due to the deficiency of TUM1, which converts the former to pyruvate [18,19]. Patients with mercaptolactate–cysteine disulfuiduria (MCDU) have been shown to have mental retardation [19], while in some cases, mental retardation was not recorded [20]. MPST knockout mice presented an increased anxiety-like behavior [21]. In addition, investigation of MPST knockout mouse brains revealed lack of cysteine-SSH and GSSH production with 50% decreased levels of total persulfated species [22].

The interaction of TUM1 with MOCS3 suggested that TUM1 is involved in tRNA thiolation and molybdenum cofactor (Moco) biosynthesis [7]. In Moco biosynthesis, two sulfur atoms are inserted into the cyclic pyranopterin monophosphate (cPMP) backbone, forming the dithiolene group of molybdopterin (MPT), which ligates the molybdenum atom and forms the molybdenum cofactor (Moco) [23]. The conversion of cPMP to MPT is catalyzed by MPT synthase, which is composed of MOCS2A and MOCS2B [24]. For regeneration of the thiocarboxylate group at the C-terminal glycine of MOCS2A in MPT synthase [25] MOCS3, TUM1 and NFS1 are suggested to be involved [7]. Moco biosynthesis and tRNA thiolation were suggested to share the same sulfur delivery pathway composed of NFS1, TUM1 and MOCS3 [7].

In humans, there are four molybdoenzymes, namely sulfite oxidase (SO) aldehyde oxidase (AOX), xanthine oxidase (XO) and the two mitochondrial amidoxime reducing components, mARC1 and mARC2 [26]. SO catalyzes the metabolic detoxification of sulfite to sulfate within the intermembrane space of the mitochondria [27]. In mammals, SO is highly expressed in the liver, kidney and heart and has very low expression in the spleen, brain, skeletal muscle and blood [28]. Sulfite toxicity is proposed to arise from the conversion of excess sulfite to sulfite radicals in the absence and presence of oxidative stress due to deficiency in SO [29]. In humans, deficiency in sulfite oxidase deficiency, which can arise from the mutation of genes encoding for proteins responsible for Moco biosynthesis (MocoCD) [30], can lead to mental retardation, epileptic seizures, brain atrophy and (dislocated ocular lenses) [31]. Recently, it was shown that, in Moco deficient patients, highly interconnected mitochondria are present, similar to what has been shown in mouse-derived fibroblasts [32]. It has been therefore concluded that altered mitochondrial dynamics are an important contributor to the disease phenotype of sulfite oxidase deficiency in Moco-deficient patients, and it has been suggested that MoCD should be included among the mitochondrial disorders [32].

Transfer RNAs from all organisms contain modified nucleosides, which are derivatives of the four major nucleosides: adenosine (A), guanosine (G), cytosine (C) and uridine (U) [33]. tRNAs specific for lysine, glutamate and glutamine in most organisms have a 2-thiouridine derivative (xm^5s^2U) at the wobble uridine at position 34 [34–37]. Thiolation modifications at the wobble uridine at position 34 (U34) present in tRNA of lysine, glutamine and glutamate are suggested to be important for enhanced translation efficiency and higher stability of tRNA binding to the ribosomal A site [38]. For the thiolation and formation of the mcm^5s^2U in the cytosol of eukaryotes, the biosynthesis of the 5 methoxy-carbonylmethyl group of the uracil ring is required for efficient 2 thiouri-dine formation in the cytoplasm [8]. In humans, it was shown that the proteins MOCS3, URM1, TUM1, CTU1 and CTU2 are involved in s^2U34 formation [39,40], while proteins of the ELP pathway synthesize the mcm5-group [41]. The ELP pathway includes the six subunits of the ELP-complex (ELP1–6) and the tRNA methyltransferase complex con-

taining TRM9 and TRM112 [42]. The URM1 protein (ubiquitin-related modifier) was shown to have a ubiquitin-like b-grasp-fold and to contain a conserved C-terminal double glycine-motif on which a thiocarboxylate group is formed for direct sulfur-transfer to mcm^5U34 in tRNA [25,36,43,44]. In contrast, the formation of τm^5s^2U34 for mitochondrial tRNALys, Gln, Glu requires different protein components compared to the ones identified in the cytosol, whereas details of the pathway are not completely resolved to date [45]. It was shown that lack of the τm^5s^2U modification in mitochondrial tRNALys from individuals with myoclonus epilepsy associated with ragged red fibers (MERRF) resulted in a marked defect in mitochondrial translation [46]. In this pathway, the MTU1 protein—which is a mitochondria-specific 2-thiouridylase responsible for the generation of τm^5s^2U in mammals—is required [47]. The sulfur is derived from mitochondrial NFS1, which is transferred via TUM1-Iso2 [7,48]. For the formation of the taurine group, the proteins GTPBP3 and MTO1 are required [47].

TUM1 catalyses the conversion of 3-mercaptopyruvate to pyruvate and a protein-bound persulfide, which is released as H_2S [9]. Three H_2S producing enzymes exist in humans, besides TUM1/MPST, the cystathionine-γ-lyase (CTH) and the cystathionin β-synthase (CBS). CBS and CTH are pyridoxal-phosphate (PLP)-dependent enzymes, which are differently expressed throughout tissues [49,50]. In the L-cysteine catabolism, the three enzymes are partly overlapping and complementary functions. Dysregulation of the H_2S producing system has been linked to increased cellular dysfunction in case of diseased/stressed states [51].

We have recently shown that human interaction studies most interestingly revealed interaction of TUM1 with the only L-cysteine desulfurase of human cells NFS1, which is central for sulfur transfer in FeS biosynthesis [52], Moco biosynthesis and tRNA thiolation [53]. TUM1-Iso1 was further shown to bind MOCS3 [7], a sulfur transferase implicated in Moco biosynthesis and tRNA thiolation [39]. We hence proposed a role for human TUM1 Moco biosynthesis and tRNA thiolation. Here, we show for the first time that knockout of TUM1 in human embryonic kidney (HEK) cells impacts cytosolic tRNA thiolation as well as the Moco-dependent enzyme Sulfite oxidase (SO). Further, we show that TUM1 impacts H_2S biosynthesis and cellular bioenergetics in HEK293T cells.

2. Materials and Methods

2.1. Materials

Sodium hydrosulfide (NaHS) obtained from (Sigma-Aldrich, Darmstadt, Hesse, Germany) was freshly dissolved in millipore water shortly before cell treatment.

2.2. Cultivation of Mammalian Cell Lines

HEK293T (DSMZ) cells were cultured in Dulbecco's modified Eagle's medium (DMEM, PAN-Biotech, Aidenbach, Bavaria, Germany) supplemented with 10% fetal bovine serum (FBS, PAN-Biotech, Aidenbach, Bavaria, Germany) and 2 mM L-glutamine (PAN-Biotech, Aidenbach, Bavaria, Germany). The cells were maintained at 37 °C and 5% CO_2 adherently in T75 or T25 cell culture flasks (Sarstedt, Nümbrecht, North Rhine-Westaphalia, Germany) until the cells were 90% confluent. The cells were detached via trypsin/EDTA (Gibco, Life Technologies, Darmstadt, Hesse, Germany) and passaged every 3–4 days.

2.3. Generating TUM1 Knockout Cells with CRISPR/Cas9

The CRISPR/Cas9 method was used to generate stable TUM1 knockout cell lines. The protocol was adapted from [54]. The method is based on a complementary gRNA to target the gene of interest providing a cleavage site for the Cas9 nuclease. The cleaved DNA is repaired by error prone nonhomologous end joining (NHEJ) leading to deletions, insertions or frameshifts preferentially resulting in loss of function mutations. gRNAs complementary to DNA near the start codon of the TUM1 gene were designed using MIT opensource (https://crispr.mit.edu/, accessed on 16 August 2017) [55]. The forward guide and the reverse guide were annealed using a standard protocol. They were constructed with *Bbs*I restriction

sites to enable cloning into the pSpCas9(BB)-2A-Puro vector (https://addgene.org/crispr/, on accessed on 1 September 2017) [56]. This vector already contains the scaffolding part of the gRNA and the gene for Cas9. The resulting plasmid was transiently transfected into the HEK293T cells. Positively transfected cells were selected with puromycin. Single cells were grown into colonies and analyzed via sequencing (GATC) and immunoblotting using an α-TUM1 antibody (Abcam, Rozenburg, Amsterdam, Netherlands).

2.4. Immunoblotting

Whole cell lysates (50–100 µg) were separated by sodium dodecyl sulfate–polyacrylamide gel electrophoresis (SDS–PAGE) and transferred onto a polyvinylidene fluoride (PVDF) membrane (Amersham Hybond, GE Healthcare, Freiburg, Baden-Württemberg). Protein transfer was performed using Mini-Protean 2 Cell chambers (Bio-Rad, Kabelsketal, Saxony-Anhalt, Germany). The primary antibodies TUM1 (1:3500., Abcam, Rozenburg, Amsterdam, Netherlands), CBS (1:1000., Sigma-Aldrich, Darmstadt, Hesse, Germany), CTH(1:1000., Sigma-Aldrich, Darmstadt, Hesse, Germany), CTU1 (1:1000, Sigma-Aldrich, Darmstadt, Hesse, Germany), CTU2 (1:1000, Sigma-Aldrich, Darmstadt, Hesse, Germany), URM1 (1:500, Sigma-Aldrich, Darmstadt, Hesse, Germany), α-MOCS3 (1:4000, Abcam, Rozenburg, Amsterdam, Netherlands), α-SO (1:1000, Abcam, Rozenburg, Amsterdam, Netherlands) and α-actin (1:7500, Sigma-Aldrich, Darmstadt, Hesse, Germany) were used for protein detection together with the peroxidase-coupled secondary antibodies (α-rabbit POD, 1:10,000, Sigma-Aldrich, Darmstadt, Hesse, Germany; α-mouse POD, 1:5000, Sigma-Aldrich, Darmstadt, Hesse, Germany). The blots were developed with chemiluminescence via the Fusion SL Vilber Lourmat (peqlab, Erlangen, Bavaria, Germany) imaging system.

2.5. MTT Assay

MTT [3-(4,5-dimethylthiazol-2-yl)-2,5-diphenyltetrazolium bromide] is converted to insoluble purple formazan by dehydrogenases in living cells, thereby measuring the growth rate [57]. Formazan can be solubilized by isopropanol and measured spectrophotometrically. 10×10^3 cells per well were seeded in a 96-well plate, and 50 µL of the MTT solution was added to each well and incubated for 3 h at 37 °C. Subsequently, 150 µL of the MTT solvent was added, and the MTT formazan was detected after 15 min at 590 nm.

2.6. Aconitase Activity Assay

Aconitase is an [4Fe-4S] cluster-containing TCA cycle protein that catalyzes the isomerization of citrate to isocitrate via cis-aconitate [58]. HEK293T cells were grown in T75 culture flasks until the cells were 90% confluent. The cells were harvested and lysed in nondenaturing lysis buffer [50 mM Tris-HCl and 1% NP-40 (pH 8)]. The protein concentration was determined via a Bradford assay. The aconitase activity was measured using 50 µL of cell lysate mixed with 250 µL of reaction buffer [50 mM Tris-HCl, 50 mM NaCl, 5 mM MgCl2, 0.5 mM NADP+ and 0.05 unit of isocitrate-dehydrogenase (Sigma) (pH 8)]. This was incubated for 5 min at 37 °C before the addition of 200 µL of starting buffer (50 mM Tris-HCl, 50 mM NaCl, 5 mM $MgCl_2$ and 2.5 mM cis-aconitate). The reaction was followed at 340 nm by the reduction of NADPH as ICDH converted the product of aconitase. The specific activity was calculated using the extinction coefficient of NADPH ($\epsilon 340 = 6220\ mM^{-1}$) [59].

2.7. Sulfite Oxidase Activity Assay

The activity assay of the Moco-dependent enzyme sulfite oxidase was adapted from [60]. Cells were grown in a T75 cell culture flask until they were 90% confluent. They were harvested, and the pellet was resuspended with extraction buffer [50 mM Tris-acetate, 0.1 mM EDTA and 1% NP-40 (pH 8.5)]. The probes were vortexed and centrifuged (12,000 × *g* for 15 min at 4 °C) to obtain the cell lysate. The protein concentration was determined with Bradford reagent. The enzyme activity was measured using 150 µL of cell lysate in a total reaction volume of 1 mL. The reaction buffer consisted of 800 µL of 50 mM Tris-acetate,

0.1 mM EDTA and 1% NP-40 (pH 8.5) to which 10 µL of 17 mM sodium deoxycholic acid, 5 µL of 10 µM potassium cyanide, 33 µL of cytochrome c (6 mg/mL) and 2 µL of 100 mM sodium sulfite had been added. The reduction of cytochrome c was monitored at 550 nm for 5 min. The specific activity using the extinction coefficient of cytochrome c(ϵ550 = 19.36 M^{-1}) was calculated.

2.8. tRNA Extraction and Analysis

Using nucleoside separation by HPLC, it is possible to distinguish and quantify non-modified nucleosides as well as the modified nucleosides, as the mcm^5s^2-modification on Uridine of Lys, Gln and Glu. Nucleosides can be distinguished by the respective UV-spectra. Forty-eight hours before being harvested, the cells were seeded on three T75 cell culture flasks until the cells were 90% confluent. The cells were taken up with TriFast (Peqlab, Erlangen, Bavaria, Germany), and a 1:5 volume of chloroform was added. After centrifugation, the upper, aqueous phase was transferred into a new falcon and precipitated with 1 times the volume of isopropanol overnight at − 20 °C. The samples were spun down (13,000× *g* for 1.5 h at 4 °C), and the resulting pellet was washed thrice with 70% ethanol. The pellet was dried at 37 °C for 10–15 min. The precipitated RNA was dissolved in 100 µL of 0.3 M NaOAc (pH 4.5) for 15 min at 55 °C. One hundred micrograms of total RNA per gel was separated by 10% urea–PAGE run at 200 V for 75 min. Subsequently, the gels were stained with an ethidium bromide solution, and the tRNA bands were cut out and placed in crush-n-soak buffer [50 mM sodium acetate and 150 mM sodium chloride (pH 7.0)] at 4 °C overnight to release the RNA from the gel. This was then precipitated overnight at −20 °C with a 1:1 dilution with isopropanol before being washed twice with 70% ethanol. The tRNA pellets were dried at 37 °C for 10–15 min. They were dissolved in 50 µL of 0.3 M NaOAc for approximately 15 min at 55 °C. High-performance liquid chromatography (HPLC) analysis was performed as described by [61].

2.9. Quantification of Moco and cPMP in HEK293T Cells

Moco and cPMP can be oxidized into their fluorescent degradation products FormA and Compound Z, respectively. These degradation products can then be eluted via QAE chromatography and quantified via HPLC [62]. Briefly, HEK293T cells were grown in T75 cell culture flasks until the cells were 90% confluent. They were harvested and resuspended in 800 µL 100 mM Tris-HCl (pH 7.2), followed by cell lysis through sonification (on 2 s, off 2 s, 20%, 45 s). The protein concentrations were determined via Bradford reagent. For both Moco and cPMP measurements, 50 µL of solution A (1063 µL of I2/KI and 100 µL of 37% HCl) was added to 400 µL of the cell lysate followed by the addition of 150 µL of the I2/KI solution. The samples were kept in the dark overnight at RT. Subsequently, 100 µL of 1% ascorbic acid was added to 400 µL of the supernatant after centrifugation. This was followed by the addition of 200 µL of 1 M Tris to change the pH to 8.3. The cPMP samples were loaded on QAE column. The FormA samples were further dephosphorylated with 30 µL of 1 M $MgCl_2$ and 2 µL of fast alkaline phosphatase for 2 h. Purification of FormA and Compound Z was performed using QAE chromatography. FormA was eluted with 10 mM acetic acid from which nine fractions were collected (500 µL). The cPMP samples were eluted with 100 mM HCl collecting nine times 500 µL fractions. Thereafter, the fractions were loaded onto the HPLC system and quantified after separation on a reversed phase C18 column.

2.10. Measurement of Free H_2S via Methylene Blue

Sulfides are able to convert N,N-dimethyl-*p*-phenylenediamine (DMPD) directly to methylene blue in the presence of a mild oxidizing agent (acidified ferric chloride). The methylene blue assay was employed according to [63]. Using cysteine, the reaction containing 50 mM Tris buffer pH 8.0, 2 mg cell lysate, 1 mM DTT, 10 µM PLP in a total volume of 500 µL was started with 1 mM L-cysteine and incubated at 37 °C for 1 h. For mitochondria substrate 3-mercaptopyruvate (3-MP), reaction containing CAPS buffer pH 10.5, 300 µg cell

lysate, 1 mM DTT in a total volume of 500 µL was started with 1 mM 3-MP and incubated at 37 °C for 1 h. Both reactions were stopped by simultaneous addition of 50 µM DMPD and 30 mM Iron (III)-chloride. Methylene blue was formed and quantified at 670 nm against a sulfide standard curve.

2.11. Reactive Oxygen Species Quantification

To analyze the amount of ROS in the cells, the nonfluorescent molecule carboxy-(2′,7′-dichloro-hydrofluorescein diacetate)—which is readily converted to its highly fluorescent 2′,7′-dichlorofluorescein when the acetate groups are removed by activity of ROS—was employed and adapted from [64]. Cells were plated at 25,000 cells/well in a 96-well plate 24 h before treatment, cells were treated with (carboxy-DCFDA, Sigma-Aldrich, Darmstadt, Hesse, Germany) at a concentration of 10 µM of serum-free culture media and incubated at 37 °C for 30 min. The serum-free media containing the dye was removed and washed. Fluorescence evaluation was carried out at emission 560 nm and excitation at 488 nm.

2.12. Measurement of Cellular Bioenergetics

The cellular bioenergetics were measured using the seahorse extracellular flux mito stress test, which quantifies the oxygen consumption rate as described in [65]. Briefly, cells (15,000/well) were seeded on a 24-well seahorse plate in DMEM medium a night prior to analysis; the medium was replaced with seahorse medium supplemented with L-glutamine (2 mM, Gibco, Life Technologies, Darmstadt, Hesse, Germany), sodium pyruvate (1 mM, Sigma, Sigma-Aldrich, Saint Quentin-Fallavier, Lyon, France) and glucose (10 mM, Sigma, Sigma-Aldrich, Saint Quentin-Fallavier, Lyon, France). After 1 h incubation at 37 °C in CO_2-free incubator, the oxygen consumption rate (OCR) after oligomycin (1 µM) was used to estimate the rate of ATP production. In addition, carbonyl cyanide-4-trifluoromethoxy phenylhydrazone (FCCP, 0.5 µM) was used to estimate the maximal mitochondrial respiratory capacity. The flux of electrons through complex III and I was blocked with antimycin A (0.5 µM) and rotenone (0.5 µM), respectively; any residual activity in the presence of these inhibitors was assessed as non-mitochondrial OCR. Results were normalized to the number of cells.

3. Results

3.1. Generation of HEK293T TUM1 KO Cell Lines with CRISPR/Cas9 System

HEK293T cells were used to generate the TUM1 knockout cell line. HEK293T cells have a near triploid karyotype and contain three copies of chromosome 22 on which the TUM1 gene is localized. Co-transfection of the short guide RNA-containing Cas9-encoding plasmid with a repair-oligonucleotide that contains several stop codons at the 5′ end directs the cell repair mechanism towards homology-directed repair (HDR) and insertion of the desired genetic sequence (Figure 1A), which preferentially led to random mutations with a desired premature termination of TUM1 transcription. DNA sequencing revealed the mutations and identified several homozygous (−/−) TUM1 KO cell line (Figure 1C). Additionally, the absence of the TUM1 protein in the knockout cell line was confirmed by immunodetection, using a TUM1 specific antibodies (Figure 1D). As control, we used our MOCS3 KO cell line, reported previously [66] which shows the presence of both TUM1 isoforms, confirming that the TUM1 KO was successful and both isoforms are mutated in the produced homozygous cell line. The MTT assay was applied to analyze changes in the cell growth caused by the absence of TUM1. Here, we compared the TUM1 KO cell line to the MOCS3 KO since that cell line was shown before to have a growth defect. The results in (Figure 1E) show that the TUM1 KO strain has a higher impact on cell division in comparison to the MOCS3 KO strain. The cells were able to divide, but the growth rate was shown to be significantly reduced by 50% in the homozygous (−/−) TUM1 KO strain compared to that in wild-type cells. Treatment with exogenous H_2S donors like NaHS in a neutral solution like water leads to about 20% H_2S and 80% (HS-) [67]. Treatment of TUM1 KO cells with 10 µM of NaHS (as exogenous hydrogen sulfide donor) reverted the

growth deficit. NaHS was applied due to previous results showing that hydrogen sulfide stimulates cellular bioenergetics at lower concentrations [68] and the known involvement of TUM1 in hydrogen sulfide production in mitochondria [69]. Conclusively, TUM1 KO cells might lower the rate of cell proliferation based on a lower hydrogen sulfide production in the mitochondria.

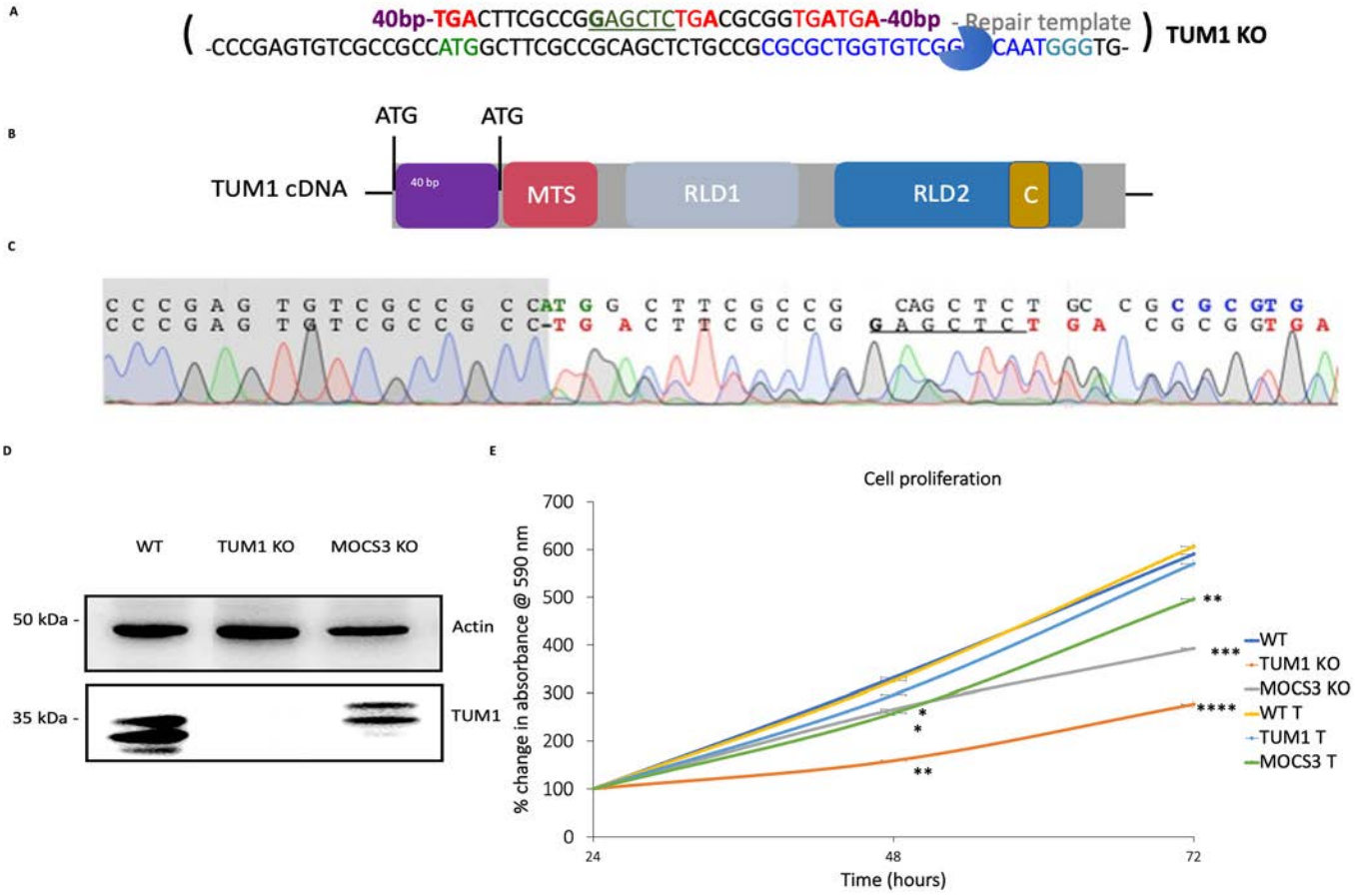

Figure 1. Generation of *TUM1* knockout cell lines using the CRISPR/Cas9 system. (**A**) Schematic diagram of Repair template (upper) and genomic sequence (lower) of the respective Cas9 targetingsite. Homology sequences not shown (40 bp). The guide RNA (blue) with the respective PAM-site (turquoise), exon regions (yellow box), start codons (green), silent mutations (orange), restriction sites(brown), resulting in stop codons (red). (**B**) Diagrammatic representation of *TUM1* cDNA showingthe ATG (start codon), MTS (mitochondria targeting sequence), RLD (rhodanese like domains) andthe C terminal cysteine. (**C**) Sequence of PCR product with mutations spanning from the start codon. (**D**) Immunodetection of TUM1 in different HEK293T cell lines. The generated HEK293T CRISPR/Cas9 cell lines with knockout cells in TUM1 were analyzed for the presence of the TUM1 protein by immunodetection. (**E**) Proliferation rate with (T) and without NaHS treatment of HEK293T cell lines. MTT was added at 0.5 mg/mL to the culture media and incubated at atmosphere of 5% CO_2 for 3 h at 37 °C. The formazan dye formed was dissolved using the permeabilization solution and measured at 570 nm. Independent samples *t*-test with SPSS was performed as indicated * $p < 0.05$,
** $p < 0.01$, *** $p < 0.005$, **** $p < 0.001$ ($n = 3$) (n represents number of biological replicates).

3.2. *Effect of TUM1 KO on Sulfite Oxidase Activity and Moco Biosynthesis*

Prior studies have shown that TUM1 interacts with the L-cysteine desulfurase (NFS1) and the Molybdenum cofactor biosynthesis protein 3 (MOCS3) [7]. These two proteins are involved in two important sulfur requiring pathways; Cytosolic tRNA thiolation and Moco biosynthesis [39,53]. However, the previous studies did not investigate the role of TUM1 in these pathways in humans. To analyze a potential role of TUM1 in Moco

biosynthesis, we determined the activity of the most abundant human molybdoenzyme, Sulfite oxidase, in the *TUM1 KO* cell line in comparison to the *MOCS3 KO* cell line. Again, we compared the activity to the *MOCS3 KO* cell line, which was shown before to largely reduce sulfite oxidase activity. Sulfite oxidase activity was found to be reduced to 75% of the activity of the wild type (Figure 2A) in the *TUM1 KO* cells. SO activity in *MOCS3 KO* cells a negative control was decreased to 15% of the wild type activity, in consistency with previous results [66]. Sulfite oxidase abundance was slightly reduced in *TUM1 KO* cells compared to the wild type and undetectable in *MOCS3 KO* cells (Figure 2B,C). These results confirm the past results [70] showing that SO is degraded in the absence of Moco which is evident in *MOCS3 KO* cells and a slight reduction of SO abundance in *TUM1 KO* cells. The low amount of SO activity present in the *TUM1 KO* cells might be due to sulfur availability for MOCS3 transferred from other sulfurtransferases.

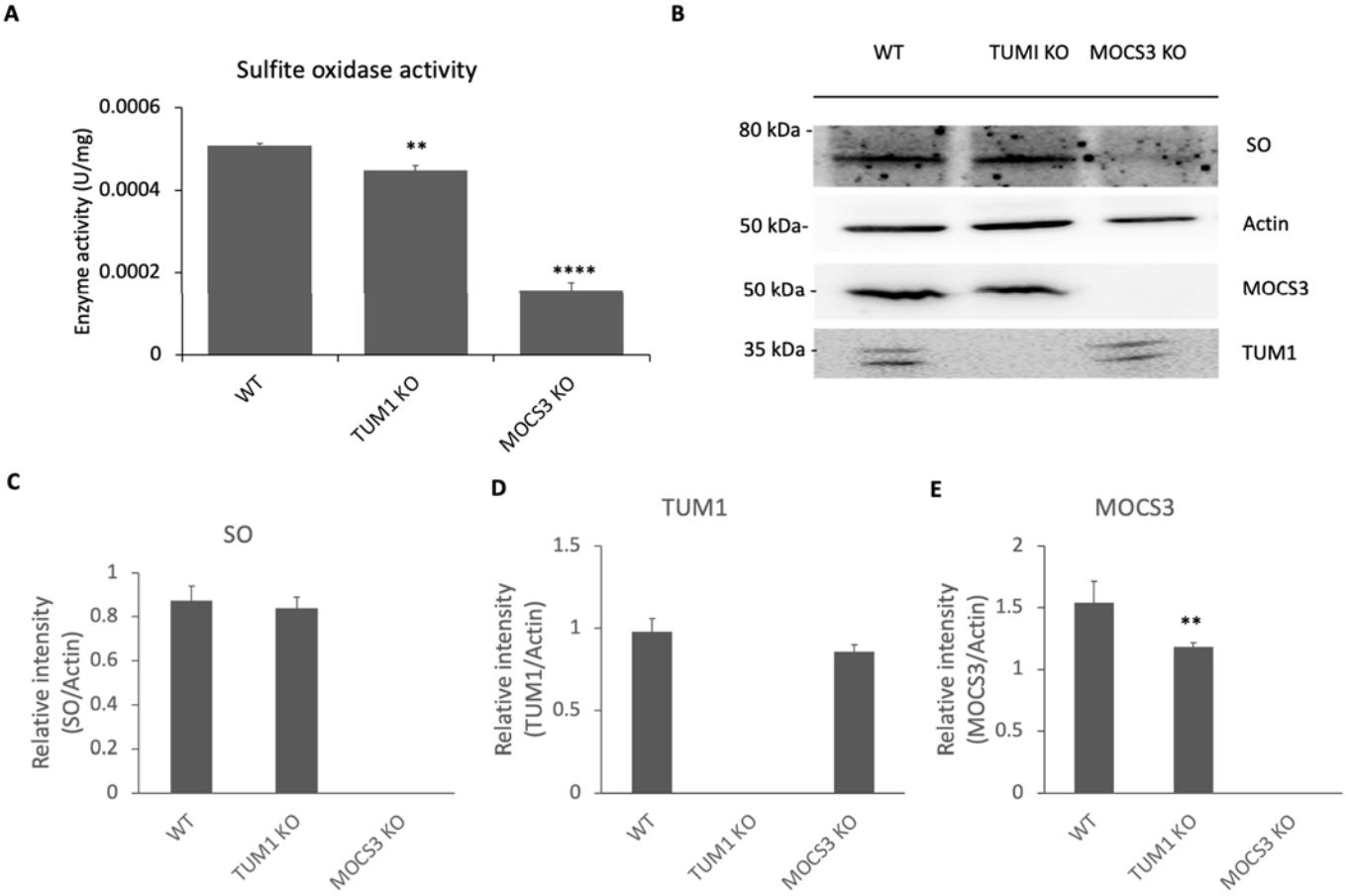

Figure 2. Sulfite oxidase activity in HEK293T cell lines. (**A**) Sulfite oxidase activity in wild type, *TUM1 KO*, and *MOCS3 KO*(−/−) were determined using sodium sulfite as substrate; the reaction was monitored by the reduction of cytochrome c at 550 nm for 5 min. (**B**) Immunodetection of SO,MOCS3 and TUM1 using the corresponding antibodies. 100 µg of cell lysates were loaded on a 12% SDS-PAGE and transferred to a PVDF membrane, followed by incubation with correspondingantibodies. Proteins were visualized using POD-labeled secondary antibodies. Image J intensity quantification (**C**) SO (**D**)TUM1 (**E**) MOCS3. Independent samples *t*-test with SPSS was performed as indicated ** $p < 0.005$, **** $p < 0.001$ (n = 3) (n represents number of biological replicates).

3.3. Effect of TUM1 KO on Moco and cPMP Levels

Since sulfite oxidase activity was reduced in *TUM1 KO* cells, it was of interest to analyze the effect on Moco and cPMP production in these cells, which we compared again to the *MOCS3 KO* cell line, in which both cofactor levels were shown previously to be affected [66]. The results show that *TUM1 KO* cells had a 45% decrease in the amount of

Moco compared to WT, while Moco was not detected in *MOCS3 KO* cells as reported before (Figure 3A). Additionally, cPMP accumulated 50% more in *TUM1 KO* cells compared to the WT while *MOCS3 KO* cells accumulated 120% cPMP compared to the WT (Figure 3B). These results show an effect of TUM1 for Moco production by a reduced cPMP conversion, that is the consequence of the results for the reduction of sulfite oxidase activity as shown (Figure 2).

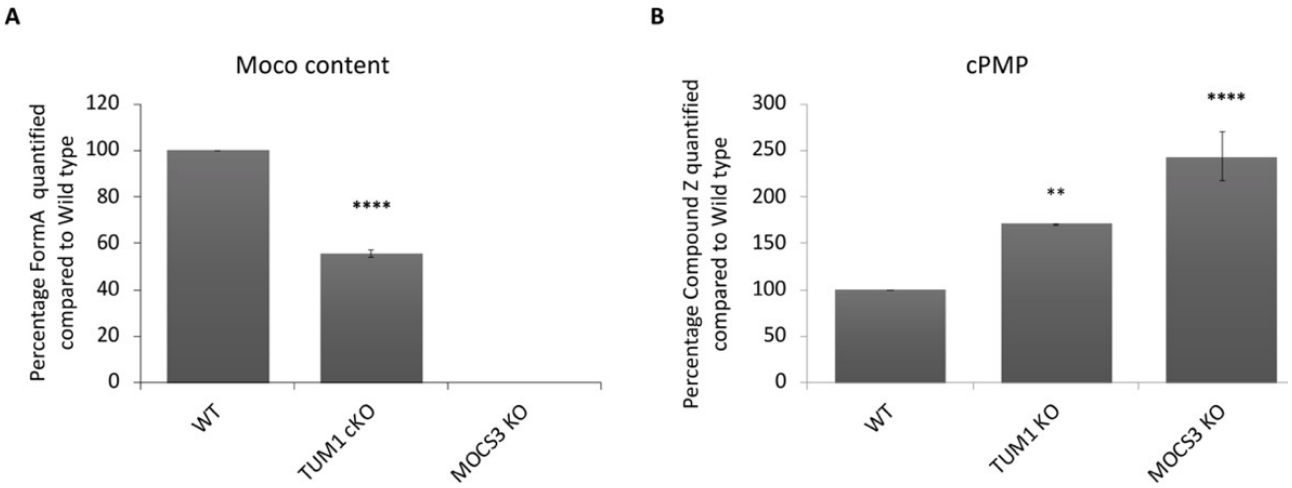

Figure 3. Quantification of Moco and cPMP in HEK 293T cell lines. Cells were oxidized overnight to convert Moco and cPMP to their fluorescent degradation products Form A and Compound Z, respectively. cPMP samples were separated by QAE ion-exchange chromatography and quantifiedby HPLC after separation on a C-18 column. 20 µL of 50% acetic acid was added to Form A samplesbefore loading on the column. The elution of Form A and Compound Z was monitored with an Agilent 1100 series system. The fluorescence excitation at 383 nm and emission 450 nm. (**A**) Mococontent after normalizing to protein concentration (**B**) cPMP content after normalizing to protein concentration. Independent samples *t*-test with SPSS was performed as indicated ** $p < 0.005$, **** $p < 0.001$ ($n = 2$).

3.4. Repair of Sulfite Oxidase Activity in TUM1 KO Cells with NaHS

H_2S has been mentioned to act via *S*-sulfhydration of target proteins. NaHS could also serve as direct sulfur donor through NaHS dissociation in neutral solution (H_2S, HS-, S2), thereby leading to pool of sulfide [67]. The cell proliferation experiments showed that NaHS can complement the growth deficit of *TUM1 KO* cells but not of *MOCS3 KO* cells. To investigate the enzyme that is repaired by NaHS, we investigated the effect on sulfite oxidase activity. Therefore, we investigated whether the treatment of the cells with NaHS could repair the low SO activity in *TUM1* and *MOCS3 KO* cells. Here, we show that the SO activity of *TUM1 KO* cells were rescued to almost the WT level, but not the *MOCS3 KO* cells (Figure 4A). NaHS treated WT cells also showed an increase in SO activity compared to the untreated control. These data suggest that NaHS is a sulfur donor only in *TUM1 KO* cells (containing MOCS3), hence increasing the amount of Moco formed while *MOCS3 KO* cells did not respond to the NaHS treatment since MOCS3 is crucial for the sulfurtransfer reaction. One possibility is that either the transfer of sulfur from NFS1 to MOCS3 is facilitated by hydrogen sulfide by the action of TUM1. Further, it was shown previously that sulfite oxidase deficiency can be suppressed by mutation in CTH [71]. CTH was found to be present in lower amounts in TUM1 cells (Figure 4C,D); NaHS might also suppress the sulfite production from cystathionine due to the availability of hydrogen sulfide. However, this effect is not so pronounced in the *MOCS3 KO* cells since the hydrogen sulfide biosynthesis is less perturbed in *MOCS3 KO* cells compared to the*TUM1 KO* cells.

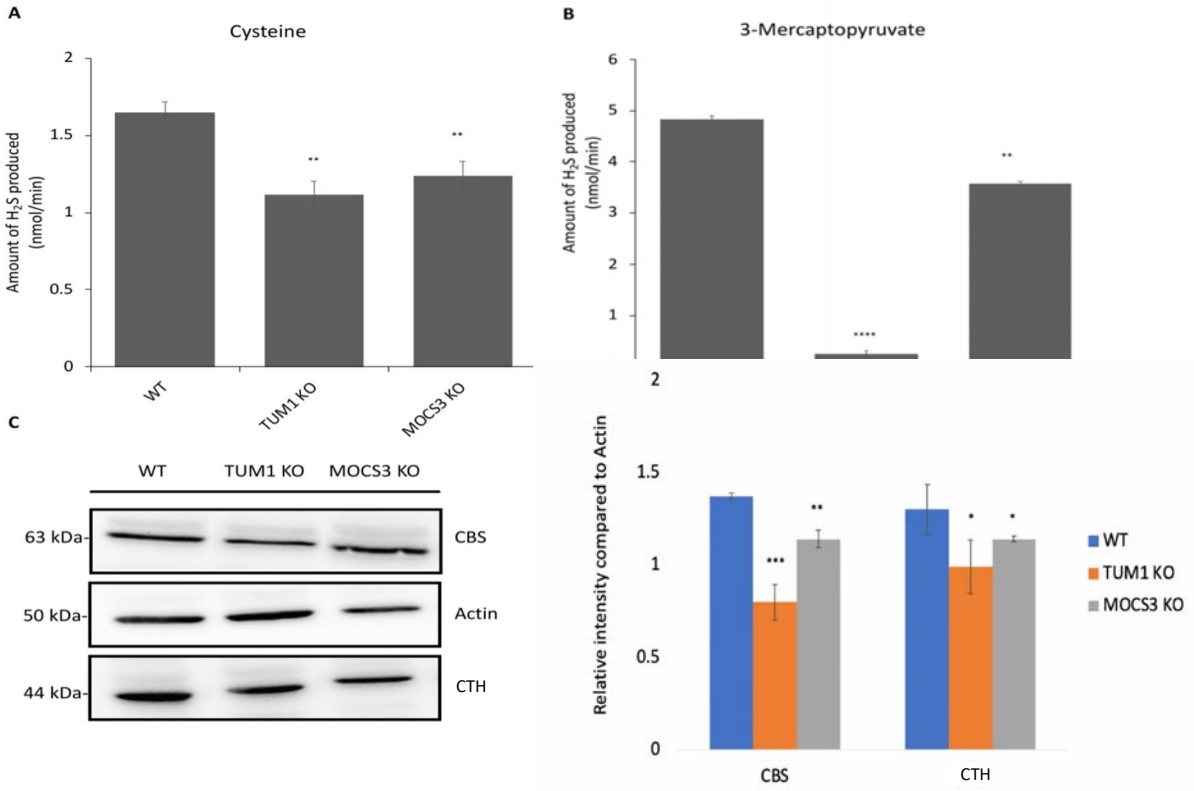

Figure 4. Effect of NaHS on sulfite oxidase activity in HEK293T cell lines. (**A**) Sulfite oxidase activity in WT, *TUM1 KO* and *MOCS3 KO* (−/−) were determined using sodium sulfite as substrate; the reaction was monitored by the reduction of cytochrome c at 550 nm for 5 min. (**B**) Immunodetection ofSO, MOCS3 and TUM1 using respective antibodies. (**C**) Immunodetection of other H_2S biosynthesis enzyme CBS and CTH in WT, *TUM1 KO*, and *MOCS3 KO* cells (−/−) cell lines. Proteins were visualized using POD-labeled secondary antibodies. (**D**) Image J quantification of relative intensity of blot bands of CBS and CTH compared to Actin. Independent samples *t*-test with SPSS was performedas indicated ND; no statistical difference, * $p < 0.05$, ** $p < 0.01$, *** $p < 0.005$, **** $p < 0.001$, ($n = 3$).

3.5. Effect of TUM1 KO on tRNA Thiolation

TUM1 has been initially identified in a screening for mcm^5s^2U modified tRNA deficient mutants in yeast [8], in which TUM1 was shown to be involved, but not essential for mcm^5s^2U formation. Further, human TUM1 was identified to interact with NFS1 and MOCS3 in the cytosol [7], showing its involvement as a sulfur transferase for mcm^5s^2U formation. Therefore, we investigated the role of TUM1 on cytosolic tRNA thiolation in *TUM1 KO* cells. It is possible to distinguish and quantify non-modified nucleosides mcm^5U from the sulfur-modified nucleosides mcm^5s^2U, as the mcm^5s^2U have a different elution time after separation on a C18 reversed phase column (LiCrospher 100, 5 µm particle size, 250 × 4.6 mm) by HPLC [61]. Quantifying the modified nucleosides, the level of mcm^5s^2U in *TUM1 KO* was decreased to 70% of the wild type level but undetectable in the *MOCS3 KO* cells (Figure 5A). In consistency, a higher amount of unmodified mcm^5U was detected in *TUM1 KO* cells compared to the *MOCS3 KO* cells and below the detection limit in wild type cells (Figure 5B). This shows the role of TUM1 in sulfur transfer for cytosolic tRNA thiolation. Further, we treated the cells with NaHS to investigate the effect of extra sulfur supply on mcm^5s^2U formation. Here, mcm^5s^2U level in NaHS treated *TUM1 KO* cells were similar to mcm^5s^2U levels observed in control wild type cells. However, there was a similar increase in the level of mcm^5s^2U in the NaHS treated wild type cells (Figure 5C). This implies that H_2S is not directly transferred to MOCS3, and the positive effect on sulfite oxidase activity is likely based on the reduced abundance of CBS and CTH (Figure 4C,D). Protein expression of CTU1, CTU2 and URM1 proteins necessary for

cytosolic tRNA thiolation were also reduced in TUM1 knockout cells compared to the wild type and were largely reduced in *MOCS3 KO* cells. This suggests that the proteins might degrade in the absence of their interaction partners (Figure 5F), which is in line with previous findings where it was shown that URM1 is down-regulated under sulfur starvation conditions as other partner proteins involved in cytosolic tRNA thiolation [72].

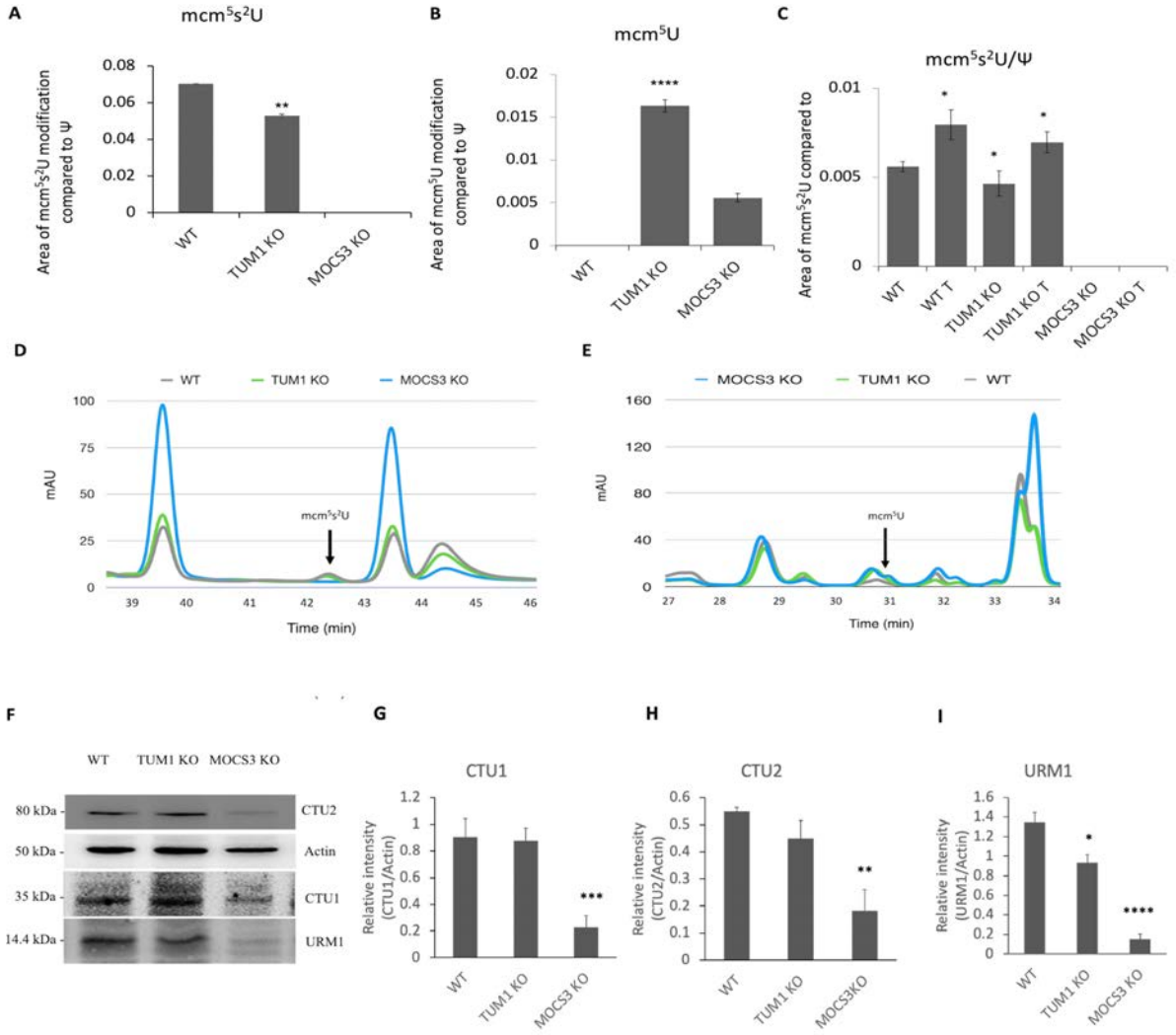

Figure 5. Quantification of mcm^5s^2U and mcm^5U in HEK293T cell lines. Total RNAs were extracted using phenol-isopropanol precipitation. tRNAs were separated afterward from total RNA using Urea- gel. Respective tRNA were digested and corresponding nucleosides were separated and quantified by the HPLC on a C18 reversed phase column (LiCrospher 100, 5 µm particle size, 250 × 4.6 mm)
(A) mcm^5s^2U (**B**) mcm^5U (**C**) Influence of NaHS to mcm^5s^2U and mcm^5U levels. T: treated with50 µM NaHS for 16 h. (**D**) Chromatogram displaying mcm^5s^2U and (**E**) mcm^5U modification at 33 and 43.4 min, respectively, of the respective cell lines using R plot (**F**) Immunoblot showing the abundance of URM1, CTU-1, CTU-2 and Actin in WT, *TUM1 KO*, and *MOCS3 KO* cells (−/−) cell lines using the respective antibodies. Proteins were visualized using POD-labeled secondary antibodies. Representative Image J intensity quantification of band intensity (**G**) CTU1 (**H**) CTU2
(I) URM1 Independent samples *t*-test with SPSS was performed as indicated ND; no statistical difference, * $p < 0.05$, ** $p < 0.01$, *** $p < 0.005$, **** $p < 0.001$ ($n = 3$).

3.6. Effect of TUM1 on H_2S Biosynthesis

H_2S is produced from sulfur-containing amino acids cysteine and homocysteine, or from 3-mercaptopyruvate, in a reaction that is catalyzed mainly by three enzymes: cystathio-

nine beta-synthase (CBS); cystathionine gamma-lyase (CTH); and 3-mercaptopyruvate sulfurtransferase (TUM1). Of these, the first two reside in the cytosol and comprise the transsulfuration pathway. TUM1 is among the three major H_2S producing enzymes in humans. Here, we quantified the H_2S production in *TUM1 KO* cell lines with different substrates. When using cysteine as substrate, the total H_2S production via all the three H_2S producing enzymes is measured. Here, the amount of H_2S generated in *TUM1 KO* cells was only 60% of that generated in the wild type cells. *MOCS3 KO* cells produced only 70% of H_2S compared to the wild type (Figure 6A). When using 3-MP as substrate *TUM1 KO* cells produced only 5% of the H_2S produced in the wild type, while the *MOCS3 KO* cells produced 75% of that of the wild type which might be consistent with the low TUM1 abundance in *MOCS3 KO* cells (Figure 6B). These results are in accordance with previous findings using different experimental approaches showing that TUM1 is the major H_2S producing when 3-MP is available as substrate in mitochondria. Further, we validated using the methylene blue assay where we measured the activity of the H_2S producing enzymes. To achieve this, we used the commercially available CTH and CBS inhibitors propargylglycine and aminooxyacetate (AOAA), respectively. *TUM1 KO* cells had 44% inhibition compared to 20 and 25% observed in the wild type and *MOCS3 KO* cells, respectively (Figure 6C). It was, however, impossible to measure the extent of CBS inhibition due to unselective property of the available inhibitor AOAA. This inhibitor completely inhibited the activity of all PLP dependent enzyme (Figure 6D). These results also further suggest a coping mechanism of the cell to ameliorate the effect of sulfite toxicity due to the deficiency in sulfite oxidase. CTH and CDO suppression have been found to undermine the effect of Moco deficiency in *C. elegans* [71]

3.7. Effect of TUM1 on Cellular Bioenergetics

H_2S is mainly produced by cystathionine gamma-lyase (CTH), cystathionine beta-synthase (CBS) and 3-mercaptopyruvate sulfur transferase (3-MST) [73]. In contrast to the inhibitory effect of H_2S on Complex IV, at high concentrations above 200 μM, at lower concentrations a stimulatory role of electron transport has been shown [68]. It has been suggested that H_2S enhances the activity of FoF1-ATP (adenosine triphosphate) synthase and lactate dehydrogenase via their S-sulfhydration, thereby stimulating mitochondrial electron transport [74]. Further, H_2S serves as an electron donor for the mitochondrial respiratory chain via sulfide quinone oxidoreductase and cytochrome c oxidase at low H_2S levels. The latter enzyme is inhibited by high H_2S concentrations, resulting in the reversible inhibition of electron transport and ATP production in mitochondria [75]. Mainly SQR is responsible for the oxidation of H_2S in the mitochondria [68], from two H_2S molecules, two disulfides (-SSH) bounds are created on the SQR, two electrons derived from two H_2S molecules also enter the mitochondrial electron transport chain, promoting mitochondrial ATP generation [68]. Among the H_2S producing enzymes described above, TUM1 is the major H_2S producing enzyme in the mitochondria [73]. Therefore, we investigated the effect of TUM1 on cellular bioenergetics using the Seahorse XFe96 analyzer. Measuringthe O_2 consumption rate (OCR), an indicator of mitochondria respiration, the *TUM1 KO* cells displayed lower oxygen consumption compared to the wild-type. The *MOCS3 KO* cells also displayed a lower O_2 consumption compared to the wild type; however, the levels were higher compared to the *TUM1 KO* cells (Figure 7A). Measuring the extracellular acidification rate (ECAR), an indicator of glycolytic respiration, *TUM1 KO* cells were higher compared to wild type, while the *MOCS3 KO* cells had similar ECAR compared to the wild type (Figure 7B). TUM1 absence led to reduced mitochondria generated ATP (Figure 7C). However, the TUM1 knockout cells produced more ATP via the glycolytic pathway(Figure 7D). Overall, ATP production was nevertheless reduced by 25% in *TUM1 KO* cells compared to wild type (Figure 7E). Data from the OCR can be used to calculate other relevant mitochondria parameters (Figure 7F). Basal respiration indicates the minimal rate of metabolism for essential maintenance function of the cell. Here, the wild type displayed higher basal respiration compared to the *MOCS3 KO* cells and *TUM1 KO* cells.

However, the *MOCS3 KO* cells had higher basal respiration compared to the *TUM1 KO* cells. This suggests that the wild type cells, which proliferate much faster, require more ATP for basic metabolism and vice versa for the *TUM1 KO* cells. ATP linked respiration was higher in the wild type compared to the *TUM1 KO* cells and *MOCS3 KO* cells. However, the *MOCS3 KO* cells had more ATP linked respiration in contrast to the TUM1 knockout cells. Addition of Rotenone/Antimycin abolishes the mitochondria-linked respiration; through this, the non-mitochondria O_2 can be measured. Here, the *MOCS3 KO* cells compared to the wild type and *TUM1 KO* cells displayed higher non-mitochondria O_2 consumption while *TUM1 KO* cells displayed higher in comparison to the wild type. This indicates other cellular oxidative reactions like ROS, this result is in accordance with the high amount of ROS quantified in the *MOCS3 KO* cells (Figure S1). Further, there was more proton leak in the *MOCS3 KO* cells compared to the *TUM1 KO* cells and wild type, while the *TUM1 KO* cells displayed an increased proton leak in contrast to the wild type. This result implicates possible mitochondria membrane damage in the *MOCS3 KO* cells. Conclusively, the energy map shows again the dependency of *TUM1 KO* cells on the glycolytic ATP production pathway rather than the mitochondria ATP production pathway (Figure 7G). These results indicate that TUM1 impacts mitochondria bioenergetics and, consequently, ATP production, mainly in the mitochondria.

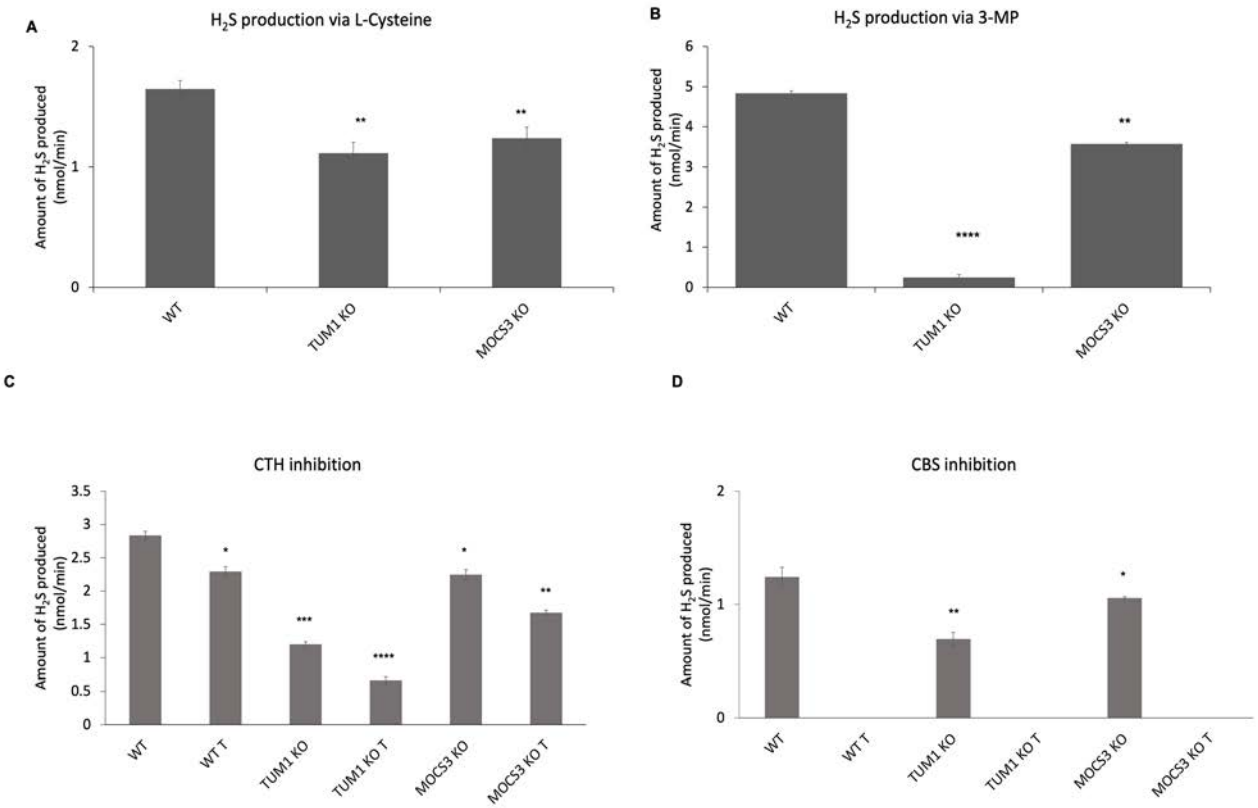

Figure 6. Invitro H_2S production in HEK 293 T cell lines. Cells from WT, *TUM1 KO*, *MOCS3 KO* were lysed in NP-40 containing Tris buffer. Protein concentrations of resulting lysates were determined by the Bradford assay. H_2S production was measured using Methylene blue assay. The activity was started by the addition of (**A**) 500 µM L-cysteine as substrate and incubated for 1 h (**B**) 1 mM 3- mercaptopyruvate as substrate and incubated for 15 min (**C**) with 2 mM propargylglycine (CTHinhibitor) treatment (**D**) with 2 mM aminooxyacetate (CBS inhibitor). Each reaction was stopped by simultaneous addition 20 mM-DMPD and 30 mM $FeCl_3$ and incubated further for 20 min. The absorbance was measured at 670 nm. Independent samples *t*-test with SPSS was performed as indicated ND; no statistical difference, * $p < 0.05$, ** $p < 0.01$, *** $p < 0.005$, **** $p < 0.001$ ($n = 3$).

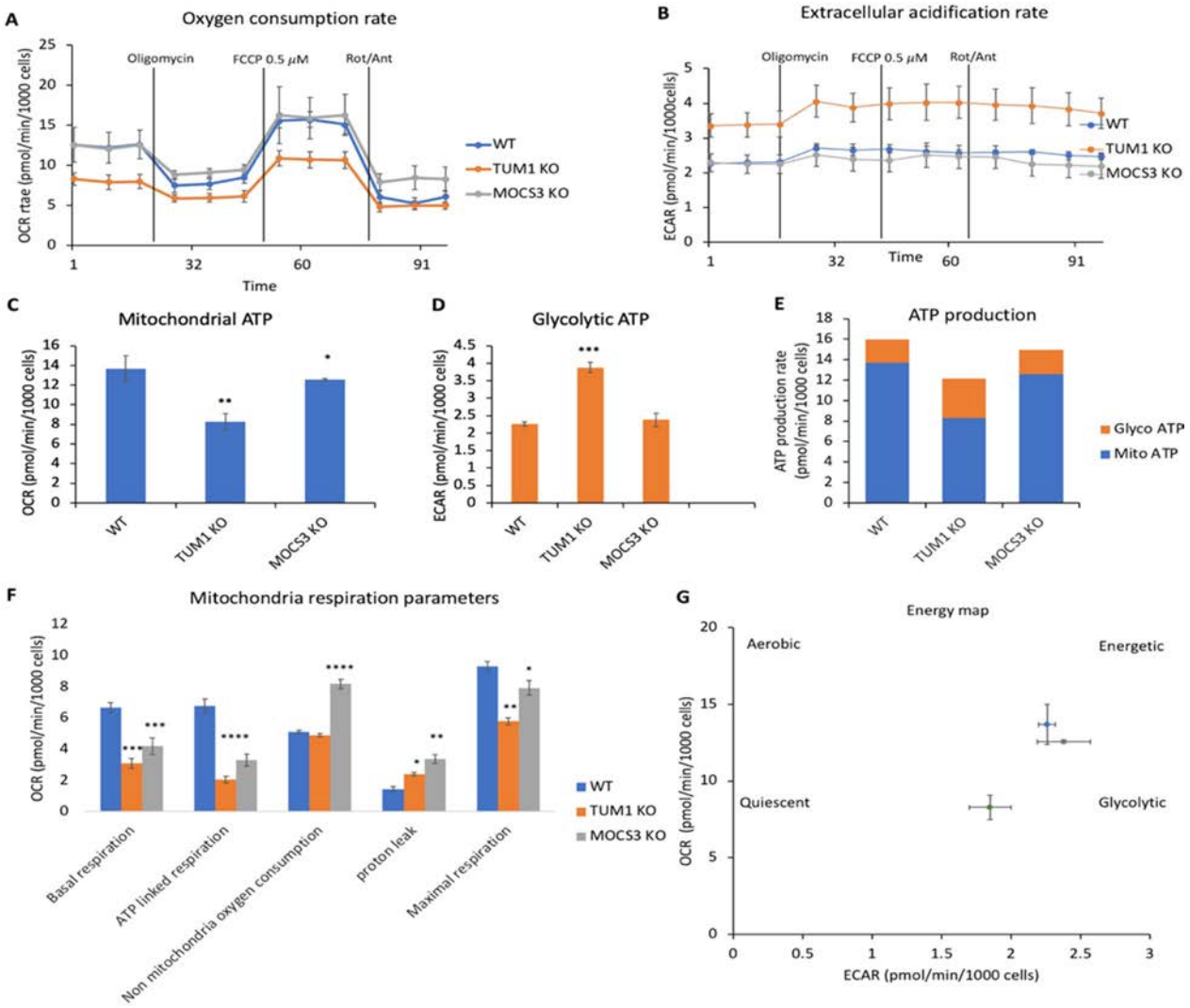

Figure 7. Effect of *TUM1 KO* on oxidative phosphorylation parameters in HEK 293T cells: (**A**) Oxygen consumption rate (OCR) profiles. Lines indicate the addition of specific mitochondrial stressors. Results are indicated as mean ± SD of four replicates per condition; (**B**) Representative extracellular acidification rate (ECAR). Lines indicate the addition of specific mitochondria stressors into the media. Results are indicated as mean ± SD of four replicates per condition; (**C**) analysis of mitochondrial ATP production (**D**) analysis of glycolytic ATP production (**E**) Total ATP production (**F**) analysis of oxidative phosphorylation-related bioenergetics parameters. (**G**) Energy map. All measurements were normalized to the number of cells after the seahorse measurements with Hoechst dye. Indepen- dent samples *t*-test with SPSS was performed as indicated ND; no statistical difference, * $p < 0.05$,
** $p < 0.01$, *** $p < 0.005$, **** $p < 0.001$. ($n = 3$).

3.8. Effect of TUM1 KO on TCA Cycle

Aconitase is an Fe-S cluster dependent enzyme which is oxidative sensitive. There are two isoenzymes of Aconitase 1 localizing in the cytosol and Aconitase 2 localizing in the mitochondria [76]. The suppression of gene encoding for aconitase has been previously linked to reduction in cell growth and ATP [77]. Therefore, herein we investigate the effect of the two isoenzymes by measuring the aconitase activity in the cytosolic and mitochondria compartments of the cell. Measuring the cytosolic aconitase activity, there was70% reduction aconitase activity in the *TUM1 KO* compared to the wild-type. *MOCS3 KO* also had about 50% reduction in aconitase activity compared to the wild-type (Figure 8A). In the mitochondria, the *TUM1 KO* had only 20% of aconitase activity compared to the wild-

type, while the *MOCS3 KO* had only 40% of the wild-type aconitase activity (Figure 8B). These results suggest possible involvement of aconitase down regulation on the retarded growth in *TUM1* and *MOCS3 KO*.

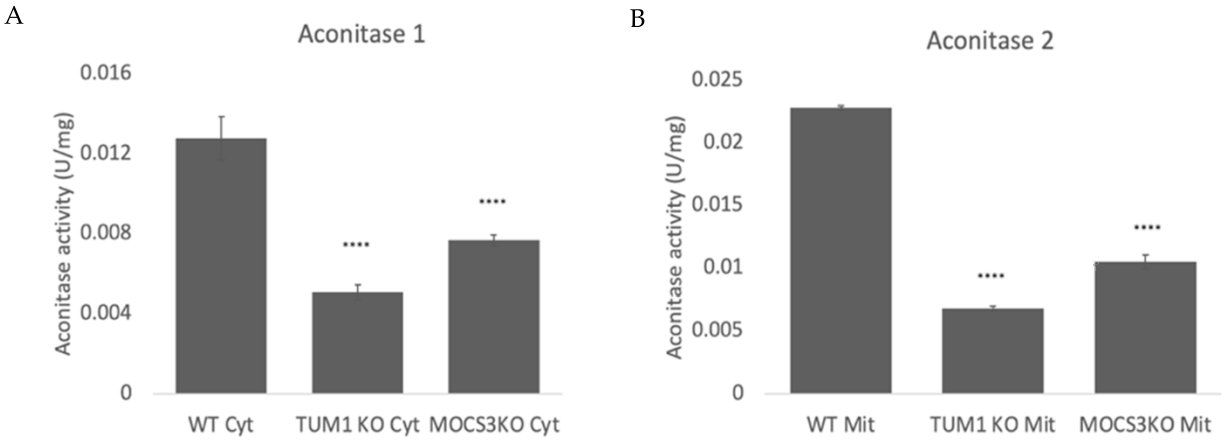

Figure 8. Determination of TCA cycle enzyme Aconitase in HEK293T. Cells were lysed in reaction buffer containing 0.1% NP-40. Cells were separated into cytosolic (cyt) and mitochondria (mit) fractions. The activity measurement was carried out as stated above. Enzyme activity was determined by the reduction of NAD+ at 340 nm for 3 min (**A**) Activity of Aconitase 1 (**B**) activity of Aconitase.Independent samples t-test with SPSS was performed as indicated. **** $p < 0.001$ ($n = 3$).

4. Discussion

TUM1 had been identified in yeast in a reverse genetic approach identifying genes involved in 2-thiouridine formation [8]. In that approach, five genes responsible for 2-thiouridine formation of mcm^5s^2U, were identified, namely NFS1, TUM1, Urm1, NCS2 and NCS6. While the other proteins were essential in that approach, TUM1 was not [8]. TUM1 contains a tandem rhodanese-like domain (RLDs). Rhodanese is a widespread and versatile sulfur-carrier enzyme catalyzing the sulfur-transfer reaction in distinct metabolic and regulatory pathway [8]. Using an in vitro sulfur transfer reaction revealed that yeast TUM1p stimulated yeast Nfs1p and accepted a persulfide sulfur atom from Nfs1p [8]. In addition, it was shown that Cys259 in RLD2 of TUM1 is responsible for efficient 2-thiouridine formation [8]. RLD1 of TUM1p, in contrast, is rather a catalytically inactive RLD, often found in various rhodanese-containing proteins because it has no conserved cysteine residue [78,79]. Those results demonstrated that NFS1 not only provides a sulfur atom to Fe/S cluster formation but also directly supplies a sulfur atom to the formation of 2-thiouridine. Yeast TUM1 therefore might act as an activator for the desulfurase of Nfs1p as well as a mediator of the persulfide from Nfs1p. Sulfur transfer for Moco biosynthesis has not been investigated in that approach or any other approach so far, based on the fact that *S. cerevisiae* is lacking Moco biosynthesis and active molybdoenzymes [80]. In this present study we report a mild effect of TUM1 on cytosolic tRNA thiolation and Moco biosynthesis leading to the proposed mechanism for sulfur transfer for the pathways (Figure 9). This similar effect was reported in cytosolic tRNA thiolation in *S.cerevisiae*. It was proposed that L-cysteine desulfurase can directly transfer the sulfur to Uba4p, the yeast homologue for MOCS3. There, TUM1p was proposed to be an activator of Nfs1p or a mediator of persulfide from the L-cysteine desulfurase. It was also shown that Uba4p could receive the persulfide directly from Nfs1p but with a reduced efficiency compared to the presence of TUM1p [8].

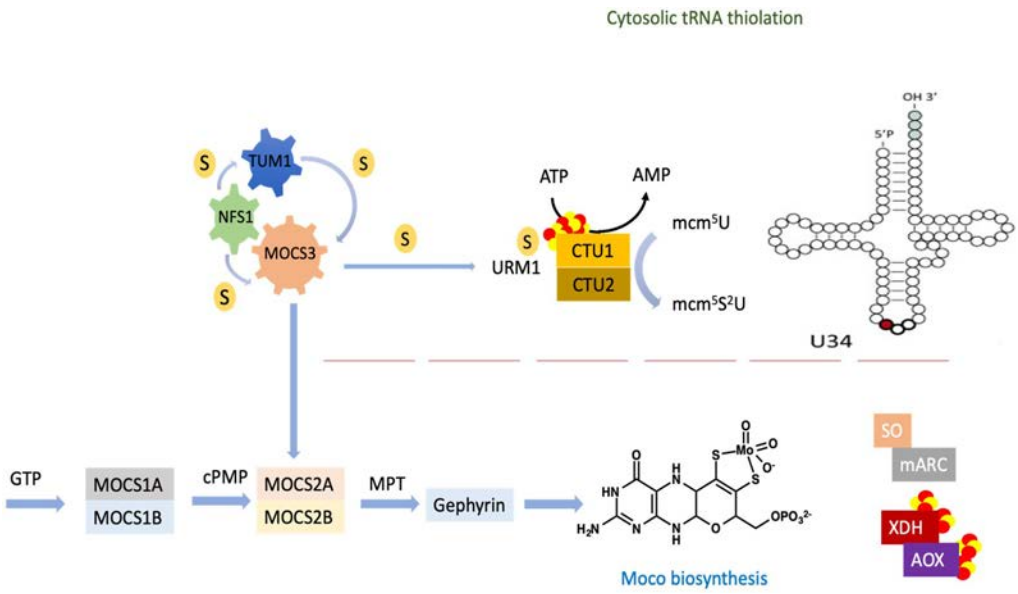

Figure 9. Pathway showing the transfer of sulfur from NFS1 to MOCS3 with/without the involvement of TUM1 for sulfur transfer to MOCS3. MOCS3 further activates URM1 by adenylation followed by the sulfur transfer step, which results in the formation of a thiocarboxylate group at the C-terminalGly of URM1. URM1 subsequently interacts with the CTU1–CTU2 complex before final transfer of the sulfur to the tRNA. MOCS3 transfers two sulfur atoms to MOCS2A. MPT dithiolate is formed byincorporating two sulfur atoms from MOCS2A followed by the insertion of molybdate. This reactionis catalyzed by MPT synthase formed by the MOCS2A, MOCS2B complex.

In general, sulfur transfer in organisms involves a network of several proteins that are conserved among organisms [81,82]. Sulfur transfer in organisms is handled by specific sulfur transferases, among which are the L-cysteine desulfurase (NFS1) rhodaneses and thiosulfate or 3-mercaptopyruvate sulfur transferases [83]. L-cysteine desulfurases generally are the initial sulfur mobilizing enzymes for many processes like FeS biosynthesis, biotin, lipoic acid biosynthesis, Moco and biogenesis of 2-thiouridines in tRNA [40]. TUM1, the 3-mercaptopyruvate sulfurtransferase in human mitochondria and the cytosol has been shown to interact with NFS1 and MOCS3 [7] proteins involved in sulfur transfer for Moco biosynthesis and cytosolic and mitochondrial tRNA thiolation [39,53]. The product of the Moco biosynthesis pathway Moco, is the active site of the four molybdoenzymes present in humans [23]. Impairment in the activity of sulfite oxidase among these enzymes has been reported to cause neurological disorders and other diseases [60]. TUM1 deficiency has been implicated to be responsible for a rare inheritable disorder known as mercaptolactate-cysteine disulfiduria (MCDU), which is associated with mental disorder [19,84] since, in *TUM1 KO* cells, sulfite oxidase activity is reduced; the mental disorder of TUM1 deficiency might be related to the symptoms of sulfite oxidase deficiency which is also characterized by neurological disorders [85]. In this report, we show that human TUM1 is involved in Moco biosynthesis and 2-thiouridine formation in addition to cellular bioenergetics through H_2S formation. We show a decrease in the activity of sulfite oxidase activity on human embryonic kidney cell lines, in which we generated a homozygous *TUM1 KO*. The reduced sulfate oxidase activity is based on lower Moco levels in these cells, showing that TUM1 is involved in Moco biosynthesis. These results are in agreement with a previous report showing the absence of sulfite oxidase activity in *MOCS3 KO* cells [66]. It has been reported that sulfite oxidase is being degraded in the absence of Moco [70]. Hence, the reduction in sulfite oxidase activity in *TUM1 KO* cells resulted from the reduction in the amount of Moco, and reduced amounts of sulfite oxidase are likely based on the degradation of the protein in the absence of Moco.

Recently, H_2S has been described as acting as a sulfur donor for mitochondrial respiration [86]. H_2S can be exogenously donated to the cells through sodium hydrosulfide (NaHS) and sodium sulfide (Na_2S). These compounds dissociate to form HS^-, and then partially binding to H^+ to form undissociated hydrogen sulfide [87]. In previous experiments, sulfide has been shown to directly transfer sulfur in an invitro MPT biosynthesis assay [7]. In this study, we show that exogenous treatment of cells with NaHS rescues the deficit of sulfite oxidase activity in *TUM1 KO* cells. However, it has been reported that H_2S acts by sulfurhydration of proteins in which H_2S modulates cysteine persulfidation [88]. MPST has been shown to produce similar persulfides like cysteine persulfide (CysSSH) and GSH persulfide (GSSH) [89,90] It has also been reported that the presence of the three proteins NFS1, TUM1 and MOCS3 led to increase in Moco compared to NFS1 and MOCS3 alone [7]. Therefore, TUM1 is also involved in sulfur transfer from NFS1 to MOCS3 by enhancing the sulfur transfer to the recipient protein, a reaction that can be displaced by NaHS in *TUM1 KO* cells but not in *MOCS3 KO* cells since MOCS3 is required for Moco biosynthesis. The tRNA thiolation is also not rescued by NaHS treatment. Here, the main effect might be a higher level of oxidative stress in these cells (Figure S1) which leads to the dethiolation of tRNA (Figure S2). The dethiolated tRNA likely cannot be repaired by NAHS. Further, CTH level in *TUM1 KO* cells and *MOCS3 KO* cells were found to be reduced. This suggests a coping mechanism by the cell to reduce the toxic effect of sulfite due to Moco deficiency. CTH is known to catalyze the formation of cysteine from Cysthathionine and also the forward production of hydrogen sulfide from cysteine [91]. Increased production in H_2S could also add up to the sulfite pool in the cell. In close cooperation with SQR, glutathione persulfide (GSSH) is generated since it is the preferred physiological co-substrate [92]. Then PDO converts GSSH + oxygen into sulfite + GSH. Sulfite is then converted (together with another GSSH molecule) into thiosulfate + GSH by rhodanese [92].

Cytosolic tRNA thiolation is an important pathway in humans that ensures properand efficient translation [93]. Perturbation of this process has been shown to cause suscepti-bility to oxidative stress conditions and could also lead to misreading and misfolding of proteins [8]. Formation of mcm^5s^2U is dependent on the URM1 pathway, also involving MOCS3 and CTU1 and CTU2. Our results show that human TUM1 impacts cytosolic tRNA $cmcm^5s^2U$ thiolation. The yeast homolog TUM1p has been described to partici- pate in cytosolic tRNA thiolation for the mcm^5s^2U modification of the wobble uridine at position 34 (U34) in lysine, glutamine and glutamate [8]. In yeast, it has been reported that L-cysteine desulfurase relays the sulfur to TUM1 or directly transfers it to the Uba4 for the biogenesis of 2-thiouridine, which makes TUM1 important, but not essential for efficient transfer of sulfur [8]. In accordance to the data from yeast, human TUM1 is required but not essential for the efficient transfer of sulfur for the formation of cytosolic mcm^5s^2U modification, and the levels in the *TUM1 KO* are only reduced to 60% of wild type levels.We further show that CTU1, CTU2 and URM1 protein levels are reduced *TUM1 KO* cells, a reduction that is also observed in *MOCS3 KO* cells. This correlates with previous data on URM1, in which down regulation of URM1 under sulfur starvation conditions was reported in yeast [72]. We further observed an increase in the amount of mcm^5s^2U after exogenous supplementation of cells with NaHS, thereby repairing the loss of TUM1 function in *TUM1 KO* cell (Figure 3).

In this present research, we show retarded growth in *TUM1* and *MOCS3 KO* and subsequently demonstrated that the retarded growth rate could be due to a reduced level of H_2S production compared to the wild-type or the reduced activity of the mitochondria aconitase. The TCA cycle is essential for the production of energy in form of ATP for maintaining high energy demanding physiological functions like cell growth [94]. Recently, it has been reported that the suppression of TCA cycle enzymes using genetic silencing siRNA showed that aconitase 2 affected the growth of CHO cells [77]. The other TCA cycle enzymes did not have significant effect on the growth rate and viability of the CHO cells. A reduction in aconitase 1 and 2 was observed in *TUM1 KO* cells as well as retarded cell growth. However, complementation of *TUM1 KO* cells with exogenous NaHS

complemented for the retarded growth rate. The retarded growth can therefore be ascribed to the cellular bioenergetics influencing the aconitase activity.

Cysteine is the major H_2S biosynthesis substrate in humans using transsulfuration pathways [95]. H_2S is long viewed as toxic gas, and environmental hazard is emerging as a biological mediator with remarkable physiological and pathophysiological relevance [96]. TUM1 was described to be involved in H_2S production and signaling in the mitochon- dria [97]. Recently, H_2S has been described to act as a sulfur donor for mitochondrial respiration [86]. H_2S is also produced in the cytosol by cystathionine β-synthase (CBS) and cystathionine γ-lyase (CTH) [97]. In addition, CTH and CBS are mainly located in the cytosol but translocate into mitochondria under oxidative conditions [98]. TUM1 has been previously characterized to have two distinct isoforms TUM1 Iso1 which localizesonly in the cytosol and TUM1 Iso2 localizing both in the cytosol and mitochondria [7].In the mitochondria, 3-mercaptopyruvate sulfurtransferase (3-MPST) produces H_2S from 3MP (3-mercaptopyruvate), which is generated by CAT (cysteine aminotransferase) from L-cysteine and α-ketoglutarate [2,17]. We demonstrated that TUM1 has significant involve- ment in H_2S biosynthesis in both cytosol and mitochondria, following the reduction of free H_2S biosynthesis using cysteine and 3-MP as substrate. H_2S produced in the vicinity of the mitochondria, in cooperation with the sulfide-oxidizing unit (SOU), stimulates and balances mitochondrial electron transport [68]. The SOU is constituted of mitochondrial membrane-bound sulfide quinone reductase (SQR) and two other enzymes the sulfur dioxygenase (ETHE1, also called dioxygenase ethylmalonic encephalopathy) and the thio- sulfate sulfurtransferase (TST, also known as one isoenzyme of the rhodanese), ensuring the final oxidation of the two disulfides consuming molecular oxygen and water [68]. SQR is responsible for the oxidation of H_2S in the mitochondria [68], from two H_2S molecules, two disulfides (-SSH) bounds are created on the SQR, two electrons derived from two H_2S molecules enter the mitochondrial electron transport chain, promoting mitochondrial ATP generation. Although higher concentrations of H_2S can also inhibit Complex IV, thereby inhibiting mitochondrial potential [68]. However, in ΔMST mouse models, the activity of the complex IV was found to be similar to the WT [99]. It has been reported that the silencing of 3-MST in liver cell cultures led to reduced bioenergetics and concomitant stimulation by 3-MP, at low concentrations [96]. In ΔMST mouse, the expression of CTH was found to be reduced compared to the wild type mouse. Here, we also reported similar reduction in the abundance of CTH in the *TUM1 KO* cells [99]. The effect of the other two H_2S producing enzymes CBS and CTH could not be annulled since H_2S can diffuse intothe mitochondria [100]. However, studies reported that CTH did not affect the cellular bioenergetics in smooth muscle cells under normal conditions [98]. It was also reported that CTH deficiency promotes ETC in blood cells [101]. Mice deficient in CTH were also shown to have decreased mitochondria biogenesis. These alternating outcomes suggest that the effect of H_2S enzymes may defer between different tissues and complexity. We reported significant reduction in the total ATP production in the *TUM1 KO* cells and were more dependent on the glycolytic ATP production pathway rather than the mitochondria ATP production pathway. High proton leak was observed in the *TUM1* and *MOCS3 KO* cells, causing damage to the mitochondria membrane. Sulfite has been reported to alter the mitochondria in molybdenum cofactor deficiency [32], following the sulfite dependent increase in ROS with concordant decrease in ATP [102]. Non mitochondria O_2 consumption is caused by ROS production and other oxidative reactions [103]. We observed that non- mitochondria O_2 consumption is increased in both *MOCS3* and *TUM1 KO* and an increase in ROS level (Figure S1). Furthermore, inhibition of glutamate dehydrogenase was linked to ATP production via sulfite accumulation [102]. In accordance to this, a decreased rate of glutamate oxidation indicating low level of glutamate dehydrogenase was observed in *TUM1 KO* although not so pronounced in the *MOCS3 KO* (Figure S3). Therefore, the lower ATP level in the *TUM1 KO* compared to the *MOCS3 KO* could be a combined alteration in H_2S biosynthesis and glutamate dehydrogenase inhibition (Figure S3). This could also be explained by the low expression of CTH and CBS in the *TUM1 KO* cells but not less

pronounced in the *MOCS3 KO*. In *C. elegans*, suppression of CTH and CDO has been shown to alleviate the effect of Moco deficiency on growth in the cell. CTH and CDO through cysteine produces sulfite, thereby inhibiting growth rate [71]. Therefore, TUM1 is not only important for Moco biosynthesis and 2-thiouridine formation but also for cellular respiration and ATP production. The fact that we see an impairment of cellular bioenergetics, ATP production in mitochondria in addition to the reduced sulfite oxidase activity in *TUM1* and *MOCS3 KO* cells, fits well into what has been observed in fibroblasts from sulfite oxidase KO patients, where an impaired ATP production and an SO_3^{2-} induced mitochondrial fragmentation has been observed [32]. Therefore, our results fit well into what has been observed before in cells with higher SO_3^{2-} levels based on a reduced sulfite oxidase activity where decreased ATP levels, impaired cellular respiration, inhibition of glutamate dehydrogenase and malate dehydrogenase were reported [102].

Supplementary Materials: The following supporting information can be downloaded at: https://www.mdpi.com/article/10.3390/biom13010144/s1, Figure S1: Quantification of reactive oxygen species in HEK293T; Figure S2: Effect of oxidative stress on tRNA thiolation. Figure S3: Effect of oxidative stress on tRNA thiolation.

Author Contributions: Conceptualization, M.O.O. and S.L.; methodology, M.O.O., S.L., F.F. and G.G.-C.; software, M.O.O.; validation, M.O.O., S.L.; formal analysis, M.O.O. and S.L.; investigation, M.O.O. and S.L.; data curation, M.O.O. and S.L.; writing—original draft preparation, M.O.O. andS.L.; writing—review and editing, M.O.O. and S.L.; visualization, M.O.O.; supervision, S.L.; funding acquisition, S.L. All authors have read and agreed to the published version of the manuscript.

Funding: The work was funded by the Deutsche Forschungsgemeinschaft grant [LE11-71/11-2] Projektnummer 491466077 to (S.L.). The Seahorse experiments were funded by the CNRS.

Institutional Review Board Statement: Not applicable.

Informed Consent Statement: Not applicable.

Data Availability Statement: Not applicable.

Conflicts of Interest: The authors declare no conflict of interest.

References

1. Bordo, D.; Bork, P. The rhodanese/Cdc25 phosphatase superfamily. *EMBO Rep.* **2002**, *3*, 741–746. [CrossRef] [PubMed]
2. Shibuya, N.; Tanaka, M.; Yoshida, M.; Ogasawara, Y.; Togawa, T.; Ishii, K.; Kimura, H. 3-Mercaptopyruvate Sulfurtransferase Produces Hydrogen Sulfide and Bound Sulfane Sulfur in the Brain. *Antioxid. Redox Signal.* **2009**, *11*, 703–714. [CrossRef] [PubMed]
3. Yadav, P.K.; Yamada, K.; Chiku, T.; Koutmos, M.; Banerjee, R. Structure and Kinetic Analysis of H_2S Production by Human Mercaptopyruvate Sulfurtransferase. *J. Biol. Chem.* **2013**, *288*, 20002–20013. [CrossRef] [PubMed]
4. Palenchar, P.M.; Buck, C.J.; Cheng, H.; Larson, T.J.; Mueller, E.G. Evidence That ThiI, an Enzyme Shared between Thiamin and 4-Thiouridine Biosynthesis, May Be a Sulfurtransferase That Proceeds through a Persulfide Intermediate. *J. Biol. Chem.* **2000**, *275*, 8283–8286. [CrossRef] [PubMed]
5. Ubuka, T.; Ohta, J.; Yao, W.-B.; Abe, T.; Teraoka, T.; Kurozumi, Y. l-Cysteine metabolism via 3-mercaptopyruvate pathway and sulfate formation in rat liver mitochondria. *Amino Acids* **1992**, *2*, 143–155. [CrossRef]
6. Westley, J.; Adler, H.; Westley, L.; Nishida, C. The sulfurtransferases. *Fundam. Appl. Toxicol.* **1983**, *3*, 377–382. [CrossRef]
7. Fräsdorf, B.; Radon, C.; Leimkühler, S. Characterization and Interaction Studies of Two Isoforms of the Dual Localized 3-Mercaptopyruvate Sulfurtransferase TUM1 from Humans. *J. Biol. Chem.* **2014**, *289*, 34543–34556. [CrossRef]
8. Noma, A.; Sakaguchi, Y.; Suzuki, T. Mechanistic characterization of the sulfur-relay system for eukaryotic 2-thiouridine biogenesisat tRNA wobble positions. *Nucleic Acids Res.* **2009**, *37*, 1335–1352. [CrossRef]
9. Pedre, B.; Dick, T.P. 3-Mercaptopyruvate sulfurtransferase: An enzyme at the crossroads of sulfane sulfur trafficking. *Biol. Chem.* **2020**, *402*, 223–237. [CrossRef]
10. Wróbel, M.; Bronowicka-Adamska, P.; Bentke, A. Hydrogen sulfide generation from L-cysteine in the human glioblastoma-astrocytoma U-87 MG and neuroblastoma SHSY5Y cell lines. *Acta Biochim. Pol.* **2017**, *64*, 171–176. [CrossRef]
11. Gai, J.-W.; Wahafu, W.; Guo, H.; Liu, M.; Wang, X.-C.; Xiao, Y.-X.; Zhang, L.; Xin, Z.-C.; Jin, J. Further evidence of endogenous hydrogen sulphide as a mediator of relaxation in human and rat bladder. *Asian J. Androl.* **2013**, *15*, 692–696. [CrossRef]
12. Ramasamy, S.; Singh, S.; Taniere, P.; Langman, M.J.S.; Eggo, M.C. Sulfide-detoxifying enzymes in the human colon are decreasedin cancer and upregulated in differentiation. *Am. J. Physiol.-Gastrointest. Liver Physiol.* **2006**, *291*, G288–G296. [CrossRef] [PubMed]

13. Zuhra, K.; Sousa, P.M.F.; Paulini, G.; Lemos, A.R.; Kalme, Z.; Bisenieks, I.; Bisenieks, E.; Vigante, B.; Duburs, G.; Bandeiras, T.M.; et al. Screening Pyridine Derivatives against Human Hydrogen Sulfide-synthesizing Enzymes by Orthogonal Methods. *Sci.Rep.* **2019**, *9*, 684. [CrossRef] [PubMed]
14. Fiedler, H.; Wood, J.L. SPECIFICITY STUDIES ON THE β-MERCAPTOPYRUVATE-CYANIDE TRANSSULFURATION SYSTEM. *J. Biol. Chem.* **1956**, *222*, 387–397. [CrossRef]
15. Shen, X.; Pattillo, C.B.; Pardue, S.; Bir, S.C.; Wang, R.; Kevil, C.G. Measurement of plasma hydrogen sulfide in vivo and in vitro. *Free. Radic. Biol. Med.* **2011**, *50*, 1021–1031. [CrossRef] [PubMed]
16. Vachek, H.; Wood, J.L. Purification and properties of mercaptopyruvate sulfur transferase of Escherichia coli. *Biochim. et Biophys.Acta (BBA)—Enzym.* **1972**, *258*, 133–146. [CrossRef]
17. Taniguchi, T.; Kimura, T. Role of 3-mercaptopyruvate sulfurtransferase in the formation of the iron-sulfur chromophore of adrenal ferredoxin. *Biochim. et Biophys. Acta (BBA)—Enzym.* **1974**, *364*, 284–295. [CrossRef]
18. Crawhall, J.C.; Parker, R.; Sneddon, W.; Young, E.P.; Ampola, M.G.; Efron, M.L.; Bixby, E.M. Beta Mercaptolactate-Cysteine Disulfide: Analog of Cystine in the Urine of a Mentally Retarded Patient. *Science* **1968**, *160*, 419–420. [CrossRef]
19. Hannestad, U.; Mårtensson, J.; Sjödahl, R.; Sörbo, B. 3-Mercaptolactate cysteine disulfiduria: Biochemical studies on affected and unaffected members of a family. *Biochem. Med.* **1981**, *26*, 106–114. [CrossRef]
20. Niederwieser, A.; Giliberti, P.; Baerlocher, K. β-mercaptolactate cysteine disulfiduria in two normal sisters. Isolation and characterization of β-mercaptolactate cysteine disulfide. *Clin. Chim. Acta* **1973**, *43*, 405–416. [CrossRef]
21. Nagahara, N.; Nagano, M.; Ito, T.; Shimamura, K.; Akimoto, T.; Suzuki, H. Antioxidant enzyme, 3-mercaptopyruvate sulfurtransferase-knockout mice exhibit increased anxiety-like behaviors: A model for human mercaptolactate-cysteine disulfiduria. *Sci. Rep.* **2013**, *3*, srep01986. [CrossRef] [PubMed]
22. Kimura, H.; Shibuya, N.; Kimura, Y. Hydrogen Sulfide Is a Signaling Molecule and a Cytoprotectant. *Antioxidants Redox Signal.* **2012**, *17*, 45–57. [CrossRef] [PubMed]
23. Mendel, R.R.; Leimkühler, S. The biosynthesis of the molybdenum cofactors. *JBIC J. Biol. Inorg. Chem.* **2014**, *20*, 337–347. [CrossRef] [PubMed]
24. Stallmeyer, B.; Drugeon, G.; Reiss, J.; Haenni, A.; Mendel, R. Human Molybdopterin Synthase Gene: Identification of a Bicistronic Transcript with Overlapping Reading Frames. *Am. J. Hum. Genet.* **1999**, *64*, 698–705. [CrossRef]
25. Schmitz, J.; Chowdhury, M.M.; Hänzelmann, P.; Nimtz, M.; Lee, E.-Y.; Schindelin, H.; Leimkühler, S. The Sulfurtransferase Activity of Uba4 Presents a Link between Ubiquitin-like Protein Conjugation and Activation of Sulfur Carrier Proteins. *Biochemistry* **2008**,*47*, 6479–6489. [CrossRef]
26. Hille, R.; Hall, J.; Basu, P. The Mononuclear Molybdenum Enzymes. *Chem. Rev.* **2014**, *114*, 3963–4038. [CrossRef]
27. Cohen, H.J.; Fridovich, I. Hepatic Sulfite Oxidase. Purification and Properties. *J. Biol. Chem.* **1971**, *246*, 359–366. [CrossRef]
28. Woo, W.H.; Yang, H.; Wong, K.P.; Halliwell, B. Sulphite oxidase gene expression in human brain and in other human and rat tissues. *Biochem. Biophys. Res. Commun.* **2003**, *305*, 619–623. [CrossRef]
29. Velayutham, M.; Hemann, C.F.; Cardounel, A.J.; Zweier, J.L. Sulfite oxidase activity of cytochrome c: Role of hydrogen peroxide. *Biochem. Biophys. Rep.* **2016**, *5*, 96–104. [CrossRef] [PubMed]
30. Kohl, J.B.; Mellis, A.-T.; Schwarz, G. Homeostatic impact of sulfite and hydrogen sulfide on cysteine catabolism. *J. Cereb. Blood Flow Metab.* **2018**, *176*, 554–570. [CrossRef] [PubMed]
31. Johnson, J.L.; Duran, M. Molybdenum Cofactor Deficiency and Isolated Sulfite Oxidase Deficiency. In *The Online Metabolic and Molecular Bases of Inherited Disease*; Valle, D.L., Antonarakis, S., Ballabio, A., Beaudet, A.L., Mitchell, G.A., Eds.; McGraw-Hill Education: New York, NY, USA, 2019.
32. Mellis, A.-T.; Roeper, J.; Misko, A.L.; Kohl, J.; Schwarz, G. Sulfite Alters the Mitochondrial Network in Molybdenum Cofactor Deficiency. *Front. Genet.* **2021**, *11*, 594828. [CrossRef] [PubMed]
33. Agris, P.F. The importance of being modified: An unrealized code to RNA structure and function. *RNA* **2015**, *21*, 552–554. [CrossRef]
34. Björk, G.R.; Huang, B.; Persson, O.P.; Byström, A.S. A conserved modified wobble nucleoside (mcm^5s^2U) in lysyl-tRNA is required for viability in yeast. *RNA* **2007**, *13*, 1245–1255. [CrossRef] [PubMed]
35. Klassen, R.; Grunewald, P.; Thüring, K.L.; Eichler, C.; Helm, M.; Schaffrath, R. Loss of Anticodon Wobble Uridine Modifications Affects tRNALys Function and Protein Levels in Saccharomyces cerevisiae. *PLoS ONE* **2015**, *10*, e0119261. [CrossRef] [PubMed]
36. Leidel, S.; Pedrioli, P.G.A.; Bucher, T.; Brost, R.; Costanzo, M.; Schmidt, A.; Aebersold, R.; Boone, C.; Hofmann, K.; Peter, M. Ubiquitin-related modifier Urm1 acts as a sulphur carrier in thiolation of eukaryotic transfer RNA. *Nature* **2009**, *458*, 228–232.[CrossRef] [PubMed]
37. Nedialkova, D.D.; Leidel, S.A. Optimization of Codon Translation Rates via tRNA Modifications Maintains Proteome Integrity. *Cell* **2015**, *161*, 1606–1618. [CrossRef]
38. Yarian, C.; Townsend, H.; Czestkowski, W.; Sochacka, E.; Malkiewicz, A.J.; Guenther, R.; Miskiewicz, A.; Agris, P.F. Accurate Translation of the Genetic Code Depends on tRNA Modified Nucleosides. *J. Biol. Chem.* **2002**, *277*, 16391–16395. [CrossRef]
39. Chowdhury, M.M.; Dosche, C.; Löhmannsröben, H.-G.; Leimkühler, S. Dual Role of the Molybdenum Cofactor Biosynthesis Protein MOCS3 in tRNA Thiolation and Molybdenum Cofactor Biosynthesis in Humans. *J. Biol. Chem.* **2012**, *287*, 17297–17307.[CrossRef] [PubMed]

40. Leimkühler, S.; Bühning, M.; Beilschmidt, L. Shared Sulfur Mobilization Routes for tRNA Thiolation and Molybdenum Cofactor Biosynthesis in Prokaryotes and Eukaryotes. *Biomolecules* **2017**, *7*, 5. [CrossRef]
41. Van der Veen, A.G.; Schorpp, K.; Schlieker, C.; Buti, L.; Damon, J.R.; Spooner, E.; Ploegh, H.L.; Jentsch, S. Role of the ubiquitin-likeprotein Urm1 as a noncanonical lysine-directed protein modifier. *Proc. Natl. Acad. Sci. USA* **2011**, *108*, 1763–1770. [CrossRef][PubMed]
42. Chen, C.; Huang, B.; Eliasson, M.; Rydén, P.; Byström, A.S. Elongator Complex Influences Telomeric Gene Silencing and DNA Damage Response by Its Role in Wobble Uridine tRNA Modification. *PLOS Genet.* **2011**, *7*, e1002258. [CrossRef]
43. Pedrioli, P.G.A.; Leidel, S.; Hofmann, K. Urm1 at the crossroad of modifications. *EMBO Rep.* **2008**, *9*, 1196–1202. [CrossRef] [PubMed]
44. Xu, J.; Zhang, J.; Wang, L.; Zhou, J.; Huang, H.; Wu, J.; Zhong, Y.; Shi, Y. Solution structure of Urm1 and its implications for the origin of protein modifiers. *Proc. Natl. Acad. Sci. USA* **2006**, *103*, 11625–11630. [CrossRef] [PubMed]
45. Suzuki, T.; Wada, T.; Saigo, K.; Watanabe, K. Taurine as a constituent of mitochondrial tRNAs: New insights into the functions of taurine and human mitochondrial diseases. *EMBO J.* **2002**, *21*, 6581–6589. [CrossRef]
46. Kirino, Y.; Suzuki, T. Human Mitochondrial Diseases Associated with tRNA Wobble Modification Deficiency. *RNA Biol.* **2005**, *2*, 41–44. [CrossRef]
47. Umeda, N.; Suzuki, T.; Yukawa, M.; Ohya, Y.; Shindo, H.; Watanabe, K.; Suzuki, T. Mitochondria-specific RNA-modifying Enzymes Responsible for the Biosynthesis of the Wobble Base in Mitochondrial tRNAs. *J. Biol. Chem.* **2005**, *280*, 1613–1624. [CrossRef] [PubMed]
48. Suzuki, T. Biosynthesis and function of tRNA wobble modifications. In *Fine-Tuning of RNA Functions by Modification and Editing*; Springer: Berlin/Heidelberg, Germany, 2005; pp. 23–69. [CrossRef]
49. Abe, K.; Kimura, H. The possible role of hydrogen sulfide as an endogenous neuromodulator. *J. Neurosci.* **1996**, *16*, 1066–1071. [CrossRef]
50. Hosoki, R.; Matsuki, N.; Kimura, H. The Possible Role of Hydrogen Sulfide as an Endogenous Smooth Muscle Relaxant in Synergy with Nitric Oxide. *Biochem. Biophys. Res. Commun.* **1997**, *237*, 527–531. [CrossRef]
51. Nakai, Y.; Nakai, M.; Hayashi, H. Thio-modification of Yeast Cytosolic tRNA Requires a Ubiquitin-related System That Resembles Bacterial Sulfur Transfer Systems. *J. Biol. Chem.* **2008**, *283*, 27469–27476. [CrossRef]
52. Land, T.; Rouault, T.A. Targeting of a Human Iron–Sulfur Cluster Assembly Enzyme, nifs, to Different Subcellular CompartmentsIs Regulated through Alternative AUG Utilization. *Mol. Cell* **1998**, *2*, 807–815. [CrossRef]
53. Marelja, Z.; Chowdhury, M.M.; Dosche, C.; Hille, C.; Baumann, O.; Löhmannsröben, H.-G.; Leimkühler, S. The L-Cysteine Desulfurase NFS1 Is Localized in the Cytosol where it Provides the Sulfur for Molybdenum Cofactor Biosynthesis in Humans. *PLoS ONE* **2013**, *8*, e60869. [CrossRef]
54. Ran, F.A.; Hsu, P.D.; Wright, J.; Agarwala, V.; Scott, D.A.; Zhang, F. Genome engineering using the CRISPR-Cas9 system. *Nat. Protoc.* **2013**, *8*, 2281–2308. [CrossRef] [PubMed]
55. Guide design resources—Zhang Lab. Available online: https://zlab.bio/guide-design-resources (accessed on 16 August 2022).
56. Addgene: CRISPR Plasmids and Resources. Available online: https://www.addgene.org/crispr/ (accessed on 1 September 2017).
57. Freimoser, F.M.; Jakob, C.A.; Aebi, M.; Tuor, U. The MTT [3-(4,5-Dimethylthiazol-2-yl)-2,5-Diphenyltetrazolium Bromide] Assay Is a Fast and Reliable Method for Colorimetric Determination of Fungal Cell Densities. *Appl. Environ. Microbiol.* **1999**, *65*, 3727–3729. [CrossRef] [PubMed]
58. Beinert, H.; Kennedy, M.C. Aconitase, a two-faced protein: Enzyme and iron regulatory factor [1 2]. *FASEB J.* **1993**, *7*, 1442–1449. [CrossRef] [PubMed]
59. Uhrigshardt, H.; Singh, A.; Kovtunovych, G.; Ghosh, M.; Rouault, T.A. Characterization of the human HSC20, an unusual DnaJ type III protein, involved in iron–sulfur cluster biogenesis. *Hum. Mol. Genet.* **2010**, *19*, 3816–3834. [CrossRef] [PubMed]
60. Johnson, J.L.; Rajagopalan, K.V.; Lanman, J.T.; Schutgens, R.B.H.; van Gennip, A.H.; Sorensen, P.; Applegarth, D.A. Prenatal diagnosis of molybdenum cofactor deficiency by assay of sulphite oxidase activity in chorionic villus samples. *J. Inherit. Metab.Dis.* **1991**, *14*, 932–937. [CrossRef]
61. Gehrke, C.W.; Kuo, K.C. Ribonucleoside analysis by reversed-phase high-performance liquid chromatography. *J. Chromatogr. A* **1989**, *471*, 3–36. [CrossRef] [PubMed]
62. Johnson, J.L.; Hainline, B.E.; Rajagopalan, K.V.; Arison, B.H. The pterin component of the molybdenum cofactor. Structural characterization of two fluorescent derivatives. *J. Biol. Chem.* **1984**, *259*, 5414–5422. [CrossRef]
63. Fogo, J.K.; Popowsky, M. Spectrophotometric Determination of Hydrogen Sulfide. *Anal. Chem.* **1949**, *21*, 732–734. [CrossRef]
64. Wu, D.; Yotnda, P. Production and Detection of Reactive Oxygen Species (ROS) in Cancers. *J. Vis. Exp.* **2011**, *57*, e3357. [CrossRef] [PubMed]
65. van der Windt, G.J.; Chang, C.; Pearce, E.L. Measuring Bioenergetics in T Cells Using a Seahorse Extracellular Flux Analyzer. *Curr. Protoc. Immunol.* **2016**, *113*, 3.16B.1–3.16B.14. [CrossRef] [PubMed]
66. Neukranz, Y.; Kotter, A.; Beilschmidt, L.; Marelja, Z.; Helm, M.; Gräf, R.; Leimkühler, S. Analysis of the Cellular Roles of MOCS3 Identifies a MOCS3-Independent Localization of NFS1 at the Tips of the Centrosome. *Biochemistry* **2019**, *58*, 1786–1798. [CrossRef] [PubMed]
67. Greiner, R.; Pálinkás, Z.; Bäsell, K.; Becher, D.; Antelmann, H.; Nagy, P.; Dick, T.P. Polysulfides Link H_2S to Protein Thiol Oxidation. *Antioxidants Redox Signal.* **2013**, *19*, 1749–1765. [CrossRef]

68. Szabo, C.; Ransy, C.; Módis, K.; Andriamihaja, M.; Murghes, B.; Coletta, C.; Olah, G.; Yanagi, K.; Bouillaud, F. Regulation of mitochondrial bioenergetic function by hydrogen sulfide. Part I. Biochemical and physiological mechanisms. *Br. J. Pharmacol.* **2014**, *171*, 2099–2122. [CrossRef]
69. Módis, K.; Coletta, C.; Erdélyi, K.; Papapetropoulos, A.; Szabo, C. Intramitochondrial hydrogen sulfide production by 3-mercaptopyruvate sulfurtransferase maintains mitochondrial electron flow and supports cellular bioenergetics. *FASEB J.* **2012**, *27*, 601–611. [CrossRef] [PubMed]
70. Klein, J.M.; Schwarz, G. Cofactor-dependent maturation of mammalian sulfite oxidase links two mitochondrial import pathways. *J. Cell Sci.* **2012**, *125*, 4876–4885. [CrossRef] [PubMed]
71. Warnhoff, K.; Ruvkun, G. Molybdenum cofactor transfer from bacteria to nematode mediates sulfite detoxification. *Nat. Chem.Biol.* **2019**, *15*, 480–488. [CrossRef] [PubMed]
72. Jüdes, A.; Ebert, F.; Bär, C.; Thüring, K.L.; Harrer, A.; Klassen, R.; Helm, M.; Stark, M.J.; Schaffrath, R. Urmylation and tRNA thiolation functions of ubiquitin-like Uba4 Urm1 systems are conserved from yeast to man. *FEBS Lett.* **2015**, *589*, 904–909. [CrossRef]
73. Cao, X.; Ding, L.; Xie, Z.Z.; Yang, Y.; Whiteman, M.; Moore, P.K.; Bian, J.S. A Review of Hydrogen Sulfide Synthesis, Metabolism, and Measurement: Is Modulation of Hydrogen Sulfide a Novel Therapeutic for Cancer? *Antioxidants Redox Signal.* **2019**, *31*, 1–38. [CrossRef]
74. Módis, K.; Ju, Y.; Ahmad, A.; Untereiner, A.A.; Altaany, Z.; Wu, L.; Szabo, C.; Wang, R. S- Sulfhydration of ATP synthase by hydrogen sulfide stimulates mitochondrial bioenergetics. *Pharmacol. Res.* **2016**, *113*, 116–124. [CrossRef] [PubMed]
75. Borisov, V.B.; Forte, E. Impact of Hydrogen Sulfide on Mitochondrial and Bacterial Bioenergetics. *Int. J. Mol. Sci.* **2021**, *22*, 12688. [CrossRef] [PubMed]
76. Lushchak, O.V.; Piroddi, M.; Galli, F.; Lushchak, V.I. Aconitase post-translational modification as a key in linkage between Krebs cycle, iron homeostasis, redox signaling, and metabolism of reactive oxygen species. *Redox Rep.* **2013**, *19*, 8–15. [CrossRef] [PubMed]
77. Dhami, N.; Trivedi, D.K.; Goodacre, R.; Mainwaring, D.; Humphreys, D.P. Mitochondrial aconitase is a key regulator of energy production for growth and protein expression in Chinese hamster ovary cells. *Metabolomics* **2018**, *14*, 136. [CrossRef] [PubMed]
78. Ray, W.K.; Zeng, G.; Potters, M.B.; Mansuri, A.M.; Larson, T.J. Characterization of a 12-Kilodalton Rhodanese Encoded by *glpE* of *Escherichia coli* and Its Interaction with Thioredoxin. *J. Bacteriol.* **2000**, *182*, 2277–2284. [CrossRef] [PubMed]
79. Spallarossa, A.; Donahue, J.L.; Larson, T.J.; Bolognesi, M.; Bordo, D. Escherichia coli GlpE Is a Prototype Sulfurtransferase for the Single-Domain Rhodanese Homology Superfamily. *Structure* **2001**, *9*, 1117–1125. [CrossRef]
80. Zhang, Y.; Gladyshev, V.N. Molybdoproteomes and Evolution of Molybdenum Utilization. *J. Mol. Biol.* **2008**, *379*, 881–899. [CrossRef]
81. Kessler, D. Enzymatic activation of sulfur for incorporation into biomolecules in prokaryotes. *FEMS Microbiol. Rev.* **2006**, *30*, 825–840. [CrossRef]
82. Hidese, R.; Mihara, H.; Esaki, N. Bacterial cysteine desulfurases: Versatile key players in biosynthetic pathways of sulfur-containing biofactors. *Appl. Microbiol. Biotechnol.* **2011**, *91*, 47–61. [CrossRef]
83. Rydz, L.; Wróbel, M.; Jurkowska, H. Sulfur Administration in Fe–S Cluster Homeostasis. *Antioxidants* **2021**, *10*, 1738. [CrossRef]
84. Billaut-Laden, I.; Rat, E.; Allorge, D.; Crunelle-Thibaut, A.; Cauffiez, C.; Chevalier, D.; Lo-Guidice, J.-M.; Broly, F. Evidence for a functional genetic polymorphism of the human mercaptopyruvate sulfurtransferase (MPST), a cyanide detoxification enzyme.*Toxicol. Lett.* **2006**, *165*, 101–111. [CrossRef] [PubMed]
85. Duran, M.; Beemer, F.A.; Heiden, C.V.D.; Korteland, J.; de Bree, P.K.; Brink, M.; Wadman, S.K.; Lombeck, I. Combined deficiency of xanthine oxidase and sulphite oxidase: A defect of molybdenum metabolism or transport? *J. Inherit. Metab. Dis.* **1978**, *1*, 175–178. [CrossRef]
86. Benchoam, D.; Cuevasanta, E.; Möller, M.N.; Alvarez, B. Hydrogen Sulfide and Persulfides Oxidation by Biologically Relevant Oxidizing Species. *Antioxidants* **2019**, *8*, 48. [CrossRef]
87. Łowicka, E.; Bełtowski, J. Hydrogen sulfide (H_2S)—The third gas of interest for pharmacologists. *Pharmacol Rep.* **2007**, *59*, 4–24. [PubMed]
88. Paul, B.D.; Snyder, S.H. H_2S signalling through protein sulfhydration and beyond. *Nat. Rev. Mol. Cell Biol.* **2012**, *13*, 499–507. [CrossRef]
89. Koike, S.; Nishimoto, S.; Ogasawara, Y. Cysteine persulfides and polysulfides produced by exchange reactions with H_2S protectSH-SY5Y cells from methylglyoxal-induced toxicity through Nrf2 activation. *Redox Biol.* **2017**, *12*, 530–539. [CrossRef] [PubMed]
90. Kimura, H. Hydrogen Sulfide and Polysulfide Signaling. *Antioxidants Redox Signal.* **2017**, *27*, 619–621. [CrossRef] [PubMed]
91. Chiku, T.; Padovani, D.; Zhu, W.; Singh, S.; Vitvitsky, V.; Banerjee, R. H_2S Biogenesis by Human Cystathionine γ-Lyase Leads to the Novel Sulfur Metabolites Lanthionine and Homolanthionine and Is Responsive to the Grade of Hyperhomocysteinemia.*J. Biol. Chem.* **2009**, *284*, 11601–11612. [CrossRef] [PubMed]
92. Paul, B.D.; Snyder, S.H.; Kashfi, K. Effects of hydrogen sulfide on mitochondrial function and cellular bioenergetics. *Redox Biol.* **2020**, *38*, 101772. [CrossRef]
93. Damon, J.R.; Pincus, D.; Ploegh, H.L. tRNA thiolation links translation to stress responses in *Saccharomyces cerevisiae*. *Mol. Biol.Cell* **2015**, *26*, 270–282. [CrossRef]

94. Martínez-Reyes, I.; Diebold, L.P.; Kong, H.; Schieber, M.; Huang, H.; Hensley, C.T.; Mehta, M.M.; Wang, T.; Santos, J.H.; Woychik, R.; et al. TCA Cycle and Mitochondrial Membrane Potential Are Necessary for Diverse Biological Functions. *Mol. Cell* **2015**, *61*, 199–209. [CrossRef]
95. Finkelstein, J.D. Methionine metabolism in mammals. *J. Nutr. Biochem.* **1990**, *1*, 228–237. [CrossRef] [PubMed]
96. Módis, K.; Asimakopoulou, A.; Coletta, C.; Papapetropoulos, A.; Szabo, C. Oxidative stress suppresses the cellular bioenergetic effect of the 3-mercaptopyruvate sulfurtransferase/hydrogen sulfide pathway. *Biochem. Biophys. Res. Commun.* **2013**, *433*, 401–407.[CrossRef] [PubMed]
97. Hildebrandt, T.M.; Grieshaber, M.K. Three enzymatic activities catalyze the oxidation of sulfide to thiosulfate in mammalian andinvertebrate mitochondria. *FEBS J.* **2008**, *275*, 3352–3361. [CrossRef]
98. Fu, M.; Zhang, W.; Wu, L.; Yang, G.; Li, H.; Wang, R. Hydrogen sulfide (H_2S) metabolism in mitochondria and its regulatory rolein energy production. *Proc. Natl. Acad. Sci. USA* **2012**, *109*, 2943–2948. [CrossRef] [PubMed]
99. Trautwein, B.; Merz, T.; Denoix, N.; Szabo, C.; Calzia, E.; Radermacher, P.; McCook, O. ΔMST and the Regulation of Cardiac CSEand OTR Expression in Trauma and Hemorrhage. *Antioxidants* **2021**, *10*, 233. [CrossRef] [PubMed]
100. Murphy, B.; Bhattacharya, R.; Mukherjee, P. Hydrogen sulfide signaling in mitochondria and disease. *FASEB J.* **2019**, *33*, 13098–13125. [CrossRef] [PubMed]
101. Módis, K.; Ramanujam, V.-M.S.; Govar, A.A.; Lopez, E.; Anderson, K.E.; Wang, R.; Szabo, C. Cystathionine-γ-lyase (CSE) deficiency increases erythropoiesis and promotes mitochondrial electron transport via the upregulation of coproporphyrinogen III oxidase and consequent stimulation of heme biosynthesis. *Biochem. Pharmacol.* **2019**, *169*, 113604. [CrossRef] [PubMed]
102. Zhang, X.; Vincent, A.S.; Halliwell, B.; Wong, K.P. A Mechanism of Sulfite Neurotoxicity. *J. Biol. Chem.* **2004**, *279*, 43035–43045. [CrossRef] [PubMed]
103. Herst, P.M.; Tan, A.S.; Scarlett, D.-J.G.; Berridge, M.V. Cell surface oxygen consumption by mitochondrial gene knockout cells. *Biochim. et Biophys. Acta* **2004**, *1656*, 79–87. [CrossRef] [PubMed]

Manuscript II

Sulfur transferases in the pathways of molybdenum cofactor biosynthesis and tRNA thiolation in

Sulfur transferases in the pathways of molybdenum cofactor biosynthesis and tRNA thiolation in humans

Silke Leimkühler* and Moses Olalekan Ogunkola

Institute of Biochemistry and Biology, Department of Molecular Enzymology, University of Potsdam, 14476 Potsdam, Germany.

* Correspondence: sleim@uni-potsdam.de; Tel.: +49-331-977-5603

Abstract:

Sulfur is an essential element for all living organisms. Modifications of tRNA have been shown to play critical roles in the biogenesis, metabolism, structural stability and function of RNA molecules and the specific modifications of nucleobases with sulfur atoms in tRNA are present in pro- and eukaryotes. Here, especially the thiomodifications xm^5s^2U at the wobble position 34 in tRNAs for Lys, Gln and Glu, were suggested to have an important role during the translation process by ensuring accurate deciphering of the genetic code and by stabilization of the tRNA structure. The trafficking and delivery of sulfur to the molybdenum cofactor and to nucleosides in tRNA is a complex process that is carried out by sulfur relay systems involving numerous proteins, and is a highly regulated process which proceeds in a complex pathway involving several sulfur transferring proteins.

In humans, the cytosolic sulfur modification of mcm^5s^2U34 in $tRNAs^{Lys, Gln, Glu}$ requires the proteins NFS1, TUM1, MOCS3, URM1, CTU1 and CTU2. In contrast, the sulfur insertion for τm^5s^2U34 modifications in mitochondrial $tRNA^{Lys, Gln, Glu}$ involves the proteins NFS1, TUM1 and MTU1. Further, for the synthesis of the dithiolene group of Moco, the proteins MOCS2A, MOCS3, TUM1 and NFS1 are involved, a reaction which occurs in the cytosol of humans. Conclusively, Moco biosynthesis and tRNA thiolation are connected in the cytosol and share the same sulfur delivery pathway proteins composed of NFS1, MOCS3 and possibly TUM1.

Introduction

Sulfur adds considerable functionality to a wide variety of biomolecules because of its unique properties: its chemical bonds are made and broken easily and sulfur equally well serves as an electrophile or a nucleophile (Beinert, 2000; Kessler, 2006). Sulfur is an indispensable component of certain cofactors like thiamine, biotin, lipoic acid,

molybdopterin and the iron sulfur clusters starting with the simpler [2Fe-2S] clusters to the highly complex [4Fe-4S] clusters(Figure1).

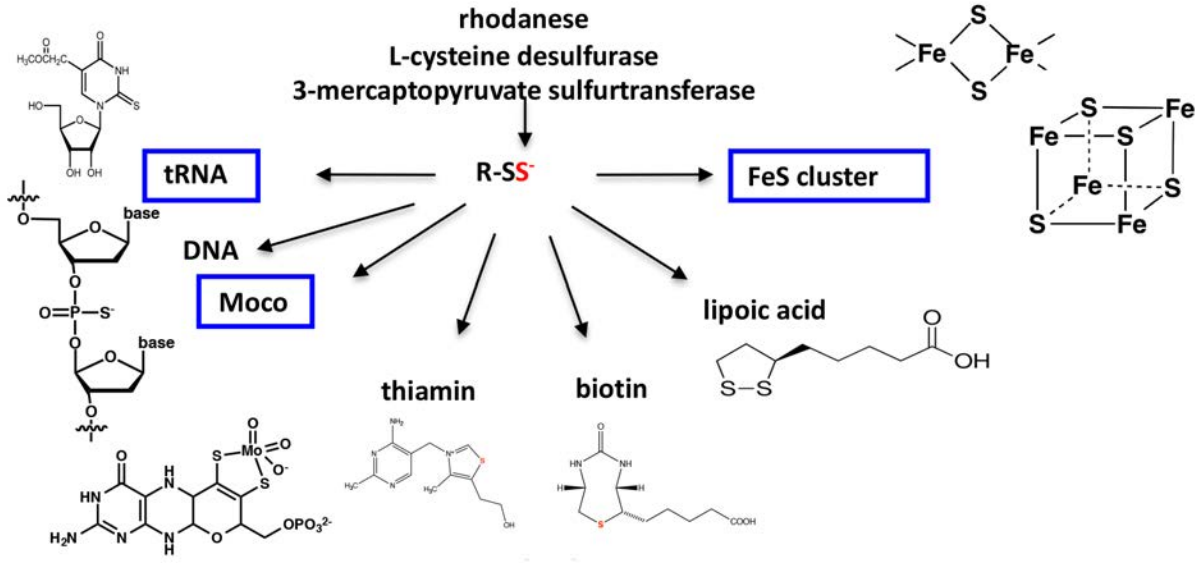

Figure 1: Sulfur compounds relying on persulfide transfer via sulfur transferases involving L-cysteine desulfurases, rhodaneses or β-mercaptopyruvate sulfur transferases.

In addition, nucleosides in RNA and DNA can be sulfurated, using mechanisms related to the biosynthesis of components like the Moco or Fe-S clusters and play an important role for cell viability (Hidese, Mihara, & Esaki, 2011; Leimkuhler, Buhning, & Beilschmidt, 2017). For incorporation into biomolecules, sulfur must be reduced or activated (Kessler, 2006) (Figure 1). In general, L-cysteine serves as a central building block for the insertion of sulfur into various biomolecules (Hidese et al., 2011). From L-cysteine the sulfur is provided as persulfide by sulfur carrier proteins (Black & Dos Santos, 2015). The other way to transfer sulfur is as thiocarboxylate group (Hochstrasser, 2000). Thiocarboxylate sulfur is formed on ubiquitin-like proteins (Hochstrasser, 2000; Leidel et al., 2009), which further transfer the sulfur by thioester intermediates to sulfur acceptor proteins or the final biomolecule. Ubiquitin-like proteins are the link to sulfur carrier proteins for the transpersulfidation and thiocarboxylate pathway(Pedrioli, Leidel, & Hofmann, 2008; Schlieker, Van der Veen, Damon, Spooner, & Ploegh, 2008). L-cysteine desulfurases are the proteins that mobilize the sulfur primarily from L-cysteine and form a protein-bound persulfide that can be transferred to acceptor proteins (Black & Dos Santos, 2015; Cupp-Vickery,

Urbina, & Vickery, 2003; Zheng, White, Cash, Jack, & Dean, 1993) (Figure 1). Pathways that combine both, the transpersulfidation of sulfur mobilized by L-cysteine desulfurases and the thiocarboxylate formation by ubiquitin-like proteins with thioester intermediates are the pathways for molybdenum cofactor biosynthesis, the formation of s^2U-modified nucleosides in tRNAs and the synthesis of thiamine (Leimkuhler et al., 2017). Here, we will focus on the first two pathways that even share protein components (Figure 2).

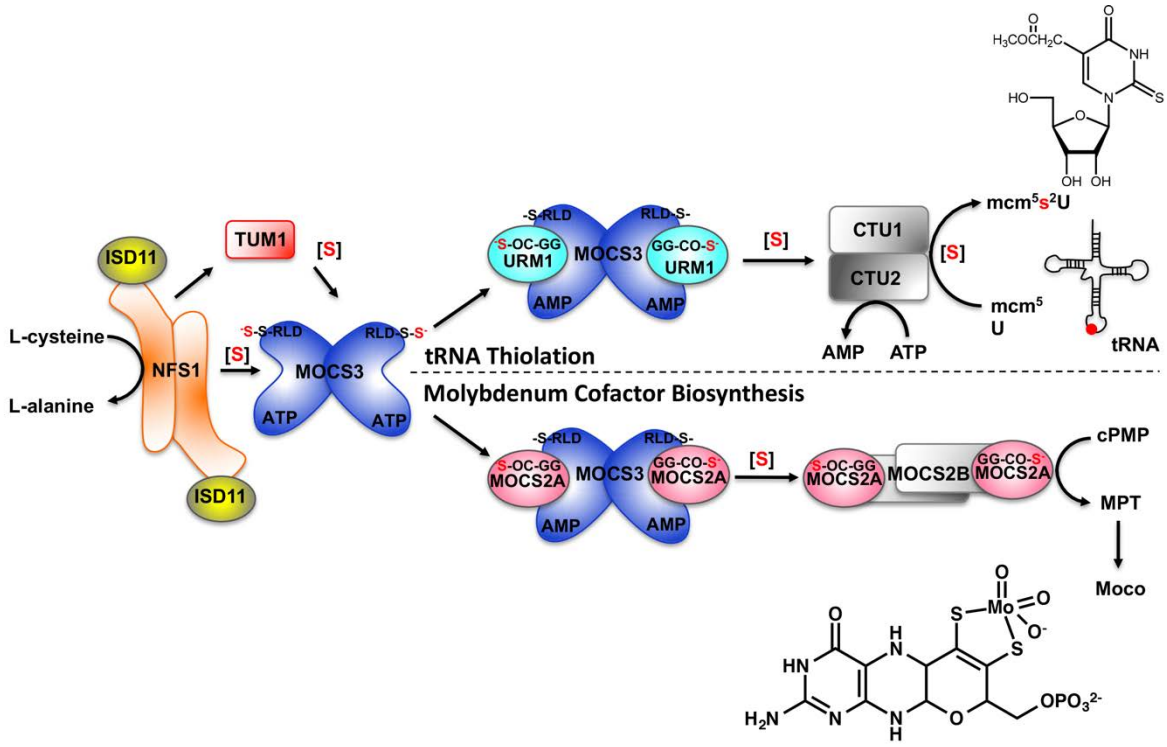

Figure 2: The dual role of MOSC3 in Moco biosynthesis and tRNA thiolation. Depicted are the sulfur transferase pathways and the involved proteins for Moco biosynthesis and tRNA thiolation. Details are given in the text.

Mechanisms involved in the thiolation of all these cofactors are shared and highly conserved among all species(Leimkuhler, 2017). Mobilization of sulfur is primarily catalyzed by L-cysteine desulfurases using L-Cysteine as substrate and resulting in the formation of a persulfide on a conserved cysteine residue that can be transferred to acceptor proteins by transpersulfidation. In *Saccharomyces cerevisiae* the L-cysteine desulfurase NFS1 was shown to be involved in cell viability and the thiolation of tRNA (Nakai, Nakai, Hayashi, & Kagamiyama, 2001);(Lill & Mühlenhoff, 2006) and is the proposed sulfur donor for Moco synthesis in humans (Marelja et al., 2013; Marelja, Stöcklein, Nimtz, & Leimkühler, 2008a; Neukranz et al., 2019). The sulfur can

be further transferred to rhodanese-like proteins in form of an enzyme-bound persulfide. Sulfur transferases/rhodaneses are widespread enzymes; that catalyze the transfer of a sulfane sulfur from a donor molecule to a thiophilic acceptor (Bordo & Bork, 2002) (Figure 1). Rhodaneses (thiosulfate:cyanide sulfur transferases) are able to transfer sulfur from thiosulfate to cyanide in vitro (Bordo & Bork, 2002). 3 Mercaptopyruvate:cyanide sulfur transferases (MSTs, EC 2.8.1.2) catalyze a similar reaction, using 3-mercaptopyruvate as the sulfur donor (Kessler, 2006; Pedre & Dick, 2021). The final step in the sulfur transfer to thio- containing cofactors can involve the thiocarboxylation of sulfur carrier proteins (Pedre & Dick, 2021). Besides the mobilization of sulfur, mechanisms for the activation of the sulfur carriers are highly conserved.

thiolation of tRNA

Post-transcriptional RNA modifications are a characteristic structural feature of RNA molecules. The diverse modifications have been shown to play critical roles in biogenesis, metabolism, structural stability and function of RNA molecules (El Yacoubi, Bailly, & de Crecy-Lagard, 2012). Transfer RNAs (tRNAs) are key for efficient and accurate protein translation. Up to 100 different modification in tRNAs were identified so far. Growing evidences indicate that tRNA modifications and the enzymes catalyzing such modifications play an important role in complex human pathologies. The thio-modification at the wobble position U34 of nucleotides present in lysine, glutamine or glutamate tRNAs were suggested to be responsible for enhanced translation efficiency by enhancing aminoacylation kinetics, assisting proper codon-anticodon pairing and preventing frameshifting during translation (El Yacoubi et al., 2012; Suzuki, 2005). In particular, the wobble bases of tRNAs for Glu, Gln and Lys are modified and sulfurated to form 5-methyl-2-thiouridine derivatives (xm^5s^2U), such as 5-taurinomethyl-2-thiouridine (τm^5s^2U) in mammalian mitochondrial tRNAs, and 5-methoxycarbonylmethyl-2-thiouridine (mcm^5s^2U) in eukaryotic cytoplasmic tRNAs (Noma, Shigi, & Suzuki, 2009)(Figure 3).

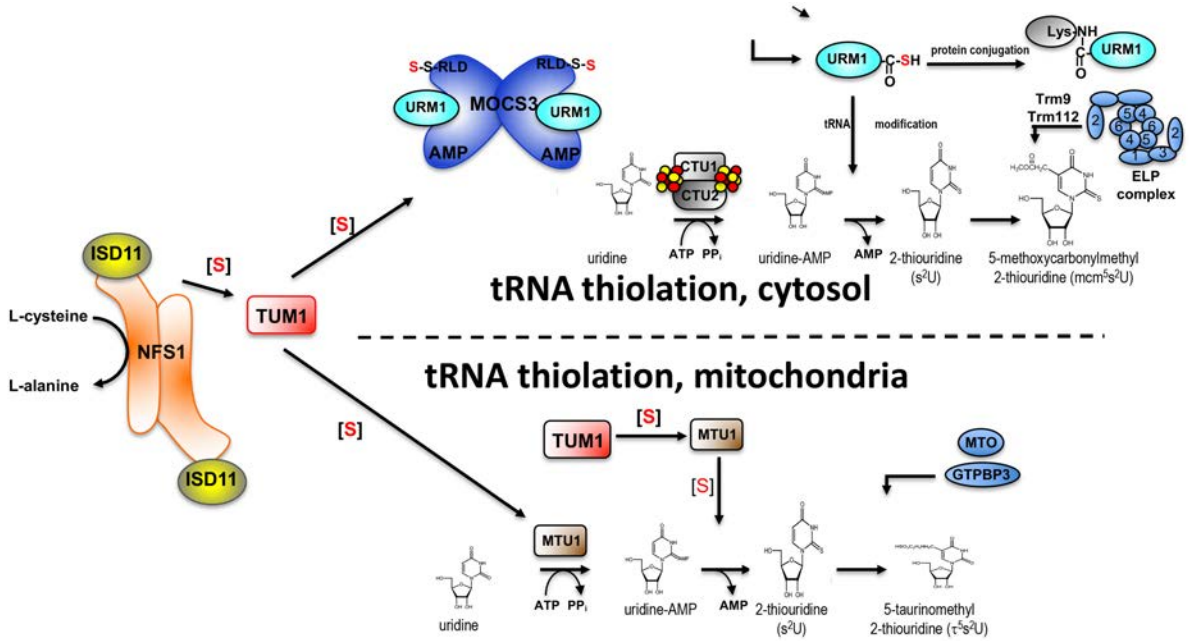

Figure 3: The sulfur transfer pathways for Moco biosynthesis and tRNA thiolation. Depicted are the sulfur transferase pathways and the involved proteins for Moco biosynthesis and tRNA thiolation. Details are given in the text. **Proposed mechanism of 5-taurinomethyl-2-thiouridine (□m^{5}s^{2}U^{34}) formation in mitochondria of humans.** MTO1 and GTPBP3 are essential for the formation of the taurine group at the C5 position of uridine 34 in tRNA Lys, Gln and Glu in mitochondria. However, details on the formation of the taurine group are not known so far. The MTU1 protein is involved in the activation of the τm^{5}U-modified tRNA under ATP consumption. In the activated form, sulfur can be transferred to the C2 position of the uridine. The sulfur is mobilized by the NFS1/ISD11 complex from L-cysteine in mitochondria and further transferred to TUM1-Iso2, which then transfers the sulfur to the MTU1/tRNA complex and τm^{5}s^{2}U^{34} is formed.

The result of these thiomodifications is that the conformation of xm^{5}s^{2}U is trapped in the C3'-*endo* form of the ribose, since the large van der Waals' radius of the 2-thio group causes a steric clash with its 2'-OH group (Noma, Shigi, et al., 2009; Yokoyama et al., 1985). This conformational rigidity causes preferential pairing of the xm^{5}s^{2}U modified bases with purines, and prevents misreading of codons ending in pyrimidines (Agris, Soll, & Seno, 1973; Durant, Bajji, Sundaram, Kumar, & Davis, 2005; Yokoyama et al., 1985). The mcm^{5}s^{2}U34 modification in the cytosol of eukaryotes is highly conserved and was identified to involve the same protein components in humans, yeast and plants, while the τm^{5}s^{2}U modification seem to be restricted to mitochondria of mammals (Figure 3).

For the **thiolation and formation of the mcm^{5}s^{2}U** in the cytosol of eukaryotes, the biosynthesis of the 5-methoxycarbonylmethyl-group of the uracil ring is required for efficient 2-thiouridine formation in the cytoplasm (Noma, Sakaguchi, & Suzuki, 2009) (Figure 3). In humans, it was shown that the proteins MOCS3, URM1,TUM1, CTU1 and CTU2 are involved in s^{2}U34 formation, while proteins of the ELP pathway synthesize the mcm^5-group (Van der Veen et al., 2011) (Figure 3). The *ELP* pathway includes the six subunits of the ELP-complex (ELP1–6) and the tRNA methyltransferase complex containing TRM9 and TRM112 (Chen, Huang, Eliasson,

Ryden, & Bystrom, 2011). The URM1 protein (ubiquitin-related modifier) was shown to have a ubiquitin-like β-grasp-fold and contains a conserved C-terminal double glycine-motif on which a thiocarboxylate group is formed for direct sulfur-transfer to mcm^5U34 in tRNA (Leidel et al., 2009; Pedrioli et al., 2008; Schmitz et al., 2008; Xu et al., 2006). The components essential for Urm1-mediated tRNA thiolation are MOCS3, NFS1, TUM1, CTU1 and CTU2 in humans (Figure 4).

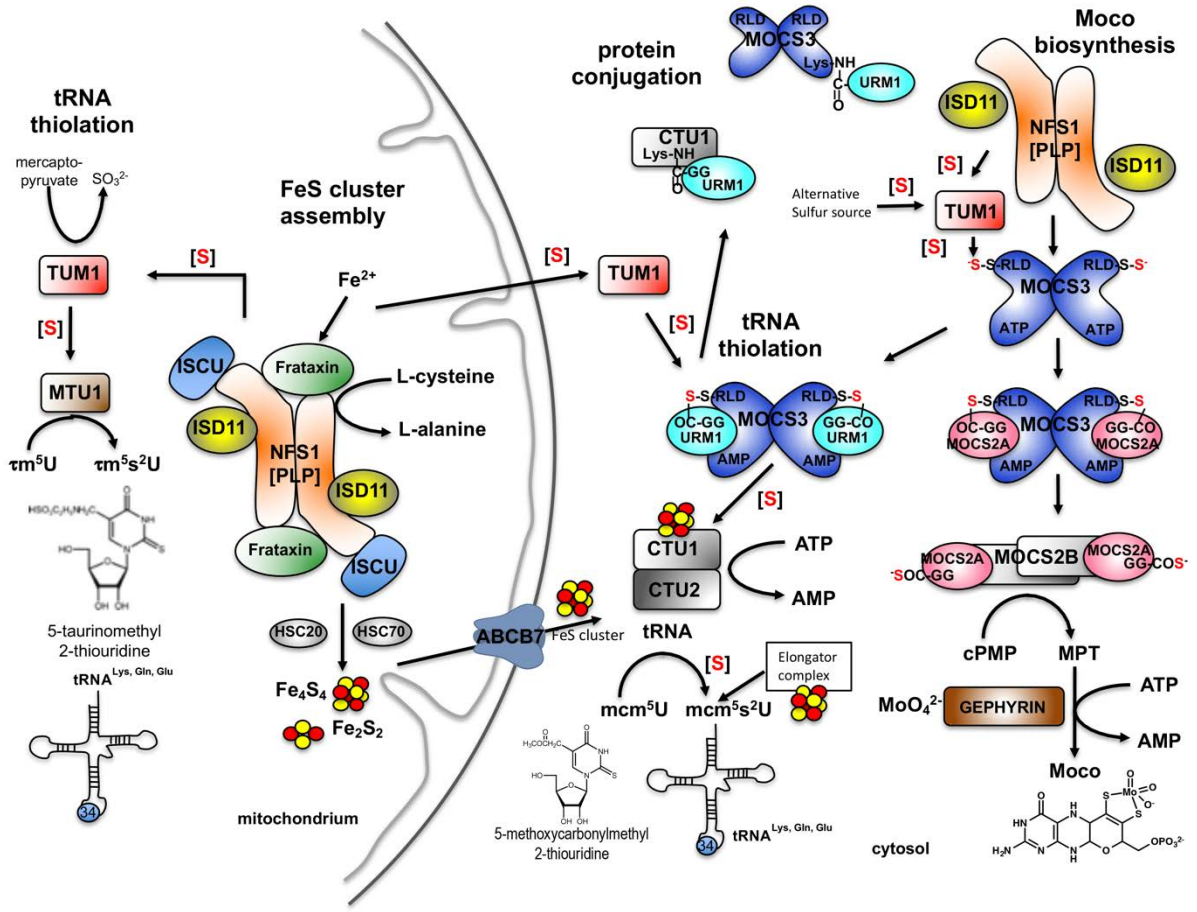

Figure 4: The different compartments for the biosynthesis of Moco in humans and the link to Fe-S cluster assembly in mitochondria. The first step of Moco biosynthesis, the conversion of 5'GTP to cPMP catalyzed by MOCS1A and MOCS1B, is localized in mitochondria. This is also the main compartment for Fe-S cluster biosynthesis in eukaryotes. Fe-S clusters assemble on the scaffold protein ISCU2, which receives the sulfur from the L-cysteine desulfurase complex NFS1/ISD11. The iron donor in this reaction has not been identified so far. Frataxin (FDN) is able to interact with the NFS1/Isd11-ISCU2 complex. Ferredoxin (FDX2) delivers the electrons for Fe-S cluster assembly. Assembly and release of the clusters is catalyzed by the chaperones HSC20/HSPA9. The carrier proteins GLRX5, ISCA2 and/or IBA57 deliver the Fe-S clusters to target proteins. Synthesized cPMP further is transferred to the cytosol, where all further modification steps are catalyzed. These steps involve the conversion of cPMP to MPT by MOCS2A/MOCS2B (which are activated by MOCS3), the insertion of molybdate by GEPHYRIN (GEPH), and the insertion of Mo-MPT either into sulfite oxidase (localized in the mitochondrial intermembrane space) or to the mARC protein (localized at the outer mitochondrial membrane). A further modification step of Moco is catalyzed by HMCS for the enzymes aldehyde oxidase and xanthine dehydrogenase, which involves the formation of the equatorial sulfido-ligand at the Mo atom, an essential requirement for the activity of these enzymes. A dual localization of NFS1 both in mitochondria and the cytosol is

predicted. Cytosolic NFS1 acts as a sulfur donor for MOCS3.

The sulfur is transferred to URM1 via MOCS3, which was originally recognized for its role in Moco biosynthesis (see below) (Chowdhury, Dosche, Löhmannsröben, & Leimkühler, 2012)

The formation of mcm^{5}s^{2}U in the cytosol of eukaryotes is directly linked to two other sulfur-containing cofactors, Moco biosynthesis and FeS cluster biosynthesis (Figure 4). It was suggested that CTU1 is a FeS cluster containing protein, ensuring tRNA thiolation only when functional FeS clusters are formed (Shigi, 2014). In addition, the MOCS3 protein is a dual-function protein which is directly shared in tRNA thiolation and Moco biosynthesis serving as an adenyltransferase not only for URM1, but also for MOCS2A (Chowdhury et al., 2012; Neukranz et al., 2019)(Figures 3 + 5).

In **Moco biosynthesis**, two sulfur atoms are inserted into the cyclic pyranopterin monophosphate (cPMP) backbone, forming the dithiolene group of molybdopterin (MPT), which ligates the molybdenum atom and forms the molybdenum cofactor (Moco). The conversion of cPMP to MPT is catalyzed by MPT synthase, which is composed of MOCS2A and MOCS2B (R. R. Mendel & Leimkühler, 2015). For regeneration of the thiocarboxylate group at the C-terminal glycine of MOCS2A in MPT synthase, MOCS3, TUM1 and NFS1 are involved (Figures 3 + 4). Thus, Moco biosynthesis and tRNA thiolation are connected and share the same sulfur delivery pathway composed of NFS1, TUM1 and MOCS3 (Frasdorf, Radon, & Leimkuhler, 2014).

In contrast, the formation of **τm^{5}s^{2}U34 for mitochondrial tRNA$^{Lys,\ Gln,\ Glu}$** requires different protein components compared to the ones identified in the cytosol, whereas details of the pathway are not completely resolved to date (Suzuki, Wada, Saigo, & Watanabe, 2002). It was shown that lack of the τm^{5}s^{2}U modification in mitochondrial tRNA^{Lys} from individuals with myoclonus epilepsy associated with ragged-red fibers (MERRF) resulted in a marked defect in mitochondrial translation (Suzuki, 2005). In this pathway the MTU1 protein which is a mitochondria-specific 2-thiouridylase responsible for the generation of τm^{5}s^{2}U in mammals is required (Umeda et al., 2005). The sulfur is derived from mitochondrial NFS1 which is transferred via TUM1-Iso2 (see

below). For the formation of the taurine group the proteins GTPBP3 and MTO1 are required (Figure 3).

Recently, a role of a further protein component has been suggested to be involved in both pathways of tRNA thiolation for cytosolic and mitochondrial tRNAs. Here, an involvement of **the TUM1 protein** (tRNA thiouridine modification protein) was suggested in yeast and humans (Frasdorf et al., 2014). Human TUM1, also designated as 3-mercaptopyruvate sulfurtrans ferase (MPST), has been implicated in a wide range of physiological processes in the cell. The roles range from an involvement in thiolation of cytosolic tRNAs, to the generation of H_2S as signaling molecule both in mitochondria and the cytosol. TUM1 is a member of the sulfur transferase family and catalyzes the conversion of 3-mercaptopyruvate to pyruvate and a protein-bound persulfide. Recently, two so far uncharacterized TUM1 splice variants, designated as TUM1-Iso1 and TUM1-Iso2, were purified and their cellular localization and interaction partners were characterized. Cellular localization studies showed a different localization pattern of the isoforms. TUM1-Iso1 is exclusively localized in the cytosol, while TUM1-Iso2 showed a dual localization both in the cytosol and mitochondria (Figure 5).

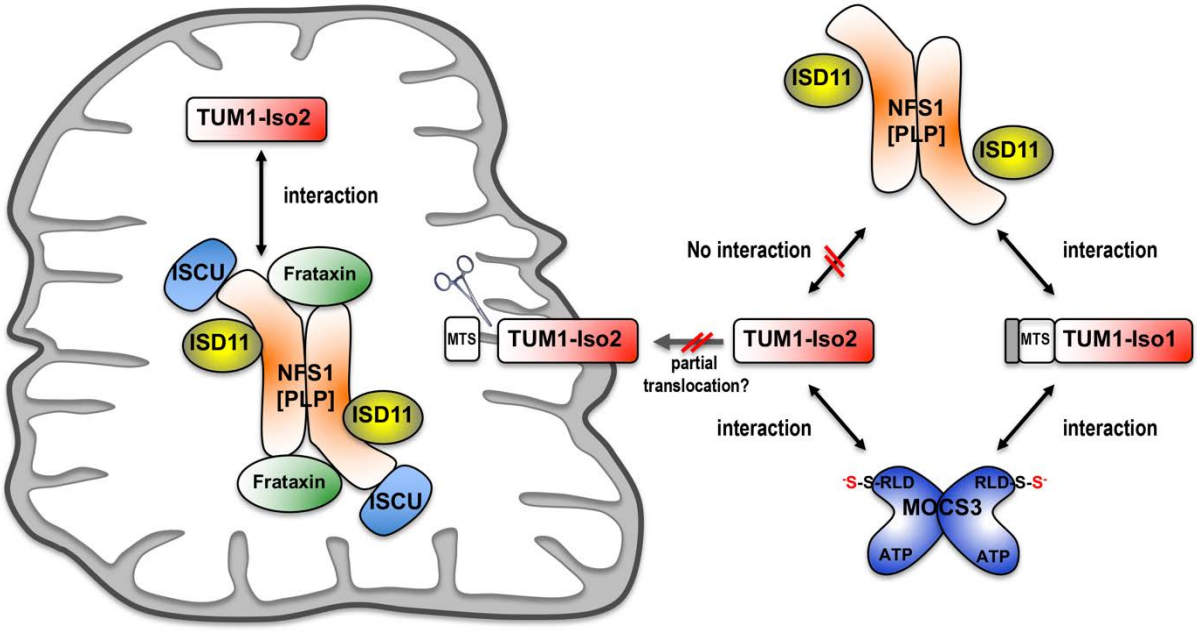

Figure 5: Summary of the interaction network of the TUM1 isoforms. TUM1-Iso1 is exclusively localized in the cytosol where it interacts with both NFS1 and MOCS3. TUM1-Iso2, in contrast, has a dual localization in mitochondria and in the cytosol. In mitochondria TUM1-Iso2 interacts with NFS1, however, in the cytosol solely an interaction with MOCS3 was shown.

Further, the interaction partners of the two isoforms proofed to be different. While TUM1-Iso1 interacted with both NFS1 and MOCS3 in the cytosol, TUM1-Iso2 exclusively interacted with MOCS3 in the cytosol and with NFS1 in mitochondria (Figure 5). These studies implied distinct roles of each TUM1 isoform in the sulfur transfer processes in the cell, with different compartmentalization of the two splice variants of TUM1.

Thiocarboxylate formation on the URM1 protein

Urm1 was identified in a study to identify unknown UBLs distantly related to ubiquitin. The bacterial MoaD and ThiS proteins were chosen in this query to search for distantly related ubiquitin-like conjugation systems(UBLs) (Schindelin, 2005). The MoaD-MoeB and ThiS-ThiF systems provide the sulfur for the biosynthesis of the cofactors molybdopterin and thiamin, respectively. In these systems, MoaD is adenylated by their cognate E1-like activating enzyme MoeB and subsequently thiocarboxylated at their C-terminus(Lake, Wuebbens, Rajagopalan, & Schindelin, 2001; Schmitz, Wuebbens, Rajagopalan, & Leimkühler, 2007). Urm1, MoaD and ThiS, like UBLs share a characteristic diglycine motif at their C-termini, which ensures recognition for activation. It is believed that UBLs and sulfur carrier proteins (SCPs) have emerged from a single, multifunctional ancestral system capable of both adenylating and sulfurtransfer activities, which is combined in the human MOCS3 protein, interacting with a ubiquitin-like SCP (Leidel et al., 2009; Termathe & Leidel, 2021). Then SCPs have further specialized for sulfur-transfer reactions. Urm1 possesses both sequence and structural features of the last common ancestor, therefore Urm1 is believed to be a molecular fossil (Pabis et al., 2020). The Urm1 pathway consists of four cytosolic proteins essential for 2-thiolation and several effector proteins (Pabis et al., 2020). The mitochondrial NFS1 protein and its stabilizing interaction partner Isd11, mobilize the sulfur by converting L-cysteine to L-alanine(Lim et al., 2013; Maio, Jain, & Rouault, 2020). During this step, a persulfide is formed on NFS1(Cory et al., 2017). It was proposed that TUM1 accepts sulfur from NFS1 and shuttles between mitochondria and the cytosol, here the sulfur is transferred to MOCS3 (Frasdorf et al., 2014). MOCS3 activates the sulfur C-terminus of URM1 by adenylation and subsequently generates URM1 thiocarboxylate via a thioester intermediate (Figure 3). As the final

step, a protein complex of CTU1 and CTU2 inserts the sulfur on U34 in tRNA after an adenylation step (Cavuzic & Liu, 2017; Van der Veen et al., 2011).

Moco Biosynthesis

Many enzymes coordinating Moco have been identified. In total, bacteria contain the largest variety of more than 60 different molybdoenzymes being involved in specific, however, usually non-essential redox-reactions. In contrast, in humans only four different molybdoenzymes have been identified, namely sulfite oxidase, being essential to humans, in addition to xanthine dehydrogenase, aldehyde oxidase and the mitochondrial amidoxime reducing compound (mARC). A defect in Moco biosynthesis is lethal due to the loss of sulfite oxidase activity. A therapy for Moco deficiency of patients has been developed (Veldman et al., 2010), however, to date no effective therapy exists for the treatment of isolated sulfite oxidase deficiency.

Moco is a tricyclic pyranopterin containing a unique dithiolene group to which the molybdenum atom is coordinated (Johnson & Rajagopalan, 1982). In general, the biosynthesis of Moco can be divided into three steps in eukaryotes, and four steps in bacteria and archaea (R. R. Mendel & Leimkühler, 2015): *i)* the starting point is the formation of the cyclic pyranopterin monophosphate (cPMP) from 5'GTP, *ii)* in the second step two sulfur molecules are inserted into cPMP leading to the formation of MPT, *iii)* in the third step the molybdenum atom is inserted into molybdopterin to form Moco, and *iv)* additional modification of Moco occurs in bacteria and archaea with the attachment of a nucleotide (CMP or GMP) to the phosphate group of MPT, forming the dinucleotide variants of Moco. Form these dinucleotide variants, the bis-molybdopterin guanine dinucleotide (bis-MGD) cofactor is the most abundant one, being present in most bacterial molybdoenzymes.

The first step of Moco biosynthesis, the conversion from 5'GTP to cyclic pyranopterin monophosphate (cPMP), is catalyzed by MOCS1A and MOCS1B in mitochondria in humans, (Hänzelmann et al., 2004). The MOCS1A protein belongs to the group of radical SAM proteins, which require a [Fe_4S_4] cluster for their catalytic activity. In case of MOCS1A, the protein binds an additional [Fe_4S_4] cluster at its C-terminus, being involved in binding of the substrate 5'GTP. During the conversion of 5'GTP to cPMP a (8S)-3',8-cyclo-7,8-dihydroguanosine 5'triphosphate (3',8-cH_2GTP) intermediate is formed. All further steps for the formation of Moco from cPMP are localized in the cytosol in eukaryotes and do not require FeS-containing proteins (R.

R. Mendel & Kruse, 2012; Schwarz, Mendel, & Ribbe, 2009). For the formation of MPT from cPMP, two sulfur atoms are incorporated to the C1' and C2' positions of cPMP, a reaction catalyzed by MPT synthase (Figure 3). (Stallmeyer, Drugeon, Reiss, Haenni, & Mendel, 1999). It was shown that MPT synthase carries the sulfur in form of a thiocarboxylate at the C-terminal glycine of MOCS2A (Gutzke, Fischer, Mendel, & Schwarz, 2001; Leimkühler, Freuer, Araujo, Rajagopalan, & Mendel, 2003). The central dimer is formed by two MOCS2B subunits containing one MOCS2A at each end, as revealed by the crystal structure of the bacterial homologues (Rudolph, Wuebbens, Rajagopalan, & Schindelin, 2001). It was shown for the *E. coli* proteins that the two MOCS2A/MOCS2B dimers act independently. Thus, for the insertion of two sulfurs into cPMP, two MOCS2A proteins are required at each end of the MPT synthase tetramer (Wuebbens & Rajagopalan, 2003). The first sulfur is added by one MOCS2A molecule at the C2' position of cPMP, a reaction which is coupled to the hydrolysis of the cPMP cyclic phosphate (Daniels, Wuebbens, Rajagopalan, & Schindelin, 2007). During the course of this reaction, a hemi-sulfurated intermediate is formed in which the MOCS2A C-terminus is covalently linked to the substrate via a thioester linkage, which subsequently is hydrolyzed by a water molecule (Figure 6).

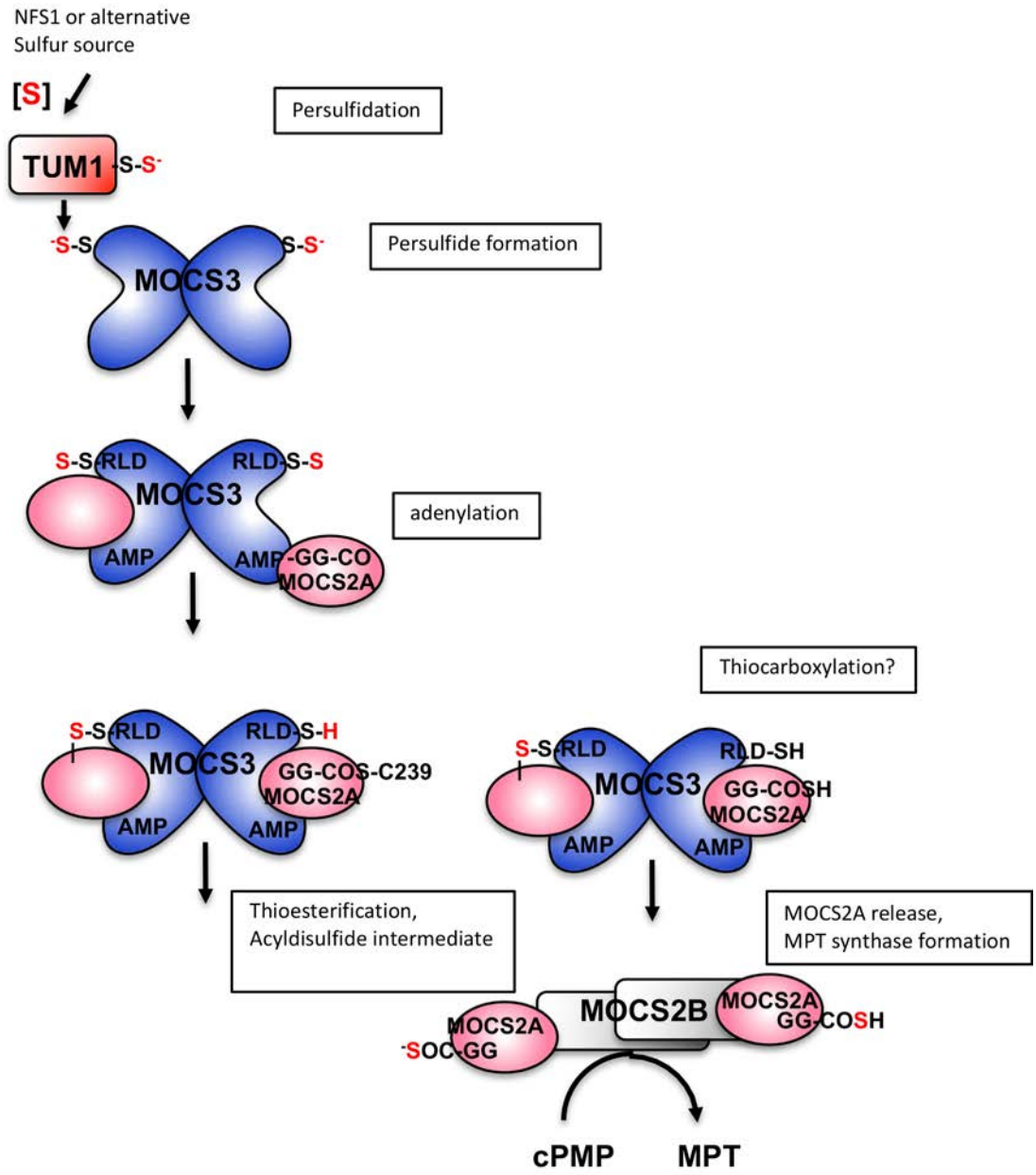

Figure 6: **Formation of the thiocarboxylate group on MOCS2A.** cPMP is converted to MPT by the transfer of two sulfur groups from the C-terminal thiocarboxylate of the MOCS2A subunit of MPT synthase. Regeneration of the MOCS2A-SH sulfur occurs in a MOCS2A/MOCS3 complex. Here, adenylated MOCS2A is formed by attachment of an AMP moiety at the N-terminal E1-like domain of MOCS3. MOCS2A-AMP is then sulfurated by a protein-bound persulfide from the C-terminal rhodanese-like domain. The sulfur donor for the persulfide group on MOCS3-RLD is NFS1, which acquires the sulfur from L-cysteine. An additional involvement of TUM1 in this reaction is suggested based on the interaction determined between NFS1 and MOCS3 of the TUM1 isoforms in the cytosol. After formation of the thiocarboxylate group, MOCS2A-SH dissociates from the MOCS3 dimer and reassociates with MOCS2B, forming the active MPT synthase.

After transfer of its thiocarboxylate sulfur to cPMP, the first MOCS2A subunit dissociates from the MPT synthase complex (Daniels et al., 2007; Wuebbens &

Rajagopalan, 2003). During the reaction of the first sulfur transfer, the opening of the cyclic phosphate is proposed to shift the location of the intermediate within the protein so that the C1' position now becomes more accessible to attack by the second MOCS2A thiocarboxylate. This results in a second covalent intermediate that is converted to MPT via the elimination of a water molecule and hydrolysis of the thioester intermediate. During the reaction, cPMP and the hemisulfurated intermediate remain bound to one MOCS2B subunit (R.R. Mendel & Schwarz, 2011). This reaction has been mainly revealed by studies with the homologous proteins MoaD and MoaE from *E. coli*; however, the same reaction can be catalyzed by hybrid complexes formed between the bacterial and mammalian proteins, indicating that conservation of the reaction components is high among species (Leimkühler et al., 2003).

For the MPT synthase to act catalytically, it is necessary to regenerate its transferable sulfur in an ATP-dependent reaction, catalyzed by the MOCS3 protein in humans. It was shown that the N-terminal domain of MOCS3 activates the C-terminus of MOCS2A by formation of an acyl-adenylate (Figure 6). Human MOCS3 contains an additional C-terminal domain at its C-terminus, which is fused to the N-terminal MoeB-like adenylation domain and shares amino acid sequence homologies to rhodaneses (Leimkühler et al., 2003; A. Matthies, K. V. Rajagopalan, R. R. Mendel, & S. Leimkühler, 2004b). In humans, this rhodanese-like domain on MOCS3 acts as direct sulfur donor for the formation of the thiocarboxylate group on MOCS2A (Figure 6), However, it is also believed that the sulfur for MOCS3 originates from L-cysteine, which is mobilized by NFS1 in the cytosol (Marelja et al., 2013; Marelja et al., 2008a). Thus, NFS1 would mobilize the sulfur for two pathways in humans, Moco biosynthesis in the cytosol and FeS cluster assembly in mitochondria (Figures 3 + 4). Crucially, MOCS3 is not only involved in Moco biosynthesis: besides interacting with MOCS2A, MOCS3 also interacts with URM1, which acts as a sulfur acceptor protein involved in the thiolation of some tRNAs (Chowdhury et al., 2012) (Figure 4). Thus, Moco biosynthesis and tRNA thiolation are directly connected in humans by sharing the sulfur delivery pathway composed of NFS1 and MOCS3.

MOCS3

MOCS3 is the non-canonical E1-like activating enzyme and consists of two catalytically active domains: an adenylation domain (AD) and a rhodanese-like domain (RLD) (A. Matthies, K.V. Rajagopalan, R.R. Mendel, & S. Leimkühler, 2004a). The AD

is a common feature that MOCS3 shares with other E1-like enzyme. All E1-like enzymes use an identical mechanism to activate their respective UBL by adenylating its C-terminal diglycine motif. Following this initial step, the C-terminus of Urm1 or MOCS2A is further activated by forming a thioester with the catalytic cysteine of AD of MOCS3 (however, this has only been proven for the yeast homologues Urm1-Uba4, so far(Termathe & Leidel, 2018). Chemically, thioesters are high-energy bonds, that are more susceptible to nucleophilic attacks than their oxyester counterparts, since thiols constitute better leaving groups. The formation of the thioester is the central step of classical UBLs the thioester between the C-terminus of Urm1 or MOCS2A and the catalytic cysteine, likely C239 in the AD of MOCS3 positions the thioester in close proximity to the RLD (Figure 6). In the second reaction, the MOCS2A or URM1acyl-adenylate is converted to a thiocarboxylate by sulfur-transfer from a persulfide present at MOCS3-RLD (Matthies, Nimtz, & Leimkühler, 2005; R.R. Mendel & Schwarz, 2011). In this reaction, the deprotonated persulfide group of RLD-C412 serves as a nucleophile at the activated MOCS2A/URM1-adenylate to form a disulfide intermediate (Figure 6). Reductive cleavage of the disulfide bond could then occur by attack of another thiol group e.g. the conserved MOCS3-C239 to form a disulfide bond with C412, and in turn, thiocarboxylated MOCS2A or URM1 are generated and released (Matthies et al., 2005). In analogy to the *E. coli* system, it was shown that the sulfur for MOCS3 originates from the L-cysteine desulfurase NFS1 or the TUM1-Iso1 protein in the cytosol in humans cells, transferring sulfur from L-cysteine in a sulfur relay system via a persulfide group formed on the L-cysteine desulfurase via TUM1-Iso1 and MOCS3-RLD further onto MOCS2A or URM1 (Krepinsky & Leimkühler, 2007; Marelja et al., 2013; Marelja, Stöcklein, Nimtz, & Leimkühler, 2008b) (Figures 2+ 6). The RLD ensures a specific reaction between the MOCS2/URM1 thioester and the MOCS3 persulfide, preventing cross-reactivity of the activated thioester intermediate. The acyl-persulfide is the key difference to classical UBLs, where an isopeptide bond is formed with the target protein (Figure 6). Hence, the activation of the C-terminal diglycine motif of a SCP by adenylation was likely a feature of the last common ancestor. This might have been the point from which other systems emerged and further developed into UBL systems with specialized E2 and E3 enzymes (Termathe & Leidel, 2021). The absence of E2 and E3 proteins in the MOCS2A-MOC3 systems clearly distinguishes it from classical UBLs and underlines MOCS2As function as an SCP. In addition to the necessity of a rhodanese-homology domain (RLD). MOCS3-

RLD was additionally shown to act as direct sulfur donor for the formation of the thiocarboxylate group on URM1 (Chowdhury et al., 2012; Matthies et al., 2004a) in s^2U thiomodification (as described above). Rhodaneses or rhodanese-like proteins are Thiosulfate:cyanide sulfur transferases (EC 2.8.1.1) belong to the large family of sulfur transferases (EC 2.8.1). They are forming a protein-bound persulfide using thiosulfate as *in vitro* substrate or another persulfide-containing protein as sulfur-donor. In nature, sulfur transferases are generally accepting sulfur from L-cysteine desulfurases, but in some prokaryotes sulfur can be also mobilized from their substrates (Bordo & Bork, 2002).

Rhodaneses or rhodanese-like proteins are either composed of a single catalytic rhodanese domain, or a fusion of two rhodanese domains, with an inactive N-terminal domain (i.e. where the active-site cysteine is replaced by another residue) and an active C-terminal domain containing the putative catalytic cysteine (Bordo & Bork, 2002). The tandem domains are proposed to have evolved from a common ancestor protein by gene duplication and have lost most of sequence similarity during evolution, while the tertiary structure was kept conserved. Furthermore, rhodanese domains either catalytic or inactive, are also found (Ploegman *et al*., 1978) in MAP-kinase phosphates, Cdc25 phosphatases or in several ubiquitinating and deubiquitinating enzymes (Keyse & Ginsburg, 1993; Fauman *et al*., 1998; Hofmann *et al*., 1998). Due to these similarities, rhodaneses also belong to the rhodanese/Cdc25 phosphatase superfamily since it was shown that the two human Cdc25 phosphatases, Cdc25A and Cdc25B, two key enzymes involved in cell cycle control, display a rhodanese-like three-dimensional fold and maintain the active-site cysteine at the first position of an active-site loop consisting of six amino acids in rhodaneses and seven amino acids in Cdc25 phosphatases (Bordo & Bork, 2002)

The best characterized rhodanese is the bovine liver rhodanese, a member that consists of two rhodanese domains (Bergsma et al., 1975; Ploegman, Drent, Kalk, & Hol, 1978, 1979; Ploegman, Drent, Kalk, Hol, et al., 1978; Westley, 1973, 1981). The *in vitro* catalysis of rhodaneses involves a double displacement mechanism for the transfer of a sulfane sulfur atom from thiosulfate to cyanide via a protein-bound persulfide intermediate.

The physiological role of rhodaneses is still largely debated. It seems unlikely that the physiological sulfur acceptor is cyanide due to the high K_M value; however, proposed functions include cyanide detoxification (Sorbo, 1957), formation of prosthetic groups

in Fe-S proteins, maintenance of the sulfane pool (Westley, 1973), sulfur transfer for thiamine or thiouridine biosynthesis (Kambampati & Lauhon, 2000; Palenchar, Buck, Cheng, Larson, & Mueller, 2000),(Chowdhury et al., 2012)) as well as the beforehand mentioned potential regulatory roles in signaling pathways.

In total, MOCS3 can be regarded as a multi-functional and multi-domain protein combining the adenylation of MOCS2A and URM1 with the subsequent sulfurtransfer reaction (Figure 2) (Matthies et al., 2004b). In the second reaction, the MOCS2A acyl-adenylate is converted to a thiocarboxylate by sulfur-transfer from a persulfide present at MOCS3-RLD (Matthies et al., 2005; R.R. Mendel & Schwarz, 2011). In this reaction, the deprotonated persulfide group of RLD-C412 serves as a nucleophile at the activated MOCS2A-adenylate to form a disulfide intermediate. Reductive cleavage of the disulfide bond could then occur by attack of another thiol group e.g. the conserved MOCS3-C239 to form a disulfide bond with C412, and in turn, thiocarboxylated MOCS2A is generated and released (Matthies et al., 2004a) (Figure 6).

Crucially, MOCS3 is not only involved in Moco biosynthesis but also in the formation of thio-modified mcm^5U34 nucleosides in tRNA for Gln, Glu and Lys in the cytosol of human cells (Chowdhury et al., 2012; Neukranz et al., 2019). To perform this shared function role in tRNA thiolation, MOCS3 interacts with the ubiquitin-related modifier protein1 (URM1). In analogy to the MOCS2A protein (Figure 2), URM1 contains a conserved C-terminal double glycine-motif on which a thiocarboxylate group is formed for sulfur-transfer for the mcm^5s^2U34 modification in tRNA (Leidel et al., 2009; Pedrioli et al., 2008; Schmitz et al., 2008; Xu et al., 2006). In detail, MOCS3 activates URM1 in the presence of ATP by formation of activated URM1-AMP. URM1 is further transferred to the persulfide group formed on Cys412 of MOCS3-RLD via a disulfide bond. After cleavage of the disulfide bond, thiocarboxylated URM1 is released. The sulfur of URM1-COSH is further transferred to mcm^5U34 group of the $tRNA^{Glu,Gln,Lys}$ aided by the CTU1 and CTU2 proteins under ATP consumption(Chowdhury et al., 2012) (Figure 2).
In total, Moco biosynthesis and tRNA thiolation are directly connected in humans by sharing the role of MOCS3(Chowdhury et al., 2012). Further, the sulfur delivery pathway to MOCS3 involves the L-cysteine desulfurase NFS1 in the cytosol (Figure 4) (Marelja et al., 2013; Marelja et al., 2008a). In eukaryotes, however, NFS1 was described to be mainly localized in the mitochondria where it is involved in the assembly of FeS clusters (Biederbick et al., 2006). A role of NFS1 for the CIA pathway of FeS cluster biosynthesis in the cytosol has not been described so far. Thus, the role of the cytosolic form of NFS1 might be specifically restricted to Moco biosynthesis and

thio-modification of tRNAs.

Nfs1

Sulfur transfer to MOCS3 involves the NFS1 protein in the cytosol

L-cysteine desulfurases are pyridoxal phosphate (PLP)-dependent enzymes that use L-cysteine as substrate and convert it by the help of protein-bound PLP to L-alanine and a protein-bound persulfide (Zheng et al., 1993). This persulfide serves as reactive and transferable sulfur that can be directly transferred to target compounds or acceptor proteins. L-cysteine desulfurases have been identified to provide the sulfur for the biosynthesis of sulfur-containing nucleotides, vitamins and cofactors, such as molybdopterin (MPT), iron-sulfur (FeS) clusters, thiamine, lipoic acid, and biotin (Hidese *et al*., 2011) (Figure 1). The protein-bound persulfide formation and the involvement of the PLP cofactor in the desulfuration of L-cysteine. In the first step, the α-amino group of the L-cysteine binds to the PLP in the active site leading to the formation of an external aldimine, which then converts to a ketimine intermediate. This reaction can be monitored by UV–visible spectroscopy, since the light absorption band of PLP at around 390 nm is shifted to around 420 nm (Zheng *et al*., 1993; Behshad *et al*., 2004) (Figure 7).

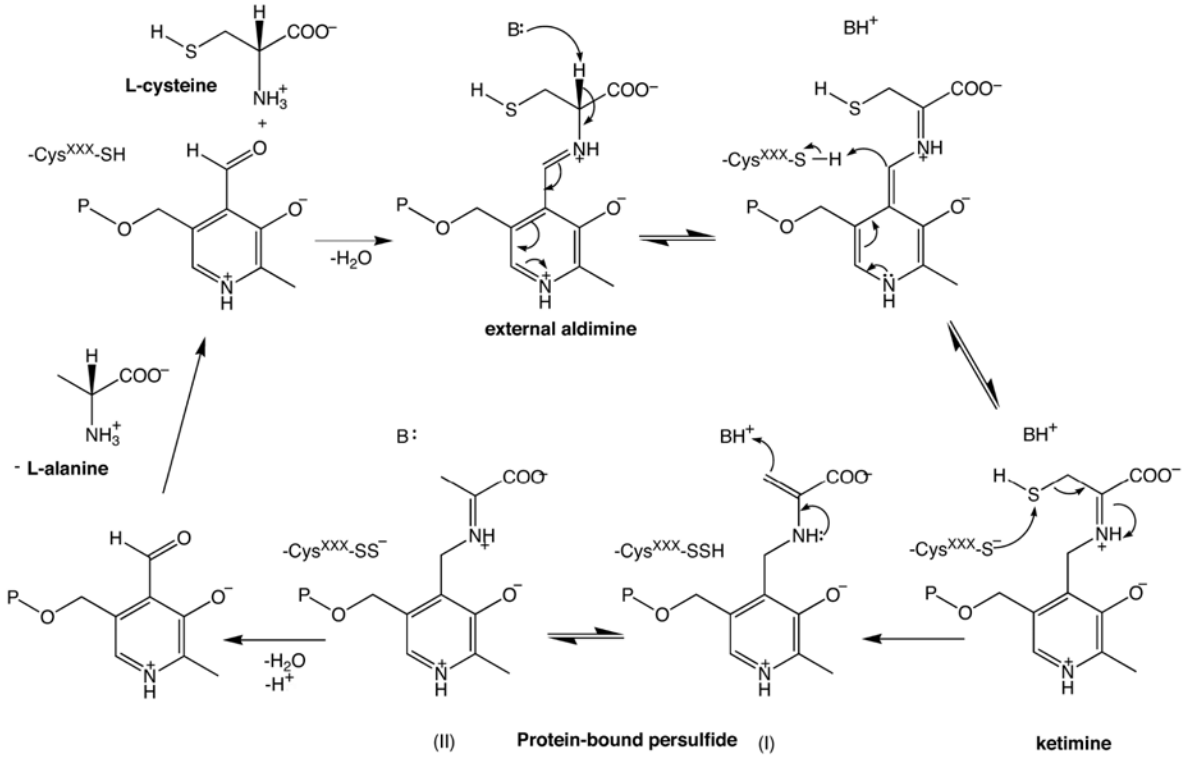

Figure 7**: The role of PLP in the catalytic reaction of L-cysteine desulfurases.**

The α-amino group of the substrate L-cysteine binds to PLP and forms an external aldimine. The cleavage of the C – S bond of L-cysteine bound to the PLP cofactor occurs due to the nucleophilic attack from the L-cysteine sulfur of the substrate to an active-site cysteine residue of the L-cysteine desulfurase (-Cys^{XXX}-S^-), resulting in the formation of an enzyme-bound persulfide (-Cys^{XXX}-SS^-) and alanine enamine bound to PLP. Subsequently the L-alanine must be released in order to bind another L-cysteine molecule.

The second step involves an essential active-site cysteine. It is supposed to be in a deprotonated cysteinate state in order to carry out a nucleophilic attack on the electrophilic sulfur atom of the ketimine intermediate. This process generates a stable protein-bound persulfide together with a novel ketimine (Zheng *et al*., 1994; Lima, 2002). A following hydrolysis of the ketimine results in the formation and release of L-alanine and regenerates PLP for a new catalytic cycle (Figure 7) . A new catalytic cycle can only start after the release of the terminal electrophilic persulfide-sulfur atom and liberation of the active-site cysteine to its active form. This occurs through a nucleophilic attack on the persulfido sulfur by a sulfur acceptor, for instance a cysteinate of a target protein (Fontecave & Ollagnier-de-Choudens, 2008).

It is well-recognized that the amino acid cysteine serves as the sulfur source for most, if not all, sulfur containing biomolecules in bacterial and eukaryotic systems. The first step of sulfur mobilization is catalyzed by a pyridoxal-5′-phosphate (PLP) enzymatic reaction of cysteine desulfurases. This class of enzymes promotes the abstraction of sulfur from cysteine and transfers it to acceptor molecules participating in the biosynthesis of thio-cofactor. A single L-cysteine desulfurase homologue, named NFS1, was identified in humans (Biederbick et al., 2006; Land & Rouault, 1998; Maio et al., 2020; Maio & Rouault, 2020; Maio et al., 2014). NFS1 converts cysteine to alanine, while generating a persulfide species on a mobile cysteine-containing loop (Cys381 in human NFS1) that delivers sulfane sulfur to the scaffold protein ISCU. The accessory protein ISD11 (also known as LYRM4;), a member of the LYRM family, characterized by the presence of the highly conserved Leu Tyr Arg motif (Angerer, 2015), is uniquely present in eukaryotes and was shown to stabilize NFS1 and to interact with the acyl carrier protein ACP (NDUFAB1 in human) (Van Vranken et al., 2016).

However, it was suggested that two distinct NFS1 isoforms are produced through alternative utilization of in-frame AUGs (Land & Rouault, 1998; Li, Tong, Hughes, & Rouault, 2006; Tong & Rouault, 2000). The major form is generated by initiation of the first AUG of the NFS1 transcript and contains a mitochondrial targeting signal at the N-terminus that undergoes cleavage to yield a mature mitochondrial protein of 47 kDa in size (Land & Rouault, 1998) (Figure 8) .

:

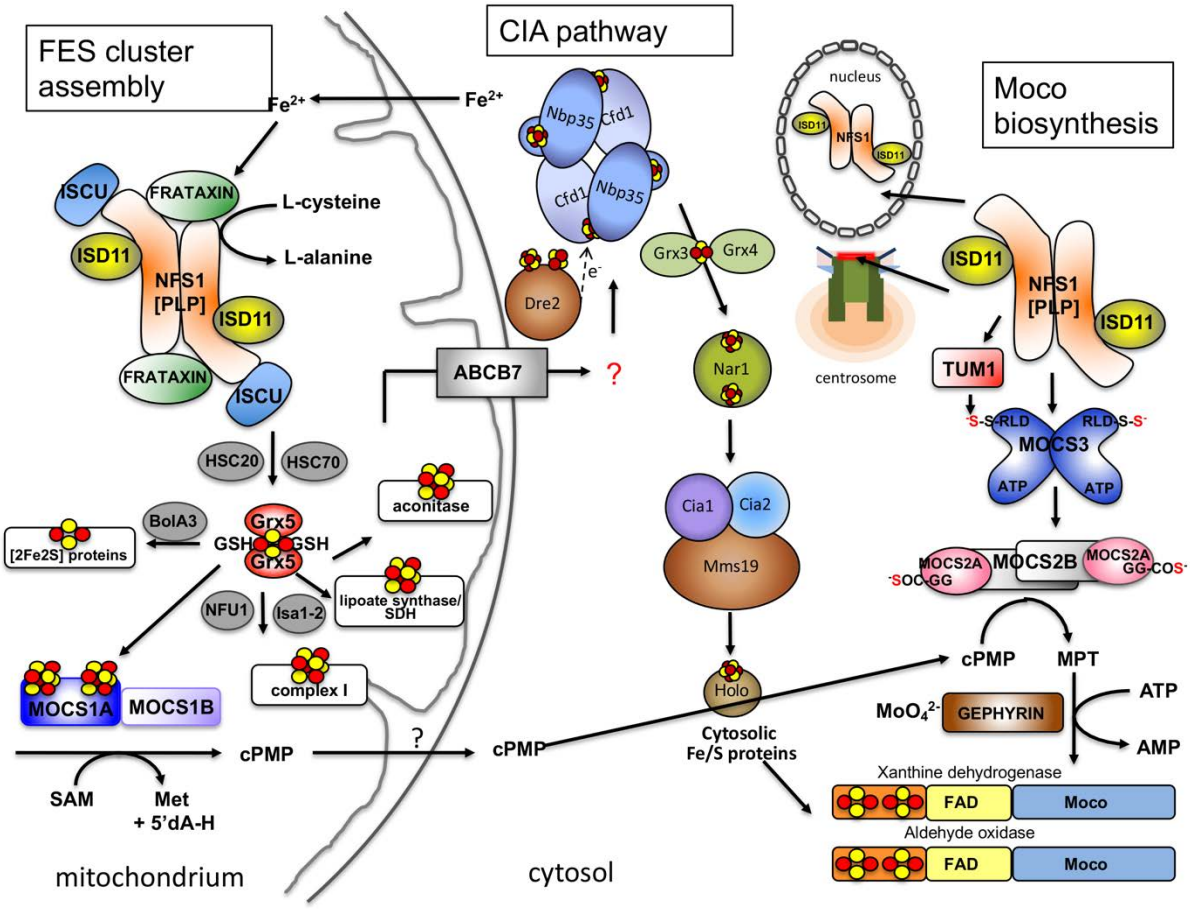

Figure 8: **The different compartments for the biosynthesis of Moco in humans and the link to Fe-S cluster assembly in mitochondria.** The first step of Moco biosynthesis, the conversion of 5'GTP to cPMP catalyzed by MOCS1A and MOCS1B, is localized in mitochondria. This is also the main compartment for Fe-S cluster biosynthesis in eukaryotes. Fe-S clusters assemble on the scaffold protein ISCU2, which receives the sulfur from the L-cysteine desulfurase complex NFS1/ISD11. The iron donor in this reaction has not been identified so far. Frataxin (FDN) is able to interact with the NFS1/Isd11-ISCU2 complex. Ferredoxin (FDX2) delivers the electrons for Fe-S cluster assembly. Assembly and release of the clusters is catalyzed by the chaperones HSC20/HSPA9. The carrier proteins GLRX5, ISCA2 and/or IBA57 deliver the Fe-S clusters to target proteins. Synthesized cPMP further is transferred to the cytosol, where all further modification steps are catalyzed. These steps involve the conversion of cPMP to MPT by MOCS2A/MOCS2B (which are activated by MOCS3), the insertion of molybdate by GEPHYRIN (GEPH), and the insertion of Mo-MPT either into sulfite oxidase (localized in the mitochondrial

intermembrane space) or to the mARC protein (localized at the outer mitochondrial membrane). A further modification step of Moco is catalyzed by HMCS for the enzymes aldehyde oxidase and xanthine dehydrogenase, which involves the formation of the equatorial sulfido-ligand at the Mo atom, an essential requirement for the activity of these enzymes. A dual localization of NFS1 both in mitochondria and the cytosol is predicted. Cytosolic NFS1 acts as a sulfur donor for MOCS3. NFS1 was also localized in the nucleus and at the centrosome.

In mitochondria, NFS1 is involved in FeS cluster biosynthesis (Tong & Rouault, 2006). A less abundant isoform generated by initiation of translation at the second in-frame AUG lacks the first 60 residues of the mitochondrial precursor form, and this 44 kDa protein resides both in the cytosol and in the nucleus (Land & Rouault, 1998).
Recently, the Isd11 protein was identified to be essential for FeS cluster biosynthesis in mitochondria and it was shown that Isd11 forms a complex with NFS1 (Adam, Bornhovd, Prokisch, Neupert, & Hell, 2006; Boniecki, Freibert, Muhlenhoff, Lill, & Cygler, 2017; Wiedemann, Urzica, Guiard, Muller, Lohaus, Meyer, Ryan, Meisinger, Muhlenhoff, et al., 2006) . Isd11 is suggested to function as an adapter and stabilizer of NFS1 (Shan, Napoli, & Cortopassi, 2007). Homologues of Isd11 have been identified in plant, fungi and animal genomes, which contain mitochondria, but no prokaryotic homologue has been identified (Richards & van der Giezen, 2006).

It has been reported that NFS1 is additionally localized in small amounts in the cytosol, where it interacts with MOCS3 (Marelja et al., 2013) for Moco biosynthesis and s^2U tRNA thiomodification (Figure 8).The interaction of NFS1 and MOCS3 was revealed by using Förster resonance energy transfer and a split-EGFP system. The colocalization of NFS1 and MOCS3 in the cytosol was additionally confirmed by immunodetection of fractionated cells and localization studies using confocal fluorescence microscopy (Marelja et al., 2013). However, while the role of NFS1 in the cytosol for sulfur transfer to MOCS3 seems to be established, an involvement of ISD11 in this reaction still remains unclear. So far, ISD11 was described as a stabilizing factor of NFS1 in eukaryotes that is essential for its activity in FeS cluster formation in mitochondria (Shi, Ghosh, Tong, & Rouault, 2009). In the absence of ISD11, NFS1 is prone to aggregation and FeS clusters cannot be formed (Marelja et al., 2008a; Wiedemann, Urzica, Guiard, Muller, Lohaus, Meyer, Ryan, Meisinger, Mühlenhoff, et al., 2006). However, localization studies showed that ISD11 mainly is located in mitochondria and the nucleus in human cells (Shi et al., 2009) (Figure 8). Thus, the role of ISD11 and its involvement in the interaction of NFS1 and MOCS3 in the cytosol still

needs to be investigated in more detail. MOCS3 might replace the role of ISD11 as a stabilizing protein to NFS1 in the cytosol.

For cytosolic Fe-S cluster assembly, the mitochondrial ISC system has been proposed to be essential (Netz, Mascarenhas, Stehling, Pierik, & Lill, 2014; Paul & Lill, 2015). Studies by several groups have shown that the mitochondrial ISC machinery generates a sulfur-containing factor “X-S” that is exported to the cytosol via the mitochondrial ABC transporter ABCB7 and is used for cytosolic Fe-S cluster assembly by the CIA machinery (Figure 8) (Biederbick et al., 2006; Gerber, Comellas-Bigler, Goetz, & Locher, 2008; Kispal, Csere, Prohl, & Lill, 1999; Stehling et al., 2008). However, models also exists that propose that cytosolic versions of NFS1, ISCU and FDN are involved in cytosolic Fe-S cluster formation (Maio & Rouault, 2020). The CIA machinery is composed of up to 13 known proteins that assemble both cytosolic and nuclear Fe-S proteins. Initially, a [4Fe-4S] cluster is assembled on the CIA scaffold complex formed between CFD1-NBP35 (Figure 8) (Stehling et al., 2018; Stehling et al., 2008). The initial cluster synthesis on CFD1-NBP35 further requires the electron transfer chain composed of the flavin-dependent oxidoreductase NDOR1 and CIAPIN1, however, the precise role of the electron-transfer for cluster synthesis is not completely understood yet (Netz et al., 2016; Netz et al., 2010). The insertion of the two Fe-S clusters of CIAPIN1 additionally requires the cytosolic monothiol glutaredoxin reductase GLRX3 (Banci, Ciofi-Baffoni, et al., 2015; Frey, Palenchar, Wildemann, & Philpott, 2016; Haunhorst et al., 2013). GLRX3 binds a bridging [2Fe-2S] cluster with BOLA2 which is further transferred to CIAPIN1 (Figure 8) (Banci, Camponeschi, Ciofi-Baffoni, & Muzzioli, 2015; Frey et al., 2016). CIAPIN1 can coordinate a pair of [2Fe-2S] clusters or a [2Fe-2S] cluster and a [4Fe-4S] cluster (Banci et al., 2014; Banci et al., 2013; Netz et al., 2016; Zhang et al., 2008). While the BOLA2-GLRX3 complex is able to transfer [2Fe-2S] clusters to CIAPIN1, the formation of the [4Fe-4S] cluster in CIAPIN1 is still fully undefined.

The next step of cytosolic Fe-S assembly involves the trafficking of the [4Fe-4S] cluster from the CFD1-NBP35 complex to CIAO3 and then to the CIA targeting complex (CTC) which is composed of CIAO1, CIAO2B, and MMS19 (Gari et al., 2012; Srinivasan et al., 2007). From this complex, which can be formed with different protein components, the cluster is transferred directly to target proteins (Figure 8). The specific interaction with the target proteins is mediated by the CTC proteins.

This could imply that cytosolic NFS1 is only involved in Moco biosynthesis and tRNA thiolation in conjunction with MOCS3, while in the absence of ISD11 it has no role in FeS cluster biosynthesis.

Additionally, a localization of NFS1 to be present at the centrosome has been identified (Neukranz et al., 2019) (Figure 8). So far, NFS1 was described to be mainly localized to the mitochondria and the nucleus. In mitochondria, the main role of NFS1 has been described to form a complex with ISD11, ISCU and frataxin for Fe-S cluster biosynthesis. Recent crystal structures of the quaternary complex also identified the acyl carrier protein (ACP) to be present in this complex under certain conditions.(Boniecki et al., 2017; Cory et al., 2017). In the nucleus, the NFS1/ISD11 complex is also predicted to be involved in Fe-S cluster biosynthesis for nuclear proteins.

The recent identification of NFS1 at the centrosome in human cells is another proof for the cytosolic localization of NFS1 (Figure 8) . Another report investigating the centrosomal proteins in *Drosophila* already identified NFS1 (CG12264) as a centrosomal protein (Hughes et al., 2008). This localization was verified for human cell lines in a recent study (Neukranz et al., 2019). The role of NFS1 at the centrosome still remains to be identified, however, a role in Fe-S cluster insertion for centrosomal proteins has been suggested previously. Additionally, in the recent report by Kim et al. (2018), NFS1 was co-immunoprecipitated with the centrosomal protein NUBP2.(Kim, Maio, Singh, & Rouault, 2018) NUBP2 itself interacts with the kinesin-like protein HSET (KIFC5A in mice) and is an important factor of the cytosolic iron-sulfur cluster machinery (CIA).(Christodoulou, Lederer, Surrey, Vernos, & Santama, 2006). For the CIA pathway, NUBP2 forms a larger complex with Cfd1-Nbp35 acting as a scaffold for [4Fe4S] cluster assembly and insertion (Stehling et al., 2008). Conclusively, the role of NFS1 at the centrosome might be to insert Fe-S clusters into centrosomal proteins, thereby influencing cell division. The exact role of NFS1 at the centrosome in addition to its interaction partners need to be investigated in further detail in future studies.

Tum1

Recently, a role of a further protein component has been suggested to be involved in both pathways of tRNA thiolation for cytosolic and mitochondrial tRNAs. Here, an involvement of **the TUM1 protein** (tRNA thiouridine modification protein) was suggested in yeast and humans (Frasdorf et al., 2014). Human TUM1, also designated

as 3-mercaptopyruvate sulfur transferase (MPST), has been implicated in a wide range of physiological processes in the cell. 3-Mercaptopyruvate sulfur transferase (MPST) catalyzes the desulfuration of 3-mercaptopyruvate to generate an enzyme-bound hydropersulfide (Pedre & Dick, 2021). Subsequently, MPST transfers the persulfide's outer sulfur atom to proteins or small molecule acceptors. MPST activity is known to be involved in hydrogen sulfide generation, tRNA thiolation, protein urmylation and cyanide detoxification. Tissue-specific changes in MPST expression correlate with ageing and the development of metabolic disease. Recently, high expression of MPST has been reported in cancer tissues due to its H_2S biosynthesis capability and subsequent influence on the cellular bioenergetics (Bronowicka-Adamska, Bentke, & Wrobel, 2017; Gai et al., 2013; Ramasamy, Singh, Taniere, Langman, & Eggo, 2006; Zuhra et al., 2019) Deletion and overexpression experiments suggest that MPST contributes to oxidative stress resistance, mitochondrial respiratory function and the regulation of fatty acid metabolism. MPST belongs to the rhodanese/Cdc25 phosphatase superfamily (Bordo & Bork, 2002). All known MPSTs contain two rhodanese domains. The active site lies at the interface of these two domains, but most of the residues involved in binding and catalysis are located in the C-terminal domain. The catalytic cysteine is part of a conserved six amino acid motif (CG[S/T]GVT) that folds into a cradle-like loop and defines the active site pocket. Variations on the active site motif appear to determine substrate specificity within the rhodanese family. The catalysis occurs as follows (Pedre & Dick, 2021): Following binding into the active site pocket, 3MP is desulfurated, to generate a persulfidated active site cysteine and pyruvate as products. Pyruvate is then released from the active site, allowing acceptor molecules to enter. MPST facilitates transfer of the outer sulfur atom of the enzyme-bound persulfide to the acceptor molecule, either the MTU1 protein in mitochondria or the MOCS3 protein in the cytosol (a process also known as 'transpersulfidation'), after which the sulfurated acceptor is released (Figure 5). The individual steps of the ping-pong mechanism are separated by kinetic pauses (Hanaoka et al. 2017; Lec et al. 2018)(Takano et al., 2017). 3MP desulfuration is very fast, with a rate constant in the 106 M^{-1} s^{-1} range (Misslinger, Lechner, Bacher, & Haas, 2018). The release of pyruvate is thought to be the rate limiting step of the MPST catalytic cycle, in the specific case of the MPST client protein MOCS3 the situation is different. The persulfidated MOCS3 does not release H_2S, but instead transfers sulfur to the AMP-activated URM1 protein, generating a thiocarboxylate at

its C-terminus. Thiocarboxylated URM1 has the known fate: it transfers the sulfur further on to CTU1 for s^2-uridine formation in the cytosol(Pabis et al., 2020).

TUM1 is a member of the sulfur transferase family and catalyzes the conversion of 3-mercaptopyruvate to pyruvate and a protein-bound persulfide. Recently, two so far uncharacterized TUM1 splice variants, designated as TUM1-Iso1 and TUM1-Iso2, were purified and their cellular localization and interaction partners were characterized. Cellular localization studies showed a different localization pattern of the isoforms. TUM1-Iso1 is exclusively localized in the cytosol, while TUM1-Iso2 showed a dual localization both in the cytosol and mitochondria (Figure 5). Further, the interaction partners of the two isoforms proofed to be different. While TUM1-Iso1 interacted with both NFS1 and MOCS3 in the cytosol, TUM1-Iso2 exclusively interacted with MOCS3 in the cytosol and with NFS1 in mitochondria (Figure 5). These studies implied distinct roles of each TUM1 isoform in the sulfur transfer processes in the cell, with different compartmentalization of the two splice variants of TUM1.
So far, the sulfur transfer pathway for thionucleotides in tRNA has been mostly investigated in *S. cerevisiae*. The sulfur transferase protein Tum1p (tRNA thiouridine modification protein, also designated MPST as 3-mercaptopyruvate sulfur transferase or Yor251c) catalyzes the conversion of 3-mercaptopyruvate to pyruvate and a protein-bound persulfide. The yeast protein has been implicated in yeast cytosolic mcm^5s^2U34 modification together with Uba4p (MOCS3 homologue) and Urm1p as well as Nfs1p (Noma, Sakaguchi, et al., 2009). Furthermore, a conjugation of Urm1p to the stress protein Ahp1p was reported, Tum1p was shown to be required but not essential for cytosolic tRNA thiolation in yeast (Jüdes, Bruch, Klassen, Helm, & Schaffrath, 2016; Noma, Sakaguchi, et al., 2009).

A role of the TUM1 protein has been suggested to be involved in tRNA thiolation in humans accordingly (Frasdorf et al., 2014). Still numerous questions remain on the function of TUM1. Splice variants for Tum1p were not reported in yeast so far and tRNA thiolation differs between yeast and humans. Human mitochondrial tRNAs contain a taurine modification, which is not present in yeast mitochondrial tRNA, containing the $cmnm^5U34$ modification instead. Furthermore, in yeast Moco biosynthesis is not present making yeast an ideal and simple system to study tRNA thiolation as a separate pathway. Therefore, major differences between tRNA thiolation and Moco biosynthesis exists from human to yeast. In humans, the protein network appears more complex

since Moco biosynthesis is an essential cellular pathway, which is required for the activity of sulfite oxidase (SUOX) as detoxifying enzyme(Neukranz et al., 2019).

MTU1

In eukaryotic mitochondria, NFS1 and the mitochondrial tRNA-specific 2-thiouridylase 1 (MTU1) are responsible for 2-thiolation of cmnm^{5}s^{2}U in yeast and 5-taurinomethyl-2-thiouridine (τm^{5}s^{2}U) in mammals (Umeda et al., 2005) (Figure 3). Here, the taurine modification (τm^{5}s^{2}U) seems to be restricted to the mitochondria of mammals. MTU1 was shown to be a homologue of the bacterial MnmA protein involved in mnm^{5}s^{2}U34 modification in *E. coli* (Shigi, 2014). While the 5-taurinomethyluridine (τm^{5}U34) is found in mitochondrial tRNAs for Leu and Trp, its 2-thiouridine derivative (τm^{5}s^{2}U34) is present in mitochondrial tRNAs for Glu, Gln and Lys. These modifications allow tRNAs to precisely recognize their cognate codons and to ensure accurate translation in the mitochondria. Two enzymes, the mitochondrial tRNA translation optimization 1 (MTO1) and the GTP binding protein 3 (GTPBP3) were shown to be responsible for the taurine modification/insertion for the formation of τm^{5}U34 (Umeda et al., 2005) (Figure 3). However, the proteins involved in the formation of the taurine group itself remain to be identified. MTU1 catalyzes the subsequent step of the 2-thiolation of τm^{5}U34 to form τm^{5}s^{2}U34. The sulfur for this modification is derived from mitochondrial NFS1 and mitochondrial TUM1 isoform 2. (Frasdorf et al., 2014; Suzuki, 2005) (Figure 5).

CTU1

In eukaryotes and archaea, CTU1 and its archaeal homolog NcsA catalyze the direct 2-thiolation reaction of uridine in tRNA at position 34 In eukaryotes(Chavarria et al., 2014; Nilsson, Jager, & Bjork, 2017), CTU1 forms a heterocomplex with the CTU2 protein that apparent role in catalysis is currently unknown. (Dewez et al., 2008; Esberg, Huang, Johansson, & Bystrom, 2006). CTU1 receives the sulfur from the thiocarboxylate group of URM1(Figure 2). In some thermophilic bacteria and archaea, such as T. thermophilus, the TtuA protein catalyzes the same 2-thiouridylation reaction at different positions (e.g., position 54) 2017)(Arragain et al., 2017; Bouvier et al., 2014; Mulliez, Duarte, Arragain, Fontecave, & Atta, 2017; Shigi et al., 2006).The mechanism by which sulfur is incorporated into tRNA s2 U34 in eukaryotic cytosol

differs greatly from that in bacteria. This process requires the Fe–S cluster assembly machinery. A small amount of the cysteine desulfurase Nfs1 is present in yeast cytosol and participates in tRNA thiolation. Similar to methanogenic archaeal ThiI, Ncs6 has a PP-loop motif and three conserved Cys residues (two from a CXXC motif) in its putative catalytic domain. The PP-loop binds ATP that is used to adenylate U34, resembling the reaction schemes of ThiI and MnmA. The three Cys residues coordinate a [3Fe-4S] cluster (Liu et al., 2016), which is probably involved in sulfur transfer. CTU1 utilizes an oxygen-sensitive Fe-S cluster and a unique thiocarboxylate (RCOSH) that is formed on the carboxy terminus of the sulfur carrier protein URM1, believed to be ancient ubiquitin-like post-translational modifiers In an alternative mechanism that is used as sulfur donor, a sulfide ion released from URM1-COSH may bind to the free iron atom of the Fe-S cluster, and become incorporated into s^2U. A sulfide captured by the iron-sulfur cluster was observed in the crystal structure (Arragain et al., 2017), By contrast, another study observed that MmNcs6, after anaerobic reconstitution of the cluster, contains a [4Fe–4S] cluster that is essential for U34-tRNA thiolation(Bimai, Arragain, & Golinelli-Pimpaneau, 2020). The [4Fe–4S] is the active state, not the [3Fe–4S] cluster, in agreement with the fact that there is no known example of a [3Fe–4S] cluster being an active state in bioorganic chemistry and that [3Fe–4S] clusters are the first intermediates appearing upon air-degradation of [4Fe–4S] clusters(Liu et al., 2016).

In analogy to the bacterial TtuA system for s^2T synthesis the mechanism of sulfurtransfer involving URM1 and CTU1 might occur as follows:
one reaction mechanism for CTU1 to remove sulfur from URM1-COSH is therefore proposed to be as follows: (1) CTU1 captures the C-terminal of URM1 with an Fe-S cluster; (2) waits until adenylation is complete; and (3) releases sulfur from URM1 by nucleophilic attack with a hydroxide ion, benefitting from a charge on the side chain at Lys137. (4) Finally, the sulfide bound to the unique Fe site attacks the adenylated tRNA and substitutes the adenyl group (Figure 9).

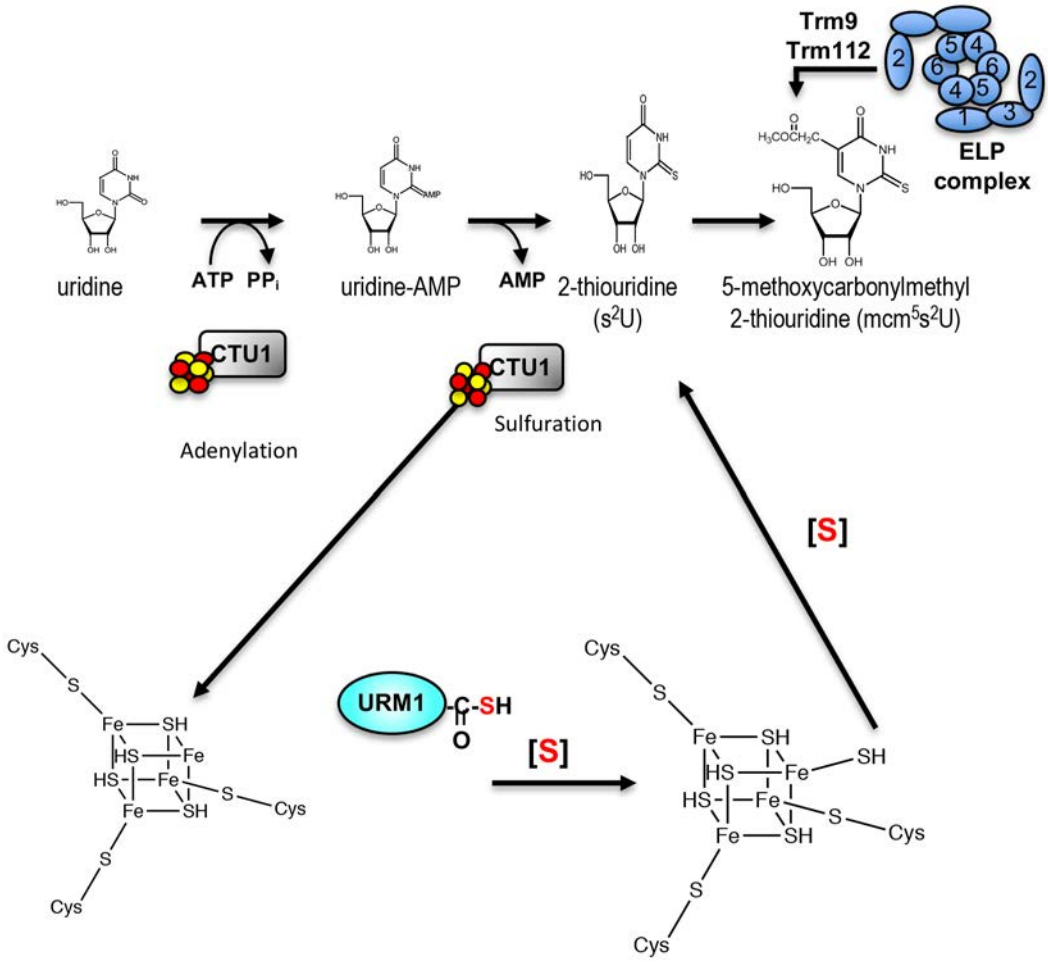

Figure 9: **Proposed mechanism for cytosolic 5-methoxycarbonylmethyl-2-thiouridine ($mcm^5s^2U^{34}$) formation in humans.** Proteins of the ELP pathway and the TRM9 and TRM112 proteins are involved in the formation of the 5-methoxycarbonylmethyl group at the C5 position of U34. The sulfur is mobilized by cytosolic NFS1 from L-cysteine which either transfers the sulfur directly to MOCS3 or to cytosolic TUM1-Iso1. Additionally, TUM1-Iso2 also can interact directly with MOCS3. MOCS3 activates URM1 in the presence of ATP by formation of an acyl-adenylate bond. URM1 is further transferred to a persulfide group on Cys412 of MOCS3-RLD, forming a disulfide bond. After sulfurtransfer, URM1-thiocarboxylate is released and transfers the sulfur further onto uridine 34 on the lysine tRNA, which is activated by the CTU1 and CTU2 proteins under ATP consumption. URM1 can alternatively be conjugated to target proteins via a lysine-isopeptide bond.

In fact, persulfides are formed on cysteines that ligate an [Fe–S] cluster. Although a general mechanism for tRNA thiolation was initially proposed, in which a persulfide attached to a catalytic cysteine is the sulfur donor for tRNA thiolation, there is increasing evidence that a sulfur-containing species bound to a [4Fe–4S] cluster, forming an [4Fe5S] intermediate (Figure 9)(Bimai et al., 2020), ligated to three cysteines only, can be the sulfurating agent. (Figure 9) According to this finding, the

tRNA thiolation enzymes for which a low in vitro activity has been detected and/or for which the catalytic residues remain undetermined, should have their mechanism revisited for the possibility that it involves a [4Fe–4S] cluster. The role of CTU2 is still unknown.

Conclusions:

The biosynthetic pathways of sulfur-containing tRNA nucleosides are very complex since they usually involve a cascade of sulfur carrier proteins, including persulfidation and thiocarboxylate formation with thioester intermediates. rather than a direct transfer from the ultimate sulfur donor to the substrate; and the sulfur flows to different biomolecules involving proteins that are shared with different sulfurtransfer pathways. How this direction of Sulfur flow is controlled is still unknown.
Further, the reaction mechanisms of a [4Fe-4S] cluster containing CTU1 with a persulfide [4Fe5S] intermediate, still need to be verified.

References:

Adam, A. C., Bornhovd, C., Prokisch, H., Neupert, W., & Hell, K. (2006). The Nfs1 interacting protein Isd11 has an essential role in Fe/S cluster biogenesis in mitochondria. *EMBO J, 25*(1), 174-183. doi:10.1038/sj.emboj.7600905

Agris, P. F., Soll, D., & Seno, T. (1973). Biological function of 2-thiouridine in Escherichia coli glutamic acid transfer ribonucleic acid. *Biochemistry, 12*(22), 4331-4337.

Angerer, H. (2015). Eukaryotic LYR Proteins Interact with Mitochondrial Protein Complexes. *Biology (Basel), 4*(1), 133-150. doi:10.3390/biology4010133

Arragain, S., Bimai, O., Legrand, P., Caillat, S., Ravanat, J. L., Touati, N., . . . Golinelli-Pimpaneau, B. (2017). Nonredox thiolation in tRNA occurring via sulfur activation by a [4Fe-4S] cluster. *Proceedings of the National Academy of Sciences of the United States of America, 114*(28), 7355-7360. doi:10.1073/pnas.1700902114

Banci, L., Brancaccio, D., Ciofi-Baffoni, S., Del Conte, R., Gadepalli, R., Mikolajczyk, M., . . . Winkelmann, J. (2014). [2Fe-2S] cluster transfer in iron-sulfur protein biogenesis. *Proceedings of the National Academy of Sciences of the United States of America, 111*(17), 6203-6208. doi:10.1073/pnas.1400102111

Banci, L., Camponeschi, F., Ciofi-Baffoni, S., & Muzzioli, R. (2015). Elucidating the Molecular Function of Human BOLA2 in GRX3-Dependent Anamorsin Maturation Pathway. *Journal of the American Chemical Society, 137*(51), 16133-16143. doi:10.1021/jacs.5b10592

Banci, L., Ciofi-Baffoni, S., Gajda, K., Muzzioli, R., Peruzzini, R., & Winkelmann, J. (2015). N-terminal domains mediate [2Fe-2S] cluster transfer from glutaredoxin-3 to anamorsin. *Nat Chem Biol, 11*(10), 772-778. doi:10.1038/nchembio.1892

Banci, L., Ciofi-Baffoni, S., Mikolajczyk, M., Winkelmann, J., Bill, E., & Pandelia, M. E. (2013). Human anamorsin binds [2Fe-2S] clusters with unique electronic properties. *Journal of biological inorganic chemistry : JBIC : a publication of the Society of Biological Inorganic Chemistry, 18*(8), 883-893. doi:10.1007/s00775-013-1033-1

Beinert, H. (2000). A tribute to sulfur. *European journal of biochemistry / FEBS, 267*(18), 5657-5664.

Bergsma, J., Hol, W. G., Jansonius, J. N., Kalk, K. H., Ploegman, J. H., & Smit, J. D. (1975). The double domain structure of rhodanese. *J Mol Biol, 98*(3), 637-643. doi:10.1016/s0022-2836(75)80092-1

Biederbick, A., Stehling, O., Rosser, R., Niggemeyer, B., Nakai, Y., Elsasser, H. P., & Lill, R. (2006). Role of human mitochondrial Nfs1 in cytosolic iron-sulfur protein biogenesis and iron regulation. *Mol Cell Biol, 26*(15), 5675-5687.

Bimai, O., Arragain, S., & Golinelli-Pimpaneau, B. (2020). Structure-based mechanistic insights into catalysis by tRNA thiolation enzymes. *Curr Opin Struct Biol, 65*, 69-78. doi:10.1016/j.sbi.2020.06.002

Black, K. A., & Dos Santos, P. C. (2015). Shared-intermediates in the biosynthesis of thio-cofactors: Mechanism and functions of cysteine desulfurases and sulfur acceptors. *Biochimica et biophysica acta, 1853*(6), 1470-1480. doi:10.1016/j.bbamcr.2014.10.018

Boniecki, M. T., Freibert, S. A., Muhlenhoff, U., Lill, R., & Cygler, M. (2017). Structure and functional dynamics of the mitochondrial Fe/S cluster synthesis complex. *Nat Commun, 8*(1), 1287. doi:10.1038/s41467-017-01497-1

Bordo, D., & Bork, P. (2002). The rhodanese/Cdc25 phosphatase superfamily. *Embo reports, 3*, 741-746.

Bouvier, D., Labessan, N., Clemancey, M., Latour, J. M., Ravanat, J. L., Fontecave, M., & Atta, M. (2014). TtcA a new tRNA-thioltransferase with an Fe-S cluster. *Nucleic Acids Res, 42*(12), 7960-7970. doi:10.1093/nar/gku508

Bronowicka-Adamska, P., Bentke, A., & Wrobel, M. (2017). Hydrogen sulfide generation from l-cysteine in the human glioblastoma-astrocytoma U-87 MG and neuroblastoma SHSY5Y cell lines. *Acta Biochim Pol, 64*(1), 171-176. doi:10.18388/abp.2016_1394

Cavuzic, M., & Liu, Y. (2017). Biosynthesis of Sulfur-Containing tRNA Modifications: A Comparison of Bacterial, Archaeal, and Eukaryotic Pathways. *Biomolecules, 7*(1). doi:10.3390/biom7010027

Chavarria, N. E., Hwang, S., Cao, S., Fu, X., Holman, M., Elbanna, D., . . . Maupin-Furlow, J. A. (2014). Archaeal Tuc1/Ncs6 homolog required for wobble uridine tRNA thiolation is associated with ubiquitin-proteasome, translation, and RNA processing system homologs. *PLoS One, 9*(6), e99104. doi:10.1371/journal.pone.0099104

Chen, C., Huang, B., Eliasson, M., Ryden, P., & Bystrom, A. S. (2011). Elongator complex influences telomeric gene silencing and DNA damage response by its role in wobble uridine tRNA modification. *PLoS genetics, 7*(9), e1002258. doi:10.1371/journal.pgen.1002258

Chowdhury, M. M., Dosche, C., Löhmannsröben, H. G., & Leimkühler, S. (2012). Dual role of the molybdenum cofactor biosynthesis protein MOCS3 in tRNA thiolation and molybdenum cofactor biosynthesis in humans. *The Journal of biological chemistry, 287*(21), 17297-17307. doi:10.1074/jbc.M112.351429

Christodoulou, A., Lederer, C. W., Surrey, T., Vernos, I., & Santama, N. (2006). Motor protein KIFC5A interacts with Nubp1 and Nubp2, and is implicated in the regulation of centrosome duplication. *J Cell Sci, 119*(Pt 10), 2035-2047. doi:10.1242/jcs.02922

Cory, S. A., Van Vranken, J. G., Brignole, E. J., Patra, S., Winge, D. R., Drennan, C. L., . . . Barondeau, D. P. (2017). Structure of human Fe-S assembly subcomplex reveals unexpected cysteine desulfurase architecture and acyl-ACP-ISD11 interactions. *Proceedings of the National Academy of Sciences of the United States of America, 114*(27), E5325-E5334. doi:10.1073/pnas.1702849114

Cupp-Vickery, J. R., Urbina, H., & Vickery, L. E. (2003). Crystal structure of IscS, a cysteine desulfurase from Escherichia coli. *Journal of molecular biology, 330*(5), 1049-1059.

Daniels, J. N., Wuebbens, M. M., Rajagopalan, K. V., & Schindelin, H. (2007). Crystal Structure of a Molybdopterin Synthase-Precursor Z Complex: Insight into Its Sulfur Transfer Mechanism and Its Role in Molybdenum Cofactor Deficiency(,). *Biochemistry*.

Dewez, M., Bauer, F., Dieu, M., Raes, M., Vandenhaute, J., & Hermand, D. (2008). The conserved Wobble uridine tRNA thiolase Ctu1-Ctu2 is required to maintain genome integrity. *Proceedings of the National Academy of Sciences of the United States of America, 105*(14), 5459-5464. doi:10.1073/pnas.0709404105

Durant, P. C., Bajji, A. C., Sundaram, M., Kumar, R. K., & Davis, D. R. (2005). Structural effects of hypermodified nucleosides in the Escherichia coli and human tRNALys anticodon loop: the effect of nucleosides s2U, mcm5U, mcm5s2U, mnm5s2U, t6A, and ms2t6A. *Biochemistry, 44*(22), 8078-8089. doi:10.1021/bi050343f

El Yacoubi, B., Bailly, M., & de Crecy-Lagard, V. (2012). Biosynthesis and function of posttranscriptional modifications of transfer RNAs. *Annual review of genetics, 46*, 69-95. doi:10.1146/annurev-genet-110711-155641

Esberg, A., Huang, B., Johansson, M. J., & Bystrom, A. S. (2006). Elevated levels of two tRNA species bypass the requirement for elongator complex in transcription and exocytosis. *Mol Cell, 24*(1), 139-148. doi:10.1016/j.molcel.2006.07.031

Frasdorf, B., Radon, C., & Leimkuhler, S. (2014). Characterization and interaction studies of two isoforms of the dual localized 3-mercaptopyruvate sulfurtransferase TUM1 from humans. *The Journal of biological chemistry, 289*(50), 34543-34556. doi:10.1074/jbc.M114.605733

Frey, A. G., Palenchar, D. J., Wildemann, J. D., & Philpott, C. C. (2016). A Glutaredoxin.BolA Complex Serves as an Iron-Sulfur Cluster Chaperone for the Cytosolic Cluster Assembly Machinery. *The Journal of biological chemistry, 291*(43), 22344-22356. doi:10.1074/jbc.M116.744946

Gai, J. W., Wahafu, W., Guo, H., Liu, M., Wang, X. C., Xiao, Y. X., . . . Jin, J. (2013). Further evidence of endogenous hydrogen sulphide as a mediator of relaxation in human and rat bladder. *Asian J Androl, 15*(5), 692-696. doi:10.1038/aja.2013.32

Gari, K., Leon Ortiz, A. M., Borel, V., Flynn, H., Skehel, J. M., & Boulton, S. J. (2012). MMS19 links cytoplasmic iron-sulfur cluster assembly to DNA metabolism. *Science, 337*(6091), 243-245. doi:10.1126/science.1219664

Gerber, S., Comellas-Bigler, M., Goetz, B. A., & Locher, K. P. (2008). Structural basis of trans-inhibition in a molybdate/tungstate ABC transporter. *Science, 321*(5886), 246-250. doi:10.1126/science.1156213

Gutzke, G., Fischer, B., Mendel, R. R., & Schwarz, G. (2001). Thiocarboxylation of molybdopterin synthase provides evidence for the mechanism of dithiolene formation in metal-binding pterins. *J. Biol. Chem., 276*, 36268-36274.

Hänzelmann, P., Hernandez, H. L., Menzel, C., Garcia-Serres, R., Huynh, B. H., Johnson, M. K., . . . Schindelin, H. (2004). Characterization of MOCS1A, an oxygen-sensitive iron-sulfur protein involved in human molybdenum cofactor biosynthesis. *The Journal of biological chemistry, 279*(33), 34721-34732.

Haunhorst, P., Hanschmann, E. M., Brautigam, L., Stehling, O., Hoffmann, B., Muhlenhoff, U., . . . Lillig, C. H. (2013). Crucial function of vertebrate glutaredoxin 3 (PICOT) in iron homeostasis and hemoglobin maturation. *Mol Biol Cell, 24*(12), 1895-1903. doi:10.1091/mbc.E12-09-0648

Hidese, R., Mihara, H., & Esaki, N. (2011). Bacterial cysteine desulfurases: versatile key players in biosynthetic pathways of sulfur-containing biofactors. *Applied microbiology and biotechnology, 91*(1), 47-61. doi:10.1007/s00253-011-3336-x

Hochstrasser, M. (2000). Evolution and function of ubiquitin-like protein-conjugation systems. *Nat Cell Biol, 2*(8), E153-157.

Hughes, J. R., Meireles, A. M., Fisher, K. H., Garcia, A., Antrobus, P. R., Wainman, A., . . . Wakefield, J. G. (2008). A microtubule interactome: complexes with roles in cell cycle and mitosis. *PLoS Biol, 6*(4), e98. doi:10.1371/journal.pbio.0060098

Johnson, J. L., & Rajagopalan, K. V. (1982). Structural and metabolic relationship between the molybdenum cofactor and urothione. *Proc. Natl. Acad. Sci. U. S. A., 79*, 6856-6860.

Jüdes, A., Bruch, A., Klassen, R., Helm, M., & Schaffrath, R. (2016). Sulfur transfer and activation by ubiquitin-like modifier system Uba4•Urm1 link protein urmylation and tRNA thiolation in yeast. *Microbial Cell, 3*(423-433).

Kambampati, R., & Lauhon, C. T. (2000). Evidence for the transfer of sulfane sulfur from IscS to ThiI during the in vitro biosynthesis of 4-thiouridine in *Escherichia coli* tRNA. *The Journal of biological chemistry, 275*(15), 10727-10730.

Kessler, D. (2006). Enzymatic activation of sulfur for incorporation into biomolecules in prokaryotes. *FEMS microbiology reviews, 30*(6), 825-840. doi:10.1111/j.1574-6976.2006.00036.x

Kim, K. S., Maio, N., Singh, A., & Rouault, T. A. (2018). Cytosolic HSC20 integrates de novo iron-sulfur cluster biogenesis with the CIAO1-mediated transfer to recipients. *Hum Mol Genet, 27*(5), 837-852. doi:10.1093/hmg/ddy004

Kispal, G., Csere, P., Prohl, C., & Lill, R. (1999). The mitochondrial proteins Atm1p and Nfs1p are essential for biogenesis of cytosolic Fe/S proteins. *The EMBO journal, 18*(14), 3981-3989. doi:10.1093/emboj/18.14.3981

Krepinsky, K., & Leimkühler, S. (2007). Site-directed mutagenesis of the active-site loop of the rhodanese-like domain of the human molybdopterin synthase sulfurase MOCS3: Major differences in substrate specificity between eukaryotic and bacterial homologues. *FEBS J., 274*, 2778-2787.

Lake, M. W., Wuebbens, M. M., Rajagopalan, K. V., & Schindelin, H. (2001). Mechanism of ubiquitin activation revealed by the structure of a bacterial MoeB-MoaD complex. *Nature, 414*, 325-329.

Land, T., & Rouault, T. A. (1998). Targeting of a human iron-sulfur cluster assembly enzyme, Nifs, to different subcellular compartments is regulated through alternative AUG utilization. *Mol Cell, 2*, 807-815.

Leidel, S., Pedrioli, P. G., Bucher, T., Brost, R., Costanzo, M., Schmidt, A., . . . Peter, M. (2009). Ubiquitin-related modifier Urm1 acts as a sulphur carrier in thiolation of eukaryotic transfer RNA. *Nature, 458*(7235), 228-232. doi:10.1038/nature07643

Leimkuhler, S. (2017). Shared function and moonlighting proteins in molybdenum cofactor biosynthesis. *Biol Chem, 398*(9), 1009-1026. doi:10.1515/hsz-2017-0110

Leimkuhler, S., Buhning, M., & Beilschmidt, L. (2017). Shared Sulfur Mobilization Routes for tRNA Thiolation and Molybdenum Cofactor Biosynthesis in Prokaryotes and Eukaryotes. *Biomolecules, 7*(1). doi:10.3390/biom7010005

Leimkühler, S., Freuer, A., Araujo, J. A., Rajagopalan, K. V., & Mendel, R. R. (2003). Mechanistic studies of human molybdopterin synthase reaction and characterization of mutants identified in group B patients of molybdenum cofactor deficiency. *The Journal of biological chemistry, 278*(28), 26127-26134. doi:10.1074/jbc.M303092200

Li, K., Tong, W. H., Hughes, R. M., & Rouault, T. A. (2006). Roles of the mammalian cytosolic cysteine desulfurase, ISCS, and scaffold protein, ISCU, in iron-sulfur cluster assembly. *The Journal of biological chemistry, 281*(18), 12344-12351. doi:10.1074/jbc.M600582200

Lill, R., & Mühlenhoff, U. (2006). Iron-sulfur protein biogenesis in eukaryotes: components and mechanisms. *Annu Rev Cell Dev Biol, 22*, 457-486.

Lim, S. C., Friemel, M., Marum, J. E., Tucker, E. J., Bruno, D. L., Riley, L. G., . . . Compton, A. G. (2013). Mutations in LYRM4, encoding iron-sulfur cluster biogenesis factor ISD11, cause deficiency of multiple respiratory chain complexes. *Human molecular genetics*. doi:10.1093/hmg/ddt295

Liu, Y., Vinyard, D. J., Reesbeck, M. E., Suzuki, T., Manakongtreecheep, K., Holland, P. L., . . . Soll, D. (2016). A [3Fe-4S] cluster is required for tRNA thiolation in archaea and eukaryotes. *Proceedings of the National*

Academy of Sciences of the United States of America, 113(45), 12703-12708. doi:10.1073/pnas.1615732113

Maio, N., Jain, A., & Rouault, T. A. (2020). Mammalian iron-sulfur cluster biogenesis: Recent insights into the roles of frataxin, acyl carrier protein and ATPase-mediated transfer to recipient proteins. *Curr Opin Chem Biol, 55*, 34-44. doi:10.1016/j.cbpa.2019.11.014

Maio, N., & Rouault, T. A. (2020). Outlining the Complex Pathway of Mammalian Fe-S Cluster Biogenesis. *Trends Biochem Sci, 45*(5), 411-426. doi:10.1016/j.tibs.2020.02.001

Maio, N., Singh, A., Uhrigshardt, H., Saxena, N., Tong, W. H., & Rouault, T. A. (2014). Cochaperone binding to LYR motifs confers specificity of iron sulfur cluster delivery. *Cell Metab, 19*(3), 445-457. doi:10.1016/j.cmet.2014.01.015

Marelja, Z., Mullick Chowdhury, M., Dosche, C., Hille, C., Baumann, O., Löhmannsröben, H. G., & Leimkühler, S. (2013). The L-cysteine desulfurase NFS1 is localized in the cytosol where it provides the sulfur for molybdenum cofactor biosynthesis in humans. *PLoS One, 8*(4), e60869. doi:10.1371/journal.pone.0060869

Marelja, Z., Stöcklein, W., Nimtz, M., & Leimkühler, S. (2008a). A novel role for human Nfs1 in the cytoplasm: Nfs1 acts as a sulfur donor for MOCS3, a protein involved in molybdenum cofactor biosynthesis. *The Journal of biological chemistry, 283*(37), 25178-25185. doi:10.1074/jbc.M804064200

Marelja, Z., Stöcklein, W., Nimtz, M., & Leimkühler, S. (2008b). A novel role for human Nfs1 in the cytoplasm: Nfs1 acts as a sulfur donor for MOCS3, a protein involved in molybdenum cofactor biosynthesis. *J. Biol. Chem., 283*, 25178-25185.

Matthies, A., Nimtz, M., & Leimkühler, S. (2005). Molybdenum cofactor biosynthesis in humans: identification of a persulfide group in the rhodanese-like domain of MOCS3 by mass spectrometry. *Biochemistry, 44*(21), 7912-7920.

Matthies, A., Rajagopalan, K. V., Mendel, R. R., & Leimkühler, S. (2004a). Evidence for the physiological role of a rhodanese-like protein for the biosynthesis of the molybdenum cofactor in humans. *Proceedings of the National Academy of Sciences of the United States of America, 101*, 5946-5951.

Matthies, A., Rajagopalan, K. V., Mendel, R. R., & Leimkühler, S. (2004b). Evidence for the physiological role of a rhodanese-like protein for the biosynthesis of the molybdenum cofactor in humans. *Proceedings of the National Academy of Sciences of the United States of America, 101*(16), 5946-5951. doi:10.1073/pnas.0308191101

Mendel, R. R., & Kruse, T. (2012). Cell biology of molybdenum in plants and humans. *Biochimica et biophysica acta, 1823*(9), 1568-1579. doi:10.1016/j.bbamcr.2012.02.007

Mendel, R. R., & Leimkühler, S. (2015). The biosynthesis of the molybdenum cofactors. *Journal of biological inorganic chemistry : JBIC : a publication of the Society of Biological Inorganic Chemistry, 20*(2), 337-347. doi:10.1007/s00775-014-1173-y

Mendel, R. R., & Schwarz, G. (2011). Molybdenum cofactor biosynthesis in plants and humans. *Coordination Chemistry Reviews, 255*, 1145-1158.

Misslinger, M., Lechner, B. E., Bacher, K., & Haas, H. (2018). Iron-sensing is governed by mitochondrial, not by cytosolic iron-sulfur cluster biogenesis in Aspergillus fumigatus. *Metallomics : integrated biometal science, 10*(11), 1687-1700. doi:10.1039/c8mt00263k

Mulliez, E., Duarte, V., Arragain, S., Fontecave, M., & Atta, M. (2017). On the Role of Additional [4Fe-4S] Clusters with a Free Coordination Site in Radical-SAM Enzymes. *Front Chem, 5*, 17. doi:10.3389/fchem.2017.00017

Nakai, Y., Nakai, M., Hayashi, H., & Kagamiyama, H. (2001). Nuclear localization of yeast Nfs1p is required for cell survival. *The Journal of biological chemistry, 276*(11), 8314-8320. doi:10.1074/jbc.M007878200

Netz, D. J., Genau, H. M., Weiler, B. D., Bill, E., Pierik, A. J., & Lill, R. (2016). The conserved protein Dre2 uses essential [2Fe-2S] and [4Fe-4S] clusters for its function in cytosolic iron-sulfur protein assembly. *Biochem J, 473*(14), 2073-2085. doi:10.1042/BCJ20160416

Netz, D. J., Mascarenhas, J., Stehling, O., Pierik, A. J., & Lill, R. (2014). Maturation of cytosolic and nuclear iron-sulfur proteins. *Trends in cell biology, 24*(5), 303-312. doi:10.1016/j.tcb.2013.11.005

Netz, D. J., Stumpfig, M., Dore, C., Mühlenhoff, U., Pierik, A. J., & Lill, R. (2010). Tah18 transfers electrons to Dre2 in cytosolic iron-sulfur protein biogenesis. *Nature chemical biology, 6*(10), 758-765. doi:10.1038/nchembio.432

Neukranz, Y., Kotter, A., Beilschmidt, L., Marelja, Z., Helm, M., Graf, R., & Leimkuhler, S. (2019). Analysis of the Cellular Roles of MOCS3 Identifies a MOCS3-Independent Localization of NFS1 at the Tips of the Centrosome. *Biochemistry, 58*(13), 1786-1798. doi:10.1021/acs.biochem.8b01160

Nilsson, K., Jager, G., & Bjork, G. R. (2017). An unmodified wobble uridine in tRNAs specific for Glutamine, Lysine, and Glutamic acid from Salmonella enterica Serovar Typhimurium results in nonviability-Due to increased missense errors? *PLoS One, 12*(4), e0175092. doi:10.1371/journal.pone.0175092

Noma, A., Sakaguchi, Y., & Suzuki, T. (2009). Mechanistic characterization of the sulfur-relay system for eukaryotic 2-thiouridine biogenesis at tRNA wobble positions. *Nucleic acids research, 37*(4), 1335-1352. doi:10.1093/nar/gkn1023

Noma, A., Shigi, N., & Suzuki, T. (2009). Biogenesis and Functions of Thio-Compounds in transfer RNA: Comparison of bacterial and eukaryotic thiolation machineries. *Landes Bioscience, DNA and RNA modification*(Grosjean eds.), 392-405.

Pabis, M., Termathe, M., Ravichandran, K. E., Kienast, S. D., Krutyholowa, R., Sokolowski, M., . . . Glatt, S. (2020). Molecular basis for the bifunctional Uba4-Urm1 sulfur-relay system in tRNA thiolation and ubiquitin-like conjugation. *EMBO J, 39*(19), e105087. doi:10.15252/embj.2020105087

Palenchar, P. M., Buck, C. J., Cheng, H., Larson, T. J., & Mueller, E. G. (2000). Evidence that ThiI, an enzyme shared between thiamin and 4-thiouridine biosynthesis, may be a sulfurtransferase that proceeds through a persulfide intermediate. *J. Biol. Chem., 275*, 8283-8286.

Paul, V. D., & Lill, R. (2015). Biogenesis of cytosolic and nuclear iron-sulfur proteins and their role in genome stability. *Biochimica et biophysica acta, 1853*(6), 1528-1539. doi:10.1016/j.bbamcr.2014.12.018

Pedre, B., & Dick, T. P. (2021). 3-Mercaptopyruvate sulfurtransferase: an enzyme at the crossroads of sulfane sulfur trafficking. *Biol Chem, 402*(3), 223-237. doi:10.1515/hsz-2020-0249

Pedrioli, P. G., Leidel, S., & Hofmann, K. (2008). Urm1 at the crossroad of modifications. 'Protein Modifications: Beyond the Usual Suspects' Review Series. *EMBO reports, 9*(12), 1196-1202. doi:10.1038/embor.2008.209

Ploegman, J. H., Drent, G., Kalk, K. H., & Hol, W. G. (1978). Structure of bovine liver rhodanese. I. Structure determination at 2.5 A resolution and a comparison of the conformation and sequence of its two domains. *J Mol Biol, 123*(4), 557-594.

Ploegman, J. H., Drent, G., Kalk, K. H., & Hol, W. G. (1979). The structure of bovine liver rhodanese. II. The active site in the sulfur-substituted and the sulfur-free enzyme. *J Mol Biol, 127*(2), 149-162. doi:10.1016/0022-2836(79)90236-5

Ploegman, J. H., Drent, G., Kalk, K. H., Hol, W. G., Heinrikson, R. L., Keim, P., . . . Russell, J. (1978). The covalent and tertiary structure of bovine liver rhodanese. *Nature, 273*(5658), 124-129. doi:10.1038/273124a0

Ramasamy, S., Singh, S., Taniere, P., Langman, M. J., & Eggo, M. C. (2006). Sulfide-detoxifying enzymes in the human colon are decreased in cancer and upregulated in differentiation. *Am J Physiol Gastrointest Liver Physiol, 291*(2), G288-296. doi:10.1152/ajpgi.00324.2005

Richards, T. A., & van der Giezen, M. (2006). Evolution of the Isd11-IscS complex reveals a single alpha-proteobacterial endosymbiosis for all eukaryotes. *Mol Biol Evol, 23*(7), 1341-1344.

Rudolph, M. J., Wuebbens, M. M., Rajagopalan, K. V., & Schindelin, H. (2001). Crystal structure of molybdopterin synthase and its evolutionary relationship to ubiquitin activation. *Nat Struct Biol, 8*(1), 42-46.

Schindelin, H. (2005). Evolutionary Origin of the Activation Step During Ubiquitin-dependent Protein Degradation. In R. J. Mayer, A. Ciechanover, & M. Rechsteiner (Eds.), *Protein Degradation: Ubiquitin and the Chemistry of Life* (Vol. I, pp. 21-43). Weinheim: WILEY-VCH.

Schlieker, C. D., Van der Veen, A. G., Damon, J. R., Spooner, E., & Ploegh, H. L. (2008). A functional proteomics approach links the ubiquitin-related modifier Urm1 to a tRNA modification pathway. *Proceedings of the National Academy of Sciences of the United States of America, 105*(47), 18255-18260. doi:10.1073/pnas.0808756105

Schmitz, J., Mullick Chowdhury, M., Hänzelmann, P., Nimtz, M., Lee, E. Y., Schindelin, H., & Leimkühler, S. (2008). The sulfurtransferase activity of Uba4 presents a link between ubiquitin-like protein conjugation and activation of sulfur carrier proteins. *Biochemistry, 47*(24), 6479-6489. doi:10.1021/bi800477u

Schmitz, J., Wuebbens, M. M., Rajagopalan, K. V., & Leimkühler, S. (2007). Role of the C-Terminal Gly-Gly Motif of Escherichia Coli MoaD, a Molybdenum Cofactor Biosynthesis Protein with a Ubiquitin Fold. *Biochemistry, 46*(3), 909-916.

Schwarz, G., Mendel, R. R., & Ribbe, M. W. (2009). Molybdenum cofactors, enzymes and pathways. *Nature, 460*(7257), 839-847. doi:10.1038/nature08302

Shan, Y., Napoli, E., & Cortopassi, G. (2007). Mitochondrial frataxin interacts with ISD11 of the NFS1/ISCU complex and multiple mitochondrial chaperones. *Hum Mol Genet, 16*(8), 929-941.

Shi, Y., Ghosh, M. C., Tong, W. H., & Rouault, T. A. (2009). Human ISD11 is essential for both iron-sulfur cluster assembly and maintenance of normal cellular iron homeostasis. *Human molecular genetics, 18*(16), 3014-3025. doi:10.1093/hmg/ddp239

Shigi, N. (2014). Biosynthesis and functions of sulfur modifications in tRNA. *Frontiers in genetics, 5*, 67. doi:10.3389/fgene.2014.00067

Shigi, N., Suzuki, T., Terada, T., Shirouzu, M., Yokoyama, S., & Watanabe, K. (2006). Temperature-dependent biosynthesis of 2-thioribothymidine of Thermus thermophilus tRNA. *The Journal of biological chemistry, 281*(4), 2104-2113. doi:10.1074/jbc.M510771200

Sorbo, B. (1957). A colorimetric method for the determination of thiosulfate. *Biochimica et biophysica acta, 23*(2), 412-416.

Srinivasan, V., Netz, D. J., Webert, H., Mascarenhas, J., Pierik, A. J., Michel, H., & Lill, R. (2007). Structure of the yeast WD40 domain protein Cia1, a component acting late in iron-sulfur protein biogenesis. *Structure, 15*(10), 1246-1257. doi:10.1016/j.str.2007.08.009

Stallmeyer, B., Drugeon, G., Reiss, J., Haenni, A. L., & Mendel, R. R. (1999). Human molybdopterin synthase gene: identification of a bicistronic transcript with overlapping reading frames. *Am. J. Hum. Genet., 64*, 698-705.

Stehling, O., Jeoung, J. H., Freibert, S. A., Paul, V. D., Banfer, S., Niggemeyer, B., . . . Lill, R. (2018). Function and crystal structure of the dimeric P-loop ATPase CFD1 coordinating an exposed [4Fe-4S] cluster for transfer to apoproteins. *Proceedings of the National Academy of Sciences of the United States of America, 115*(39), E9085-E9094. doi:10.1073/pnas.1807762115

Stehling, O., Netz, D. J., Niggemeyer, B., Rosser, R., Eisenstein, R. S., Puccio, H., . . . Lill, R. (2008). Human Nbp35 is essential for both cytosolic iron-sulfur protein assembly and iron homeostasis. *Molecular and cellular biology, 28*(17), 5517-5528. doi:10.1128/MCB.00545-08

Suzuki, T. (2005). Biosynthesis and function of tRNA wobble
modifications. *Topics in Current Genetics, 12*, 23-69.

Suzuki, T., Wada, T., Saigo, K., & Watanabe, K. (2002). Taurine as a constituent of mitochondrial tRNAs: new insights into the functions of taurine and human mitochondrial diseases. *The EMBO journal, 21*(23), 6581-6589.

Takano, Y., Hanaoka, K., Shimamoto, K., Miyamoto, R., Komatsu, T., Ueno, T., . . . Urano, Y. (2017). Development of a reversible fluorescent probe for reactive sulfur species, sulfane sulfur, and its biological application. *Chemical communications, 53*(6), 1064-1067. doi:10.1039/c6cc08372b

Termathe, M., & Leidel, S. A. (2018). The Uba4 domain interplay is mediated via a thioester that is critical for tRNA thiolation through Urm1 thiocarboxylation. *Nucleic Acids Res, 46*(10), 5171-5181. doi:10.1093/nar/gky312

Termathe, M., & Leidel, S. A. (2021). Urm1: A Non-Canonical UBL. *Biomolecules, 11*(2). doi:10.3390/biom11020139

Tong, W. H., & Rouault, T. (2000). Distinct iron-sulfur cluster assembly complexes exist in the cytosol and mitochondria of human cells. *EMBO J, 19*(21), 5692-5700.

Tong, W. H., & Rouault, T. A. (2006). Functions of mitochondrial ISCU and cytosolic ISCU in mammalian iron-sulfur cluster biogenesis and iron homeostasis. *Cell Metab, 3*(3), 199-210. doi:10.1016/j.cmet.2006.02.003

Umeda, N., Suzuki, T., Yukawa, M., Ohya, Y., Shindo, H., & Watanabe, K. (2005). Mitochondria-specific RNA-modifying enzymes responsible for the biosynthesis of the wobble base in mitochondrial tRNAs. Implications for the molecular pathogenesis of human mitochondrial diseases. *The Journal of biological chemistry, 280*(2), 1613-1624. doi:10.1074/jbc.M409306200

Van der Veen, A. G., Schorpp, K., Schlieker, C., Buti, L., Damon, J. R., Spooner, E., . . . Jentsch, S. (2011). Role of the ubiquitin-like protein Urm1 as a noncanonical lysine-directed protein modifier. *Proceedings of the National Academy of Sciences of the United States of America, 108*(5), 1763-1770. doi:10.1073/pnas.1014402108

Van Vranken, J. G., Jeong, M. Y., Wei, P., Chen, Y. C., Gygi, S. P., Winge, D. R., & Rutter, J. (2016). The mitochondrial acyl carrier protein (ACP) coordinates mitochondrial fatty acid synthesis with iron sulfur cluster biogenesis. *Elife, 5*. doi:10.7554/eLife.17828

Veldman, A., Santamaria-Araujo, J. A., Sollazzo, S., Pitt, J., Gianello, R., Yaplito-Lee, J., . . . Schwarz, G. (2010). Successful treatment of molybdenum cofactor deficiency type A with cPMP. *Pediatrics, 125*(5), e1249-1254. doi:10.1542/peds.2009-2192

Westley, J. (1973). Rhodanese. *Adv. Enzymol., 39*, 327-368.

Westley, J. (1981). Thiosulfate:Cyanide Sulfurtransferase (Rhodanese). *Methods Enzymol, 77*, 285-291.

Wiedemann, N., Urzica, E., Guiard, B., Muller, H., Lohaus, C., Meyer, H. E., . . . Pfanner, N. (2006). Essential role of Isd11 in mitochondrial iron-sulfur cluster synthesis on Isu scaffold proteins. *Embo J, 25*(1), 184-195.

Wiedemann, N., Urzica, E., Guiard, B., Muller, H., Lohaus, C., Meyer, H. E., . . . Pfanner, N. (2006). Essential role of Isd11 in mitochondrial iron-sulfur cluster synthesis on Isu scaffold proteins. *The EMBO journal, 25*(1), 184-195. doi:10.1038/sj.emboj.7600906

Wuebbens, M. M., & Rajagopalan, K. V. (2003). Mechanistic and mutational studies of *Escherichia coli* molybdopterin synthase clarify the final step of molybdopterin biosynthesis. *The Journal of biological chemistry, 278*, 14523-14532.

Xu, J., Zhang, J., Wang, L., Zhou, J., Huang, H., Wu, J., . . . Shi, Y. (2006). Solution structure of Urm1 and its implications for the origin of protein modifiers. *Proceedings of the National Academy of Sciences of the United States of America, 103*(31), 11625-11630. doi:10.1073/pnas.0604876103

Yokoyama, S., Watanabe, T., Murao, K., Ishikura, H., Yamaizumi, Z., Nishimura, S., & Miyazawa, T. (1985). Molecular mechanism of codon recognition by tRNA species with modified uridine in the first position of the anticodon. *Proceedings of the National Academy of Sciences of the United States of America, 82*(15), 4905-4909.

Zhang, Y., Lyver, E. R., Nakamaru-Ogiso, E., Yoon, H., Amutha, B., Lee, D. W., . . . Dancis, A. (2008). Dre2, a conserved eukaryotic Fe/S cluster protein, functions in cytosolic Fe/S protein biogenesis. *Mol Cell Biol, 28*(18), 5569-5582. doi:10.1128/MCB.00642-08

Zheng, L., White, R. H., Cash, V. L., Jack, R. F., & Dean, D. R. (1993). Cysteine desulfurase activity indicates a role for NIFS in metallocluster biosynthesis. *Proceedings of the National Academy of Sciences of the United States of America, 90*(7), 2754-2758.

Zuhra, K., Tome, C. S., Masi, L., Giardina, G., Paulini, G., Malagrino, F., . . . Giuffre, A. (2019). N-Acetylcysteine Serves as Substrate of 3-Mercaptopyruvate Sulfurtransferase and Stimulates Sulfide Metabolism in Colon Cancer Cells. *Cells, 8*(8). doi:10.3390/cells8080828

Manuscript III

Eprenetapopt triggers ferroptosis, inhibits NFS1 cysteine desulfurase, and synergizes with serine and glycine dietary restriction

Eprenetapopt (APR-246) triggers ferroptosis, inhibits NFS1 cystine desulfurase activity and synergizes with serine and glycine dietary restriction

Kenji M. Fujihara[1,2,*], Bonnie Z. Zhang[1,2], Thomas D. Jackson[3], Moses O. Ogunkola[4], Brunda Nijagal[5], Julia V. Milne[1,2], David A. Sallman[6], Ching-Seng Ang[3], Iva Nikolic[7], Conor J. Kearney[2,8], Simon J. Hogg[2,8,9], Carlos S. Cabalag[1,2,10], Vivien R. Sutton[2,11], Sally Watt[2,11], Asuka T. Fujihara[1], Joseph A. Trapani[2,11], Kaylene J. Simpson[2,7], Diana Stojanovski[3], Silke Leimkühler[4], Sue Haupt[2,12], Wayne A. Phillips[1,2,13], Nicholas J. Clemons[1,2,*]

[1]Gastrointestinal Cancer Program, Cancer Research Division, Peter MacCallum Cancer Centre, Melbourne, Victoria, Australia
[2]Sir Peter MacCallum Department of Oncology, The University of Melbourne, Parkville, Victoria, Australia
[3]Department of Biochemistry and Pharmacology and the Bio21 Molecular Science and Biotechnology Institute, The University of Melbourne, Parkville, Victoria, Australia
[4]Institute of Biochemistry and Biology Department for Molecular Enzymology, University of Potsdam, Potsdam, Germany
[5]Metabolomics Australia, The Bio21 Institute of Molecular Science and Biotechnology, The University of Melbourne, Parkville, Victoria, Australia
[6]Malignant Hematology Department, H. Lee Moffitt Cancer Center and Research Institute, Tampa, Florida, USA
[7]Victorian Centre for Functional Genomics, Peter MacCallum Cancer Centre
[8]Translational Hematology Program, Cancer Research Division, Peter MacCallum Cancer Centre, Melbourne, Australia
[9]Human Oncology and Pathogenesis Program, Memorial Sloan Kettering Cancer Center, New York, NY, USA
[10]Department of Surgical Oncology, Peter MacCallum Cancer Centre, Melbourne, Victoria, Australia
[11]Cancer Immunology Program, Peter MacCallum Cancer Centre, Melbourne, Australia
[12]Tumor Suppression and Cancer Sex Disparity Laboratory, Peter MacCallum Cancer Centre, Melbourne, Victoria, Australia
[13]Department of Surgery (St. Vincent's Hospital), The University of Melbourne, Parkville, Victoria, Australia

*Co-corresponding authors

Corresponding Authors:
Associate Professor Nicholas J. Clemons
Peter MacCallum Cancer Centre
Locked Bag #1, A'Beckett St, Melbourne VIC Australia 8006
Email: Nicholas.clemons@petermac.org
Tel: 03 8559 5273

Doctor Kenji M. Fujihara
Peter MacCallum Cancer Centre
Locked Bag #1, A'Beckett St, Melbourne VIC Australia 8006
Email: Kenji.fujihara@petermac.org
Tel: 03 8559 8294

Declaration: The authors declare no conflicts of interest.

ABSTRACT

The mechanism of action of eprenetapopt (APR-246, PRIMA-1^{MET}) as an anticancer agent remains unresolved, although the clinical development of eprenetapopt focuses on its reported mechanism of action as a mutant-p53 reactivator. Employing unbiased approaches, this study demonstrates that eprenetapopt depletes the cellular antioxidant glutathione by increasing its turnover, triggering a non-apoptotic, iron-dependent form of cell death known as ferroptosis. Deficiency in genes responsible for supplying cancer cells with the substrates for *de novo* glutathione synthesis (*SLC7A11*, *SHMT2* and *MTHFD1L*), as well as the enzymes required to synthesize glutathione (*GCLC* and *GCLM*), augment the activity of eprenetapopt. Eprenetapopt also inhibits iron-sulfur cluster biogenesis by limiting the cysteine desulfurase activity of NFS1, which potentiates ferroptosis and may restrict cellular proliferation. Importantly, the combination of eprenetapopt with dietary serine and glycine restriction synergize to inhibit esophageal xenograft tumor growth. These findings reframe the clinical utility of eprenetapopt from a mutant-p53 reactivator to a first-in-class ferroptosis inducer.

ONE SENTENCE SUMMARY

Using unbiased approaches, we found that the first-in-class mutant-p53 reactivator, eprenetapopt, triggers ferroptosis through increasing the turnover of glutathione and inhibiting NFS1 cysteine desulfurase activity.

KEYWORDS

Eprenetapopt, APR-246, PRIMA-1^{MET}, glutathione, ferroptosis, NFS1, iron-sulfur cluster, mitochondrial one-carbon, CRISPR screening, esophageal cancer.

INTRODUCTION

TP53 mutation occurs in ~50% of all cancers and overall is associated with poor survival (*1*), providing a strong impetus for the development of mutant-p53 (mut-p53) targeted therapeutics. Eprenetapopt (APR-246, PRIMA-1^{MET}) was developed as a mut-p53 targeted therapeutic and is currently under clinical investigation in *TP53*-mutated myelodysplastic syndromes (MDS) and acute myeloid leukemia (AML) (*2*). Recent results from two phase II clinical trials in *TP53*-mutated MDS, combining eprenetapopt with standard-of-care azacitidine, reported rates of complete remission (CR) of ~50% (*3, 4*). Furthermore, apparent improvements in median overall survival (OS) compared to previous studies of azacitidine alone were reported in *TP53*-mutated MDS (*3-5*). However, early results from the phase III randomized clinical trial in *TP53*-mutated MDS failed to meet the primary endpoint of CR rate (33.3% in eprenetapopt + azacitidine, 22.4% in azacitidine alone, *P*=0.13) (*6*).

The therapeutic effect of eprenetapopt has been understood to involve the reactivation of wild-type p53 activity to induce apoptosis through covalent modification of cysteine residues in the core domain of mut-p53 protein (*7, 8*). The specific mechanism of action (MoA) of eprenetapopt, however, remains to be thoroughly defined. Recently, we demonstrated that the expression of *SLC7A11*, which encodes the functional subunit of the cystine-glutamate antiporter, system x_c^-, is the major determinant of response to eprenetapopt across cancer lineages, and neither *TP53* mutation status nor p53 protein level were associated with sensitivity (*9*). The import of cystine through system x_c^- provides the predominant source of intracellular cysteine, which is the rate limiting substrate required for *de novo* synthesis of the cellular antioxidant glutathione (GSH) (*10*). Eprenetapopt and its structural analogue APR-017 (also known as

PRIMA-1) are prodrugs that undergo spontaneous conversion to the active compound, 2-methylene 3-quinuclidinone (MQ), releasing formaldehyde in the process (*7*). MQ is a thiol-reactive Michael acceptor that forms reversible covalent bonds with thiol-containing molecules including cysteine and the GSH (*11, 12*). As a result, the anticancer effects of eprenetapopt have been linked to GSH depletion and inhibition of the thioredoxin antioxidant system (*11-14*). Notably, we previously demonstrated that mut-p53 protein accumulation drives down the expression of *SLC7A11* through the inhibition of the transcription factor NRF2 (encoded by *NFE2L2*) – providing an explanation for the selectivity of eprenetapopt against mut-p53 cancer cells under some conditions (*12*). However, to date, limited unbiased examinations of the MoA of eprenetapopt have been attempted, and the predominant focus of prior investigations has been through the lens of eprenetapopt as a mut-p53 reactivator *a priori*.

In this study, we undertake a systematic, unbiased approach to probe the MoA of eprenetapopt, incorporating genome-wide CRISPR perturbation screening and metabolite and proteomic profiling in cancer cells with pan-cancer gene dependency and cell line sensitivity datasets. In this way, we provide a compendium of functional genomic and molecular detail into the MoA of eprenetapopt. In particular, CRISPR perturbation screens reveal that loss of mitochondrial one-carbon (mito-1C) metabolism enzymes, SHMT2 and MTHFD1L, sensitizes cancer cells to eprenetapopt – an insight that can be exploited *in vivo* to sensitize tumours to eprenetapopt with serine and glycine (SG) dietary restriction. Mechanistically, we find that eprenetapopt induces GSH depletion, triggering iron-dependent, non-apoptotic ferroptosis and limits cellular proliferation, in part, by inhibiting the cysteine desulfurase activity of NFS1. Clinically, these insights may provide a rational avenue for the expansion of

eprenetapopt utility in MDS to include patient selection based on the presence of ring sideroblasts, rather than reliance on *TP53* mutation status.

RESULTS

Multiomics strategy to determine the mechanism of action of eprenetapopt

To determine the MoA of eprenetapopt, we undertook a set of complementary approaches, including genome-wide CRISPR perturbation screens, quantitative proteomics and untargeted metabolomics in response to eprenetapopt (**Figure 1A**). We also leveraged and incorporated publicly available pan-cancer therapeutic response and cancer cell line gene dependency datasets from the Broad Institute's DepMap portal (www.depmap.org) in order to expand the validity and test the generalizability of our investigational datasets (*15, 16*). To select an appropriate model system to systematically dissect the MoA of eprenetapopt, we first analyzed cancer cell line drug sensitivity data from the Cancer Therapeutic Response Portal (CTRPv2). We found that esophageal cancer cell lines with a high rate of *TP53* mutation were the most resistant to the structural analogue of eprenetapopt, APR-017 (**Figure 1B**). Specifically, we selected the OACM5.1 esophageal cancer cell line for our investigation, which expresses the most common *TP53* missense mutation across all cancers, R248Q (mut-p53^{R248Q}). As a result, this model is amenable to identifying genetic determinants of sensitivity to eprenetapopt without precluding mut-p53 reactivation as a MoA.

We transduced OACM5.1 cells expressing Cas9-mCherry with the Brunello genome-wide CRISPR knockout (CRISPRko) library (*17*) and challenged these cells with a sublethal dose of eprenetapopt for 8 days (**Figure 1C, Figure S1A**). In parallel, we transduced OACM5.1 cells expressing dCas9-VP64 with the Calabrese Set A genome-wide CRISPR activation (CRISPRa) library (*18*) and challenged these cells with a lethal dose of eprenetapopt for 28 days. The CRISPRko screen aimed to identify

genetic deletions that increase sensitivity to eprenetapopt and thus ‘drop-out’ in the eprenetapopt treated cells compared to vehicle treated controls. Meanwhile, the CRISPRa screen aimed to identify gene overexpression that protects cells from eprenetapopt. The CRISPRa screen has the advantage of potentially identifying genetic modulators of eprenetapopt sensitivity that may not be revealed in the CRISPRko screen, where general essential genes drop-out during the puromycin selection.

Consistent with our prior observations, and those of others, that eprenetapopt triggers GSH depletion in cancer cells (*12, 19-21*), the CRISPRko screen identified genes involved in GSH synthesis, *SLC7A11* and *GCLM*, whilst *GCLC* was the top enriched gene in the CRISPRa screen (**Figure 1D**). Notably, two mitochondrial one-carbon (mito-1C) metabolism genes, *SHMT2* and *MTHFD1L*, and the S-formylglutathione hydrolase gene, *ESD*, involved in GSH-mediated formaldehyde detoxification (*22-24*) were identified in the CRISPRko screen. We confirmed that two independent sgRNA guides targeting *GCLM*, *SLC7A11*, *SHMT2*, *MTHFD1L* and *ESD*, and one sgRNA guide for *GCLC* activation, modulated sensitivity to eprenetapopt as expected (**Figure 1E**). We confirmed gene disruption in a subset of our top gene candidates (**Figure S1B**) as well as overexpression of *GCLC* following guide transduction (**Figure S1C**). In agreement, genome-wide dependency data demonstrated that *GCLC* and *GCLM* dependency correlate strongly with pan-cancer cell line sensitivity to APR-017 (**Figure 1F, Figure S1B**). *GCLC* and *GCLM* uniquely scored strongly in both our screening approaches, indicating that the modulation of the *de novo* GSH axis is central to the MoA of eprenetapopt in cancer cells (**Figure 1G**).

Complementing our functional genomics approach, we performed untargeted metabolomics and label-free quantitative proteomics in OACM5.1 cells treated with eprenetapopt prior to the onset of cell death. As expected, eprenetapopt treatment decreased reduced GSH levels, without increasing oxidized GSH (GSSG) levels (**Figure 1H**) – indicating that eprenetapopt is triggering total GSH depletion rather than the conversion of reduced GSH to GSSG in agreement with previous studies (*11, 12, 19, 25, 26*). Furthermore, cystine levels were increased following eprenetapopt treatment, which could be explained by the upregulation of *SLC7A11* expression in response to eprenetapopt treatment shown in previous studies (*11, 27*). Meanwhile, mitochondrial metabolism was altered, as demonstrated by the decrease in acetyl-CoA and NADH (**Figure 1H**). Notably, our proteomics study revealed that cells treated with eprenetapopt upregulated the levels of mitochondrial ferredoxin 1 (FDX1), a critical component of mitochondrial iron-sulfur cluster biosynthesis (*28*), as well as two other proteins, DNAJA3 and ABCF2, which have reported roles in iron metabolism (*29, 30*) (**Figure 1I**).

Altogether, these datasets provide confirmation that GSH depletion is central to the MoA of eprenetapopt and suggests as yet unappreciated roles for mito-1C metabolism and iron metabolism in the MoA of eprenetapopt.

Eprenetapopt and mitochondrial one-carbon metabolism

We next investigated the involvement of mito-1C metabolism in eprenetapopt sensitivity. Of note, mito-1C metabolism intersects with *de novo* GSH synthesis through SHMT2-mediated production of glycine from serine (*31*), and also supports cellular proliferation through formate production (*22*) (**Figure 2A**). First, we attempted

to rescue the increased sensitivity to eprenetapopt in mito-1C-deficient cells using exogenous formate. Pertinently, formate supplementation did not alter sensitivity to eprenetapopt (**Figure S2A**). Previous studies have shown that mito-1C deficient cells have altered dependency on exogenous glycine due to the loss of endogenous glycine production by SHMT2 (*32*). Indeed, cells expressing *SHMT2* and *MTHFD1L* sgRNAs displayed reduced growth in the absence of glycine, whilst cells transduced with control vectors did not (**Figure 2B, S2B**). Meanwhile, all cells displayed sensitivity to serine deprivation alone and combined serine and glycine (SG) deprivation. Importantly, the glycine auxotrophy in mito-1C deficient cells could be reversed with the exogenous supply of cell permeable GSH (**Figure 2B, S2B**) – in agreement with previous studies (*32*). This highlights that mito-1C deficient cells have a higher demand for exogenous glycine for *de novo* GSH synthesis. As a result, the increased sensitivity to eprenetapopt in mito-1C deficient cells can be reversed by supplementation of additional glycine to the cell media (**Figure 2C, S2B**). Together, these data demonstrate that mito-1C metabolism interplays with *de novo* GSH synthesis by providing endogenous glycine to regulate sensitivity to eprenetapopt in cancer cells.

Since mito-1C deficiency leads to increased demand for exogenous glycine following eprenetapopt-induced GSH depletion, we reasoned that limiting glycine availability by restricting exogenous SG would sensitize cancer cells to respond to eprenetapopt. Restriction of dietary SG has previously been shown to reduce tumour growth in a variety of xenografts and genetically engineered mouse models, and demonstrated strong efficacy in combination with biguanides, glutaminase inhibitors and phosphoglycerate dehydrogenase inhibitors (*33-37*). To this end, we tested the

combination of dietary SG restriction and eprenetapopt in an aggressive model of spontaneous metastatic esophageal cancer, FLO-1 LM (*38*). Five weeks of daily dosing of 100 mg/kg eprenetapopt monotherapy failed to inhibit primary tumour growth or limit metastatic spread (**Figure 2D, S2D,E**). Promisingly, we found that the combination of SG restriction and eprenetapopt significantly inhibited both primary tumour growth and delayed on the onset of metastatic disease, leading to prolonged overall survival (**Figure 2D, S2D**). Dietary SG restriction in combination with eprenetapopt were well tolerated (**Figure S2F**) and chow consumption remained consistent across the different diet interventions (**Figure S2G**). We also demonstrated that the combination of eprenetapopt and SG restriction limited the growth in an esophageal adenocarcinoma patient-derived xenograft (PDX) tumour model (**Figure 2E**). Of note, in the metastatic and PDX models, dietary SG restriction alone inhibited tumour growth to a degree (**Figure S2H**). Altogether, these results demonstrate that SG restriction can improve the efficacy of eprenetapopt and, for the first time, that dietary SG restriction can inhibit the growth of esophageal cancer tumours *in vivo*.

Given that *de novo* GSH synthesis pathways are central to eprenetapopt sensitivity, we hypothesized that eprenetapopt inhibits the *de novo* synthesis of GSH. First, we verified that eprenetapopt does not block cystine uptake into cells, whilst a known cystine uptake inhibitor, erastin, does (**Figure S2I**). Of note, we also found that mito-1C deficiency did not alter sensitivity to erastin (**Figure S2J**). Furthermore, in contradiction to previous investigations (*13*), we found that eprenetapopt treatment decreases the level of glutathionylation in cells (**Figure S2K)**, indicating that the GSH depletion induced by eprenetapopt is not due to loss of free GSH to protein conjugation. We tracked the incorporation of isotopically labeled cystine into GSH and

other products using LC-MS. Strikingly, we observed that eprenetapopt treatment increased the proportion of cystine-derived cysteine incorporated into *de novo* synthesis products glutamylcysteine, GSH and GSSG (**Figure 2F)**. We also detected both MQ-GSH and MQ-cysteine adducts in eprenetapopt-treated cells (**Figure 2F, S2L-N**). Meanwhile, eprenetapopt treatment also increased the proportion of incorporation into GSH breakdown intermediate, cysteinylglycine (**Figure 2F**). Furthermore, we found that eprenetapopt increased the proportion of unlabeled cystine in cells (**Figure 2F**). Given that these cells have been treated with isotopically labeled cystine, this unlabeled cystine is likely derived from the unlabeled cysteine released from degraded GSH (**Figure 2F**). This provides an alternative explanation for the increase in cystine we observed in our metabolomics study (**Figure 1H**). These data strongly indicate that eprenetapopt is not inhibiting *de novo* synthesis of GSH and instead is triggering the degradation of GSH**.** Together with our data that show mito-1C and *de novo* GSH synthesis deficiency drives increased sensitivity to eprenetapopt, this suggests that the capacity of cancer cells to regenerate *de novo* GSH from the available pool of GSH precursors, in particular cysteine and glycine, determines cancer cell sensitivity to eprenetapopt. This model is in keeping with our prior work, and confirmed by others (*11, 12, 26*), which demonstrated that inhibiting cystine uptake with erastin or sulfasalazine synergizes with eprenetapopt both *in vitro* and *in vivo*.

Eprenetapopt triggers ferroptosis

Ferroptosis is a form of non-apoptotic cell death characterized by the induction and accumulation of toxic lipid membrane peroxidation catalyzed by iron (*39*). Experimentally, the induction of ferroptosis is verified by the restoration of cell viability

by iron chelators and lipophilic antioxidants, and lack of cell death rescue by pan-caspase inhibitors. In our prior work, we showed that eprenetapopt induces lipid peroxidation following GSH depletion (*12*). However, we did not confirm that eprenetapopt induces ferroptosis as iron chelation failed to rescue cell viability following 96-hour co-treatment as determined by a resazurin-based assay, which measures the reducing capacity of cells as a surrogate for cell viability (*12*). Despite this, more recent investigation into the mechanisms of ferroptosis have highlighted that the use of metabolic based assays may obscure results. This is because ferroptosis induced by sustained cystine deprivation or erastin treatment perturbs cell proliferation beyond the induction lipid peroxidation (*40, 41*).

In order to account for these factors, we performed ferroptosis rescue experiments and utilized propidium iodide (PI) uptake to directly detect dead or irreversibly damaged cells. We found that eprenetapopt-induced cell death could be reversed by ferroptosis inhibitors (ferrostatin-1 (Fer-1): lipophilic antioxidant, and ciclopirox olamine (CPX): iron chelator), but not by the poly-caspase inhibitor, zVAD-FMK in both p53-null H1299 cells and mut-p53 expressing FLO-1 cells (**Figure 3A,B**). In contrast, zVAD-FMK blocked cell death induced by staurosporine (STS), which kills cells through the intrinsic (mitochondrial) pathway, but ferroptosis inhibitors did not (**Figure S3A**), suggesting that eprenetapopt does indeed induce ferroptosis. Furthermore, cells treated with eprenetapopt underwent catastrophic destabilization of their plasma membranes, without obvious visual evidence of nuclear fragmentation (**Movie S1**). Interestingly, ferroptosis inhibitors failed to restore cell proliferation of eprenetapopt treated cells (as assessed by confluency), which likely explains our previous results using resazurin-based assays (*12*) (**Figure 3A,B**). This suggests that eprenetapopt

perturbs cell proliferation beyond the induction of ferroptosis. However, N-acetyl-cysteine (NAC), a thiol group donor, rescued both the cell death and the proliferation defect induced by eprenetapopt (**Figure 3A,B**). This is consistent with previous studies noting that exogenously supplied thiols block eprenetapopt activity in cancer cells (*7, 11, 20, 42*). We also found that increasing the cell density completely blocked the induction of cell death by eprenetapopt (**Figure 3C**). This phenocopies previous reports of ferroptosis induced by cystine restriction and erastin being influenced by cell density (*43, 44*).

Given that previous studies reported that eprenetapopt induces apoptosis (*45-47*), we tested the effect of eprenetapopt in a cell line model incapable of undergoing apoptosis to rule out the dependency on apoptotic machinery for eprenetapopt induced cell death. To this end, we utilized MC38 mouse colon adenocarcinoma cells in which genes encoding the key mediators of apoptosis (Bax/Bak/Bid/Casp3/Casp7, **Figure 3D**) were all disrupted. As expected, STS failed to induce significant cell death in the apoptosis-resistant cells, however eprenetapopt was equally potent in killing both apoptosis-proficient and -resistant cells (**Figure 3E**). Altogether, these data demonstrate that eprenetapopt induces ferroptosis and does not require apoptotic machinery in order to elicit cell death. This is in keeping with recent findings suggesting that eprenetapopt induces ferroptosis in AML models (*26*).

Eprenetapopt inhibits NFS1 cysteine desulfurase activity

Next, we sought to explain the cell proliferation defect induced by eprenetapopt. Reflecting on recent reports suggesting that depletion of coenzyme A (CoA) contributes to the induction of ferroptosis by erastin (*48, 49*), we first referred to our

metabolomics dataset (**Figure 1H**), however we found no change to CoA in eprenetapopt-treated cells (**Figure S4A**). Our proteomics dataset indicated a possible role of iron and mitochondrial metabolism in eprenetapopt response, including upregulation of FDX1, a mitochondrial reductase involved in ISC biosynthesis (*28*) (**Figure 1I**). We hypothesized that eprenetapopt may be inhibiting mitochondrial ISC biogenesis, likely through binding to free cysteine and limiting the cysteine desulferase activity of NFS1. NFS1 harvests sulfur from cysteine for the biogenesis of ISCs (*50*), which are important co-factors for at least 48 enzymes required to support several cell essential functions, including DNA synthesis and mitochondrial respiration (electron transport chain and tricarboxylic acid cycle) (*51, 52*) (**Figure 4A**). Furthermore, the importance of NFS1 and ISC stability in regulation of cancer cell sensitivity to ferroptosis has also been demonstrated (*53, 54*). Supporting our hypothesis, the top compound in the CTRPv2 dataset that correlated to *NFS1* dependency was the eprenetapopt analogue, APR-017 (**Figure 4B**). Moreover, we observed synergy between eprenetapopt and elesclomol (**Figure 4C)**, where the latter has been shown to inhibit FDX1 (*55*). Eprenetapopt also reduced mitochondrial and cytosolic aconitase activity (**Figure 4D**), a surrogate marker for ISC stability (*56*).

Next, we utilized a cell-free NFS1 activity assay to demonstrate that the active agent of eprenetapopt, MQ, was able to inhibit the cysteine desulfurase activity of NFS1 in a dose dependent fashion (**Figure 4E**). Millimolar concentrations of MQ were required to inhibit NFS1 under these conditions in order to override the presence of 10 mM dithiothreitol (DTT) reducing agent in the reaction buffer to liberate hydrogen sulfide from the persulfide formed on NFS1 from cysteine. Therefore, we confirmed in an orthogonal fashion that MQ directly inhibits persulfide formation on NFS1 from

radioactive ^{35}S-cysteine **(Figure 4F)**. Importantly, in order to confirm that these effects of MQ on NFS1 extend to intact cells, we also demonstrated that MQ inhibits NFS1 cysteine desulfurase activity in HEK-293T (293T) cell lysates pre-treated with MQ **(Figure 4G)**. This corresponded with a decrease in aconitase activity in 293T cells (**Figure 4G**), without affecting the protein level of either mitochondrial aconitase or NFS1 (**Figure S4B**). Together, these results suggest that eprenetapopt through MQ inhibits the cysteine desulfurase activity of NFS1, likely through diminishing the availability of free cysteine by directly conjugating cysteine.

ISCs are sensitive to degradation under atmospheric oxygen conditions (standard tissue culture is 21% O_2) and thus cells require functional NFS1 to support ISC synthesis to maintain viability and proliferation (*53, 57*). Conversely, ISCs are stabilized under low oxygen conditions (3% O_2), which allows cells to proliferate in the absence of NFS1 (*53, 57*). Knowing this, we attempted to rescue the proliferation defect induced by eprenetapopt by culturing cells (with or without Fer-1) under low oxygen conditions, however we found that low oxygen failed to rescue the proliferation defect (**Figure S4B**). Interestingly, we found that low oxygen conditions alone did significantly decrease eprenetapopt induced cell death, presumably through stabilization of ISCs (**Figure S4B**). Furthermore, under these conditions, the addition of a CDK2 inhibitor, which was recently demonstrated to protect against the cell proliferation defect induced by suppression of the ISC-containing protein, DNA polymerase epsilon (POLE) (*57*), also failed to restore proliferation (**Figure S4B**). Altogether, these results demonstrate that eprenetapopt inhibits ISC biogenesis through inhibition of NFS1 cysteine desulfurase activity, which potentiates ferroptosis induced by eprenetapopt-mediated GSH depletion. It is likely that other essential

cellular functions requiring GSH as a co-factor explain the continued proliferation defect induced by eprenetapopt, even in the presence of Fer-1 and under low oxygen conditions (**Figure 4H**).

DISCUSSION

Whilst pre-clinical evidence demonstrated that eprenetapopt has p53-independent anticancer activity (*25, 26, 58*), the disappointing preliminary results from the phase III clinical trial investigating eprenetapopt in combination with azacitidine highlighted the need to reexamine the patient selection strategy for eprenetapopt (*6*). Here, using a multiomics, unbiased strategy, we determine the MoA of eprenetapopt as a GSH-depleting agent that triggers ferroptosis and inhibits the cysteine desulfurase activity of NFS1. Our work supports previous findings reporting that GSH depletion, and/or factors that regulate GSH availability, are central determinants of eprenetapopt activity in cancer cells (*9, 11, 12, 59, 60*). This is in keeping with previous unbiased investigation of the changes to the transcriptome in response to eprenetapopt treatment in cancer cells, which detected no changes to p53 target genes but upregulation of oxidative stress response genes, including *SLC7A11* (*25, 27*). Further, our findings are contrary to reports that conclude eprenetapopt induces apoptosis through mut-p53 reactivation (*61-63*) and instead supports eprenetapopt as a ferroptosis inducer (*26*). To stress this point, whilst previous reports have indicated that p53 activation may be involved in triggering ferroptosis in cancer cells (*64*), mut-p53 and p53-null cancer cells undergo ferroptosis in response to eprenetapopt treatment – demonstrating that p53 reactivation is dispensable for ferroptosis induced by eprenetapopt. As a result, our study reframes the potential clinical utility of eprenetapopt and provides three major insights.

First, as a ferroptosis inducer, eprenetapopt remains first-in-class. Whilst other clinical compounds including sorafenib (*65*), sulfasalazine (*39*), artemisinin (*66*), statins, as well as conventional chemotherapy, immune checkpoint inhibitors and radiotherapy

(*67*) have demonstrated capacity to induce or enhance sensitivity to ferroptosis, eprenetapopt is the first compound to reach a phase III clinical trial where triggering ferroptosis is central to its anticancer efficacy. Furthermore, eprenetapopt may be unique, triggering an increase in turnover of GSH, rather than restraining *de novo* GSH synthesis, as imposed by erastin though its inhibition of cystine uptake, or by L-buthionine sulfoximine through inhibition glutamate-cysteine ligase (*68*). Hematological and neurological toxicities, as well as impaired renal function have been reported in patients receiving eprenetapopt (*3, 4*), which is in line with reports demonstrating high sensitivity to ferroptosis amongst mesenchymal-derived tissues (*69-71*).

Second, patient selection for clinical trials and usage of eprenetapopt should not rely on *TP53* mutation. In the context of MDS, eprenetapopt is currently only indicated in ~7% of all MDS cases (*72*). However, dysregulated iron metabolism is a hallmark of a large subset of MDS with ringed sideroblasts (MDS-RS), characterized by aberrant iron accumulation in erythroblast mitochondria and accounting for ~30% of all MDS cases (*72, 73*). The importance of this point is highlighted by the fact that mutations driving aberrant iron accumulation in MDS-RS, such as *SF3B1* mutation, rarely co-occur with *TP53* mutations (*74*). The aberrant iron accumulation in MDS-RS likely increases erythroblast sensitivity to ferroptosis. Therefore, restricting eprenetapopt to *TP53*-mutated MDS patients, whilst being an area of unmet therapeutic need, may be obscuring the therapeutic benefit eprenetapopt could provide to a wider range of MDS patients, especially MDS-RS. As a result, reclassifying eprenetapopt as a ferroptosis inducer and not as a mut-p53 reactivator, recontextualizes the results from the phase III clinical trial to potentially be an example of poor patient selection rather than an

indication of failure of eprenetapopt as an anticancer therapy. Both phase II clinical trials demonstrated that patients who responded to eprenetapopt and azacitidine had significantly improved overall survival compared to non-responders (*3, 4*) – further highlighting the importance of patient selection.

Third, combining eprenetapopt with other agents or strategies that target cancer cell nutrient availability could provide stronger clinical efficacy. Pre-clinical evidence continues to grow, supporting the notion that dietary manipulation, including SG restriction, could be a powerful adjunct to conventional therapeutic approaches (*75*). To date, no attempts to test the safety or efficacy of SG restriction in patients with cancer have been undertaken. Here, we show that priming tumours with SG restriction improves the efficacy of eprenetapopt in esophageal cancer models. A very recent study also demonstrated synergy between eprenetapopt and asparaginase (an enzyme that degrades asparagine) in acute lymphoblastic leukemia cell lines (*76*), which could hint that GSH depletion by eprenetapopt more generally increases cancer cell dependency on exogenous amino acid uptake. Furthermore, the combination of venetoclax (BCL-2 inhibitor) and azacitidine has been shown to target mitochondrial metabolism through inhibition of the glutathionylation of complex II of the electron transport chain (*77*), and also diminishes the uptake of global amino acids in primary patient AML stem cells (*78*). Moreover, depleting GSH through exogenous cyst(e)ine degradation with cyst(e)inase demonstrated a similar MoA in AML stem cells (*79*). Together with our study, these studies provide a strong rationale for the combination of eprenetapopt, venetoclax and azacitidine, which is currently under clinical investigation in a phase I/II study in myeloid malignancies (*80*). Preliminary results from this phase I/II clinical trial report that the study successfully reached its primary

endpoint with a CR rate of 37% and found that the triple combination of eprenetapopt, venetoclax and azacitidine was well tolerated in patients (*81*). Further study should be undertaken to determine whether the response to the triple combination of eprenetapopt, venetoclax and azacitidine could be improved with SG dietary restriction.

In summary, our study demonstrates that eprenetapopt targets cancer cells through GSH depletion and inhibiting cysteine desulfurase activity of NFS1, leading to iron-dependent, non-apoptotic ferroptosis. This work not only details novel determinants of eprenetapopt activity in cancer cells, including mito-1C metabolism enzymes, but also provides a clinical roadmap for targeting antioxidant pathways in tumours with eprenetapopt – beyond *TP53*-mutant tumours.

MATERIALS AND METHODS

Compounds and reagents

Eprenetapopt was provided by Aprea Therapeutics Inc. (Boston, Massachusetts, USA). Elesclomol, erastin, staurosporine (STS) and SNS-032 were from Selleckchem (Houston, Texas, USA). 2-methylene 3-quinuclidinone (MQ), sodium formate, glycine, serine, N-acetyl-cysteine (NAC), ferrostatin-1 (Fer-1), zVAD-FMK and ciclopirox olamine (CPX) were from Sigma Aldrich (St. Louis, Missouri, USA).

Cell cultures

NCI-H1299 (H1299) (RRID:CVCL_0060), OACM5.1 (RRID:CVCL_1842), FLO-1 (RRID:CVCL_2045), and HEK-293T (293T) (RRID:CVCL_0063) were from ATCC. K562 (RRID:CVCL_0002) were provided by Prof Ricky Johnstone (Peter MacCallum Cancer Centre; PMCC). All cells were maintained at 37˚C with 5% CO_2 and their identities were authenticated by short tandem repeat analysis using the PowerPlex 16 genotyping system (Promega) and confirmed mycoplasma free by PCR every two months (Cerberus Sciences). Cells were thawed from early passage stocks and passaged for no more than 4 months. Unless otherwise specified, all culture media contained 10% fetal bovine serum (FBS) supplemented with 50 U ml^{-1} penicillin and 50 mg ml^{-1} streptomycin (Life Technologies). MC38, FLO-1 and HEK-239T cells were grown in DMEM containing 2.5 mM L-glutamine and 4.5 g l^{-1} D-glucose (Life Technologies). MC38 cells were maintained in 10% CO2. H1299, OACM5.1 and K562 were grown in RPMI 1640 medium containing 2.5 mM $_L$-glutamine. K562 were supplemented with 1× GlutaMAX (Life Technologies).

CRISPR screening

OACM5.1 cells were engineered to express the Cas9 endonuclease by transduction with the FUCas9Cherry vector (Addgene, #70182) and subsequent selection for mCherry-positive cells, or Cas9 endonuclease dead (dCas9) by transduction with the dCas9-VP64_Blast vector (Addgene, #61425) and subsequent selection for blasticidin resistance (10 μg/mL). For genome-wide CRISPR knockout (CRISPRko) and CRISPR activation (CRISPRa) screening, OACM5.1 cells expressing Cas9 or dCas9-VP64 were transduced with a genome-wide sgRNA Brunello (76,441 sgRNAs, Addgene, #73178 (*17*)) or Calabrese (56,762 sgRNAs, Addgene, #92379 (*18*)) library, respectively, at a MOI of 0.3, aiming for 500-fold starting representation of each guide. Puromycin selection (1 μg/mL) was applied for 7 days and surviving cells were subsequently split into relevant treatment conditions (CRISPRko: vehicle v 10 μM eprenetapopt; CRISPRa: vehicle v 15 μM eprenetapopt, see **Figure S1** for effect of eprenetapopt on cell number). Cells were passaged every four days in T175 flasks with 2×10^6 cells per flask for a total of 8 days for the CRISPRko screen and 28 days for the CRISPRa screen. Genomic DNA was extracted using the DNeasy Blood and Tissue Kit (Qiagen) and sequencing libraries were generated by PCR as previously detailed (*82*). The libraries were sequenced on a NextSeq 500 (Illumina) to generate 75 base pair single-end reads, which were demultiplexed with Bcl2fastq (v2.17.1.14). The sequencing reads were subsequently trimmed with Cutadapt (v1.7) to remove sgRNA vector derived sequences, then sgRNA reads were counted and the distribution analyzed using MAGeCK (v0.5.8) using read depth (--norm-method total) normalization. MAGeCK score was determined by $-\log_{10}$(neg *P*-value) + $\log_{10}$(pos *P*-value) and datasets were visualized on GraphPad Prism (v9.0). Validation experiments were performed on polyclonal OACM5.1 cells expressing individual sgRNAs (**Table S1**) following selection with puromycin. Formate and glycine rescue

experiments were performed under conditions matching the CRISPR screening procedure scaled down to T25 flask. SG auxotrophy experiments were performed in 96-well plates utilizing dialyzed FBS and media reconstituted without SG.

DepMap Analysis

Cancer cell line gene dependency data (DepMap Public 21Q1 Release) and APR-017 cancer cell line sensitivity data (CTRPv2.0) were obtained from the DepMap web-portal (www.depmap.org) and correlation analyses were performed in RStudio (v1.1.4) using the *cor.test* function. Correlation strengths were determined by adjusting the Pearson correlations with a Fisher's z-transformation in order to account for the differences in cell lines analyzed.

Metabolomics profiling

OACM5.1 cells (3.3×10^5) were plated in 6-well plates and allowed to adhere for 24 h and subsequently treated with vehicle or 50 μM eprenetapopt for 12 h in fresh media (6 replicates per condition). Media was aspirated and cells washed with water (at 37°C) for 10 sec then snap-frozen by the addition of liquid nitrogen directly to tissue culture plates. Metabolite extraction was performed with ice-cold methanol/chloroform (9:1, v/v) solvent containing ^{13}C-sorbitol, ^{13}C,^{15}N-valine, ^{13}C,^{15}N-AMP, ^{13}C,^{15}N-UMP as internal standards. Metabolite-containing supernatants were collected following centrifugation at 16,000g for 5 min to pellet insoluble material and debris.

Metabolite analysis was performed using an Agilent 6520 series quadrupole time-of-flight mass spectrometer (QTOF MS) (Agilent Technologies) with chromatographic separation on an Agilent 1200 series HPLC system (Agilent Technologies). Metabolite

separation was performed on a Merck SeQuant ZIC®-HILIC column (150 mm × 2.1 mm, 5 µm particle size) using Solvent A: 20 mM ammonium carbonate (pH 9.0; Sigma-Aldrich) and Solvent B: 100 % acetonitrile. The gradients used were as follows: negative mode – time = 0 min, 90% B; t = 0.5 min, 90% B; t= 12 min, 40 % B; t= 14 min, 40 % B; t = 15 min, 5%, t = 18 min, 5 % B; t =19 min, 90 %. Samples were stored in the autosampler at 4ºC and 7 µl injected onto the column, which was maintained at 40ºC, with a solvent flow rate of 250 µl/min.

Mass spectrometry analysis was performed on an Agilent 6545 series quadrupole time-of-flight mass spectrometer (QTOF MS) (Agilent Technologies) as described previously (*83*). Negative mode LCMS data was collected in centroid mode with a scan range of 50-1700 m/z and an acquisition rate of 1.2 spectra/sec. Samples were analyzed in the same analytical batch and randomized with a QC every 5 samples. Thirteen mixtures of authentic standards (550 metabolites) were also run to generate the library for targeted analysis. Level 1 Metabolite identification (according to the Metabolite Standard Initiative (*84*)) was based on matching accurate mass, retention time and MS/MS spectra to the 550 authentic standards in the MA in-house library. Metabolite abundance based on area under the curve (AUC) were obtained using Agilent Masshunter Quantitative Analysis B 0.7.00. Statistical analysis was performed applying the web-based platform MetaboAnalyst applying no missing value imputation, normalization to median peak area and no scaling or transformation (*85*).

For isotopic tracing analysis, OACM5.1 cells were prepared in the same fashion as steady state experiments, however cells were cultured in cystine-free RPMI-1640 media (Sigma Aldrich) with 10% dialyzed FBS supplemented with 208 µM L-[3',3'-

$^{13}C_2$]-cystine or L-^{12}C-cystine (3 replicates per condition). For enhanced resolution, identification and detection of the isotopic species metabolite analysis was performed on a Vanquish™ Horizon UHPLC System, integrated biocompatible system coupled to Thermo Scientific Orbitrap ID-X Tribrid mass spectrometer (MS) (ThermoFisher Scientific, San Jose). The polar metabolite chromatographic separation was performed on the Metabolomics Australia Merck SeQuant ZIC®-HILIC column (150 mm × 4.6 mm, 5 µm particle size) method previously with modifications.

In short, the mobile phase of A: 20 mM ammonium carbonate (pH 9.0; Sigma-Aldrich) and B: 100 % acetonitrile was run at a flow rate of 300 µl/min with the following gradient: time = 0.0 min, 80% B; t = 0.5 min, 80% B; t= 15.5 min, 50 % B; t= 17.5 min, 30 % B; t = 18.5 min, 5%, t = 21.0 min, 5 % B; t =28 min, 80 %. Samples were stored in the autosampler at 4ºC and 7 µl injected onto the column maintained at 30ºC. Full scan (MSn = 1) Orbitrap ID-X data was acquired in positive and negative ionization modes separately within the mass range of 70–1300 m/z at resolution 240,000. Ion source parameters were set as follows: Sheath gas = 40 arbitrary units, Aux gas = 10 arbitrary units, Sweep gas = 1 arbitrary unit, Spray Voltage = 3.5kV (positive ion)/ 3.2kV (negative ion), Capillary temp. = 300 °C, and Vaporizer temp = 400 °C. Metabolite and isotope abundance are based on area under the curve (AUC) deconvoluted from the labeling data using the ‘detect and analyze labeled compounds’ module and in-house mass list matching in Compound Discoverer 3.2. A 3 ppm mass error and a retention time range of 0.3 s in feature grouping and molecular formula and metabolite matching was applied. All molecules were annotated according to guidelines for reporting of chemical analysis results as proposed in Metabolomics Standards Initiative level 1 (*84*).

Quantitative proteomics

OACM5.1 cells (5.0×10^6) were plated in 15 cm plates and allowed to adhere for 24h and subsequently treated with vehicle or 50 μM eprenetapopt for 12 h in fresh media (4 replicates per condition). Media was aspirated then cells washed with ice-cold PBS and lysed at 4˚C in RIPA buffer (1 mM EDTA, 1% NP-40, 0.5% sodium deoxycholate, 0.1% SDS, 50 mM sodium fluoride, 1 mM sodium pyrophosphate in PBS) mixed with protease and phosphatase inhibitors (Roche). Debris was pelleted by centrifugation at 11,000g for 10 min. Overnight acetone precipitation of proteins was performed at -20˚C to purify the samples. Proteins were resuspended in 8 M urea in 50 mM triethylammonium bicarbonate (pH 8), reduced with 10 mM Tris(2-carboxyethy)phosphine (TCEP, Sigma Aldrich), alkylated with 55 mM iodoacetamide (IAA, Sigma Aldrich) and subjected to tryptic digest with Pierce Trypsin Protease MS-Grade (ThermoFisher Scientific) overnight at 37˚C (1:50 trypsin to protein). Formic acid (1% v/v) was added to acidify the solution before loading onto Oasis cartridges (Waters). Peptides were eluted in 80% (v/v) acetonitrile, 0.1% (v/v) trifluoroacetic acid, freeze dried and stored at -80˚C until analyzed by liquid chromatography tandem mass spectrometry (LC-MS/MS).

LC-MS/MS was carried out on a QExactive plus Orbitrap mass spectrometer (ThermoFisher Scientific) with a nanoESI interface in conjunction with an Ultimate 3000 RSLC nanoHPLC (Dionex Ultimate 3000). The LC system was equipped with an Acclaim Pepmap nano-trap column (Dinoex-C18, 100 Å, 75 μm x 2 cm) and an Acclaim Pepmap RSLC analytical column (Dinoex-C18, 100 Å, 75 μm x 50 cm). The tryptic peptides were injected to the enrichment column at an isocratic flow of 5 μL/min

of 2% v/v CH3CN containing 0.1% v/v formic acid for 5 min applied before the enrichment column was switched in-line with the analytical column. The eluents were 5% DMSO in 0.1% v/v formic acid (solvent A) and 5% DMSO in 100% v/v CH3CN and 0.1% v/v formic acid (solvent B). The flow gradient was (i) 0-6min at 3% solvent B, (ii) 6-95 min, 3-22% solvent B (iii) 95-105 min 22-40% solvent B (iv) 105-110 min, 40-80% solvent B (v) 110-115 min, 80-80% solvent B (vi) 115-117 min, 80-3% and equilibrated at 3% solvent B for 10 min before the next sample injection. The QExactive plus mass spectrometer was operated in the data-dependent mode, whereby full MS1 spectra were acquired in positive mode, 70 000 resolution, automatic target control target of 3×10^6 and maximum injection time of 50 ms. Fifteen of the most intense peptide ions with charge states ≥2 and intensity threshold of 1.7×10^4 were isolated for MSMS. The isolation window was set at 1.2 m/z and precursors fragmented using normalized collision energy of 30, 17 500 resolution, automatic target control target of 1×10^5 and maximum injection time of 100 ms. Dynamic exclusion was set to be 30 sec.

Xenograft models and treatments

All animal experiments were approved by the PMCC Animal Experimentation Ethics Committee and undertaken in accordance with the National Health and Medical Research Council Australian Code of Practise for the Care and Use of Animals for Scientific Purposes. For FLO-1 LM cell line xenografts (*38*), 5×10^6 cells suspended in 100 µL of 1:1 PBS and Matrigel (BD Bioscience) were subcutaneously injected into the right flank of ~6 week-old female NOD-SCID IL-2Rγ^{KO} (NSG) mice. Patient-derived xenografts (PDX) were established and implanted into a dorsal intramuscular pocket of NSG mice as previously described (*86*). Mice were randomized to serine/glycine (SG)-deplete or control chow *ad libitum* (AIN93G rodent diet, Specialty Feeds,

Australia) and dosed with 100 mg/kg eprenetapopt or 0.9% saline, intraperitoneally injected daily, once tumours reached 100 mm^3. Tumour volume was assessed blinded to treatment group with caliper measurements every 3-4 days and calculated using the formula (length $\times$ $weight^2$)/2. Metastatic spread was determined by bioluminescence imaging as previously described (*38*) involving weekly monitoring using a Xenogen IVIS 100 Imaging System (Caliper Life Science). At experimental endpoint (tumour volume > 1400 mm^3), the whole mouse and its organs were imaged to determine the extent and distribution of metastases. Tumours were weighed and tumour growth inhibition was calculated with the formula [1-(Tf-Ti)/mean(Cf-Ci)] $\times$ 100, where Tf, Ti and Cf, Ci represents final (f) and initial (i) tumour volume of drug treated (T) and control (C) animals respectively.

Cell death

For ferroptosis rescue experiments, cells were co-treated with rescue compounds (Fer-1, CPX, zVAD-FMK, NAC) in media containing 5 μg/mL propidium iodine (PI) in 96-well plates (FLO-1: 5,000 cells/well, H1299: 3,000 cells/well). Cell death and confluency were quantified utilizing an IncuCyte FLR (Essen BioSciences) imaging phase and red channels. Percent (%) cell death was determined by dividing the % red confluency by the % phase confluency. Note, 100% cell death was ascribed if % red confluency was greater than phase confluency.

Cell viability

For dose-response assays, 10-point log_2 serial dilutions of eprenetapopt were added to 96-well plates containing cells (OACM5.1: 10,000 cells/well, Mc38: 10,000 cells/well, K562: 5,000). After 72 h incubation, cell viability was determined using

AlamarBlue reagent (Life Technologies) and fluorescence was read at 550 nm/590 nm on a Cytation 3 Imaging Reader (BioTek).

Immunoblot

As per established protocols (*12, 87*), cells were lysed at 4˚C in RIPA buffer (1 mM EDTA, 1% NP-40, 0.5% sodium deoxycholate, 0.1% SDS, 50 mM sodium fluoride, 1 mM sodium pyrophosphate in PBS) mixed with protease and phosphatase inhibitors (Roche). Equal amounts of protein were boiled, resolved by SDS-PAGE and transferred to PVDF membranes. For total protein glutathionylation detection, lysates were not boiled and were resolved under non-reducing conditions. Membranes were incubated in blocking buffer (5% skim milk in 0.05% TBS-T) for 1 h at room temperature and probed overnight in primary antibody at 4˚C. Blots were washed thrice in 0.05% TBS-T, followed by incubation with peroxidase-conjugated secondary antibody (Dako) for 1 h at room temperature. Protein levels were detected using Amersham ECL Western Blotting Detection reagents (GE Life Sciences) or ECL Plus Western blotting substrate kit (ThermoFisher Scientific). Antibodies are detailed in **Table S2.**

NFS1 activity assays

NFS1 cell-free and in cell assays were performed as previously described (*88*). Briefly, for cell-free L-cysteine inhibition assay with MQ, a constant concentration of purified NFS1 (2 μM) was added to varying concentrations of MQ (0-2000 μM) and reaction buffer in a total volume of 1 ml. The reactions were started with varying concentrations of L-cysteine and incubated for 1 h. L-cysteine desulfurase activity was followed by

methylene blue assay as described below. Expression and purification of NFS1 are detailed in the supplemental material and methods.

Measurement of free H_2S via methylene blue

The methylene blue formation assay was performed as adapted (Fogo *et al* ., 2010). Reaction was carried out in a total volume of 400 µl containing buffer (10 mM DTT, 10 µM PLP and 2.5 mg cell lysate). The reaction was started with substrate and incubated for 1 hour at 37 °C. The reaction was stopped by simultaneous addition of 20 mM N, N- Dimethyl-4-phenylendiamin-hydrochloride (DMPD) and 30 mM Iron (III)-chloride. The resulting solution was incubated further for 20 minutes for color development and subsequently spun at 13,000 g for 5 minutes. The absorbance at the absorbance was at 670 nm using Varioskan flash (ThermoFisher Scientific, Germany).

Inhibition of persulfide formation on L-cysteine desulfurase

Purified NFS1/ISD11 was radiolabeled with 35S-cysteine for persulfide formation as adapted from (*89*). Briefly, 2 µM of NFS1 were incubated with varying concentrations of MQ in reaction buffer containing 50 mM Tris 200 mM NaCl and 150 mM NaCl in a total volume of 35 µL. The reaction was started with 10 µCi 35S-cysteine (1075 Ci/mmol) and incubated 30 °C for 1 hour. Resulting solutions were mixed with SDS loading buffer without boiling and separated on a 12% SDS-PAGE. Proteins were analyzed by autoradiography.

In-gel aconitase assay and aconitase activity assay

OACM5.1 cells (5.0×10^6) were plated in 15 cm plates and allowed to adhere for 24h and subsequently treated with 50 µM eprenetapopt for 0, 6, 12 and 24 h in fresh media.

Cells were collected and resuspended in lysis buffer containing 1% Triton-X 100 and protein content was determined. As previously described (*56*), aconitase activity gels were composed of a separating gel containing 8% acrylamide, 132 mM Tris base, 132 mM borate, 3.6 mM citrate, and a stacking gel containing 4% acrylamide, 67 mM Tris base, 67 mM borate, 3.6 mM citrate. The running buffer contained 25 mM Tris pH 8.3, 192 mM glycine, and 3.6 mM citrate. Samples contain cell lysates of equal protein content (~100 μg), 25 mM Tris-Cl, pH 8.0, 10% glycerol, and 0.025% bromophenol blue. Electrophoresis was carried out at 170 V at 4ºC. Aconitase activities were assayed by incubating the gel in the dark at 37ºC for 45 mins in 100 mM Tris (pH 8.0), 1 mM NADP, 2.5 mM cis-aconitic acid, 5 mM $MgCl_2$, 1.2 mM MTT, 0.3 mM phenazine methosulfate, and 5 U/ml isocitrate dehydrogenase (all from Sigma-Aldrich). Gels were imaged on a BioRad ChemiDoc, then stained with Coomassie to verify equal protein loading, and imaged again.

For 293T cells, the activity measurement of aconitase was adapted from (*90*). Three T-75 cm^3 flasks per cell lines were seeded and allowed to grow to 90% confluency before collection. 50 μl cell lysates were incubated with 250 μl R1 buffer (50 mM Tris-HCl, 50 mM NaCl, 5 mM $MgCl_2$, 0.5 mM $NADP^+$, 0.01 U Isocitrate dehydrogenase pH 8) for 5 mins at 37 ºC. 200 μl of R2 buffer (50 mM Tris-HCl, 50 mM NaCl, 5 mM $MgCl_2$, 2.5 mM cis-aconitate pH 8) was added to start the reaction which was monitored for 3 minutes at 340 nm using Shimadzu UV-Vis Spectrophotometer UV-2600 manufactured in Japan.

Generating apoptosis-resistant MC38 cells

Gene disruption was carried out using CRISPR/Cas 9 technology. 150 pmol of each synthetic gRNA (2 gRNAs per gene) specifically targeting BAX, BAK1, BID, CASP3 or CASP7 (**Table S3**, Synthego) in a volume of 0.5 μl were pooled in a final volume of 5 μl. 200 pmol Alt-R S.p. HiFi Cas9 Nuclease in 2 μl volume (Integrated DNA Technologies) was then added, mixed and incubated at room temperature for 10 minutes to allow formation of Cas9/gRNA complexes. Meanwhile, 3×10^5 MC38 cells for each experimental condition (harvested at 40% confluency, sub-cultured two days prior) were washed ×3 in room temperature PBS, followed by re-suspension in 20 μl of Amaxa Buffer SF. Re-suspended cells were then mixed with Cas9/gRNA complexes, transferred to a 16 well electroporation stripette (Amaxa 4D, Lonza) and electroporated using program CM-130. Immediately after electroporation, 150 μl of pre-warmed media (DMEM, 10% FBS, Pen/Strep) was added to each well and allowed to recover in an incubator for 15 mins. Cells were then transferred to 6 well plates. After at least 5 days, the effect of gene disruption on protein levels was evaluated by western blot.

Statistical analysis and replication

Data are presented as mean ± SEM and analyzed by Student's *t*-test unless otherwise indicated. GI50 dose of single agents was determined by fitting the Hill equation. Statistical analyses and data presentation were performed using Prism 9 (GraphPad). No power analyses were performed to determine sample size prior to experimentation. Blinding was undertaken during *in vivo* experiments.

ACKNOWLEDGEMENTS

We thank Aprea Therapeutics for providing the eprenetapopt used in this study. The diagrams in Figure 2A and 4F were created using www.Biorender.com.

Funding Statement: This work was supported by a National Health and Medical Research Council (NHMRC) Project Grant (APP1120293 to W.A.P., N.J.C.). N.J.C. is supported by a Fellowship (MCRF16002) from the Department of Health and Human Services acting through the Victorian Cancer Agency Fellowship. K.M.F. and T.D.J. are supported by an Australian Research Training Program (RTP) Scholarships. C.S.C is the recipient of, and supported by, The Alan & Kate Gibson Research Fellowship, 2018. The Victorian Centre for Functional Genomics (K.J.S.) is funded by the Australian Cancer Research Foundation (ACRF), Phenomics Australia (PA) through funding from the Australian Government's National Collaborative Research Infrastructure Strategy (NCRIS) program, the Peter MacCallum Cancer Centre Foundation and the University of Melbourne Research Collaborative Infrastructure Program (MCRIP).

Competing Interests: DAS receives research support from Aprea Therapeutics via financial support to the H. Lee Moffitt Cancer Center and Research Institute. All other authors declare that they have no competing interests.

Author contributions: Conception and design of the work (KMF, NJC, WAP, SH, IN, KJS); Data acquisition or contribution (KMF, BZZ, MOO, BN, DAS, C-SA, CSC, CJK, VRS, SW, ATF); Data analysis or interpretation (KMF, TDJ, BN, SJH, VRS, JAT, DS,

SL, SH, WAP, NJC); Supervision (SL, DS, NJC, WAP, SH); Manuscript drafting and editing (KMF, NJC, WAP, SH); All authors approved the final manuscript.

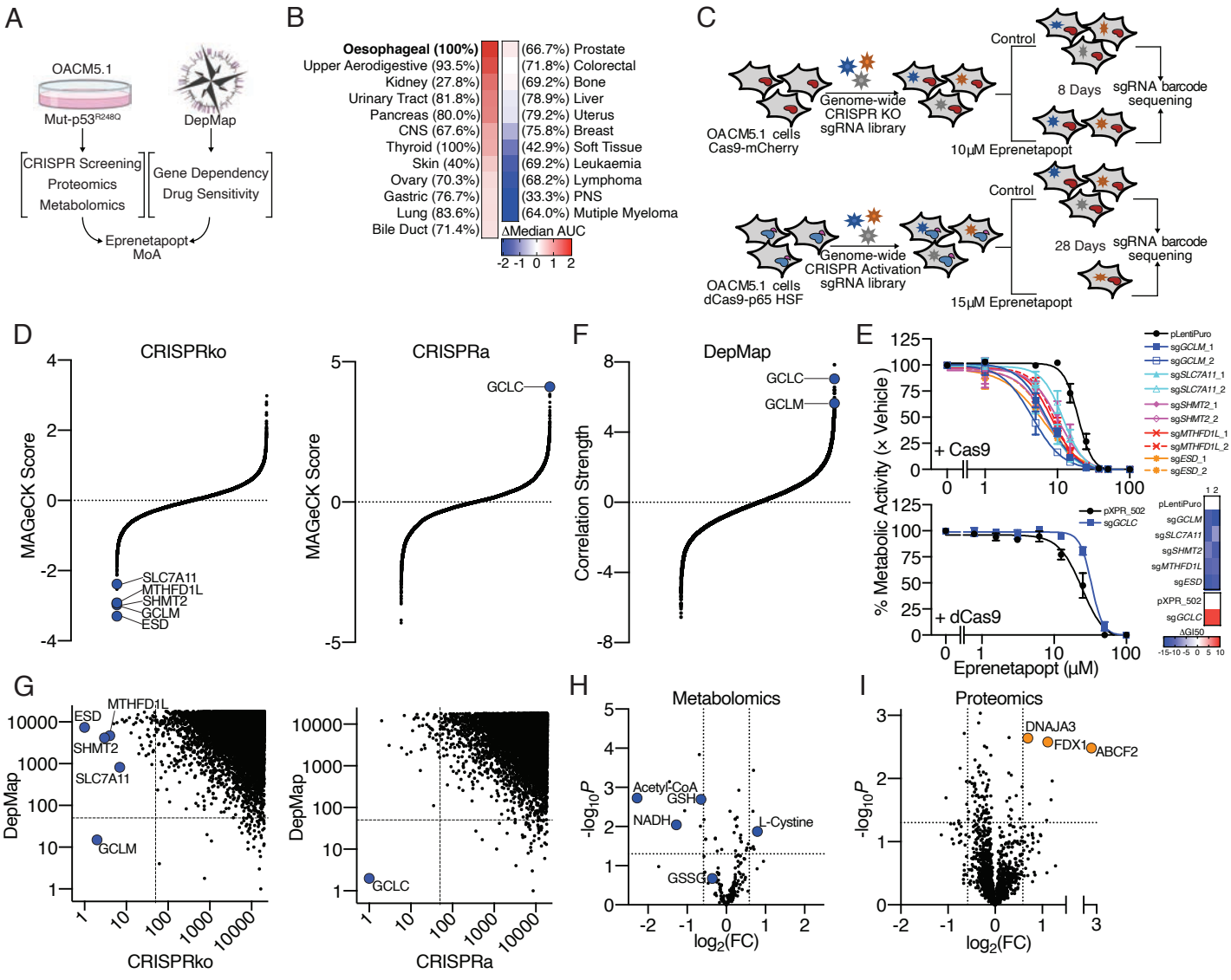

Figure 1 Multiomics strategy to determine the mechanism of action of eprenetapopt

(A) Schematic diagram showing a strategy to determine the MoA of eprenetapopt. **(B)** Heatmap of sensitivity to eprenetapopt analogue (APR-017). Cancer lineages are ordered by sensitivity determined by delta-median, area-under-the-curve (AUC) of compound activity. Percentages denote the frequency of *TP53* mutations in each lineage. **(C)** Schematic showing the workflow for the CRISPRko and CRISPRa screens in OACM5.1 cells. **(D)** MAGeCK scores (negative indicating 'dropout' and positive indicating 'enrichment') from CRISPR screens, plotted in order of magnitude. **(E)** Cellular metabolic activity measured by AlamarBlue as a surrogate readout for cell viability following 72 h exposure with eprenetapopt at indicated doses in cells transduced with individual sgRNA targeting identified hits. Heatmap represents the change in GI50 (dose where 50% growth inhibition is achieved) relative to control. **(F)** Fischer's transformed z-scored Pearson correlation strength of gene dependency from the DepMap database with eprenetapopt analogue (APR-017) sensitivity data from CTRPv2, plotted in order of magnitude. **(G)** Comparison of CRISPR screens and

DepMap gene dependency data show overlay of glutamate-cysteine ligase units (GCLC and GCLM). Plot is representing the rank of top hits (ordered by “drop-out” in CRISPRko, by “enrichment” in CRISPRa, by positive correlations in DepMap). Dotted lines indicate overlap of top 50 ranked genes. **(H)** Changes in polar metabolites determined by untargeted LC-MS metabolomics and **(I)** proteins determined by label-free quantitative proteomics in OACM5.1 cells following treatment with 50 μM eprenetapopt for 12 h compared to vehicle. Dotted lines indicate significance cut-offs ($P < 0.05$, $|\log_2(\text{Fold change, FC})| > 0.5$. Two-tailed unpaired t-test **(H,I)**. Error bars = SEM. **(D)** *N*=2 for CRISPRko, *N=1* for CRISPRa, **(E)** *N*=3-4, **(H)** *N*=6, **(I)** *N*=4. *See also Fig. S1.*

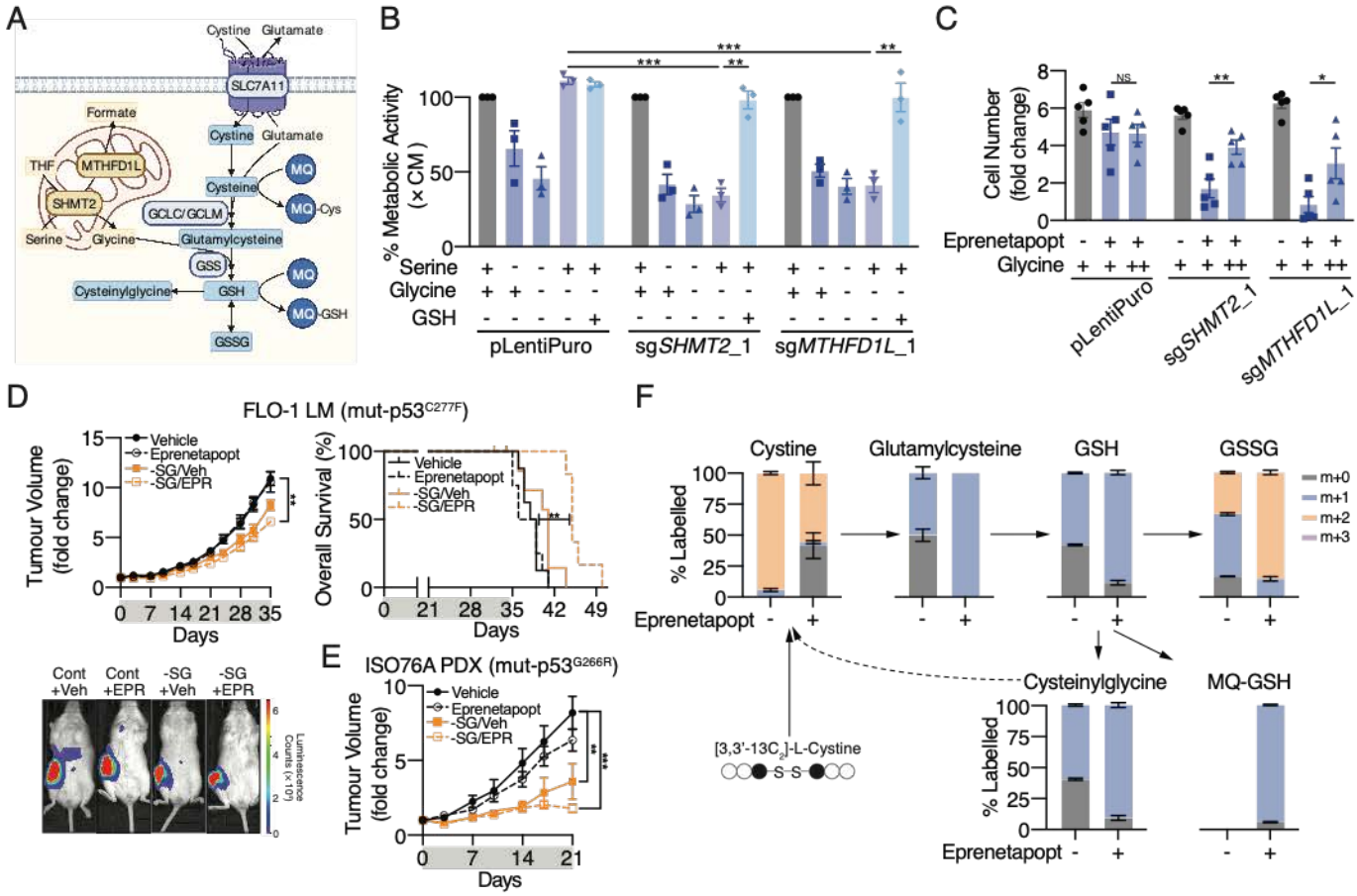

Figure 2 Eprenetapopt and mitochondrial one-carbon metabolism

(A) Schematic diagram illustrating the connections between *de novo* GSH synthesis and mito-1C metabolism. (THF, tetrahydrofolate; GSH, reduced GSH; GSSG, oxidized GSH; MQ-Cys, MQ-conjugated cysteine; MQ-GSH; MQ-conjugated GSH). **(B)** Cellular metabolic activity measured by AlamarBlue as a surrogate readout for cell viability compared to complete media (CM) following 72 h of serine, glycine or serine and glycine deprivation, and glycine deprivation rescued with 1 mM GSH-monoethyl ester (GSH) in OACM5.1 cells. **(C)** Relative cell number following treatment with 10 μM eprenetapopt ± 1 mM glycine supplementation for 4 days. + indicates glycine in RPMI media, ++ indicates supplementation with additional 1 mM glycine. **(D)** Top: Growth curves and overall survival (time to reach tumour volume ≥1400mm^3) of NSG mice inoculated with FLO-1 LM tumours treated with eprenetapopt (EPR, 100 mg/kg, daily) or vehicle on either normal or serine and glycine (SG)-free diets for 35 days. Bottom: Representative bioluminescence images illustrating the metastatic burden in mice after 35 days of treatment. **(E)** Growth curves of esophageal adenocarcinoma patient-derived xenografts (PDX) in NSG mice treated with eprenetapopt (EPR, 100 mg/kg, daily) or vehicle on either normal, or SG-free diet for 21 days. **(F)** Fractional labeling of *de novo* GSH synthesis intermediates from $^{13}C_2$-cystine following 12 h exposure to 50 μM eprenetapopt compared to vehicle in OACM5.1 cells. Two-tailed t-test **(B, C)**, one-way ANOVA with Tukey's multiple comparisons test **(D, E)**, log-rank (Mantel-Cox) test **(D)**. * $P < 0.05$, ** $P < 0.01$, *** $P < 0.001$. Error bars = SEM. **(A)** N=1, **(B, F)** N=3, **(C)** N=5. **(D)** N=8, **(E)** N=4-5. *See also Fig. S2.*

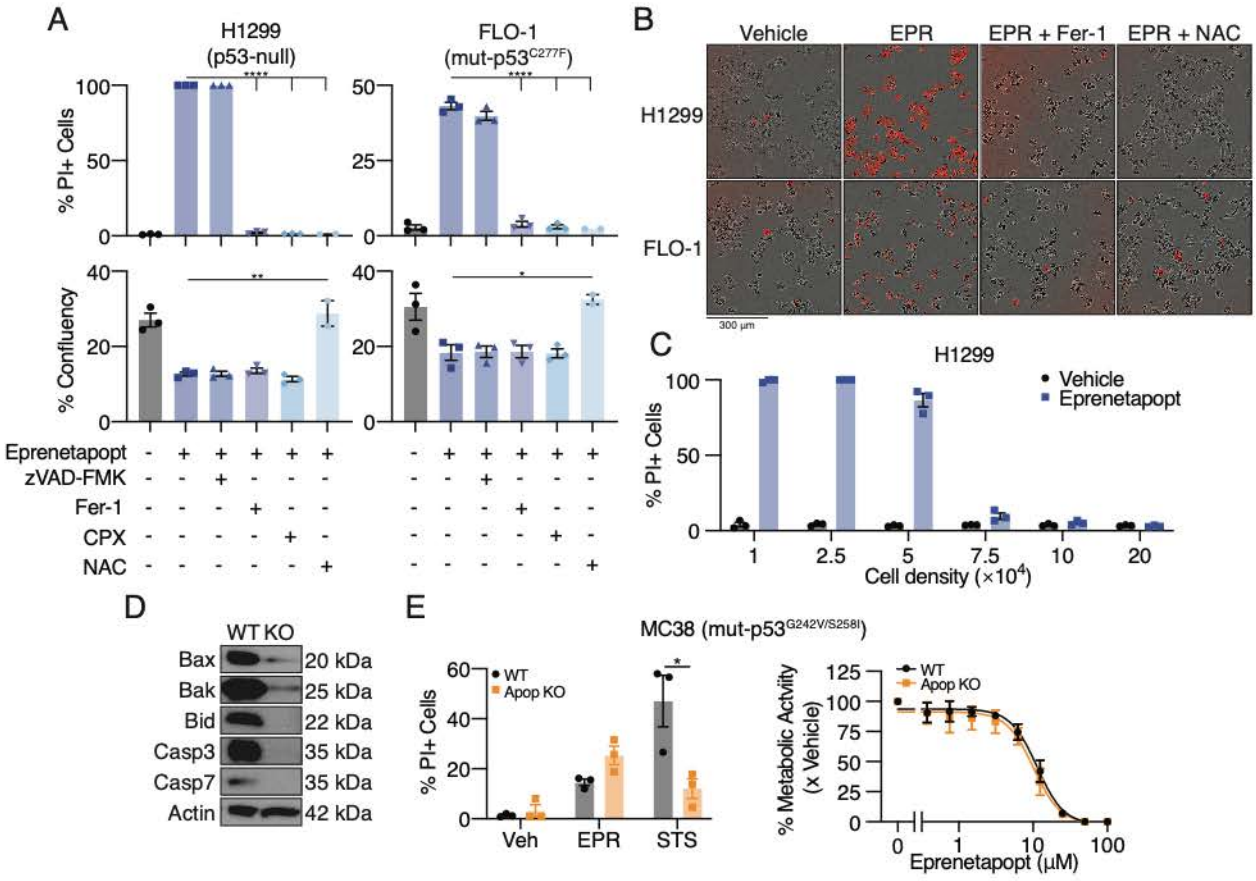

Figure 3 Eprenetapopt triggers ferroptosis

(A) Percentage (%) dead cells (as determined by % propidium iodide positive (PI+) cells) and % cell confluency following treatment for 24 h with 50 µM eprenetapopt with or without 50 µM zVAD-FMK (pan-caspase inhibitor), 12.5 µM Ferrostain-1 (Fer-1, lipophilic antioxidant), 6.25 µM ciclopirox olamine (CPX, iron chelator) or 2.5 mM N-acetyl-cysteine (NAC, cysteine supplement) in H1299 (left) and FLO-1 cells (right). **(B)** Representative merged phase and red channel images of results from **(A)** acquired on Incucyte. **(C)** % cell death determined by propidium iodide uptake following 24 h treatment with 50 µM eprenetapopt in H1299 cells at indicated cell densities. **(D)** Immunoblot of Bax, Bak, Bid, Casp3 and Casp7 illustrating the efficiency of CRISPR editing in MC38 cells. **(E)** Left: Cell death in MC38 wild-type (WT) and apoptosis-deficient (Apop KO) cells following 24 h treatment with 50 µM eprenetapopt or 12.5 µM staurosporine (STS). Right: Cellular metabolic activity measured by AlamarBlue as a surrogate readout for cell viability following 72 h exposure with eprenetapopt at indicated doses in WT and Apop KO MC38 cells. Two-way t-test **(A,E)**. * $P < 0.05$, ** $P < 0.01$, **** $P < 0.0001$ **(A)** N=2-3, **(D)** N=2, representative blots shown, **(E)** N=3. *See also Fig. S3 and Movie S1.*

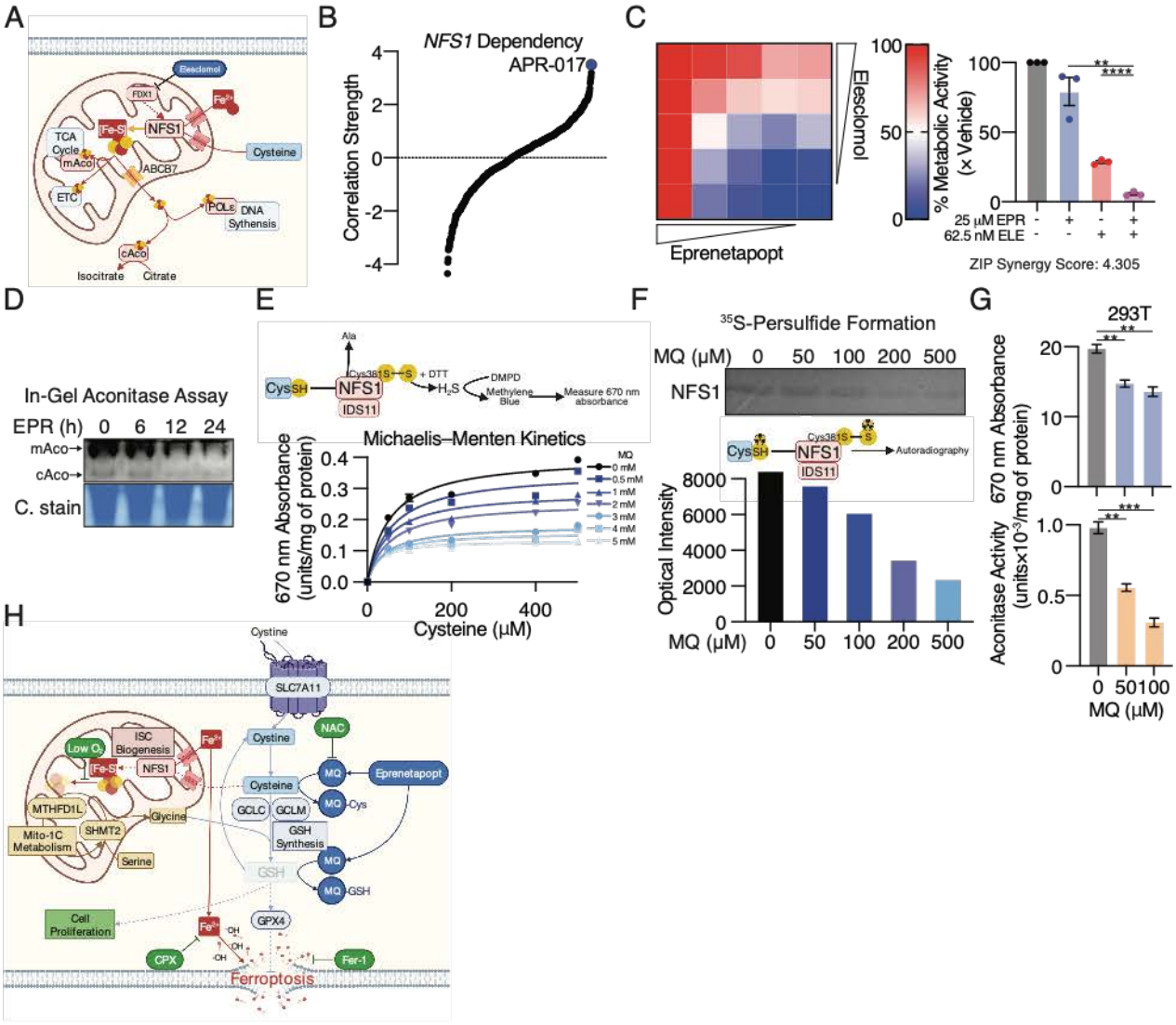

Figure 4 Eprenetapopt inhibits NFS1 cysteine desulfurase activity

(A) Schematic diagram summarizing the role of NFS1 cysteine desulfurase and important iron-sulfur cluster containing enzymes. NFS1 removes sulfur from cysteine to begin the coordination of synthesis of iron-sulfur cluster, which are essential for the function of mitochondrial protein, cytosolic and nuclear proteins. For example, mitochondrial aconitase (mAco) and cytosolic acontase (cAco) both require Fe-S clusters for their catalytic activity converting citrate to isocitrate. Of note, elesclomol inhibits FDX1, which is supports ISC formation. (TCA, tricarboxylic acid; ETC, electron transport chain; POLε, DNA polymerase epsilon) **(B)** Fischer's transformed z-scored Pearson correlation strength of *NFS1* gene dependency and the compound activity of the 481 Cancer Therapeutic Response Portal v2 (CTRPv2) compounds. Blue dot indicates eprenetapopt analogue (APR-017) is the top positive correlated compound to *NFS1* gene dependency. **(C)** Heatmap and bar chart demonstrating cell viability following 72 h eprenetapopt (EPR) and elesclomol (ELE) co-treatment in OACM5.1 cells. **(D)** In-gel aconitase assay and Coomassie stain (for protein loading) in OACM5.1 cells following treatment with 50 μM eprenetapopt for indicated times (mitochondrial: mAconitase, cytosolic: cAconitase). **(E)** Cell-free NFS1 cysteine

desulfurase assay at indicated doses of MQ and cysteine following 1 h incubation measured by the release of hydrogen sulfide (H_2S) by dithiothreitol (DTT) coupled to dimethyl-4-phenylendiamin-hydrochloride (DMPD) to produce methylene blue. **(F)** Top: 2 μM purified NFS1 was incubated with indicated concentrations of MQ and reaction was started with ^{35}S-cysteine for 1 hour at 30 °C followed by separation on 12 % non-reducing SDS-PAGE. Bottom: Image J quantification of the resulting bands. **(G)** Top: NFS1 cysteine desulfurase activity in HEK-293T (293T) following 1 h exposure with MQ at indicated doses measured by the release of H_2S mediated by DTT and NFS1 co-factor pyridoxal 5'-phosphate. Bottom: Aconitase activity following 1 h exposure with MQ at indicated doses in 293T cells. **(H)** Schematic diagram summarizing the MoA of eprenetapopt (GPX4, GSH peroxidase 4). Two-way unpaired t-test **(C,G)**, ** $P < 0.01$, **** $P < 0.00001$. Error bars = SEM. **(C,E,G)** *N*=3. **(D)** *N*=2, representative gel shown, **(F)** *N=1*.

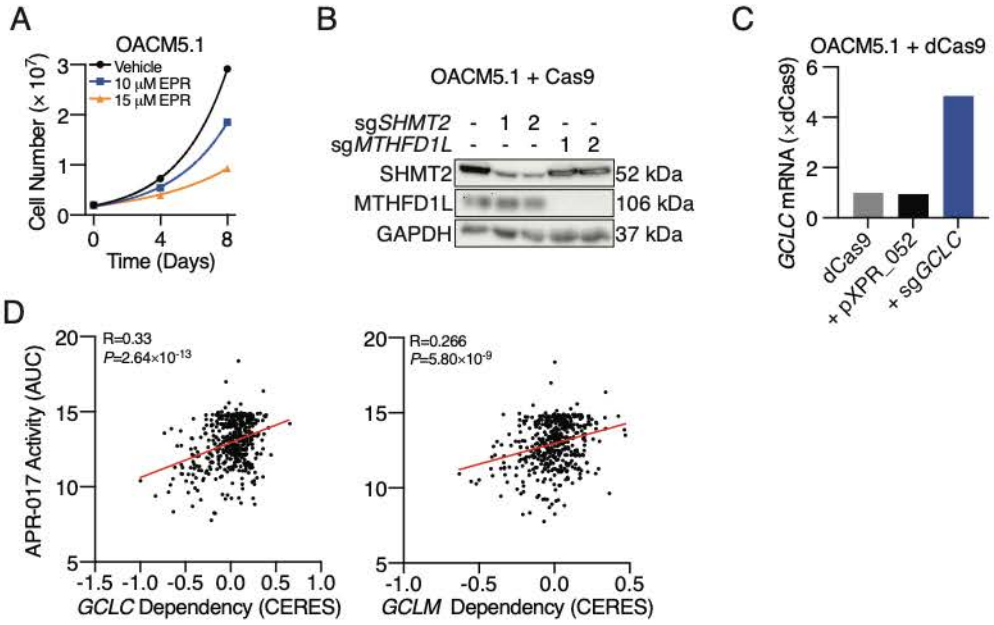

Figure S1. Related to Figure 1 Multiomics strategy to determine the mechanism of action of eprenetapopt

(A) Representative growth curve of OACM5.1 cells treated with eprenetapopt at indicated doses over 8 days. **(B)** Immunoblot of SHMT2 and MTHFD1L illustrating the efficiency of two independent sgRNA guides in bulk OACM5.1 cells following puromycin selection. **(C)** Relative gene expression of *GCLC* in OACM5.1 dCas9 cells expressing CRISPR activation sgRNA guide for *GCLC* or control guide. **(D)** Scatterplots correlating eprenetapopt analogue (APR-017) activity from CTRPv2 with CCL dependency on *GCLC* and *GCLM* in DepMap. (CERES, copy-number adjusted gene dependency score). Pearson's correlation **(D)**. **(A,B,C)** *N*=1. **(D)** *N*=466.

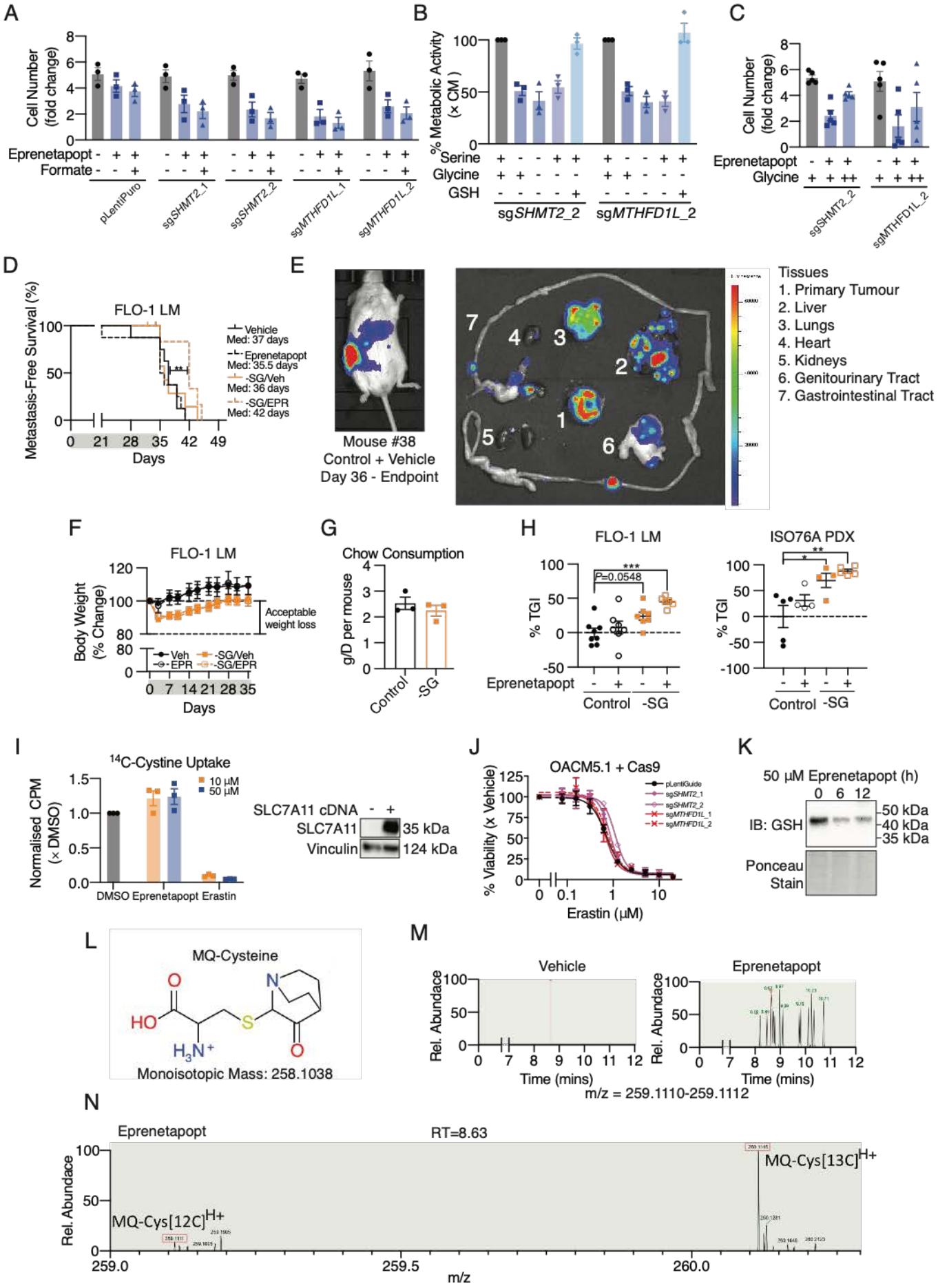
A
Cell Number (fold change)
Eprenetapopt
Formate
pLentiPuro
sgSHMT2_1
sgSHMT2_2
sgMTHFD1L_1
sgMTHFD1L_2
B
% Metabolic Activity (× CM)
Serine
Glycine
GSH
sgSHMT2_2
sgMTHFD1L_2
C
Cell Number (fold change)
Eprenetapopt
Glycine
sgSHMT2_2
sgMTHFD1L_2
D
FLO-1 LM
Metastasis-Free Survival (%)
Vehicle
Med: 37 days
Eprenetapopt
Med: 35.5 days
-SG/Veh
Med: 36 days
-SG/EPR
Med: 42 days
Days
E
Mouse #38
Control + Vehicle
Day 36 - Endpoint
Tissues
1. Primary Tumour
2. Liver
3. Lungs
4. Heart
5. Kidneys
6. Genitourinary Tract
7. Gastrointestinal Tract
F
FLO-1 LM
Body Weight (% Change)
Acceptable weight loss
Veh
EPR
-SG/Veh
-SG/EPR
Days
G
Chow Consumption
g/D per mouse
Control
-SG
H
FLO-1 LM
P=0.0548
% TGI
Eprenetapopt
Control
-SG
ISO76A PDX
% TGI
Control
-SG
I
14C-Cystine Uptake
Normalised CPM (× DMSO)
10 μM
50 μM
DMSO
Eprenetapopt
Erastin
SLC7A11 cDNA
SLC7A11
35 kDa
Vinculin
124 kDa
J
OACM5.1 + Cas9
% Viability (x Vehicle)
pLentiGuide
sgSHMT2_1
sgSHMT2_2
sgMTHFD1L_1
sgMTHFD1L_2
Erastin (μM)
K
50 μM Eprenetapopt (h)
0 6 12
IB: GSH
50 kDa
40 kDa
35 kDa
Ponceau Stain
L
MQ-Cysteine
Monoisotopic Mass: 258.1038
M
Vehicle
Eprenetapopt
Rel. Abundace
Time (mins)
m/z = 259.1110-259.1112
N
Eprenetapopt
RT=8.63
Rel. Abundace
MQ-Cys[12C]H+
MQ-Cys[13C]H+
m/z

Figure S2. Relating to Figure 2 Eprenetapopt and mitochondrial one-carbon metabolism

(A) Relative cell number following treatment with 10 μM eprenetapopt ± 1 mM formate supplementation for 4 days in OACM5.1 cells transduced with control (pLentiPuro) or *SHMT2* or *MTHFD1L* sgRNA. **(B)** Cell viability compared to complete media (CM) following 72 h of serine, glycine or serine and glycine deprivation, and glycine deprivation rescued with 1 mM GSH-monoethyl ester (GSH) in OACM5.1 cells transduced with *SHMT2 or MTHDF1L* sgRNA_2. **(C)** Relative cell number following treatment with 10 μM eprenetapopt ± 1 mM glycine supplementation for 4 days in OACM5.1 cells transduced with *SHMT2 or MTHDF1L* sgRNA_2. **(D)** Metastasis-free survival of NSG mice inoculated with FLO-1 LM tumours treated with eprenetapopt (EPR, 100 mg/kg, daily) or vehicle on either normal or SG-free diets for 35 days. **(E)** Representative bioluminescence images of the distribution of metastatic lesions before and after dissection of a NSG mouse at ethical endpoint. **(F)** % change to body weight of mice over treatment period. Loss of ≤20% body weight relative to beginning of treatment period was considered ethically acceptable. **(G)** Average daily chow consumption of mice on the indicated diets over 7 days. **(H)** % tumour growth inhibition quantified at the end of treatment (35 days for FLO-1 LM, 21 days for PDX). **(I)** Left: Relative radioactive cystine uptake in H1299-SLC7A11 overexpressing cells co-treated with DMSO (as control), pre-heated eprenetapopt and erastin (known cystine uptake inhibitor) at indicated doses. (CPM, counts per minute) Right: Immunoblot demonstrating overexpression of SLC7A11 in H1299 used for cystine uptake assay. **(J)** Cell viability following 72 h exposure with erastin at indicated doses in OACM5.1 cells transduced with indicated sgRNAs. **(K)** Changes to total glutathionylation level following 50 μM eprenetapopt treatment at indicated time points in H1299 cells. **(L)** Chemical structure and mass of MQ-conjugated cysteine. **(M)** Scan to identify MQ-cysteine from LC-MS run of OACM5.1 treated with ^{13}C-cystine and 50 μM eprenetapopt or vehicle for 12 h, over 12 mins of retention time. **(N)** Scan indicating relative abundance of species from retention time (RT) = 8.63, from LC-MS run of OACM5.1 treated with ^{13}C-cystine and 50 μM eprenetapopt. MQ-Cys[^{12}C]$^{H+}$ denotes MQ-cysteine from endogenous ^{12}C-cysteine and MQ-Cys[^{13}C]$^{H+}$ denotes MQ-cysteine from exogenous ^{13}C-cysteine. Log-rank (Mantel-Cox) test **(D)**, one-way ANOVA with Dunnett's multiple comparisons test **(H)**. Error bars = SEM. **(A,B,E,I,J)** *N*=3, **(C)** *N*=5, **(D,F)** *N*=8. **(K)** *N*=2. Representative blot.

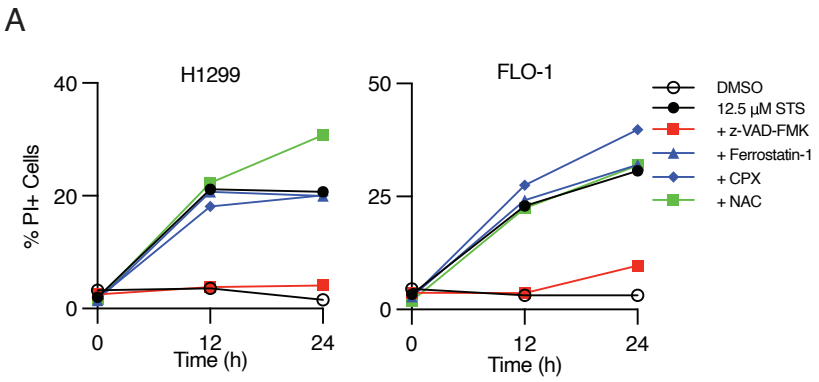

Figure S3. Relating to Figure 3 Eprenetapopt triggers ferroptosis
(A) Cell death (% PI positive) induced by staurosporine (STS, 12.5 µM) with or without apoptosis (zVAD-FMK, 50 µM) or ferroptosis inhibitors (Fer-1, 12.5 µM; CPX, 6.25 µM; NAC, 2.5 mM) in H1299 and FLO-1 cells over 24 h. **(A)** *N*=1.

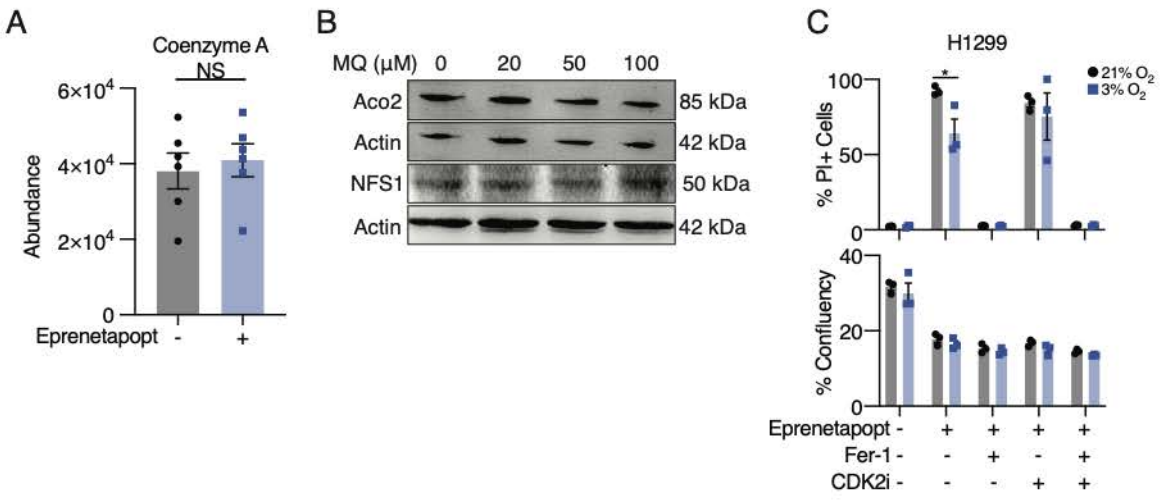

Figure S4. Relating to Figure 4 Eprenetapopt inhibits iron-sulfur cluster biogenesis

(A) Absolute abundance of coenzyme A in OACM.1 cells following treatment with 50 μM eprenetapopt from **Figure 1H**. **(B)** Immunoblot of Aco2 and NFS1 protein levels following 1 h exposure with MQ at indicated doses in 293T cells. **(C)** % cell death and % cell confluency following treatment for 24 h with 50 μM eprenetapopt with or without 12.5 μM Fer-1 and/or 625 nM CDK2 inhibitor (SNS-032) in 21% O_2 (black bars) or 3% O_2 (blue bars) in H1299. Two-tailed t-test **(C)**. * $P < 0.05$. Error bars = SEM. **(A)** *N*=6. **(B)** *N=2*, representative blots shown. **(C)** *N*=3.

SUPPLEMENTAL MATERIALS AND METHODS

Expression and purification of Human NFS1 and ISD11

Plasmids designated pZM2 expressing an N-terminal fusion protein with His_6 tag Nfs1∆1-55 and pZM4 expressing ISD11 were co-transformed into E.coli BL21 (DE3) cells. Cells were grown at 30 ^oC for in 1litre cultures of LB containing 150 µg/ml ampicillin and 50 µg/ml chloramphenicol. The expression was induced by 200 µM of IPTG (Isopropyl-β-D-thiogalactoside). Growth was continued for 16 h at 16 ^oC. Cells were clarified by centrifugation at 8000 g. Cell pellets were lysed and soluble fraction of the resulting lysed cells were obtained by centrifugation at 21000 g for 30 min. Crude extract were applied to Nickel nitrilotriacetate (Ni-NTA) resin. Nfs1∆1-55/Isd11 were eluted with 50 mM NaH_2PO_4, 300 mM NaCl, 250 mM imidazole buffer pH 8.0. Nfs1∆1-55/Isd11 were finally purified using size exclusion chromatography with Superdex 200 column (Superose12 equilibrated with 50 mM Tris, 200 mM NaCl, 10 µM PLP).

Gene expression with quantitative RT-PCR

Total RNA was extracted using NucleoSpin RNA kit (Macherey-Negal), cDNA was synthesized from 1 µg of RNA using High-capacity cDNA Reverse Transcription kit (Applied Biosystems) and gene expression was determined by SYBR-green RT-PCR on a Lightcycler 480 (Roche). Target gene expression was normalized to *ACTB* and analyzed using the ΔΔCt method. Primer sequences are detailed in **Table S4**.

SLC7A11 overexpression

SLC7A11 was ectopically expressed in H1299 using the GE Dharmacon Precision LentiORF pLOC downstream of the CMV promoter and contains turbo-GFP as a reporter gene. The turbo-RFP gene in place of *SLC7A11* was used as a control. Following transduction, GFP-positive cells were sorted. The expression of *SLC711* was confirmed by qPCR and western blotting.

Radioactive cystine uptake assay

H1299 SLC7A11-overexpressing cells were washed in pre-warmed cystine-free RPMI-1640 (uptake buffer). At this point, in each well the cystine-free-media was replaced with 300µL uptake buffer containing eprenetapopt (pre-heated at 90°C for 30 min to hydrolyze to MQ) or erastin with 0.04µCi of L-[1, 2, 1', 2'-^{14}C]-cystine (PerkinElmer) for 10 minutes at room temperature. Cells were then washed thrice with ice-cold cystine-free-media and lysed in 400µL 0.2M NaOH with 1% SDS. This lysate was added to 4mL of scintillation fluid, and radioactive counts per minute were obtained using a scintillation counter.

SUPPLEMENTAL TABLES AND DATASETS

Table S1 List of oligonucleotides used for CRISPR sgRNA guides

Gene	Forward (5'-3')	Reverse (5'-3')
GCLM sgRNA_1	CACCGAATCAACCCAGATTTGGTCA	AAACTGACCAAATCTGGGTTGATTC
GCLM sgRNA_2	CACCGACTAGAAGTGCAGTTGACAT	AAACATGTCAACTGCACTTCTAGTC
SLC7A11 sgRNA_1	CACCGAAGGGCGTGCTCCAGAACAC	AAACGTGTTCTGGAGCACGCCCTTC
SLC7A11 sgRNA_2	CACCGTGAGCTTGATCGCAAGTTCA	AAACTGAACTTGCGATCAAGCTCAC
ESD sgRNA_1	CACCGAATGTACTCTTATGTCACAG	AAACCTGTGACATAAGAGTACATTC
ESD sgRNA_2	CACCGCCTGAGAGCCAATACAGTGC	AAACGCACTGTATTGGCTCTCAGGC
SHMT2 sgRNA_1	CACCGCTACTCACAAGACTCTTCGA	AAACTCGAAGAGTCTTGTGAGTAGC
SHMT2 sgRNA_2	CACCGTCATGCGGGCGTAGTCAATG	AAACCATTGACTACGCCCGCATGAC
MTHFD1L sgRNA_1	CACCGAGGACAAACTCCAAAAGCTG	AAACCAGCTTTTGGAGTTTGTCCTC
MTHFD1L sgRNA_2	CACCGTCGACCCATCTACCATCACG	AAACCGTGATGGTAGATGGGTCGAC
GCLC activation sgRNA	CACCGACACGCCTCCTGAGCCCCCG	AAACCGGGGGGCTCAGGAGGCGTGTC

Table S2 List of antibodies

Antibody	Origin	Clone	Dilution	Source
Anti-SLC7A11	Rabbit	D2M7A	1:1000	Cell Signaling Technology
Anti-SHMT2	Mouse	F-11	1:1000	Santa Cruz Biotechnology
Anti-MTHFD1L	Rabbit	D8T7L	1:1000	Cell Signaling Technology
Anti-Bax	Rat	49F9	1:10000	Gift from Prof. Grant Dewson (WEHI)
Anti-Bak	Rabbit	N/A	1:10000	Sigma-Aldrich
Anti-Bid	Rat	4B5	1:1000	Gift from Prof. Ruth Kluck (WEHI)
Anti-Caspase-3	Rabbit	D3R6Y	1:1000	Cell Signaling Technology
Anti-Caspase-7	Rabbit	D2Q3L	1:1000	Cell Signaling Technology
Anti-NFS1	Rabbit	N/A	1:1000	Sigma-Aldrich
Anti-Aco2	Rabbit	N/A	1:4000	Sigma-Aldrich
Anti-Actin	Mouse	AC-74	1:8000	Sigma-Aldrich
Anti-Glutathione	Mouse	D8	1:1000	Abcam
Anti-Vinculin-HRP	Mouse	7F9	1:2000	Santa Cruz Biotechnology
Anti-GAPDH-HRP	Rabbit	14C10	1:10000	Cell Signaling Technology
Swine anti-rabbit	Swine	P0217	1:7000	Dako
Goat anti-mouse	Goat	P0447	1:7000	Dako
Goat anti-rat	Goat	3010	1:5000	Southern Biotech

Table S3 List of synthetic guides from Synthego for combinatorial CRISPR-editing in Mc38 cells

Gene	ID	Sequence
Casp3	2101	CATGCAGAAAGACCATACAT
Casp3	2103	AACCTCAGAGAGACATTCAT
Casp7	2107	GATATGCTTTAGGCATGCCG
Casp7	2108	TCCATGCGGTACAGATAAGT
Bid	1573	CCACAACATCCAGCCCACAC
Bid	1575	GCCAGCCGCTCCTTCAACCA
Bax	1429	GGACACGGACTCCCCCCGAG
Bax	1430	GTTTCATCCAGGATCGAGCA
Bak1	1410	GGAACTCTGTGTCGTAGCGC
Bak1	1412	GCAGGAGGCTCTTACCAGAA

Table S4 List of primers

Gene	Forward (5'-3')	Reverse (5'-3')
GCLC	CAGGACAGTTCTTAGATGCTGC	TTTGGGCCACACATAAGAAAGC
GAPDH	GGTGTGAACCATGAGAAG	CCACAGTTTCCCGGAG
ACTB	AGAAAATCTGGCACCACACC	GGGGTGTTGAAGGTCTCAAA

Dataset S1. Source data from Figure 1D and 1F. List of genes and MAGeCK scores for CRISPRko "drop-out" screen (average of two independent screens), CRISPRa "enrichment" screen (one screen) and DepMap gene dependency Fischer's z-transformed Pearson's correlation strengths.

Movie S1. H1299 cells die from 50 μM eprenetapopt treatment over 24 h. Here, we present a time-lapse video of cells with images taken every 5 min at 6 frames per second, therefore each second represents 1 h in real time, starting immediately after dosing with eprenetapopt. Images were acquired on IncuCyte FLR (Essen BioSciences).

REFERENCES

1. S. Haupt *et al.*, Identification of cancer sex-disparity in the functional integrity of p53 and its X chromosome network. *Nat Commun* **10**, 5385 (2019).
2. V. J. N. Bykov, S. E. Eriksson, J. Bianchi, K. G. Wiman, Targeting mutant p53 for efficient cancer therapy. *Nat Rev Cancer* **18**, 89-102 (2018).
3. T. Cluzeau *et al.*, Eprenetapopt Plus Azacitidine in TP53-Mutated Myelodysplastic Syndromes and Acute Myeloid Leukemia: A Phase II Study by the Groupe Francophone des Myelodysplasies (GFM). *J Clin Oncol* **39**, 1575-1583 (2021).
4. D. A. Sallman *et al.*, Eprenetapopt (APR-246) and Azacitidine in TP53-Mutant Myelodysplastic Syndromes. *J Clin Oncol* **39**, 1584-1594 (2021).
5. C. Bally *et al.*, Prognostic value of TP53 gene mutations in myelodysplastic syndromes and acute myeloid leukemia treated with azacitidine. *Leuk Res* **38**, 751-755 (2014).
6. T. Aprea. (2020).
7. J. M. Lambert *et al.*, PRIMA-1 reactivates mutant p53 by covalent binding to the core domain. *Cancer Cell* **15**, 376-388 (2009).
8. Q. Zhang, V. J. N. Bykov, K. G. Wiman, J. Zawacka-Pankau, APR-246 reactivates mutant p53 by targeting cysteines 124 and 277. *Cell Death Dis* **9**, 439 (2018).
9. K. M. Fujihara *et al.*, SLC7A11 is a superior determinant of APR-246 (Eprenetapopt) response than TP53 mutation status. *Mol Cancer Ther*, (2021).
10. S. C. Lu, Regulation of glutathione synthesis. *Mol Aspects Med* **30**, 42-59 (2009).
11. S. Ceder *et al.*, A thiol-bound drug reservoir enhances APR-246-induced mutant p53 tumor cell death. *EMBO Mol Med* **13**, e10852 (2021).
12. D. S. Liu *et al.*, Inhibiting the system xC(-)/glutathione axis selectively targets cancers with mutant-p53 accumulation. *Nat Commun* **8**, 14844 (2017).
13. L. Haffo *et al.*, Inhibition of the glutaredoxin and thioredoxin systems and ribonucleotide reductase by mutant p53-targeting compound APR-246. *Sci Rep* **8**, 12671 (2018).
14. X. Peng *et al.*, APR-246/PRIMA-1MET inhibits thioredoxin reductase 1 and converts the enzyme to a dedicated NADPH oxidase. *Cell Death Dis* **4**, e881 (2013).
15. J. M. Dempster *et al.*, Extracting biological insights from the project achilles genome-scale CRISPR screens in cancer cell lines. *BioRxiv*, 720243 (2019).
16. R. M. Meyers *et al.*, Computational correction of copy number effect improves specificity of CRISPR-Cas9 essentiality screens in cancer cells. *Nat Genet* **49**, 1779-1784 (2017).
17. J. G. Doench *et al.*, Optimized sgRNA design to maximize activity and minimize off-target effects of CRISPR-Cas9. *Nat Biotechnol* **34**, 184-191 (2016).
18. K. R. Sanson *et al.*, Optimized libraries for CRISPR-Cas9 genetic screens with multiple modalities. *Nat Commun* **9**, 5416 (2018).
19. N. Mohell *et al.*, APR-246 overcomes resistance to cisplatin and doxorubicin in ovarian cancer cells. *Cell Death Dis* **6**, e1794 (2015).
20. W. Hang *et al.*, Piperlongumine and p53-reactivator APR-246 selectively induce cell death in HNSCC by targeting GSTP1. *Oncogene* **37**, 3384-3398 (2018).
21. H. Ogiwara *et al.*, Targeting the Vulnerability of Glutathione Metabolism in ARID1A-Deficient Cancers. *Cancer Cell* **35**, 177-190 e178 (2019).

22. G. Burgos-Barragan *et al.*, Mammals divert endogenous genotoxic formaldehyde into one-carbon metabolism. *Nature* **548**, 549-554 (2017).
23. G. Burgos-Barragan *et al.*, Erratum: Mammals divert endogenous genotoxic formaldehyde into one-carbon metabolism. *Nature* **548**, 612 (2017).
24. L. Uotila, M. Koivusalo, Purification and properties of S-formylglutathione hydrolase from human liver. *J Biol Chem* **249**, 7664-7672 (1974).
25. D. Ali *et al.*, Anti-leukaemic effects induced by APR-246 are dependent on induction of oxidative stress and the NFE2L2/HMOX1 axis that can be targeted by PI3K and mTOR inhibitors in acute myeloid leukaemia cells. *Br J Haematol* **174**, 117-126 (2016).
26. R. Birsen *et al.*, APR-246 induces early cell death by ferroptosis in acute myeloid leukemia. *Haematologica*, (2021).
27. N. C. Synnott *et al.*, The Mutant p53-Targeting Compound APR-246 Induces ROS-Modulating Genes in Breast Cancer Cells. *Transl Oncol* **11**, 1343-1349 (2018).
28. K. Cai, M. Tonelli, R. O. Frederick, J. L. Markley, Human Mitochondrial Ferredoxin 1 (FDX1) and Ferredoxin 2 (FDX2) Both Bind Cysteine Desulfurase and Donate Electrons for Iron-Sulfur Cluster Biosynthesis. *Biochemistry* **56**, 487-499 (2017).
29. Z. Ye, J. R. Connor, cDNA cloning by amplification of circularized first strand cDNAs reveals non-IRE-regulated iron-responsive mRNAs. *Biochem Biophys Res Commun* **275**, 223-227 (2000).
30. C. Andreini, L. Banci, A. Rosato, Exploiting Bacterial Operons To Illuminate Human Iron-Sulfur Proteins. *J Proteome Res* **15**, 1308-1322 (2016).
31. M. Yang, K. H. Vousden, Serine and one-carbon metabolism in cancer. *Nat Rev Cancer* **16**, 650-662 (2016).
32. G. S. Ducker *et al.*, Reversal of Cytosolic One-Carbon Flux Compensates for Loss of the Mitochondrial Folate Pathway. *Cell Metab* **24**, 640-641 (2016).
33. O. D. Maddocks *et al.*, Serine starvation induces stress and p53-dependent metabolic remodelling in cancer cells. *Nature* **493**, 542-546 (2013).
34. O. D. K. Maddocks *et al.*, Modulating the therapeutic response of tumours to dietary serine and glycine starvation. *Nature* **544**, 372-376 (2017).
35. S. P. Gravel *et al.*, Serine deprivation enhances antineoplastic activity of biguanides. *Cancer Res* **74**, 7521-7533 (2014).
36. F. Polet *et al.*, Reducing the serine availability complements the inhibition of the glutamine metabolism to block leukemia cell growth. *Oncotarget* **7**, 1765-1776 (2016).
37. M. Tajan *et al.*, Serine synthesis pathway inhibition cooperates with dietary serine and glycine limitation for cancer therapy. *Nat Commun* **12**, 366 (2021).
38. D. S. Liu *et al.*, Novel metastatic models of esophageal adenocarcinoma derived from FLO-1 cells highlight the importance of E-cadherin in cancer metastasis. *Oncotarget* **7**, 83342-83358 (2016).
39. S. J. Dixon *et al.*, Ferroptosis: an iron-dependent form of nonapoptotic cell death. *Cell* **149**, 1060-1072 (2012).
40. M. Gao *et al.*, Role of Mitochondria in Ferroptosis. *Mol Cell* **73**, 354-363 e353 (2019).
41. M. Soula *et al.*, Metabolic determinants of cancer cell sensitivity to canonical ferroptosis inducers. *Nat Chem Biol* **16**, 1351-1360 (2020).
42. J. V. Milne *et al.*, Transketolase regulates sensitivity to APR-246 in p53-null cells independently of oxidative stress modulation. *Sci Rep* **11**, 4480 (2021).

43. J. Wu *et al.*, Intercellular interaction dictates cancer cell ferroptosis via NF2-YAP signalling. *Nature* **572**, 402-406 (2019).
44. W. H. Yang *et al.*, The Hippo Pathway Effector TAZ Regulates Ferroptosis in Renal Cell Carcinoma. *Cell Rep* **28**, 2501-2508 e2504 (2019).
45. N. Rokaeus *et al.*, PRIMA-1(MET)/APR-246 targets mutant forms of p53 family members p63 and p73. *Oncogene* **29**, 6442-6451 (2010).
46. R. Zandi *et al.*, PRIMA-1Met/APR-246 induces apoptosis and tumor growth delay in small cell lung cancer expressing mutant p53. *Clin Cancer Res* **17**, 2830-2841 (2011).
47. M. N. Saha, H. Jiang, Y. Yang, D. Reece, H. Chang, PRIMA-1Met/APR-246 displays high antitumor activity in multiple myeloma by induction of p73 and Noxa. *Mol Cancer Ther* **12**, 2331-2341 (2013).
48. M. A. Badgley *et al.*, Cysteine depletion induces pancreatic tumor ferroptosis in mice. *Science* **368**, 85-89 (2020).
49. J. I. Leu, M. E. Murphy, D. L. George, Functional interplay among thiol-based redox signaling, metabolism, and ferroptosis unveiled by a genetic variant of TP53. *Proc Natl Acad Sci U S A* **117**, 26804-26811 (2020).
50. A. Biederbick *et al.*, Role of human mitochondrial Nfs1 in cytosolic iron-sulfur protein biogenesis and iron regulation. *Mol Cell Biol* **26**, 5675-5687 (2006).
51. O. Stehling, C. Wilbrecht, R. Lill, Mitochondrial iron-sulfur protein biogenesis and human disease. *Biochimie* **100**, 61-77 (2014).
52. D. J. Netz, J. Mascarenhas, O. Stehling, A. J. Pierik, R. Lill, Maturation of cytosolic and nuclear iron-sulfur proteins. *Trends Cell Biol* **24**, 303-312 (2014).
53. S. W. Alvarez *et al.*, NFS1 undergoes positive selection in lung tumours and protects cells from ferroptosis. *Nature* **551**, 639-643 (2017).
54. E. M. Terzi, V. O. Sviderskiy, S. W. Alvarez, G. C. Whiten, R. Possemato, Iron-sulfur cluster deficiency can be sensed by IRP2 and regulates iron homeostasis and sensitivity to ferroptosis independent of IRP1 and FBXL5. *Sci Adv* **7**, (2021).
55. P. Tsvetkov *et al.*, Mitochondrial metabolism promotes adaptation to proteotoxic stress. *Nat Chem Biol* **15**, 681-689 (2019).
56. W. H. Tong, T. A. Rouault, Functions of mitochondrial ISCU and cytosolic ISCU in mammalian iron-sulfur cluster biogenesis and iron homeostasis. *Cell Metab* **3**, 199-210 (2006).
57. V. O. Sviderskiy *et al.*, Hyperactive CDK2 Activity in Basal-like Breast Cancer Imposes a Genome Integrity Liability that Can Be Exploited by Targeting DNA Polymerase epsilon. *Mol Cell* **80**, 682-698 e687 (2020).
58. D. Ali *et al.*, APR-246 exhibits anti-leukemic activity and synergism with conventional chemotherapeutic drugs in acute myeloid leukemia cells. *Eur J Haematol* **86**, 206-215 (2011).
59. V. Mlakar *et al.*, PRIMA-1(MET)-induced neuroblastoma cell death is modulated by p53 and mycn through glutathione level. *J Exp Clin Cancer Res* **38**, 69 (2019).
60. B. Tessoulin *et al.*, PRIMA-1Met induces myeloma cell death independent of p53 by impairing the GSH/ROS balance. *Blood* **124**, 1626-1636 (2014).
61. V. J. Bykov *et al.*, Restoration of the tumor suppressor function to mutant p53 by a low-molecular-weight compound. *Nat Med* **8**, 282-288 (2002).
62. V. J. Bykov *et al.*, PRIMA-1(MET) synergizes with cisplatin to induce tumor cell apoptosis. *Oncogene* **24**, 3484-3491 (2005).

63. P. Izetti *et al.*, PRIMA-1, a mutant p53 reactivator, induces apoptosis and enhances chemotherapeutic cytotoxicity in pancreatic cancer cell lines. *Invest New Drugs* **32**, 783-794 (2014).
64. L. Jiang *et al.*, Ferroptosis as a p53-mediated activity during tumour suppression. *Nature* **520**, 57-62 (2015).
65. S. J. Dixon *et al.*, Pharmacological inhibition of cystine-glutamate exchange induces endoplasmic reticulum stress and ferroptosis. *Elife* **3**, e02523 (2014).
66. J. Du *et al.*, DHA inhibits proliferation and induces ferroptosis of leukemia cells through autophagy dependent degradation of ferritin. *Free Radic Biol Med* **131**, 356-369 (2019).
67. X. Chen, R. Kang, G. Kroemer, D. Tang, Broadening horizons: the role of ferroptosis in cancer. *Nat Rev Clin Oncol*, (2021).
68. O. W. Griffith, A. Meister, Potent and specific inhibition of glutathione synthesis by buthionine sulfoximine (S-n-butyl homocysteine sulfoximine). *J Biol Chem* **254**, 7558-7560 (1979).
69. V. S. Viswanathan *et al.*, Dependency of a therapy-resistant state of cancer cells on a lipid peroxidase pathway. *Nature* **547**, 453-457 (2017).
70. W. S. Yang *et al.*, Regulation of ferroptotic cancer cell death by GPX4. *Cell* **156**, 317-331 (2014).
71. J. P. Friedmann Angeli *et al.*, Inactivation of the ferroptosis regulator Gpx4 triggers acute renal failure in mice. *Nat Cell Biol* **16**, 1180-1191 (2014).
72. T. Haferlach *et al.*, Landscape of genetic lesions in 944 patients with myelodysplastic syndromes. *Leukemia* **28**, 241-247 (2014).
73. E. Sabattini, F. Bacci, C. Sagramoso, S. A. Pileri, WHO classification of tumours of haematopoietic and lymphoid tissues in 2008: an overview. *Pathologica* **102**, 83-87 (2010).
74. L. Malcovati *et al.*, SF3B1 mutation identifies a distinct subset of myelodysplastic syndrome with ring sideroblasts. *Blood* **126**, 233-241 (2015).
75. N. Kanarek, B. Petrova, D. M. Sabatini, Dietary modifications for enhanced cancer therapy. *Nature* **579**, 507-517 (2020).
76. S. Ceder *et al.*, Mutant p53-reactivating compound APR-246 synergizes with asparaginase in inducing growth suppression in acute lymphoblastic leukemia cells. *Cell Death Dis* **12**, 709 (2021).
77. D. A. Pollyea *et al.*, Venetoclax with azacitidine disrupts energy metabolism and targets leukemia stem cells in patients with acute myeloid leukemia. *Nat Med* **24**, 1859-1866 (2018).
78. C. L. Jones *et al.*, Inhibition of Amino Acid Metabolism Selectively Targets Human Leukemia Stem Cells. *Cancer Cell* **34**, 724-740 e724 (2018).
79. C. L. Jones *et al.*, Cysteine depletion targets leukemia stem cells through inhibition of electron transport complex II. *Blood* **134**, 389-394 (2019).
80. NCT04214860. (2020).
81. T. Aprea. (2021).
82. J. Joung *et al.*, Genome-scale CRISPR-Cas9 knockout and transcriptional activation screening. *Nat Protoc* **12**, 828-863 (2017).
83. Y. Masukagami *et al.*, A combined metabolomic and bioinformatic approach to investigate the function of transport proteins of the important pathogen Mycoplasma bovis. *Vet Microbiol* **234**, 8-16 (2019).
84. M. S. I. B. Members *et al.*, The metabolomics standards initiative. *Nat Biotechnol* **25**, 846-848 (2007).

85. Z. Pang, J. Chong, S. Li, J. Xia, MetaboAnalystR 3.0: Toward an Optimized Workflow for Global Metabolomics. *Metabolites* **10**, (2020).
86. M. Read *et al.*, Intramuscular Transplantation Improves Engraftment Rates for Esophageal Patient-Derived Tumor Xenografts. *Ann Surg Oncol* **23**, 305-311 (2016).
87. D. S. Liu *et al.*, APR-246 potently inhibits tumour growth and overcomes chemoresistance in preclinical models of oesophageal adenocarcinoma. *Gut* **64**, 1506-1516 (2015).
88. Z. Marelja, W. Stocklein, M. Nimtz, S. Leimkuhler, A novel role for human Nfs1 in the cytoplasm: Nfs1 acts as a sulfur donor for MOCS3, a protein involved in molybdenum cofactor biosynthesis. *J Biol Chem* **283**, 25178-25185 (2008).
89. A. Pandey, H. Yoon, E. R. Lyver, A. Dancis, D. Pain, Identification of a Nfs1p-bound persulfide intermediate in Fe-S cluster synthesis by intact mitochondria. *Mitochondrion* **12**, 539-549 (2012).
90. H. Uhrigshardt, A. Singh, G. Kovtunovych, M. Ghosh, T. A. Rouault, Characterization of the human HSC20, an unusual DnaJ type III protein, involved in iron-sulfur cluster biogenesis. *Hum Mol Genet* **19**, 3816-3834 (2010).